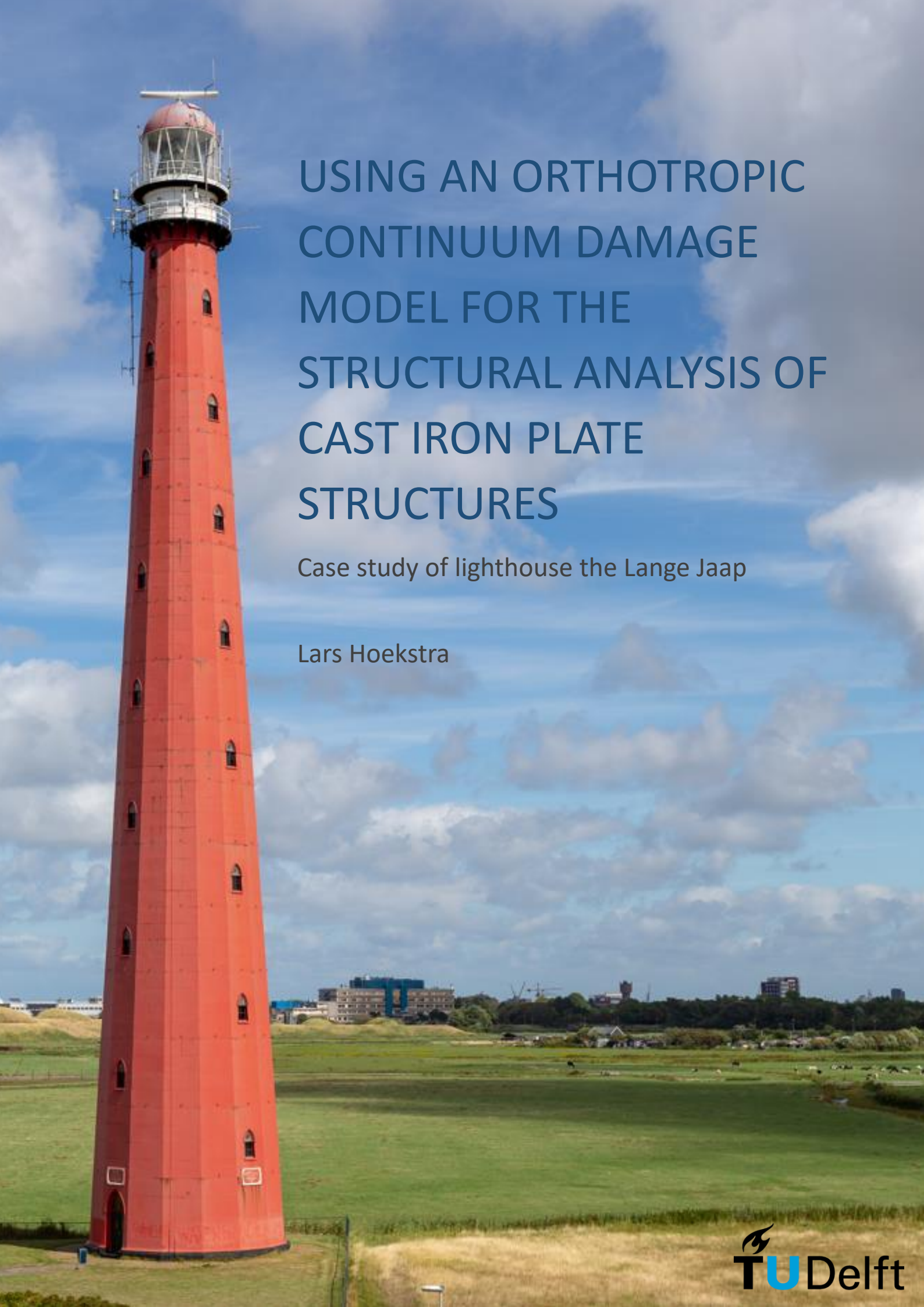

USING AN ORTHOTROPIC CONTINUUM DAMAGE MODEL FOR THE STRUCTURAL ANALYSIS OF CAST IRON PLATE STRUCTURES

Case study of lighthouse the Lange Jaap

Lars Hoekstra

TU Delft

USING AN ORTHOTROPIC CONTINUUM DAMAGE MODEL FOR THE STRUCTURAL ANALYSIS OF CAST IRON PLATE STRUCTURES

Case study of lighthouse the Lange Jaap

by

Lars Hoekstra

Preface

In this report, the research I performed for my master thesis is described. The thesis is part my Master education in Civil Engineering, with the master track Structural Engineering, at the TU Delft. The report describes how an orthotropic continuum damage model can be used for the structural analysis of a cast iron plate structure in order to reduce the complexity of a detailed finite element model for a cast iron plate structure.

I would like to thank all members of the assessment committee for enabling me to do this project and for providing me with the feedback I needed to increase the quality of my thesis. Especially Paul Korswagen, as he was the person I reached out to the most. He has guided me during everything I have done during my thesis, and I was able to ask him any questions I had at any time. Thanks to him, I was able to deliver high quality results in this project.

Delft, August 2025

Lars Hoekstra

Summary

In the Netherlands, several cast iron lighthouses were built between the years 1856-1899. Their structural state has been deteriorating and cracks have formed in the cast iron plates of the inner and outer columns, and strengthening the structures is required. Current assessment methods of such large cast iron plate structures require a very detailed finite element model. Large detailed models are very time consuming to create and analyse, which makes it a costly assessment method. In this thesis, the use of an orthotropic continuum damage model, the Engineering Masonry Model (EMM) in this case, for the structural analysis of cast iron plate structures is explored. The EMM was developed for the analysis of unreinforced brick masonry structures. In these lighthouse structures, the cast iron plates are placed in a similar pattern as bricks in masonry structures. In addition, cast iron has brittle tensile behaviour, which is also the case for bricks in masonry structures. Due to the similarities of the structures, a model is developed in this thesis which allows the use of an orthotropic continuum damage model for a cast iron plate structure. The thesis focuses on a specific case, which is the case of the lighthouse the 'Lange Jaap', located in Den Helder, the Netherlands.

In order to find a good strengthening solution for the structure of lighthouse the Lange Jaap, finite element analyses can be used. By analysing the impact of the relevant forces on a model of the lighthouse and applying a possible strengthening solution, the effectiveness of different strengthening solutions can be determined. As mentioned, creating and analysing detailed finite element models of large structure is very time consuming, so the possibilities of simplifying the model were considered. In an orthotropic continuum damage model, the material properties of the cast iron plates and the connections can be combined and one material will be used for the entire structure. By using such a material model, it is no longer required to create every single plate and connection separately, which simplifies the model significantly. Therefore, the research question of this thesis is: *How can an orthotropic continuum damage model be used to reduce the complexity of the structural analysis of a detailed finite element model for a cast iron plate structure?*

To obtain the input parameters that are required for an orthotropic continuum damage model, detailed models of small plate structures were created. Different loading conditions were applied and the resulting force-displacement curves were analysed do derive constitutive laws for the structural analysis. After performing a sensitivity study of the size effect of the structure, the failure modes changed for some of the loading types. This resulted in quite a difference in strength and ultimate strain between the small and large structures. If this method is used to simplify the complexity of a detailed finite element model, it is important to find a unit structure size for every relevant load case. This unit structure size should have the failure mode which is expected in the model of the entire structure. The unit structure size does not have to be the same for each load case.

After the input parameters for the orthotropic continuum damage model were obtained from the results of the finite element analyses of the detailed unit structure sized models, equivalent models of the exact same structure size were created in which the input parameters were applied. From the results of the equivalent models, it became apparent which parameters needed to be calibrated to increase the similarity of the results of the equivalent models, compared to results of the detailed models. In this case, the tension and compression models resulted in calibration of several parameters, as there were multiple values for the E_y and $G_{f,tension.}$ As only one value could be used, the average value was used and the other relevant parameters were calibrated. As the equivalent models are very easy to make and the running time of the analyses is very small, the calibration of the parameters did not take very long, but the accuracy of the finite element model was increased significantly.

In this project, the final, calibrated input parameters were used in an orthotropic continuum damage model for the cast iron plate structure of lighthouse the Lange Jaap and it was concluded that very similar results were obtained as from the detailed model, when all strains were in the linear-elastic regime. As the values of the bed- and head-joint tensile strengths that were obtained were quite low, tensile stresses which are larger than the tensile strength of the material appeared quite quickly in the model of the lighthouse. Once plastic deformations occurred, cracks started to form and the analysis of the thesis model quickly became unstable, which meant the results were no longer accurate. This shows that, after the calibration of the parameters, the linear-elastic behaviour of the structure is accurately captured in the model, while the plastic behaviour is not.

However, for research questions in which deformations remain in the linear-elastic regime, a finite element model in which an orthotropic continuum damage model is used can provide very accurate results. The company PT Structural Design & Analysis created a detailed finite element models of the lighthouse, and of their goals was to determine the maximum wind velocity at which (almost) no vertical tensile stresses would occur in the lighthouse. For their model, this maximum wind velocity was equal to 18.3 m/s. The same analysis was performed on the thesis model, and it was determined that the value of the maximum wind velocity is equal to 18.4 m/s in the thesis model. As the values are almost exactly the same, this confirms that the results of a finite element model in which an orthotropic continuum damage model is used for a large cast iron plate structure, very similar to the results of a detailed finite element model.

Additionally, to analyse the structural behaviour of the lighthouse in compression, an increased value was of the gravitational acceleration was applied in a separate model. This caused the self-weight load to be multiplied by a load factor of 20. The results of the analysis were mostly as expected, as the compressive stresses increased almost linearly with the load factor. Since the plates are placed under an angle in the lighthouse, the self-weight load caused out of plane displacements in the structure. As a result, tensile stresses were introduced and cracks started to form. After a load application factor of 18.7, the model became unstable and divergence was reached. It is concluded that the low values of the head- and bed-joint strength cause quite some problems in the analyses of the structure, as this allows cracks to form quite quickly, even when the tensile stresses are still relatively small.

The answer to the main research question was obtained and it was concluded that the complexity was reduced due to the following points:

- When using an orthotropic continuum damage model (such as the EMM) only small detailed models of the unit structure size that include the most realistic failure modes have to be analysed, instead of a detailed model of the entire structure. It can be concluded that this can significantly reduce the total modelling time
- The geometry of the cast iron plate structures was simplified, as the flanges and stiffeners were no longer included in the models. As a result, it was possible to use regular curved shell elements instead of structural solids. This makes it very easy to create models of very large structures
- As regular curved shell elements were used, due to the simplification of the geometry, a much larger element size can be chosen which results in a much lower amount of elements and nodes compared to a detailed model. Fewer elements and nodes means the analysis time of the model becomes shorter. It can be concluded that using an orthotropic continuum damage model, such as the EMM, can significantly reduce the total running time of the analysis of large cast iron plate structures, as shell elements can be used

Using an orthotropic continuum damage model might become a profitable method of modelling large plate structures. The total working time that is spent on creating and analysing the models, and accuracy of the final finite element models are key aspects when one considers using this method to model a certain plate structure. Especially the number of plate sizes that is considered when obtaining the input parameters, heavily impacts the total working time and the accuracy of the final model. The amount of plates that is considered should be based on which of the two aspects is of higher importance. Considering less plate sizes is faster, but reduces the accuracy of the final model.

Due to the limitations of the method, it is not applicable for all types of research. However, research types for which the method is very suitable are studies in which many finite element analyses have to be made for a structure, where small changes are made in every analysis. For the lighthouse structure, a study of the effectiveness of different strengthening solutions for the columns is a very good example. By using an orthotropic continuum damage model, the running time of the finite element model is reduced and making many different analyses of the finite element model can be achieved in a much shorter time period.

Table of contents

1 Introduction

1.1 Background problem

Cast iron became a popular building material in the 19th century and was used for different kinds of structures in the Netherlands. The first use of cast iron was in factories, where wooden columns were replaced by cast iron columns. Due to the high compressive strength of cast iron, the columns had a much smaller surface area and more space became available for machinery. However, it quickly became clear that the tensile strength of cast iron is much lower and the material is also very brittle in tension. When structures consisted only of cast iron, it had to be ensured that the elements were only loaded in compression. The material became widely used in lighthouse structures in the Netherlands and more than 10 cast iron lighthouses were built between the years 1856-1899 (Lintsen, et al., 1993).

All of those lighthouses were built more than 100 years ago and their structural state has been deteriorating. Cracks are forming in the cast iron floors and the plates of the inner and outer columns (Rijkswaterstaat, 2020). Some of the structures were demolished due to their irreparable damage. However, the government aims to maintain the remaining lighthouses, as they have become national monuments. Therefore, instead of demolishing and replacing the structures, they are looking for strengthening solutions with which the original state of the building can be maintained as much as possible. In order to find a good solution for the problem, finite element analyses can be used. By analysing the impact of the relevant forces on a model of a lighthouse and applying a possible strengthening solution, the effectiveness of the strengthening solution can be determined. However, creating detailed finite element models of large structures takes a long time. As the models will contain a large amount of nodes and elements, the running time of the analysis will be very long. If several strengthening solutions have to be analysed, this will become a very time consuming process. By simplifying certain parts of the model, the total amount of time to create and analyse different models could be reduced significantly. This would mean a conclusion can be found much faster for studies where many different models of large structures have to be analysed.

1.2 Scope and research questions

For lighthouse structures, it might be possible to simplify the model for the inner and outer columns. The columns consist of cast iron plates, which are placed in a half-brick pattern. Besides that, cast iron has brittle tensile behaviour, and is much stronger in compression. These characteristics are similar to those of masonry walls. For masonry walls, orthotropic continuum damage models, such as the Engineering Masonry Model (EMM), are used in finite element analyses. This reduces the model complexity, as it is not required to make every single brick separately in the model. If an orthotropic continuum damage model could be used for the inner and outer columns of the lighthouse, it would not be required to create every single plate separately, which simplifies the model significantly. Besides that, the flanges and stiffeners that are part of the plates can be left out of the models, which also results in a simplified model. Therefore, the research question of this thesis is:

How can an orthotropic continuum damage model be used to reduce the complexity of the structural analysis of a detailed finite element model for a cast iron plate structure?

To obtain a good answer, the research question is divided into the following sub-questions:

- *How can the required input parameters be obtained for different nonlinear failure modes of the components of a cast iron plate structure, to enable using an orthotropic continuum damage model in a structural analysis?*
- *How will those parameters be affected by increasing the size of the structure to an assembly of multiple plates and connections?*
- *How do the results of a detailed finite element model compare to the results of an orthotropic continuum damage model, when being used in a structural analysis of lighthouse the Lange Jaap?*

The first two sub-questions refer to the base of the problem, as this will show how the EMM can be used to obtain accurate results for the analysis of cast iron plate structures. The final sub-question will show a comparison between the results of a structural analysis of a detailed model and a model where the EMM is used. The case of the lighthouse the Lange Jaap, located in Den Helder, the Netherlands, is analysed in this sub-question (chapter 2 provides a description of the case study). From the comparison between the models, it will be clear whether the results will be similar, and what the main advantages and disadvantages are of using an orthotropic continuum damage model instead of a detailed model for the structural analysis of a large cast iron plate structure.

1.3 Methodology

Several steps have to be taken to find the answers to the research questions of this thesis. The main steps that will be taken during this study are presented in the flowchart below.

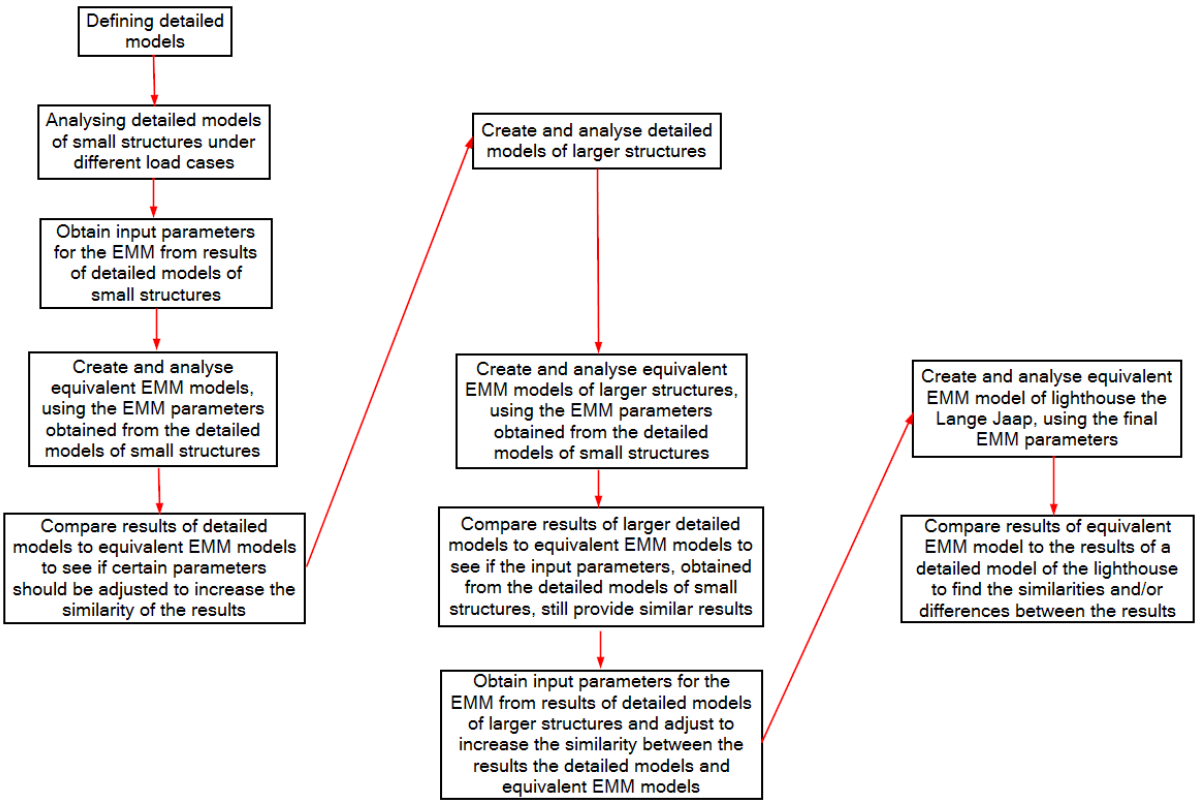

Figure 1.1: Flowchart with the main steps of the thesis

There are three different columns in the flowchart and each column will provide the answer to one of the sub-questions. Steps that have been placed on the same row are steps that are similar to each other. As the process of each column is quite similar, some steps repeat themselves during this thesis. The main content of each column is as follows:

- Analyse detailed models of a structure
- Analyse equivalent EMM models of the same structure
- Compare results to find similarities and/or differences

After the answers to all sub-questions have been obtained, the main research question can be answered as well. From all findings that were discovered during the study, conclusions can be made about the methods that were used.

1.4 Thesis outline

The structure of the report is as follows: Chapter 2 will provide a description of the case that will be studied in this thesis: lighthouse the Lange Jaap. In chapter 3, the definition of detailed models and equivalent EMM models will be clarified, and the numerical approach of both model types will be presented. Chapters 4, 5 and 6 will all provide an answer to one of the sub-questions. These chapters contain all the results of the steps that were presented in the flowchart in section 1.3. In chapter 4, the detailed models of the small structures are analysed under different load cases. From the results of those models, input parameters that can be used in the EMM are obtained. Next, these parameters will be used in equivalent EMM models and the results will be compared to the results of the detailed models. In chapter 5, the structure size will be increased and detailed models of larger structures are analysed. Again, equivalent EMM models will be analysed, where the input parameters that are used are the parameters that were obtained from the detailed models of the small structures. By comparing the results, it will be clear if these parameters provide similar results when used in equivalent EMM models of larger structures. New parameters will be obtained from the results of the detailed models of the larger structures, which are then adjusted to increase the similarity between the results of the detailed models and the equivalent EMM models. In chapter 6, the final EMM parameters are used in an equivalent EMM model of lighthouse the Lange Jaap, after which several analyses are performed. The results will be compared to the results of a detailed model of the lighthouse and all similarities and differences will be listed. Finally, chapters 7 and 8 will contain the conclusions and recommendations that will result from all previous chapters.

2 Case study: lighthouse the Lange Jaap

2.1 Description of the case study

The Lange Jaap is a cast iron lighthouse located in Den Helder, the Netherlands. The lighthouse was constructed in 1877, and was first used in 1878. The building has received a monumental status in 1988. With a total height of 63.45 meters, it is the highest functioning lighthouse in the Netherlands and the highest cast iron lighthouse in Europe (Vuurtoren Lange Jaap, 2025). The lighthouse consists of an outer column and an inner column, both made out of cast iron plates. The plates are placed in a half-brick pattern and have flanges on the edges, which allows a bolted connection between the plates. Besides that, a mixture called iron cement is used to close all openings between the edges. This method is used in older structures, to ensure a good bonding between iron elements (Oostingh, 2012). The floor plates consist of cast iron as well, which are connected to the columns via bolts. The lighthouse is placed on a foundation which consists of 249 timber piles.

The designer of the lighthouse, Quirinus Harder, chose cast iron as construction material for the Lange Jaap instead of masonry, for three main reasons (Suchtelen, 1978):

1) Faster construction time: the total construction time was approximately one year, whereas a masonry lighthouse would have taken around three years to construct. As the shipping industry was growing very fast, the lighthouse had to be constructed as fast as possible.
2) Lower costs: the total costs of a cast iron lighthouse were approximately three times lower than the costs of a masonry lighthouse.
3) Lower foundation requirements: the self-weight is significantly lower for a cast iron lighthouse compared to a masonry lighthouse. For this reason, the requirements for the foundation are lower for a cast iron lighthouse, which causes a reduction in construction complexity and costs.

Furthermore, it was chosen to use cast iron instead of sheet iron. Rolled sheet iron was only limitedly available at that time and, moreover, cast iron is a lot more resistant to the corrosive marine atmosphere, which means the structure would require less maintenance.

The structural strength of the Lange Jaap is decreasing due to the damage. To get a complete overview of the current strength and stability of the lighthouse, a structural analysis should be performed. The company PT Structural Design & Analysis bv has published a report that describes the results of their structural analysis (PT Structural Design & Analysis bv, 2022). First, the structure without any damage was analysed. From this analysis, it became clear that the maximum fundamental value of the basic wind velocity (vb,0) on the lighthouse is 18.3 m/s, as this wind load results in zero (to very little) tensile stress at the bottom of the outer column of the lighthouse. When the wind loads are increased, tensile stresses will start to occur in the plates of the outer column, which is not desired for cast iron elements. Secondly, they performed a structural analysis including cracks between the floors and the columns, which are increasing in size. This represents the current state of the lighthouse, so it can be seen what the influences are on the strength and stability, compared to the model of the lighthouse in the original state. As a result of the cracks in the floor, the force distribution becomes different in the outer column of the lighthouse, which has a negative effect on the connections between the plates. Therefore, they advise to gradually remove and replace the current floor panels. In addition, the report contains a Phased Array analysis of the bolts made by INFRATECHNIEK. They found that at least 1000 bolts have to be replaced, as they are damaged or broken. Tests have been performed on site, but replacing the bolts has been proven to be very challenging, so it is still unclear if it is feasible to replace all the bolts. However, in the conclusion of

the report, it is stated that even if all bolts are replaced, the cracks that are beginning to form in the outer column are still a large problem. These cracks will grow when tensile stresses occur in the plates, which will happen if the lighthouse is loaded by wind speeds larger than 18.3 m/s, as they found in the first analysis.

When determining the maximum wind load in the design verifications of new buildings, the value of vb,0 is based on the wind region (CEN, 2005). There are three different regions in the Netherlands, all corresponding to a different value for vb,0. As Den Helder is located in wind region I, this means that the value of vb,0 should be equal to 29.5 m/s in the design verifications. This is significantly higher than the maximum allowable value of 18.3 m/s, calculated by PT Structural Design & Analysis bv. It can be concluded that the structure, in its current condition, does not meet the strength requirements of the Eurocode. It has become clear that the floors should be replaced, because of the large amount of cracks they contain. After this step, a solution should be found to control the damage in the outer column of the lighthouse. As there are already cracks in the areas where tensile stresses have occurred, they will continue to grow when tensile stresses keep occurring. If there are no tensile stresses in the outer column of the lighthouse, the cracks will not form a big problem in terms of structural strength. PT Structural Design & Analysis bv determined that the maximum allowable wind speed is 18.3 m/s, as there are no (to very little) tensile vertical stresses in the outer column of the lighthouse for this wind speed (PT Structural Design & Analysis bv, 2022). No clear limit has been mentioned in the report for the acceptable tensile stresses, but from the curves that they present, it can be assumed that the maximum allowable tensile stresses are 0.01 MPa. When the wind loads are increased, tensile stresses will occur in the outer column of the lighthouse, which means the cracks will grow and failure of the outer column will occur at some point. As wind speeds higher than 18.3 m/s are common at the location of the Lange Jaap, a strengthening solution has to be found in order to ensure the safety of the lighthouse for higher wind loading conditions.

The government is currently trying to find an optimal solution for the strengthening of the lighthouse. They do not want to replace the building completely, as it is a national monument. The best option they found is to wrap the entire structure in a composite cocoon (Beukers, 2022). The total costs of this solution are estimated to be somewhere between 1.1 and 2.2 million euros. This solution causes a reduction of the loads on the outer column by 40 to 50%, which means the structure can endure much larger wind loads without experiencing any tension. However, the government aims to maintain the original state of the monument as much as possible, so wrapping the entire lighthouse with composite is not the most desirable solution. A solution which meets all requirements has not been found yet. As mentioned, finite element analyses can be used to determine the effectiveness of certain strengthening solutions. When a solution is applied to a finite element model of the lighthouse, it will be clear if the solution provides the desired results. For large structures such as the Lange Jaap, many different solutions are considered, which means many different finite element models would have to be analysed. As creating and analysing detailed finite element models of large structures is very time consuming, a faster analysis method is desired. By simplifying certain parts of the model, the total amount of time to create and analyse different models could be reduced significantly. However, it should first be determined what the effect of this simplification of the structure has on the results of the model. Therefore, in this study, the results of the detailed model that was created and analysed by the company PT Structural Design & Analysis bv, will be compared to the results of the equivalent EMM model of the lighthouse that will be analysed in this thesis.

2.2 Dividing the columns into different sections

The structure of the lighthouse contains an outer and an inner column. A cross section of the bottom of the lighthouse is given in the figure below.

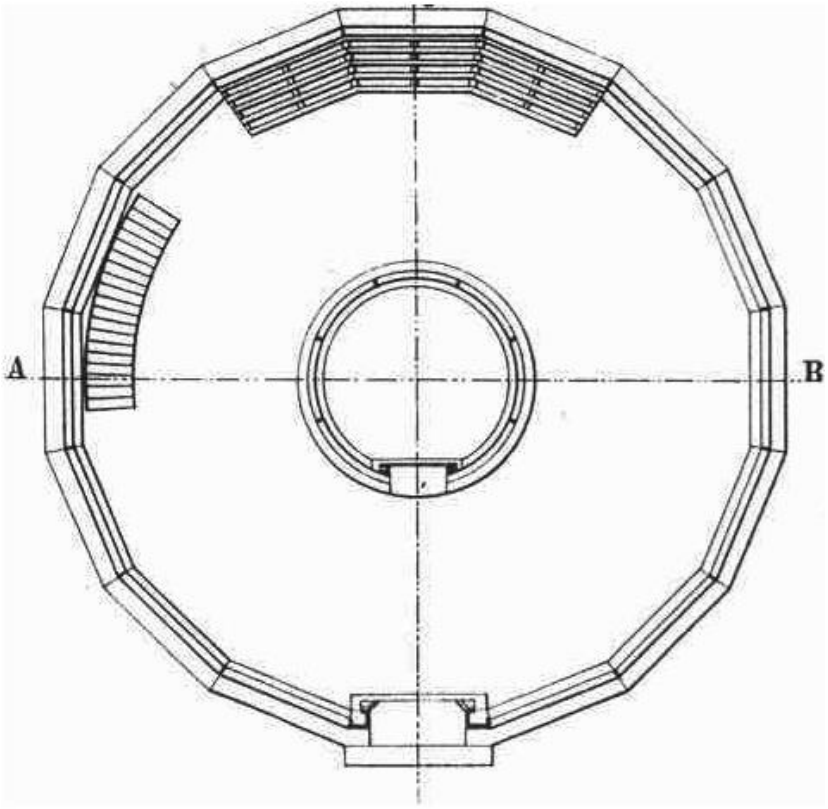

Figure 2.1: Cross section outer column of the lighthouse (Harder, 1875)

The outer column of the lighthouse consists of 68 layers of plates, divided over 17 floors, so 4 layers per floor. The plates are placed in a hexadecagon, which is a sixteen-sided shape. A document from 1875 describes the radius of the hexadecagon and plate thickness at the top and bottom of the column. The values in between can be obtained by linear interpolation. The document also provides the height of the plates on every layer. Finally, the width and thickness of the flanges are also stated here, which are 60 and 20 mm, respectively. From this information, it is possible to create an overview of the dimensions of the plates at the different layers:

Table 2.1: Overview plate dimensions per layer of outer column

Layer(s)	**Number of layers**	**h_{plate} [m]**	**t_{plate} [m]**	**h_{top} [m]**	**r_{column} [m]**	**b_{plate} [m]**
1-4	4	0.95	0.035	3.8	5.024	1.960
5-10	6	0.9	0.034	9.2	4.703	1.835
11-16	6	0.875	0.033	14.45	4.391	1.713
17-24	8	0.85	0.0317	21.25	3.986	1.555
25-34	10	0.825	0.0299	29.5	3.496	1.364
35-44	10	0.8	0.0281	37.5	3.020	1.178
45-54	10	0.775	0.0262	45.25	2.559	0.999
55-67	13	0.75	0.0241	55	1.980	0.772
68	1	0.5	0.023	55.5	1.950	0.761

By calculating h_{top} for each set of layers, the radius of the hexadecagon can be determined at the top of the set of layers. From this radius, the following formula can be used to determine the width of the plate:

$$b_{plate} = 2 * r_{column} * \sin(11.25^o)$$

The angle of 11.25° is calculated by 360°/16/2. Analysing all different plate sizes individually, would make the research very accurate, but also extremely lengthy. For this reason, the outer column of the lighthouse will be divided into three different sections instead. The sections will be chosen such that the differences between the plate dimensions within the section are not too large. The average thickness and height of the plates in the section are used. The height of the middle of the section, with respect to the total height of the column, is determined next, such that the radius of the column at this height can be calculated. By using this radius in the formula mentioned above, the width of the plates at the middle of the section can be determined, which gives the average width of the plates in that section. Names are introduced for the different plates, which refer to their respective column and section. For example, OS1 refers to a plate of the outer column, located in section 1. The dimensions of the plates of the different sections are provided in the table below.

Table 2.2: Overview plate dimensions per outer column section

Section	**$h_{section}$ [m]**	**h_{middle} [m]**	**r_{middle} [m]**	**h_{plate} [mm]**	**t_{plate} [mm]**	**b_{plate} [mm]**
OS1	21.25	10.625	4.618	885	33.2	1802
OS2	16.25	29.375	3.503	812.5	29	1368
OS3	18	46.5	2.485	750	24.9	970

Based on these dimensions, the amount of stiffeners and bolts for the connections are determined, as well as the distances between them:

Table 2.3: Overview stiffeners and bolts per outer column section

Section	**$n_{stiffeners}$**	**$d_{stiffeners}$ [mm]**	**$n_{bolts,bed}$**	**$d_{bolts,bed}$ [mm]**	**$n_{bolts,head}$**	**$d_{bolts,head}$ [mm]**
OS1	5	352.4	10	176.2	5	169
OS2	4	332	8	166	5	154.5
OS3	3	310	6	155	4	177.5

For the inner column, there are 2 layers of plates per floor. Its height reaches until the 15th floor, so there are 30 layers of plates in total. The column is a shaped as a cylinder, so not a hexadecagon like the outer column. The radius and thickness of the top and bottom of the column can be found in the same document as mentioned in the calculation of the outer column dimensions. By interpolating between these values, the dimensions of the plates for each layer can be determined. By calculating h_{top} for each set of layers, the radius of the column can be determined at the top of the set of layers. There are 8 plates at each layer, which means the width of the plate can be determined by dividing the circumference by 8. This width is therefore the arclength of 1/8 of a circle with the related radius. The dimensions of the inner column plates are given in the table below.

Table 2.4: Overview plate dimensions per layer of inner column

Layer(s)	Number of layers	h_{plate} [m]	t_{plate} [m]	h_{top} [m]	r_{column} [m]	b_{plate} [m]
1-2	2	1.9	0.025	3.8	1.443	1.133
3-5	3	1.8	0.0246	9.2	1.361	1.069
6-8	3	1.75	0.0243	14.45	1.282	1.007
9-12	4	1.7	0.0239	21.25	1.180	0.926
13-17	5	1.65	0.025	29.5	1.055	0.829
18-22	5	1.6	0.0218	37.5	0.935	0.734
23-27	5	1.55	0.021	45.25	0.818	0.642
28-30	3	1.5	0.02	49.75	0.750	0.589

Again, the column will be divided into three sections. First, the height and thickness will be calculated by determining the average of the plates in the section. Using the same method as for the outer column, the average width of the plate will be based on the plates which are located at the middle of the section. Similar as for the plates of the outer column, names are introduced for the inner column plates as well. An example here: IS2 refers to a plate of the inner column, located in section 2. The dimensions of the inner column plates are given in the table below

Table 2.5: Overview plate dimensions per inner column section

Section	$h_{section}$ [m]	h_{middle} [m]	r_{middle} [m]	h_{plate} [mm]	t_{plate} [mm]	b_{plate} [mm]
IS1	21.25	10.625	1.338	1770	24.4	1051
IS2	16.25	29.375	1.057	1624	23.4	830
IS3	12.25	43.625	0.843	1532	20.6	662

Based on these dimensions, the amount of stiffeners and bolts for the connections are determined, as well as the distances between them:

Table 2.6: Overview stiffeners and bolts per inner column section

Section	$n_{stiffeners}$	$d_{stiffeners}$ [mm]	$n_{bolts,bed}$	$d_{bolts,bed}$ [mm]	$n_{bolts,head}$	$d_{bolts,head}$ [mm]
IS1	3	337	6	168.5	10	173
IS2	2	395	4	197.5	9	176
IS3	2	311	4	155.5	8	186.5

It can be concluded that there are a few differences between the plates of the inner and outer columns, besides the shape. Due to the smaller radius of the inner column, the inner column plates are much smaller than the plates of the outer column. However, the inner column only has 2 layers of plates per floor, which means the inner column plates have a much larger height. Logically, the difference in height and width causes the difference in the amount of bolts used in the head and bed joints.

2.3 The material properties of cast iron

The first step is to establish what kind of cast iron is used in the lighthouse. The company IECRT researched the composition of the cast iron and was able to determine that EN-GJL-150 is being used (IECRT, 2010). Table A.1 and A.2 of NEN-EN 1561 provide some of the material properties that are required as input for the detailed models.

Table 2.7: Table A.1 of NEN-EN 1561 (CEN, 2023)

Table A.1 — Mechanical properties in cast samples with 30 mm as-cast diameter

Property	Symbol	SI-unit	Material designation [a]				Bibliographical references
			EN-GJL-150 (5.1200)	EN-GJL-200 (5.1300)	EN-GJL-250 (5.1301)	EN-GJL-300 (5.1302)	
			Matrix structure				
			ferritic/pearlitic			pearlitic	
Tensile strength	R_m	MPa	150 to 250	200 to 300	250 to 350	300 to 400	—
0,1 % proof strength	$R_{p0,1}$	MPa	98 to 165	130 to 195	165 to 228	195 to 260	[6]
Compression strength		MPa	$3,40 \times R_m$	$3,18 \times R_m$	$3,01 \times R_m$	$2,87 \times R_m$	[9]
0,1 % compression proof strength		MPa	195	260	325	390	[6]
Bending strength		MPa	$1,82 \times R_m$	$1,73 \times R_m$	$1,66 \times R_m$	$1,60 \times R_m$	[9]
Shear strength		MPa	170	230	290	345	[9]
Torsional strength		MPa	$1,36 \times R_m$				[9]
Modulus of elasticity [b]	E	GPa	78 to 103	88 to 113	103 to 118	108 to 137	[10]
Poisson's number	ν	—	0,26	0,26	0,26	0,26	[8]
Bending fatigue strength		MPa	70 to 115 ($0,46 \times R_m$)	90 to 140 ($0,46 \times R_m$)	115 to 160 ($0,46 \times R_m$)	140 to 185 ($0,46 \times R_m$)	[9]
Fatigue limit under reversed tension-compression stresses		MPa	50 to 85 ($0,34 \times R_m$)	70 to 100 ($0,34 \times R_m$)	85 to 120 ($0,34 \times R_m$)	100 to 135 ($0,34 \times R_m$)	[9]
Torsional fatigue strength		MPa	55 to 95 ($0,38 \times R_m$)	75 to 115 ($0,38 \times R_m$)	95 to 135 ($0,38 \times R_m$)	115 to 150 ($0,38 \times R_m$)	[9]

NOTE 1 MPa is equivalent to 1 N/mm^2.

[a] When there are special requirements relating to machinability or magnetic properties, then EN-GJL-100 (5.1100) is used. The required properties can be obtained by means of a structure-changing heat-treatment process. EN-GJL-100 (5.1100) is not cited here.

[b] Depends on the quantity and form of the graphite as well as on the loading. The tension-elongation-curve of grey cast iron is nonlinear. The modulus of elasticity is the tangent line at the origin of the tension-elongation-curve.

Table 2.8: Mass density cast iron, obtained from table A.2 of NEN-EN 1561 (CEN, 2023)

Table A.2 — Physical properties in cast samples with 30 mm as-cast diameter

Property	Symbol	SI-unit	Material designation [a]				Bibliographical references
			EN-GJL-150 (5.1200)	EN-GJL-200 (5.1300)	EN-GJL-250 (5.1301)	EN-GJL-300 (5.1302)	
Mass density	ρ	kg/dm^3	7,10	7,15	7,20	7,25	—

However, from the PT Structural report, it can be seen that the values they used for the strength, stiffness and mass density are slightly different. A mass density of 0.8541888E-05 kg/mm^3 is used. The values they use for the other parameters are given in the tables below. The top table shows the ranges they found from a document of the company 'Bouwen met Staal', the bottom table shows which values they chose to use in their model.

Table 2.9: Bouwen met staal ranges for cast iron strength (PT Structural Design & Analysis bv, 2022)

Property	**Value**
Tensile strength	105-180 [N/mm^2]
Compressive strength	340-760 [N/mm^2]
E-modulus	85-130 * 10^3 [N/mm^2]

Table 2.10: Strength values used by PT Structural Design & Analysis (PT Structural Design & Analysis bv, 2022)

Property	**Value**
Tensile strength	105 [N/mm^2]
Compressive strength	340 [N/mm^2]
E-modulus	107,5 * 10^3 [N/mm^2]

3 Numerical approach for detailed and equivalent EMM models

The first step in the process is to define the small detailed models that will be used to determine the required input parameters for the Engineering Masonry Model (EMM). This includes defining the models, the material properties of the cast iron and defining how to model the connections between the plates. The connections in the models should capture the shear and tensile behaviour accurately, such that the structural behaviour of the detailed models is a good approximation of reality. By processing the results of the detailed models, the EMM input parameters will be defined. When these parameters are used in equivalent EMM models, they should simulate similar tensile, compressive and shear failure.

3.1 Detailed models

The detailed models consist of two different parts: the cast iron plates and the bolted connections. For the cast iron plates, structural solids will be used as the element type. The material model that is used is the total strain based crack model. The bolted connection is modelled as an interface connection. Interface elements are used as the element type and the material model of combined cracking-shearing-crushing is used. Both material models were chosen due to the fact that their input values relate to the different load cases that the models will be loaded with. The figure below shows an example of what is described in this thesis as a detailed model.

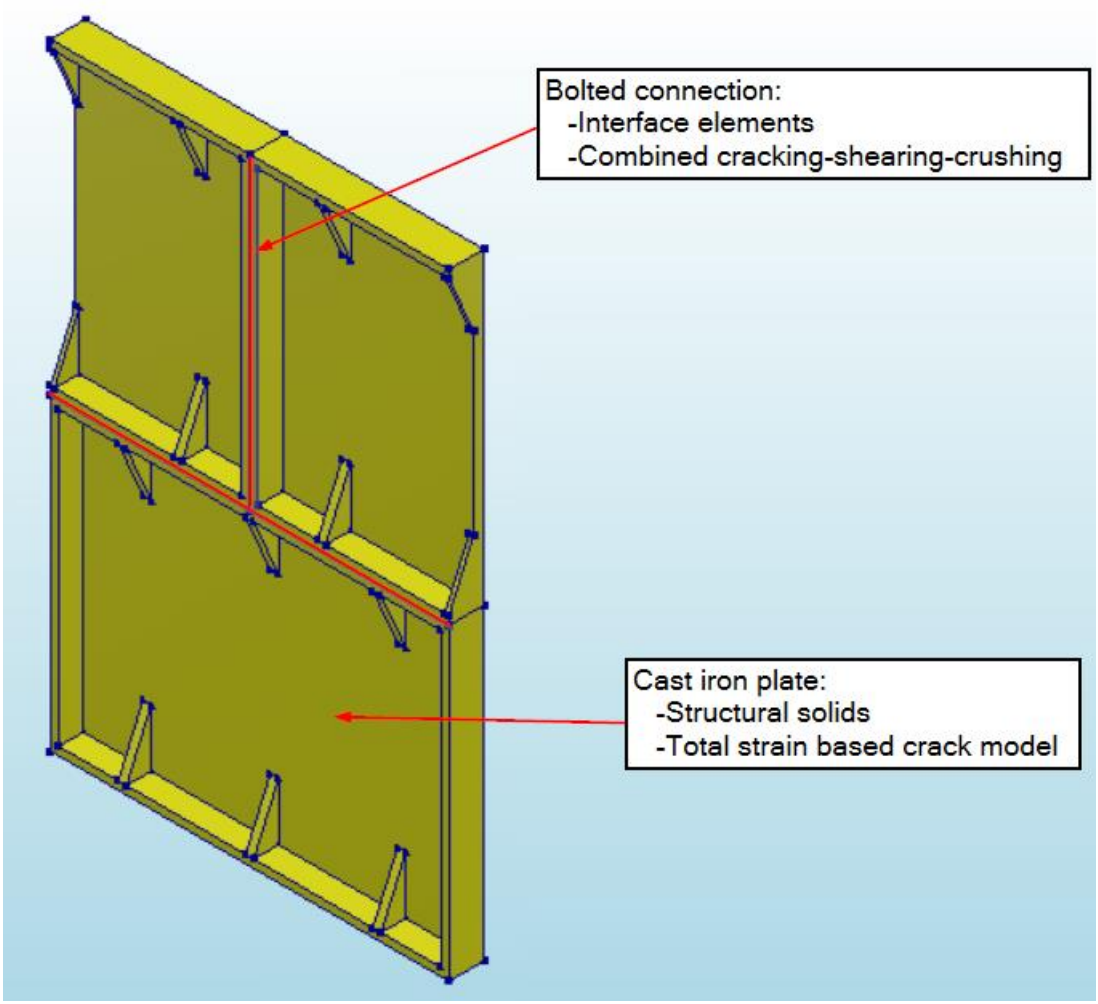

Figure 3.1: Example of what a detailed model is, as described in the thesis

3.1.1 Mesh size and elements

DIANA FEA will be used for the finite element analyses in this study. For the detailed models, structural solids will be used for the plates, and interface elements are used for the connections. Finally, the size of the elements should be chosen. The thickness of the plates varies from 20.6 to 33.2 mm. The flanges and stiffeners both have a thickness of 20 mm. Therefore, the element size in the detailed models will be chosen as 20x20 mm, approximately. The mesh will not be consisting of perfect squares only, as DIANA will automatically adjust the mesh to fit the geometry of the structure. This means there will also be different shaped elements. Element codes are used to describe the different elements, and each element has different properties. The different types of elements that are used for the detailed models in this study are given in the table below. All the relevant element properties are also provided for every element. Most properties were obtained from the DIANA FEA manual (DIANA FEA bv, 2017).

Table 3.1: Overview of the element types and their relevant properties of elements used the detailed models

Element code	HX24L	PY15L	TE12L	TP18L	Q24IF
Element type	Structural solids, brick shape	Structural solids, pyramid shape	Structural solids, tetrahedron shape	Structural solids, wedge shape	Interface elements, quadrilateral shape
Degrees of freedom	24: 8 nodes, 3 translations per node	15: 5 nodes, 3 translations per node	12: 4 nodes, 3 translations per node	18: 6 nodes, 3 translations per node	24: 2*4 = 8 nodes, 3 translations per node
Interpolation scheme	Linear	Linear	Linear	Linear	Linear
Integration scheme	2×2×2 Gauss	5-point Gauss	1-point Gauss	1-point Gauss	2×2 Newton-Cotes
Shape dimension	3D	3D	3D	3D	3D
Topological dimension	3D	3D	3D	3D	3D
Stress components	σ_{xx}, σ_{yy}, σ_{zz}, σ_{xy}, σ_{yz}, σ_{zx}	σ_{xx}, σ_{yy}, σ_{zz}, σ_{xy}, σ_{yz}, σ_{zx}	σ_{xx}, σ_{yy}, σ_{zz}, σ_{xy}, σ_{yz}, σ_{zx}	σ_{xx}, σ_{yy}, σ_{zz}, σ_{xy}, σ_{yz}, σ_{zx}	t_{sx}, t_{sy}, t_{nz}

3.1.2 Constitutive law for cast iron

As the results of the finite element analysis performed in this study will be compared to the results of the detailed model that PT Structural found, the input here should match their input. Therefore, the same values for the E-modulus, compression and tensile strengths will be used here. For the other required input parameters, the values from the Eurocode will be altered slightly such that they match the values that PT Structural used. The shear strength and the 0.1% tensile and compressive proof strength will be determined by multiplying the values from the table A.1 of NEN-EN 1561 by a factor of 105/150 = 0.7, which is the ratio of the used tensile strength over the minimal tensile strength provided in the table. Furthermore, the shear modulus is calculated by the following formula:

$$G = \frac{E}{2(1+v)}$$

This results in the following properties:

Table 3.2: Mechanical properties for cast iron used in this study

Material property	**Value**	**Unit**
E-modulus	107500	MPa
Tensile strength	105	MPa
0.1% tensile proof strength	68.6	MPa
Compression strength	340	MPa
0.1% compression proof strength	185.7	MPa
Poisson ratio	0.26	-
Shear Modulus	42658.7	MPa

With these values, it is possible to create stress-strain diagrams in tension and compression.

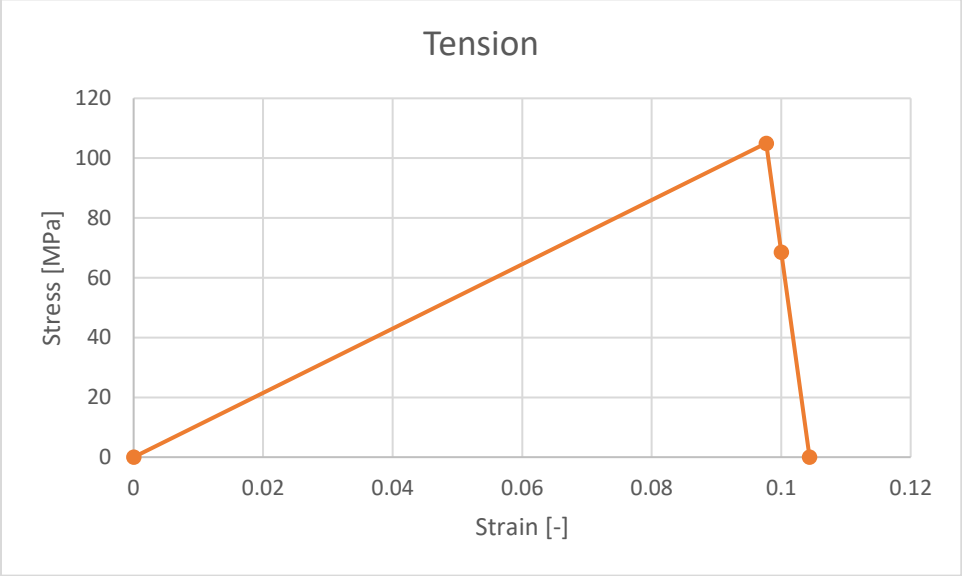

Figure 3.2: Stress-strain diagram tension

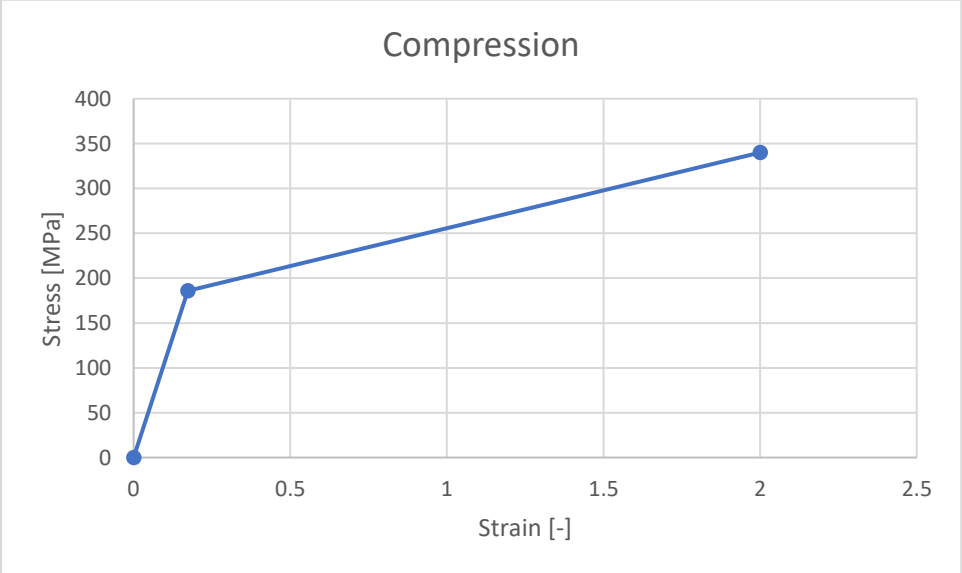

Figure 3.3: Stress-strain diagram compression

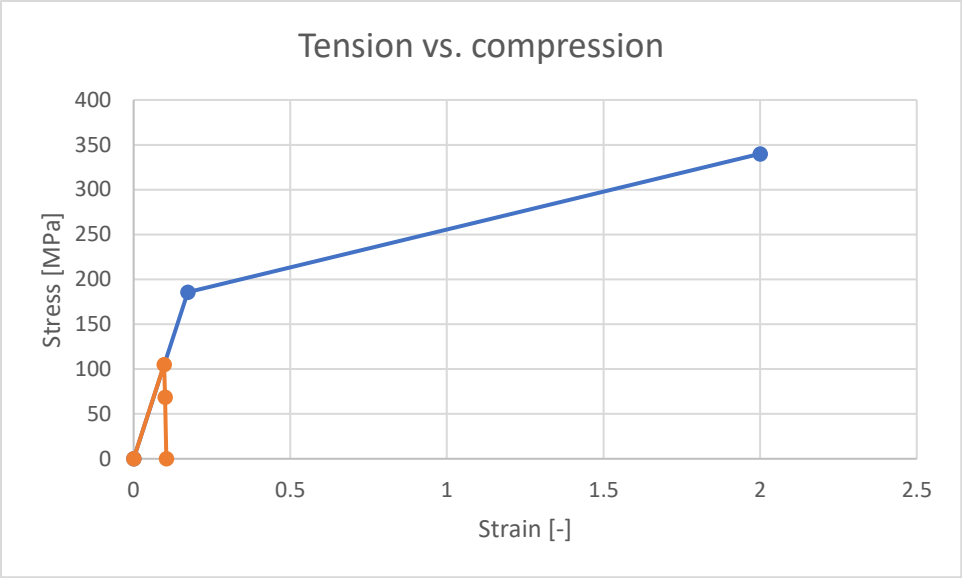

Figure 3.4: Comparison of stress-strain curves tension & compression

The figures capture the material behaviour when loaded in tension or compression. From the figures, it is clear that the material has brittle behaviour in tension and is much stronger in compression. This is due to the fact that there is softening in tension, and hardening in compression.

3.1.3 Constitutive law for connections

In order to analyse a detailed model of the cast iron plates, the strength and stiffness properties can be applied to a material in DIANA FEA, so the cast iron plates can be modelled as structural solids. For the connection between the plates, an interface connection should be defined. The combined cracking-shearing-crushing interface type of DIANA will be used. The properties will be based on the properties of the bolts and the iron cement. The stiffness in the normal direction can be calculated by relating the following formulas: $F = k * u$ and $\sigma = E * \varepsilon$. The second formula can be rewritten as: $F = EA/L * u$. This means the stiffness k equals EA/L in the normal direction. The total length is equal to the bolt length between the edges of the flanges, which is equal to the iron cement thickness plus 2 times the full flange thickness. The iron cement has a thickness of 10 mm, while the flange thickness is 20 mm, which means L = 50 mm. The formulas for the shear stiffness are derived from the figure below.

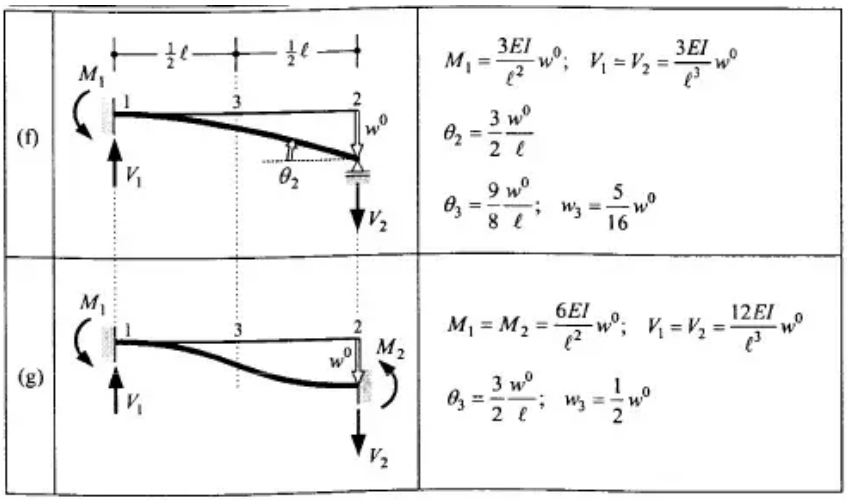

Figure 3.5: Forget-me-not situations relevant for the shear stiffness of the bolts (TU Delft, 2021)

This represents the bolts, where the supports are located in the centre of the flanges for shear, which means the length L is equal to the thickness of the iron cement plus 2 times half the thickness of the flange, so L = 30 mm. It is assumed that the top of bolt is supported by a fixed support. The bottom can be assumed to be supported by a pinned support, or by a fixed support as well. For the two options, the shear stiffness will either be $3EI/L^3$ or $12EI/L^3$, respectively. As the shear stiffness will be lower for the first option, this value will be used to be on the conservative side. The calculation of the linear stiffness in the normal direction and in shear are given below. For the area, the area of the bolt should be used (A_s). This is dependent on the bolt diameter, which is equal to 16.61 mm, according to the PT Structural report. The moment of inertia is calculated as: $I = \pi * D^4/64$.

$$k_{bolt,normal} = \frac{EA}{L}$$

$$k_{bolt,normal} = \frac{107500 * 216.69}{50} = 465883.5\ N/mm$$

$$k_{bolt,shear} = \frac{3EI}{L^3}$$

$$k_{bolt,shear} = \frac{3 * 107500 * 3727.37}{30^3} = 44521.3\ N/mm$$

The total stiffness of the joint is determined by the stiffness of a bolt, the number of bolts in the joint, and the total area of the connection. Which means the following formula is used:

$$k_{tot} = \frac{k_{bolt} * n_{bolts}}{b * h}$$

The table below provides the results of calculating the linear normal and shear stiffness for the head and bed joints of the different sections:

Table 3.3: Resulting linear normal and shear stiffness per joint

Joint	**n_{bolts}**	**$k_{bolt,normal}$ [N/mm]**	**$k_{bolt,shear}$ [N/mm]**	**$b_{connection}$ [mm]**	**$h_{connection}$ [mm]**	**$k_{tot,normal}$ [N/mm³]**	**$k_{tot,shear}$ [N/mm³]**
OS1 head	5	465883.5	44521.3	93.2	885	28.24	2.70
OS1 bed	10	465883.5	44521.3	93.2	1802	27.74	2.65
OS2 head	5	465883.5	44521.3	89	812.5	32.21	3.08
OS2 bed	8	465883.5	44521.3	89	1368	30.61	2.93
OS3 head	4	465883.5	44521.3	84.9	750	29.27	2.80
OS3 bed	6	465883.5	44521.3	84.9	970	33.94	3.24
IS1 head	10	465883.5	44521.3	84.4	1770	31.19	2.98
IS1 bed	6	465883.5	44521.3	84.4	1051	31.51	3.01
IS2 head	9	465883.5	44521.3	83.4	1624	30.96	2.96
IS2 bed	4	465883.5	44521.3	83.4	830	26.92	2.57
IS3 head	8	465883.5	44521.3	80.6	1532	30.18	2.88
IS3 bed	4	465883.5	44521.3	80.6	662	34.93	3.34

The nonlinear properties should be determined next, starting with the cracking parameters. It is assumed that the iron cement does not contribute in tension, so the forces will be completely carried by the bolts. As the characteristic strength is used in the finite element models, the bolts have a tensile strength of 105 MPa. By multiplying this stress with the area of the bolt ($A_{s,bolt}$ = 216.69 mm²), the bolt failure force can be calculated, which is equal to 22.75 kN. The tensile strength of the

interface connection is determined by the tensile strength of the bolts, the number of bolts and the total area of the connection:

$$\sigma_{t,int} = \frac{\sigma_{t,bolt} * A_{s,bolt} * n_{bolts}}{b * h}$$

Then, the fracture energy of the connection is derived from the tensile stress-strain diagram. This is equal to the area under the curve after the tensile stress is reached, which means linear tension softening is applied here due to the shape of the curve. This value is then multiplied with the length of the bolts to find the fracture energy in N/mm:

$$G_f = 0.5 * \sigma_{t,int} * (\varepsilon_{ult} - \varepsilon_t) * L_{bolt}$$

The cracking properties of the head and bed joints for the different sections are given in the table below.

Table 3.4: Cracking properties for each joint

Joint	n_{bolts}	F_{max} [N]	σ_t [N/mm^2]	ε_{ult}	ε_t	G_f [N/mm]
OS1 head	5	113.76	1.379	0.0010438	0.0009767	0.00231
OS1 bed	10	227.52	1.355	0.0010438	0.0009767	0.00227
OS2 head	5	113.76	1.573	0.0010438	0.0009767	0.00264
OS2 bed	8	182.02	1.495	0.0010438	0.0009767	0.00251
OS3 head	4	91.01	1.429	0.0010438	0.0009767	0.00240
OS3 bed	6	136.51	1.658	0.0010438	0.0009767	0.00278
IS1 head	10	227.52	1.523	0.0010438	0.0009767	0.00255
IS1 bed	6	136.51	1.539	0.0010438	0.0009767	0.00258
IS2 head	9	204.77	1.512	0.0010438	0.0009767	0.00254
IS2 bed	4	91.01	1.315	0.0010438	0.0009767	0.00220
IS3 head	8	182.02	1.474	0.0010438	0.0009767	0.00247
IS3 bed	4	91.01	1.706	0.0010438	0.0009767	0.00286

The next step is determining the parameters related to shearing. Again, it is assumed that the force will be carried by the bolts, not the iron cement. The cohesion of the interface will therefore be based on the strength of the bolts. The strength of the bolts in shear is determined, after which the cohesion of the interface can be determined:

$$F_{v,bolt} = \frac{\alpha_v * A_{s,bolt} * f_{u,bolt}}{\gamma_{M2}} = 9.1\ kN$$

$$c_{int} = \frac{F_{v,bolt} * n_{bolts}}{b * h}$$

However, after the bolts brake there will be a residual shear force the structure can still withstand. The magnitude of this force is dependent on the friction of the interface. The friction coefficient will be based on the iron cement, as this will contribute the most to the friction. Another thing to consider is that the tensile strength is limited by the cohesion and friction angle in the following way:

$$f_t = \frac{c}{tan\ \varphi}$$

As the ratio between the cohesion and the tensile strength is the same for all joints, the maximum friction angle can be determined by using the values of c and f_t of a joint. The maximum friction angle

is 0.3805 rad. Some samples of the iron cement in the lighthouse were tested (Movares, 2023) and it was determined that the compressive strength of the mortar is similar to that of C12/15 concrete. As the compressive properties match those of concrete, the frictional properties of concrete could also be used to estimate the frictional properties of the iron cement. As the cement is bonded to the cast iron, the interface is somewhat similar to that of a concrete-rebar interface. However, as rebar has quite a rough profile and the cast iron flanges will be much smoother, it is not exactly the same. A report has been found in which the bond between steel rebar and concrete is analysed (Chiriatti, Mercado-Mendoza, Apedo, Fond, & Feugeas, 2019). They found that the average value of the friction coefficient μ is equal to 0.39. As μ = tan ϕ, the value of ϕ is equal to 0.372, so this is quite close to the maximum friction angle that can be used. It is chosen to use a value of 0.38 for the friction angle in this study. Also, the parameters a and b of the mode II fracture energy should be determined. It is not exactly clear how to determine these parameters for the joints here, so for now, it is assumed that a = 0 and b = 10 * $G_{f,\,tension}$. As a result, the shearing parameters for the different sections are as follows:

Table 3.5: Shearing parameters per joint

Joint	n_{bolts}	F_{max} [N]	c [N/mm^2]	ϕ [rad]	a [mm]	b [N/mm]
OS1 head	5	45.50	0.552	0.38	0	0.231
OS1 bed	10	91.01	0.542	0.38	0	0.227
OS2 head	5	45.50	0.629	0.38	0	0.264
OS2 bed	8	72.81	0.598	0.38	0	0.251
OS3 head	4	36.40	0.572	0.38	0	0.240
OS3 bed	6	54.61	0.663	0.38	0	0.278
IS1 head	10	91.01	0.609	0.38	0	0.255
IS1 bed	6	54.61	0.616	0.38	0	0.258
IS2 head	9	81.91	0.605	0.38	0	0.254
IS2 bed	4	36.40	0.526	0.38	0	0.220
IS3 head	8	72.81	0.590	0.38	0	0.247
IS3 bed	4	36.40	0.682	0.38	0	0.286

Finally, the parameters related to crushing have to be determined. The bolts will not have any influence on the compressive failure resistance of the structure. It is assumed that when the structure is loaded in compression, there will be contact between the plates, while the bolts ensure that the plates will be held together. As a result, it can be assumed that the compressive strength of the joint is equal to the compressive strength of the plates. The other factors related to compression are C_s, $G_{f,compression}$ and the equivalent plastic relative displacement. As the structure is expected to fail in compression due to buckling, this will happen before the compressive strength has been reached. As the structure will fail before the compressive strength of the joint has been reached, the other parameters will not have much influence on the compressive failure. Therefore, assumptions are made for all parameters, such that their influence on the failure is very minimal. For C_s, a value of 0.01 is chosen. The value of $G_{f,c}$ is assumed to be much higher than the fracture energies in tension and shear, so 65 N/mm (around 25 times the value of $G_{f,shear}$). The equivalent plastic relevant displacement (EPRD) is set to 2 mm. The table below provides an overview of the joint parameters related to compression. This means all required parameters for the joints have been determined.

Table 3.6: Crushing parameters per joint

Joint	σ_t [N/mm^2]	C_s	$G_{f,c}$ [N/mm]	EPRD [mm]
All	340	0.01	65	2

The calculated values of the fracture energy in tension and shear were used in the detailed models of the small structures. However, it was discovered that it was not possible to obtain fully converging results with these fracture energy values, as the model diverged very quickly. After some research, it became clear that there is a minimum value that has to be used for $G_{f,tension}$, such that the model will not diverge. The higher the value, the larger the ultimate displacement that will be reached. Therefore, each model has been analysed many times where the value of $G_{f,tension}$ and the parameter b was lowered gradually until divergence occurred in the model. For each section, the new input values for the joints are given in the table below. The new values are around 40 times higher than the old values and they will be used for both the head- and bed-joints.

Table 3.7: New values for $G_{f,tension}$, and the parameter b, required to prevent divergence

Section	**$G_{f,tension}$ new [N/mm]**	**b new [N/mm]**
OS1	0.08	30
OS2	0.08	20
OS3	0.09	20
IS1	0.08	70
IS2	0.16	30
IS3	0.24	70

3.2 Equivalent EMM models

The equivalent EMM models consist of one polygon sheet, which represents the geometry and properties of both the cast iron plates and the bolted connection. The geometry of the flanges and stiffeners are not modelled, but their effect on the structural behaviour is part of the input parameters that are used. The thickness of the polygon sheet is taken as the plate thickness of the column section where it is located. Regular curved shells are used as the element type and the Engineering Masonry Model (EMM) is used as the material model. Finally, 7 integration points in thickness are used. An example of what is described in this thesis as an equivalent EMM model is presented in the figure below.

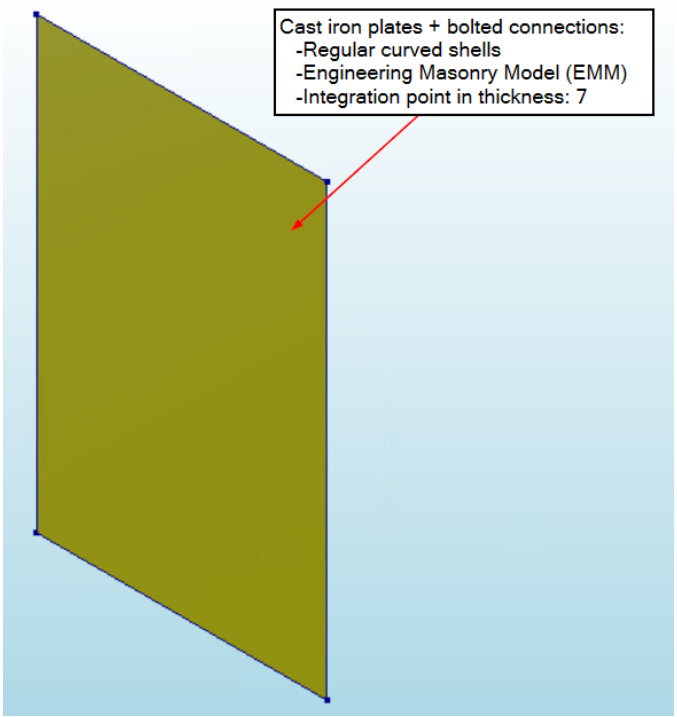

Figure 3.6: Example of what an equivalent EMM model is, as described in the thesis

3.2.1 Mesh size and elements

In the equivalent EMM models, regular curves shell elements will be used. In the model of the complete lighthouse, the element size will be chosen as approximately 200x200 mm. As the different column sections have different plate dimensions, each section will have a slightly different element size, as they will be limited by the width of the column sides. This means the element width depends on the plate width. A table is presented below where the element size of each section is specified. The crack bandwidth that is paired with the element size is also given.

Table 3.8: Element size and corresponding crack bandwidth per section, used in the equivalent EMM models

Section	Plate height	Plate width	Element height	Element width	Crack bandwidth (h)
OS1	885	1802	221.25	225.25	315.71
OS2	812.5	1368	203.125	195.43	281.77
OS3	750	970	187.5	194	269.72
IS1	1770	1051	221.25	210.2	304.98
IS2	1624	830	203	207.5	290.25
IS3	1532	662	191.5	220.67	290.72

Again, the shape of the elements will vary due to the geometry of the structure that is analysed. The different types of elements that are used for the equivalent EMM models in this study are given in the table below, as well as their most relevant properties. Again, most properties were obtained from the DIANA FEA manual (DIANA FEA bv, 2017).

Table 3.9: Overview of the element types and their relevant properties of elements used the equivalent EMM models

Element code	Q20SH	T15SH
Element type	Regular curved shells, quadrilateral shape	Regular curved shells, triangular shape
Degrees of freedom	20: 4 nodes, 3 translations and 2 rotations per node	15: 3 nodes, 3 translations and 2 rotations per node
Interpolation scheme	Linear	Linear
Integration scheme	3-point Simpson in thickness 2×2 Gauss over element area	3-point Simpson in thickness 3-point Gauss over element area
Shape dimension	3D	3D
Topological dimension	2D	2D
Stress components	σ_{xx}, σ_{yy}, σ_{xy}, σ_{yz}, σ_{zx}	σ_{xx}, σ_{yy}, σ_{xy}, σ_{yz}, σ_{zx}

3.2.2 Engineering masonry model (EMM) for cast iron plate structure

In order to use the Engineering Masonry Model (EMM), the correct input parameters are required. The plates and connections will not be modelled separately, but as a homogeneous material. This means that the material should capture the behaviour of a combination of the plates and the connections. Therefore, small detailed models will be loaded and analysed, such that the required parameters for the EMM can be extracted. The detailed models will consist of one or two plates, depending on the load case. A tensile, compressive or shear load will be introduced on one of the plates, which will result in certain forces and displacements in the model. From these models, the stiffness, strength and toughness of the plates and connection(s) can be determined. The table below

provides an overview of the required input parameters for the EMM and their respective category. It is also described in the table how the values will be obtained.

Table 3.10: Required input parameters EMM and how they will be obtained

Parameter	Category	Obtained by
E-modulus	Elasticity	The E-modulus is equal to the stiffness of the force-displacement curve of the tensile and/or compression models. Based on the values, it will be determined which value should be used: $E_{tension}$, $E_{compression}$ or a combination of these two. As the plates are rectangular, the ratio of connections per unit length is different in x and y, which means the E-modulus will most likely be different for each direction
Shear modulus	Elasticity	The G-modulus is equal to the stiffness of the force-displacement curve of the shear models
Mass density	Elasticity	This property is only dependent on the material, thus can be determined without analysing detailed models. It should match the value used in the analysis of PT Structural to enable a better comparison in the final stage of the project
Bed-joint tensile strength	Cracking	From the force-displacement curves of the tensile models, where the force acts in the normal direction of the bed joint, the maximum tensile force can be determined. From the maximum force follows the maximum tensile stress
Head-joint tensile strength	Cracking	From the force-displacement curves of the tensile models, where the force acts in the normal direction of the head joint, the maximum tensile force can be determined. From the maximum force follows the maximum tensile stress
Fracture energy in tension	Cracking	This follows from the force-displacement curves of the tensile models. The area under this curve defines the fracture energy. As failure of the bed joints is more likely when the lighthouse is loaded by wind and self-weight, the curve that follows from the model where bed joint failure occurs will be used to determine the fracture energy
Residual tensile strength	Cracking	Once the connection has fully failed, there will be no tensile strength left, so this equals 0 MPa
Angle between cracks	Cracking	The angle is dependent on the shape of the plate. The diagonal of the rectangle creates a triangle from which the angles can be determined
Compressive strength	Crushing	This will be related to the buckling strength of the plates. A hand calculation will be made first, which should then be verified with an analysis of a model containing one plate in compression
Fracture energy in compression	Crushing	This follows from the force-displacement curve of the compression models. The area under this curve defines the fracture energy
Factor to strain at compressive strength	Crushing	This factor is calculated by the following formula: $$n = \frac{E * \varepsilon_{peak}}{\sigma_c}$$ Where E is the linear stiffness and ε_{peak} the strain at the compressive strength σ_c. The values for these parameters will follow from the force-displacement curves of the compression models
Unloading factor	Crushing	Not relevant as there is no cyclic loading, but it is assumed as linear

Friction angle	Shear failure	This can be obtained from the force-displacement curves that follow from the detailed models loaded in shear (and compression). Three models will be checked, with different values for the compressive stress: 0.5, 1 and 2 MPa. A relation between the values for the peak shear stress and the compressive stress can be obtained, from which the cohesion and friction angle can be determined
Cohesion	Shear failure	This can be obtained from the force-displacement curves that follow from the detailed models loaded in shear (and compression). Three models will be checked, with different values for the compressive stress: 0.5, 1 and 2 MPa. A relation between the values for the peak shear stress and the compressive stress can be obtained, from which the cohesion and friction angle can be determined
Fracture energy in shear	Shear failure	This follows from the force-displacement curve of the shear models. The area under this curve defines the fracture energy

4 Definition of EMM parameters based on results of detailed models

Now that the detailed models have been defined, different load cases will be applied to models consisting of 1 or 2 plates. The load cases that are considered are tension, compression and shear. Each load case will be applied to every column section. From the results of the analyses, the required EMM parameters should be obtained.

4.1 Tension loading

The parameters that are related to cracking, are obtained from the detailed models loaded in tension. A tensile load will be placed on a small model with a head or bed joint, in order to determine the force-displacement curves from these analyses. However, an analytical calculation will be made first to predict the force at failure. For this prediction, the different failure modes of a ring flange connection will be used, as this is similar to the bolted connection in the lighthouse. The segment that will be looked at and the different ring flange failure modes are given in the figures below.

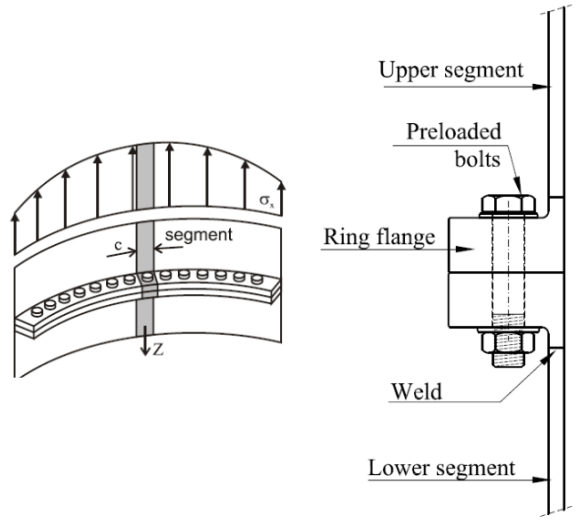

Figure 4.1: Visualisation of segment for ring flange failure (Veljkovic, 2021)

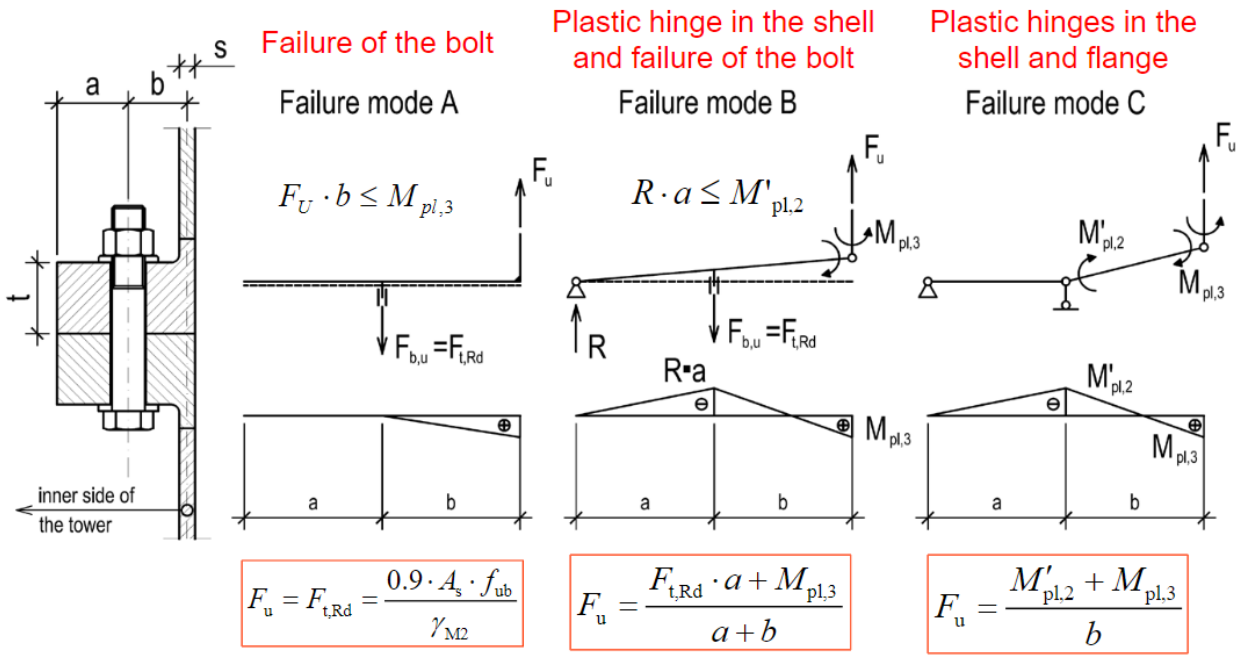

Figure 4.2: Ring flange failure modes and their corresponding formulas to calculate the force at failure (Veljkovic, 2021)

The calculation should be made for the bed and head joints of the different sections. Usually in the ring flange failure mode calculations, the section width c is the distance between the bolts. However, in this case the bolt distance for all joints is larger than 150 mm, which is not a realistic section to look at, as failure modes b and c will have a much higher resistance to failure with such a large amount of material. Therefore, an effective width will be used instead. The value for c will be assumed to be 2 times the bolt diameter. This means c will have a value of 33.22 mm for all sections. The results of the calculations are given in the table below:

Table 4.1: Force at failure for different failure modes of ring flange failure

Joint	Failure mode A [kN]	Failure mode B [kN]	Failure mode C [kN]
OS1	16.38	10.91	10.64
OS2	16.38	11.22	11.14
OS3	16.38	11.53	11.67
IS1	16.38	11.57	11.73
IS2	16.38	11.65	11.87
IS3	16.38	11.88	12.27

As the dominant failure modes are known for each section, the predicted tensile force at failure are calculated for both joint types, and given in the table below. This has been done by multiplying the force related to the dominant ring flange failure mode with the number of bolts in the joint. The failure forces that will be obtained from the finite element models should be compared to these predicted failure forces.

Table 4.2: Predicted failure force, based on most dominant ring flange failure mode

Joint	Dominant failure mode force [kN]	n_{bolts}	Predicted force at failure [kN]
OS1 head	10.64	5	53.20
OS1 bed	10.64	10	106.40
OS2 head	11.14	5	55.70
OS2 bed	11.14	8	89.12
OS3 head	11.53	4	46.12
OS3 bed	11.53	6	69.18
IS1 head	11.57	10	115.70
IS1 bed	11.57	6	69.42
IS2 head	11.65	9	104.85
IS2 bed	11.65	4	46.60
IS3 head	11.88	8	95.04
IS3 bed	11.88	4	47.52

For the head joint, a model of two half plates will be analysed, as the outer column is shaped like a hexadecagon, and each side has the width of exactly one plate. This means there will be head joints in the corners between the edges and also above every full plate in the centre, as the plates are placed in a half brick pattern. The head joints in the middle of the side will have the lower strength, as the corner joints will be much stiffer. Therefore, the model that will be analysed here consists of two half plates, connected by one head joint. The inner column has a circular shape, but using this shape in the detailed models makes it quite difficult to obtain accurate input parameters of the EMM. The shape of the structure has a big influence on the failure mode. Therefore, the failure mode of the straight plated structure should be used to determine the input parameters.

A displacement load is placed on one side of the structure, in normal direction to the head joint. The left side is supported in x and y, and the bottom is supported in z. The support in x at the right side is required for the prescribed deformation load, which is in the positive x direction. The deformation in x-direction causes a reaction force in x. The force can be displayed against the displacement in a graph for all load steps. From this force-displacement curve, it is possible to determine the input parameters for the EMM related to cracking.

The names of the models are based on the column section, the type of model, the loading condition and the size of the structure. For the models here, an example would be: section OS3, a detailed model, loaded in tension on the head-joint, and a small structure. This results in the name OS3_det_ten_head_small. Table A.1, provided in appendix A, presents all the models that have been analysed in this thesis and the names they have been given. For the remainder of the thesis, this table will be referred to when names of certain models are mentioned.

The results of OS3_det_ten_head_small and IS1_det_ten_head_small are given in the figures below. In the presentation of the results the following information is included: the structure, the finite element mesh, the displacements or strains at 4 important load steps in the analysis (A-D) which are most suitable to show the failure mode of the structure, the force-displacement curve that results from the analysis (where points A-D are highlighted as well), an overview of the elements and nodes and an overview of the iterative scheme used in the analysis. For all possible loading conditions (tension, compression and shear), only the models and analysis results of sections OS3 and IS1 will be presented. This will show the difference between results of the plates of the inner and outer columns. For the results of the other sections, see appendix B.

a)

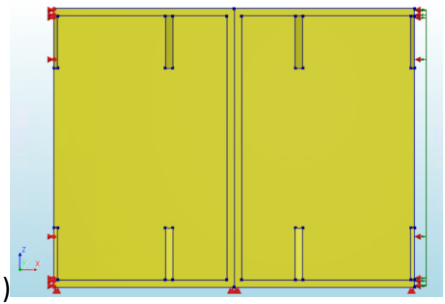

c)

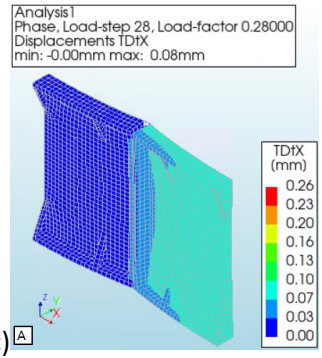

d)

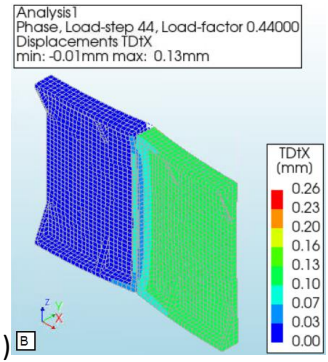

b)

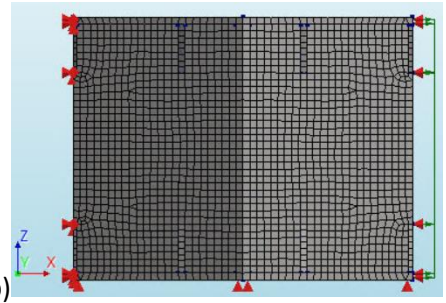

e)

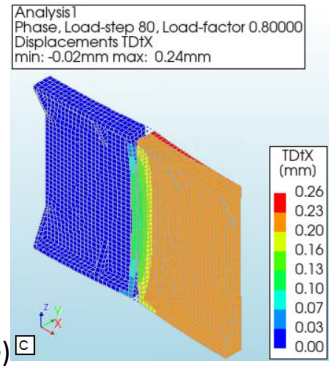

f)

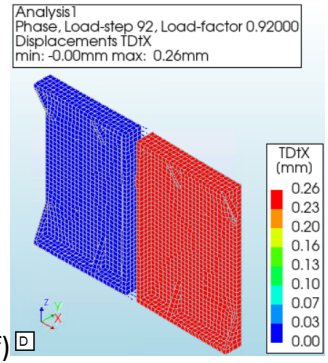

g)

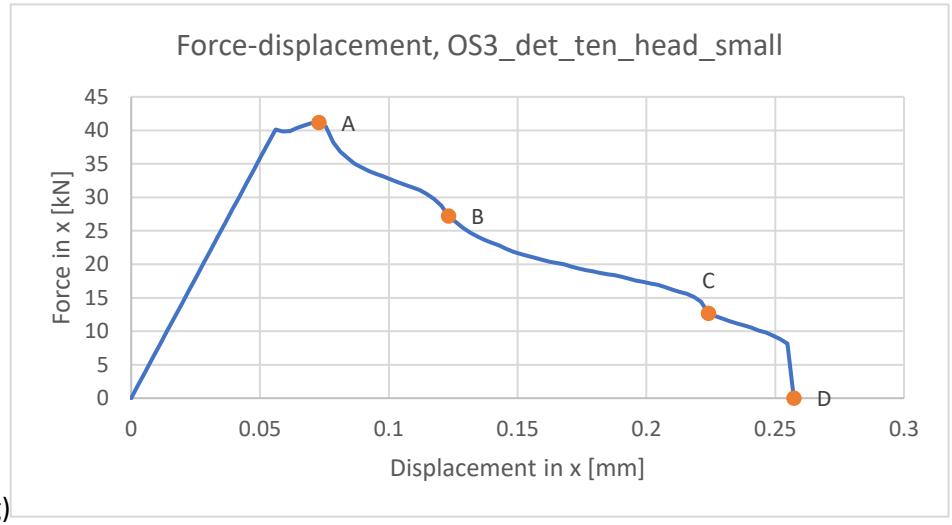

h)

Average element size [mm]		20x20
Number of elements	HX24L	2310
	PY15L	414
	TE12L	244
	TP18L	80
	Q24IF	152
Total number of nodes		5124

i)

Iteration method	Newton-Raphson	
Convergence norms	Displacement	Force
Convergence tolerances	0.01	0.01
Step size	0.01(100)	
Maximum number of iterations per step	100	
All norms satisfied	No	

Figure 4.3: Results of finite element analysis OS3_det_ten_head_small. a-i: structure (a), finite element mesh (b), displacement at point A (c), displacement at point B (d), displacement at point C (e), displacement at point D (f), force-displacement curve (g), overview elements and nodes (h), overview iterative scheme (i)

a)

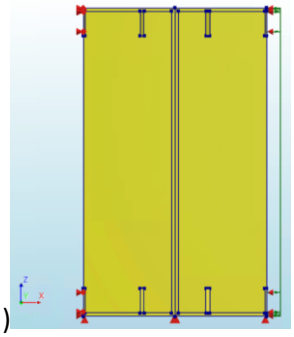

c)

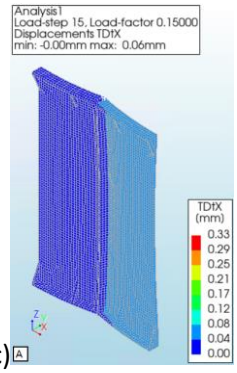

d)

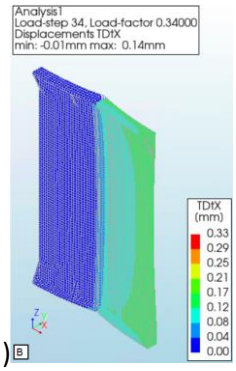

b)

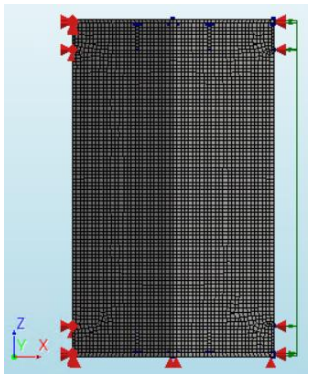

e)

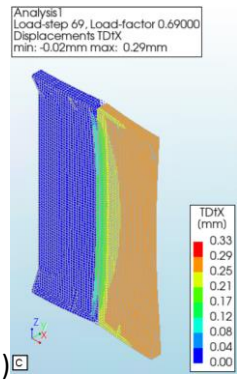

f)

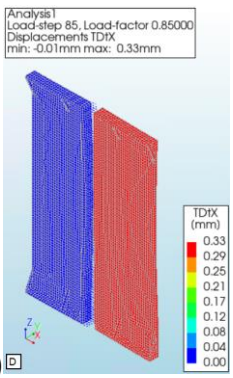

g)

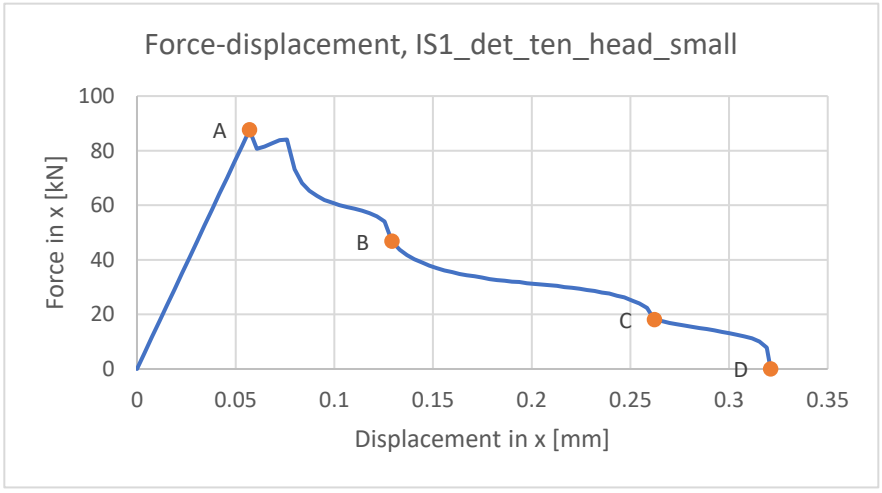

h)

Average element size [mm]		20x20
Number of elements	HX24L	5430
	PY15L	490
	TE12L	374
	TP18L	87
	Q24IF	356
Total number of nodes		11734

i)

Iteration method	Newton-Raphson	
Convergence norms	Displacement	Force
Convergence tolerances	0.01	0.01
Step size	0.01(100)	
Maximum number of iterations per step	100	
All norms satisfied	No	

Figure 4.4: Results of finite element analysis IS1_det_ten_head_small. a-i: structure (a), finite element mesh (b), displacement at point A (c), displacement at point B (d), displacement at point C (e), displacement at point D (f), force-displacement curve (g), overview elements and nodes (h), overview iterative scheme (i)

As the structures of IS1 and OS3 have different sizes, the stress-strain curves will be given below as well. The stress in this case is equal to the average stress in the plate, not including the flanges. It is determined by dividing the force by the surface area of the plates. The strain is equal to the deformation in the loading direction divided by the plate length/width in the loading direction. Presenting the stress-strain curves of both models makes it easier to compare the results of the models. In the stress-strain curves, the points A, B, C and D have been highlighted again.

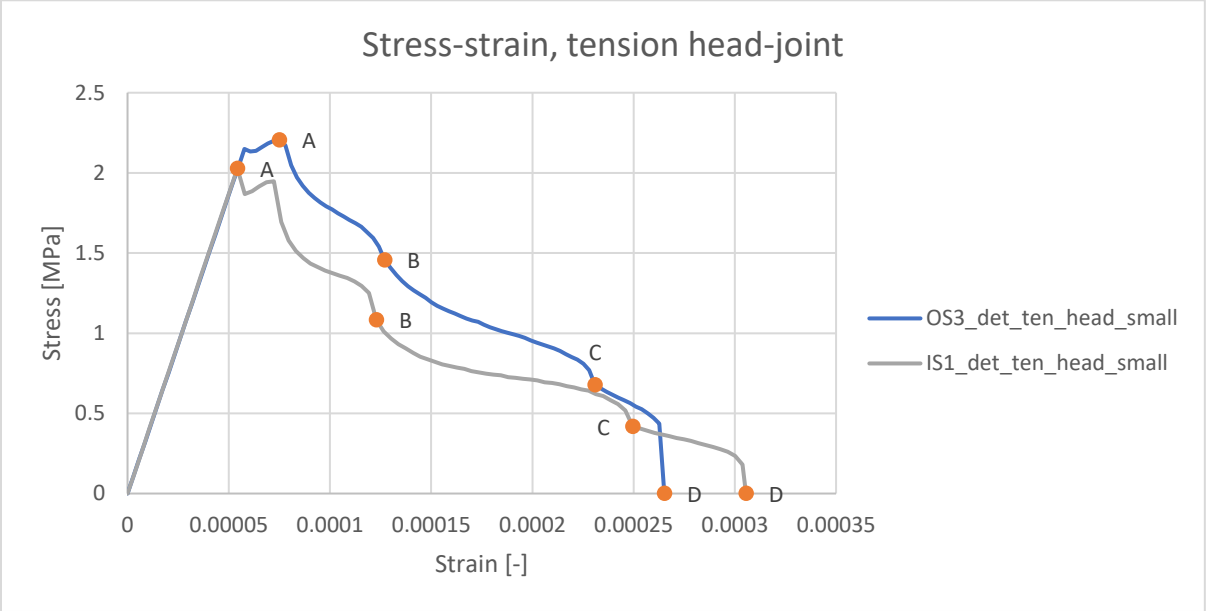

Figure 4.5: Stress-strain curves from tension head-joint models OS3_det_ten_head_small & IS1_det_ten_head_small

The points A-D have been highlighted in the curves for both models. The locations of the points show interesting steps of the analysis. In this case, point A is the step where the highest force occurs, point D is the step where the ultimate displacement occurs, and points B and C are points where there is a sudden drop in the force. From the curves, it is clear that the behaviour of OS3 and IS1 is very similar. There is linear-elastic behaviour until the peak force is reached (point A). At this point, the connection will start to open up, which weakens the force resistance of the structure. Then, a second peak appears in the curve, which can be slightly higher or slightly lower than the first peak (this varies for all column sections). After the second peak, the strength starts to reduce and plastic deformations will occur. As parts of the interface keep disconnecting, the strength is slowly lowered until the force becomes 0 kN. At this point, the interfaces are fully disconnected and the ultimate displacement is reached. The differences between the results of sections OS3 and IS1 can be seen in the stress-strain curves. The peak stress is slightly higher for the model of OS3, while the ultimate strain is a bit larger for the model of IS1. In addition, the stiffnesses are very similar for the models of OS3 and IS1.

For the bed joint, the model consists of one plate, which has two half plates on top, as the plates are placed in this way at each side of the hexadecagon (outer column). The same approach is used for the model of the inner column. A tensile displacement can be applied in the normal direction to the bed joint, which will introduce forces in this direction. The left side is supported in x and the bottom is supported in y and z. The support in z at the top is required for the prescribed deformation load, which is in the positive z direction. Again, the results of OS3 and IS1 are given below for clarification, which are models OS3_det_ten_head_small and IS1_det_ten_head_small (see appendix A for the explanation of the model names). Additionally, a figure will be presented which includes the stress-strain curves of these two models. For the results of the other sections, see appendix B.

a)

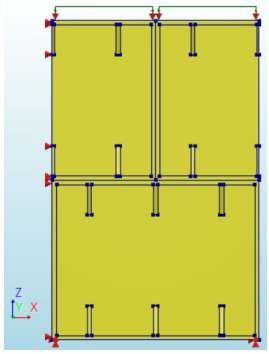

c)

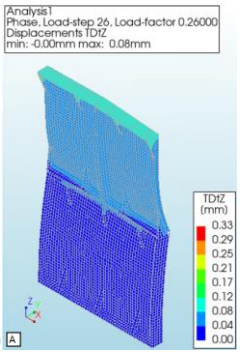

d)

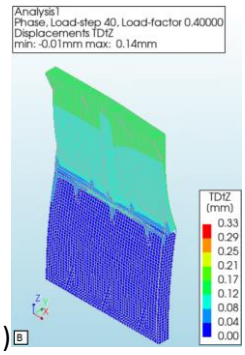

b)

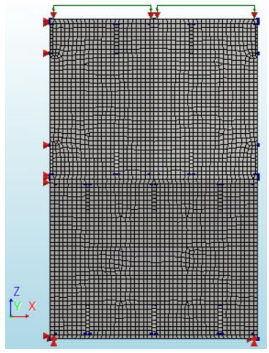

e)

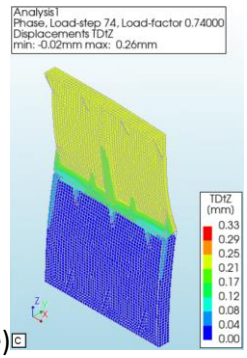

f)

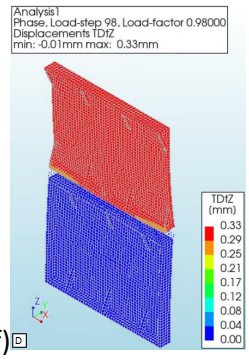

g)

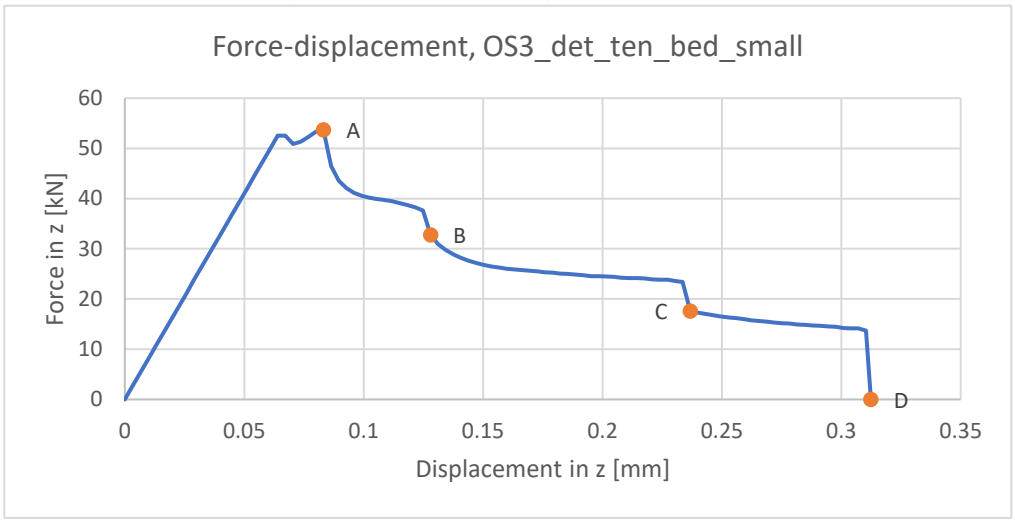

h)

Average element size [mm]		20x20
Number of elements	HX24L	4505
	PY15L	1145
	TE12L	856
	TP18L	242
	Q24IF	344
Total number of nodes		10402

i)

Iteration method	Newton-Raphson	
Convergence norms	Displacement	Force
Convergence tolerances	0.01	0.01
Step size	0.01(100)	
Maximum number of iterations per step	100	
All norms satisfied	No	

Figure 4.6: Results of finite element analysis OS3_det_ten_bed_small. a-i: structure (a), finite element mesh (b), displacement at point A (c), displacement at point B (d), displacement at point C (e), displacement at point D (f), force-displacement curve (g), overview elements and nodes (h), overview iterative scheme (i)

a) b)

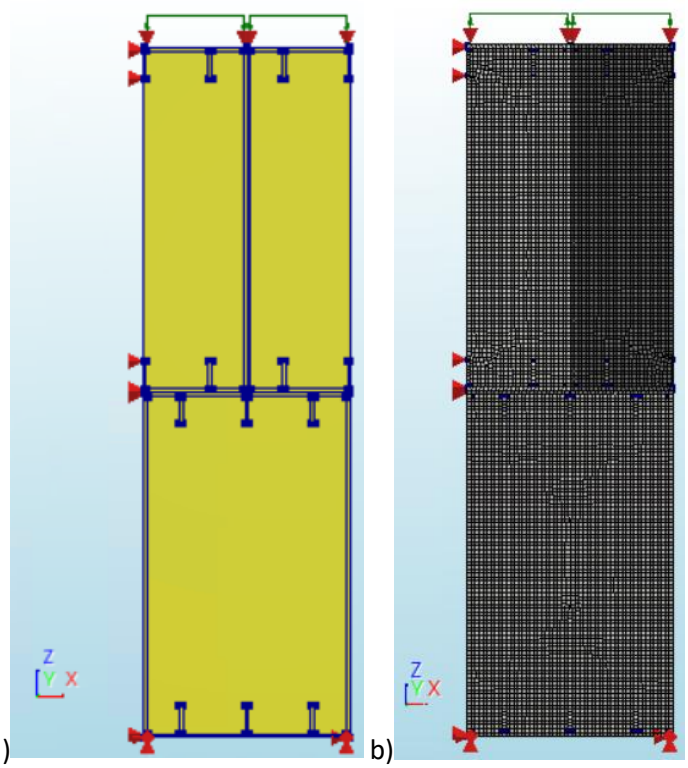

c)

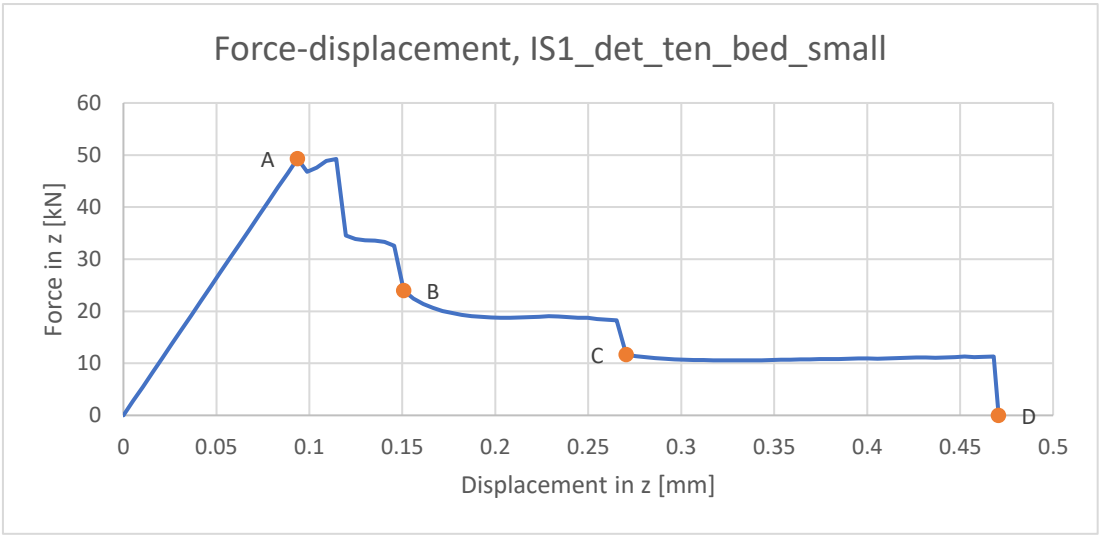

d)

Average element size [mm]		20x20
Number of elements	HX24L	10982
	PY15L	520
	TE12L	384
	TP18L	140
	Q24IF	564
Total number of nodes		23182

e)

Iteration method	Newton-Raphson	
Convergence norms	Displacement	Force
Convergence tolerances	0.01	0.01
Step size	0.01(100)	
Maximum number of iterations per step	100	
All norms satisfied	No	

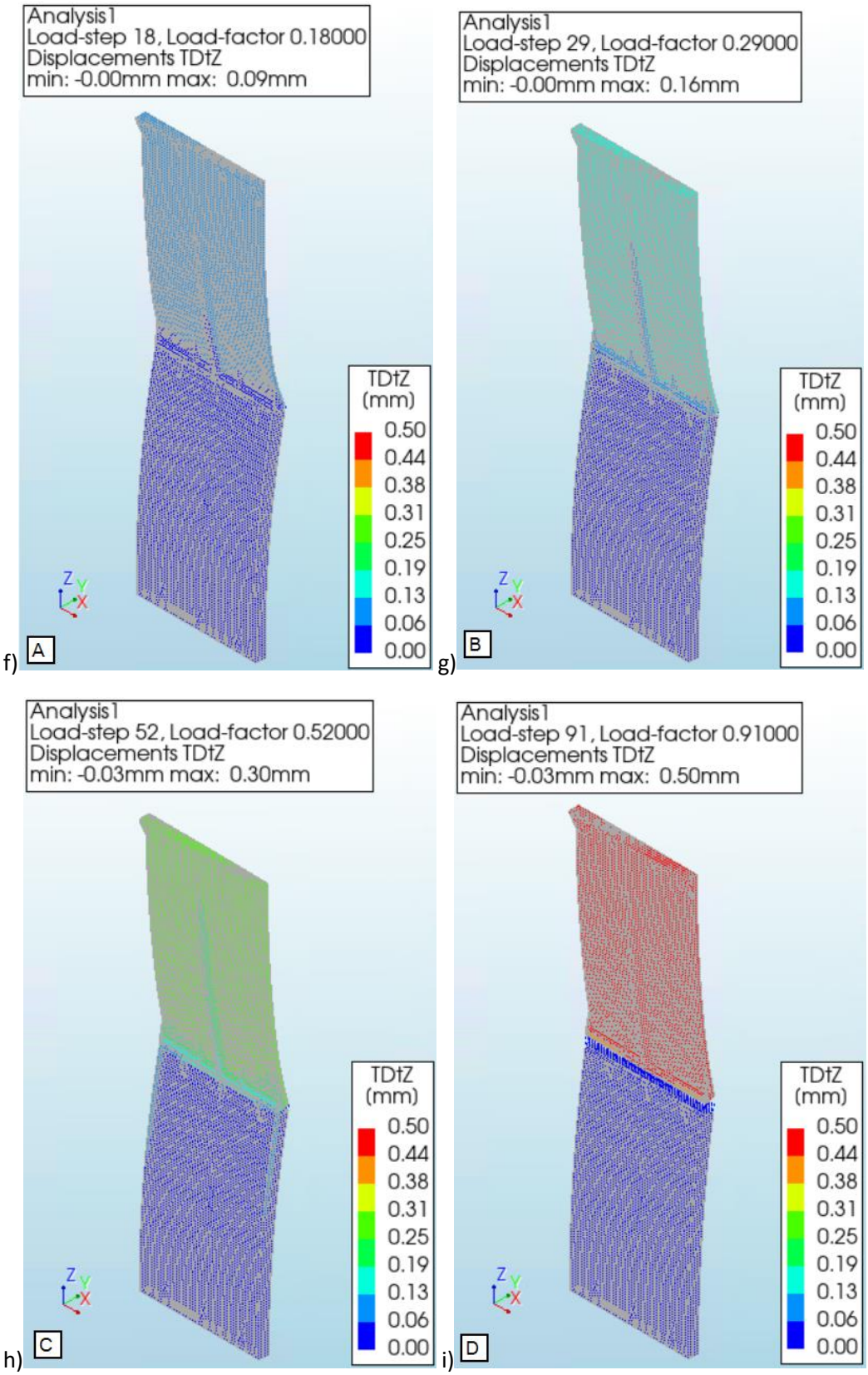

Figure 4.7: Results of finite element analysis IS1_det_ten_bed_small. a-i: structure (a), finite element mesh (b), force-displacement curve (c), overview elements and nodes (d), overview iterative scheme (e), displacement at point A (f), displacement at point B (g), displacement at point C (h), displacement at point D (i)

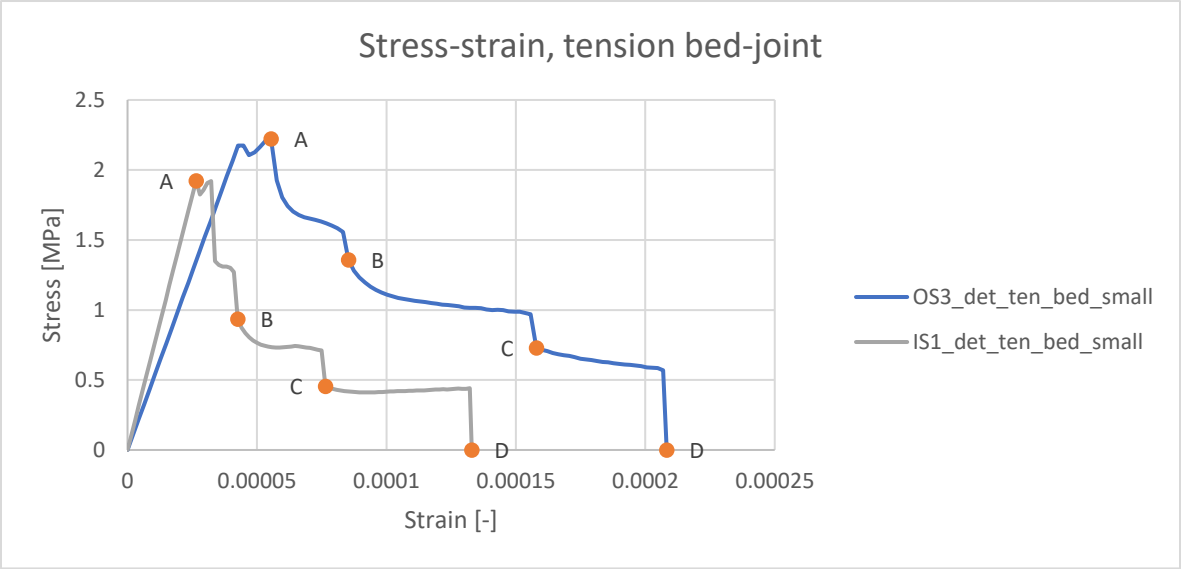

Figure 4.8: Stress-strain curves from tension bed-joint models OS3_det_ten_bed_small & IS1_det_ten_bed_small

Again, the points A-D have been highlighted in the curves for both models. The locations of the interesting points are the same as in the head-joint tension models: point A is the step where the highest force occurs, point D is the step where the ultimate displacement occurs, and points B and C are points where there is a sudden drop in the force. The F-D curves are very similar compared to the curves of the head-joint failure that were presented above. This is expected, as the connections are of the exact same type. Once the interfaces of the plates are fully disconnected, the structure is no longer able to withstand any forces, which is the point D in the curves. From the stress-strain curves it is clear that the structure of section OS3 has a larger strength, and a larger ultimate strain is reached as well. Additionally, it is clear that there is a difference in the stiffness between the models, which was not the case for the head-joint tension models. The amount of bolts and the plate dimensions heavily impact the stiffness, strength and ultimate displacement values. For this reason, it was chosen to divide the columns into different sections and not use one plate size for an entire column.

The E-modulus in tension can be obtained from the curves by determining the stiffness of the linear elastic parts. E_x follows from the head-joint models, E_y from the bed-joint models. The values of the E-moduli for each section are presented in the table below.

Table 4.3: E-modulus values based on results of tension models

Section	E_x tension [MPa]	E_y tension [MPa]
OS1	47916.2	44497.7
OS2	46164.9	47201.8
OS3	37234.6	50954.4
IS1	37385.0	72713.1
IS2	32389.3	68488.1
IS3	28253.3	79002.7

Due to the large difference in plate dimensions, there are quite some differences in the values. The widest plates result in the largest E_x values, while the highest plates result in the largest E_y values. Also, the thickness of the plates has a large impact on the resulting parameters. The maximum forces of all head- and bed-joint models loaded in tension have been determined as well. They are given in the table below, where they can be compared to the predicted maximum forces that followed from the analytical calculation, which was presented at the beginning of this section.

Table 4.4: Comparison predicted failure force vs. failure force in detailed model, tension

Joint	Predicted force at failure [kN]	Failure force detailed model [kN]	Ratio $F_{predicted}/F_{detailed}$
OS1 head	53.20	50.13	1.06
OS1 bed	106.40	95.06	1.12
OS2 head	55.70	48.99	1.14
OS2 bed	89.12	72.52	1.23
OS3 head	46.12	41.20	1.12
OS3 bed	69.18	53.67	1.29
IS1 head	115.70	87.59	1.32
IS1 bed	69.42	49.31	1.41
IS2 head	104.85	92.19	1.14
IS2 bed	46.60	41.58	1.12
IS3 head	95.04	85.65	1.11
IS3 bed	47.52	42.28	1.12

The predicted forces are quite close to the forces from the detailed models. It is clear that the outer column sections can be predicted slightly better with the ring flange failure modes, as the average ratio $F_{predicted}/F_{detailed}$ is closer to 1 for these sections. The ratio of the sections of the inner column are a bit higher, so it appears that the accuracy of the predicted forces is slightly lower for these sections. This is most likely due to the ratio of plate width/plate height, which is quite small for the inner column sections.

The cracking parameters, which are required for the input of the EMM, can all be calculated from the F-D curves of the models. The stiffness was already determined above, while the tensile strength is determined by dividing the maximum force by the surface area of the plate (not including the flanges), as the structure where the EMM will be used will have this area as well. The fracture energy is obtained by calculating the area under the force-displacement curve. This value is then divided by the area of the plate, divided by the total height and finally multiplied with the crack bandwidth (h). This is how the DIANA manual describes the value of the fracture energy (DIANA FEA bv, 2017). The value of h is dependent on the area of the elements and the crack bandwidth specification. As it was chosen to use the Rots method, h can be calculated as:

$$h = \sqrt{2A}$$

The element sizes that will be used for the different sections are given in section 3.2.1. The average size is 200x200 mm, but due to the plate dimensions, it will not be exactly 200x200 mm. This means the crack bandwidth varies per section. Finally, the angle between the cracks is based on the height and width of the plates:

$$\alpha = \arctan\left(\frac{h}{b}\right)$$

To determine the angle between the cracks for the curved plates, the distance between the edges has been used for the width, instead of the length of the curved plate side (see the figure below).

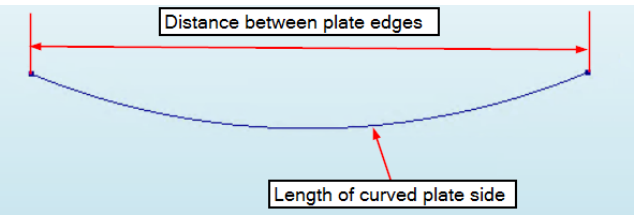

Figure 4.9: Difference between length of curved plate side and distance between plate edges

An overview of the parameters and their respective models is given below.

Table 4.5: Cracking parameters obtained from results of tension models

Joint	Bed-joint tensile strength [MPa]	Head-joint tensile strength [MPa]	Fracture energy in tension [N/mm]	Angle between cracks [rad]
OS1 head	-	1.706	0.0404	0.241
OS1 bed	1.832	-	0.0442	0.241
OS2 head	-	2.079	0.0526	0.289
OS2 bed	2.059	-	0.0494	0.289
OS3 head	-	2.206	0.0866	0.369
OS3 bed	2.447	-	0.0627	0.369
IS1 head	-	2.028	0.0835	0.700
IS1 bed	1.749	-	0.0302	0.700
IS2 head	-	2.426	0.2034	0.774
IS2 bed	2.031	-	0.0581	0.774
IS3 head	-	2.714	0.4130	0.858
IS3 bed	2.812	-	0.1007	0.858

4.2 Compression loading

The parameters that are related to crushing, will be obtained from the detailed models loaded in compression. It is be assumed that the crushing parameters are related to the buckling of a plate. The compression models in DIANA will therefore consist of a single plate loaded in compression. However, an analytical calculation is made first to predict the force at which buckling will occur. Section 4.4 of NEN-EN 1993-1-5 is used for this calculation. The chapter describes how to calculate buckling for steel plate elements without longitudinal stiffeners. The calculation will not be exactly correct, as the plates are made of cast iron, not steel. In addition, the effect of the stiffeners on the buckling strength will be neglected here. However, as the stiffeners have a small height compared to the total height of the plate, their influence will most likely not be very big anyway.

According to chapter 4.4 of NEN-EN 1993-1-5, an effective area should be used to determine the buckling strength of the plate:

$$A_{c,eff} = \rho * A_c$$

In this formula, ρ is a reduction factor, which can be determined as follows (for internal compression elements):

$$\rho = 1{,}0 \qquad \text{for } \bar{\lambda}_p \leq 0{,}673$$

$$\rho = \frac{\bar{\lambda}_p - 0{,}055\,(3+\psi)}{\bar{\lambda}_p^2} \leq 1{,}0 \qquad \text{for } \bar{\lambda}_p > 0{,}673$$

This means in order to determine ρ, the stress ratio ψ and the plate slenderness $\bar{\lambda}_p$ are required. The stress will have the same value over the width of the plate, so this is equal to 1, according to table 4.1 of EN 1993-1-5. The plate slenderness can be calculated with the following formula:

$$\bar{\lambda}_p = \frac{\bar{b}/t}{28{,}4\,\varepsilon\sqrt{k_\sigma}}$$

In this formula, b̄ and t are the width and thickness of the plate, respectively. The factor k_σ is a buckling factor, which corresponds to the stress ratio ψ and the boundary conditions. Just like the stress ratio, this factor follows from table 4.1 of EN 1993-1-5, and is equal to 4 for this case. The parameter ε is determined as follows, where f_y is the compressive strength of the cast iron:

$$\varepsilon = \sqrt{\frac{235}{f_y}}$$

$$\varepsilon = \sqrt{\frac{235}{340}} = 0.831$$

After finding $A_{c,eff}$, the effective width b_{eff} can be determined by dividing $A_{c,eff}$ by the thickness. All parameters are given in the table below.

Table 4.6: Parameters required for buckling calculation

Section	**t [m]**	**b [m]**	**A_c [m²]**	**$\bar{\lambda}_p$ [-]**	**ρ [-]**	**$A_{c,eff}$ [m²]**	**b_{eff} [m]**
OS1	0.0332	1.802	0.0598	1.149	0.703	0.0421	1.268
OS2	0.0290	1.368	0.0397	0.999	0.781	0.0310	1.068
OS3	0.0249	0.970	0.0242	0.825	0.889	0.0215	0.862
IS1	0.0244	1.051	0.0256	0.912	0.832	0.0213	0.874
IS2	0.0234	0.830	0.0194	0.751	0.941	0.0183	0.781
IS3	0.0206	0.662	0.0136	0.681	0.994	0.0136	0.658

With the effective width, the effective plate slenderness can be calculated by using the same formula as before, but now using b_{eff} instead of the total width of the plate. Chapter 6.3 of EN 1993-1-1 describes the buckling resistance of members. By using the formulas provided there, the buckling stress can be determined by using the following formulas:

$$\sigma_{b,Rd} = \mathrm{X} * f_y$$

$$\mathrm{X} = \frac{1}{\Phi + \sqrt{\Phi^2 + \lambda_{p,eff}^2}}$$

$$\Phi = 0.5 * [1 + \alpha * (\lambda_{p,eff} - 0.2) + \lambda_{p,eff}^2]$$

The final parameter to determine is the imperfection factor α, which is related to the buckling curve that corresponds to the shape of the cross-section. As the flanges and stiffeners are not considered in the calculation, it can be regarded as a solid section, which means buckling curve c should be used, so α = 0.49 here. Now the buckling stress can be calculated for each plate. The results of the calculations are given below. The buckling stresses that will be obtained from the detailed models should be compared to these values.

Table 4.7: Calculated buckling stress values per section

Section	$\bar{\lambda}_{p,eff}$ **[-]**	**Φ [-]**	**X [-]**	$\sigma_{b,Rd}$ **[MPa]**
OS1	0.809	0.976	0.657	223.30
OS2	0.780	0.946	0.675	229.45
OS3	0.733	0.900	0.704	239.35
IS1	0.759	0.925	0.688	233.92
IS2	0.707	0.874	0.720	244.90
IS3	0.677	0.846	0.739	251.27

As mentioned before, the compression model will consist of one plate, loaded by a prescribed deformation that causes a compressive stress in the plate. The bottom of the plate is supported in x, y and z, while the top face will be support in y. In addition, the top will be supported in z, which is required for the prescribed deformation load. The load is causing the top face of the plate to be displaced in the negative z direction. The total force on top of the plate, caused by the deformation, can be determined from the results of the analysis. By relating the force to the displacement in every load step, the force-displacement curve can be created. The results of the models OS3_det_comp_small and IS1_det_comp_small (see appendix A for the explanation of the model names) are presented below, after which a figure will be presented that includes the stress-strain curves of the two models. For the results of the other sections, see appendix B.

a)

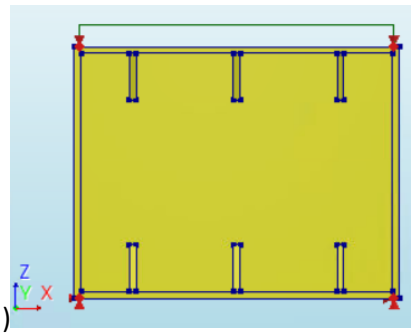

c)

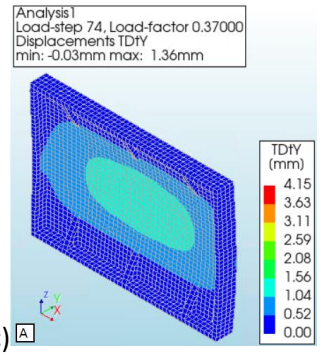

d)

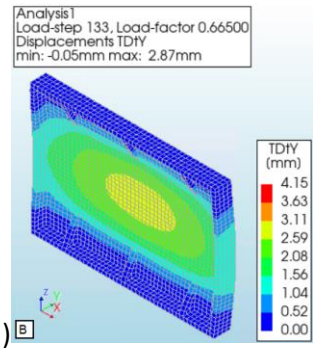

b)

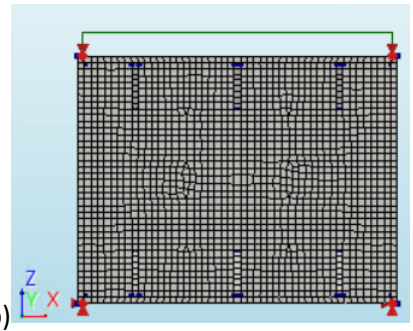

e)

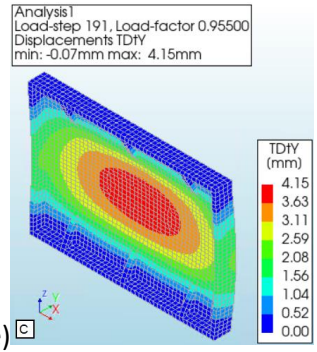

f)

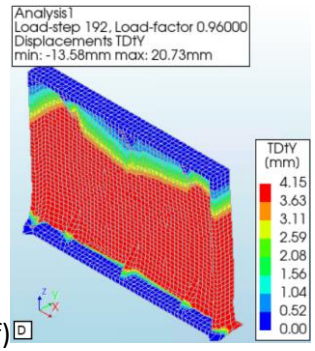

g)

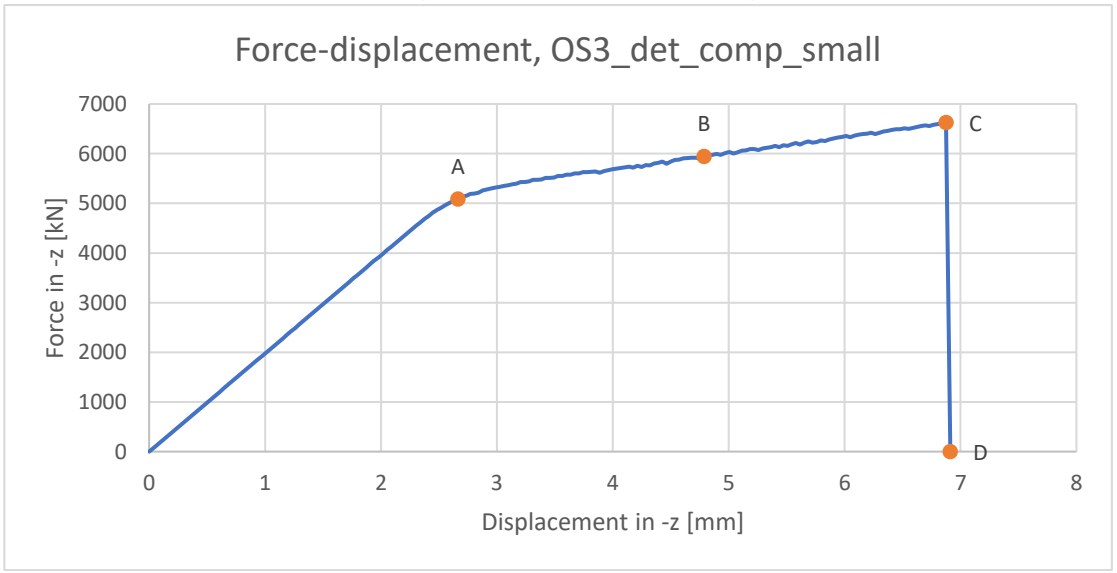

h)

Average element size [mm]		20x20
Number of elements	HX24L	2265
	PY15L	515
	TE12L	362
	TP18L	122
Total number of nodes		5143

i)

Iteration method	Newton-Raphson	
Convergence norms	Displacement	Force
Convergence tolerances	0.01	0.01
Step size	0.005(200)	
Maximum number of iterations per step	100	
All norms satisfied	No	

Figure 4.10: Results of finite element analysis OS3_det_comp_small. a-i: structure (a), finite element mesh (b), displacement at point A (c), displacement at point B (d), displacement at point C (e), displacement at point D (f), force-displacement curve (g), overview elements and nodes (h), overview iterative scheme (i)

a)

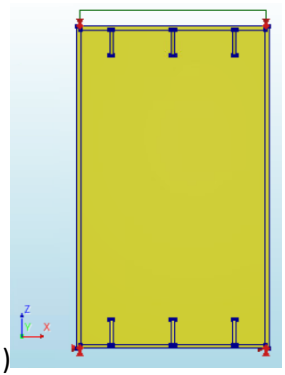

c)

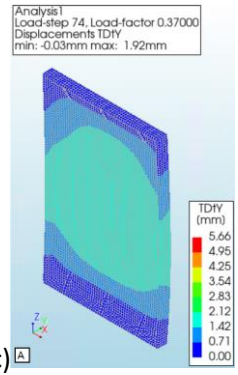

d)

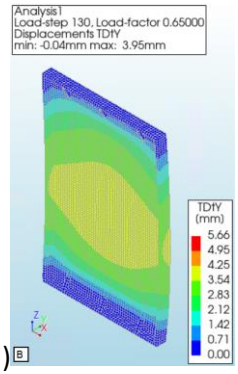

b)

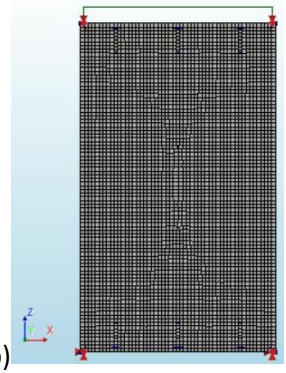

e)

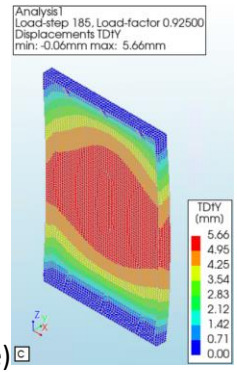

f)

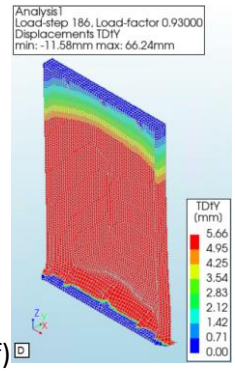

g)

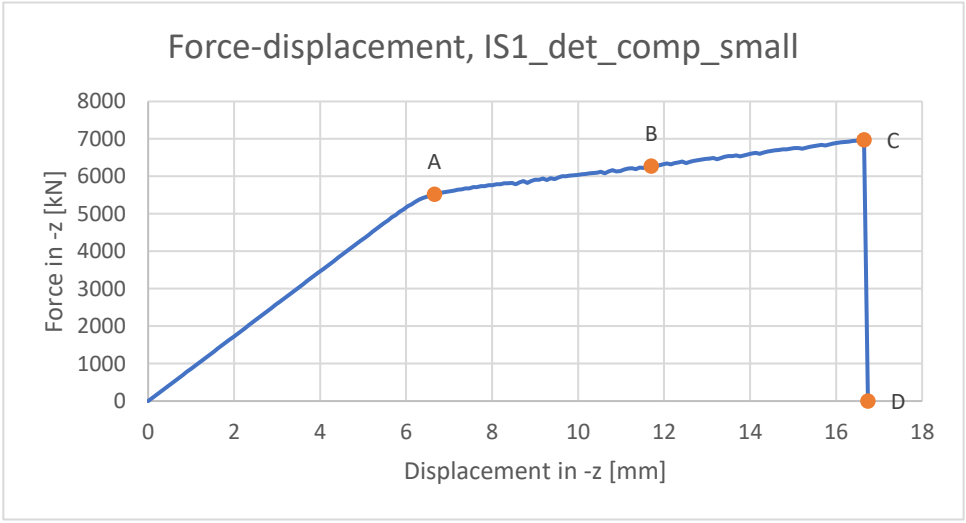

h)

Average element size [mm]		20x20
Number of elements	HX24L	5596
	PY15L	24
	TE12L	8
	TP18L	33
Total number of nodes		11514

i)

Iteration method	Newton-Raphson	
Convergence norms	Displacement	Force
Convergence tolerances	0.01	0.01
Step size	0.005(200)	
Maximum number of iterations per step	100	
All norms satisfied	No	

Figure 4.11: Results of finite element analysis IS1_det_comp_small. a-i: structure (a), finite element mesh (b), displacement at point A (c), displacement at point B (d), displacement at point C (e), displacement at point D (f), force-displacement curve (g), overview elements and nodes (h), overview iterative scheme (i)

Similar as for the models loaded in tension, the stress here is equal to the average stress in the plate, not including the flanges. It is calculated as the force divided by the surface area of the plate. The strain is equal to the deformation divided by the plate length/width in the loading direction.

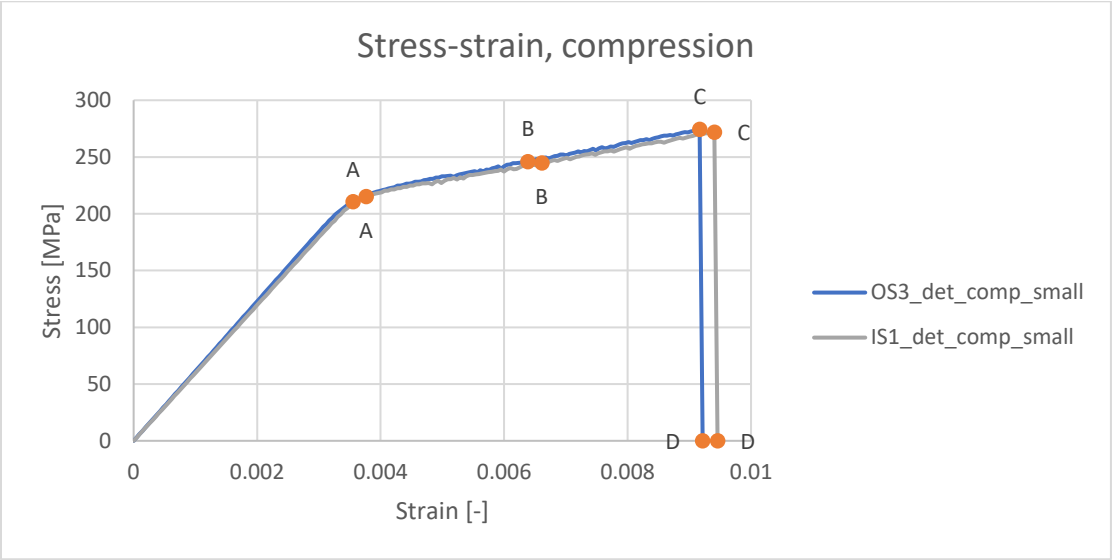

Figure 4.12: Stress-strain curves from compression models OS3_det_comp_small & IS1_det_comp_small

Again, four interesting points from the analysis have been highlighted in the curves. For the models here, the points have been chosen as follows: point A is the maximum force in the linear-elastic region, point D is where the ultimate displacement occurs and point C shows the peak force. Finally, point B is chosen such that its displacement is exactly the average of the displacements of the points A and C. For both plates, it is clear from the results that buckling occurs. It was chosen to show the contour plots of the out of plane displacement, so that the buckling patterns can be observed. After the linear-elastic part, the plastic deformation starts to occur. The deformation keeps increasing quickly, but the stress increases very slowly in the plastic region. Once buckling occurs in the plate, the model suddenly becomes unstable and the strength instantly reduces to zero. The value of the buckling stress can be determined from the maximum force that occurs. These stresses can be compared to the buckling stresses that were obtained with the analytical calculation, see the table below.

Table 4.8: Comparison calculated buckling stresses vs. buckling stresses resulting from detailed models

Section	**Calculated $\sigma_{b,Rd}$ [MPa]**	**Detailed model $\sigma_{b,Rd}$ [MPa]**	**$\sigma_{predicted}/\sigma_{detailed}$**
OS1	223.30	236.12	0.95
OS2	229.45	251.32	0.91
OS3	239.35	274.43	0.87
IS1	233.92	272.04	0.86
IS2	244.90	283.74	0.86
IS3	251.27	311.12	0.81

From the ratio $\sigma_{predicted}/\sigma_{detailed}$ it is clear that the analytical buckling stress is lower than the values that have been reached in the detailed models. In the analytical calculation, some assumptions were made to simplify the plates. This also included that the impact of the flanges and stiffeners were not taken into account, thus the obtained results are as expected. It is also observed that the ratio is closer to 1 for the wider plates. As the flanges are further away from the location of buckling, the assumed situation in the analytical calculation is more accurate for those plates.

In addition to the buckling stress, the fracture energy in compression, the factor to strain at compressive strength (n) and the E-modulus in compression have to be determined from the force-displacement curves. The values are given in the table below.

Table 4.9: Crushing parameters obtained from results of detailed models

Section	Fracture energy in compression [N/mm]	Factor to strain at compressive strength (n)	E compression [MPa]
OS1	345.02	1.683	58086.47
OS2	383.82	1.845	59132.48
OS3	477.62	2.047	61280.43
IS1	551.36	2.059	59550.62
IS2	578.36	2.141	61459.34
IS3	710.90	2.283	64347.61

It is observed that the factor to strain values are quite high. Again, as the slope becomes very flat after the linear-elastic part, the displacements increase very quickly, while the stresses only increase slightly. This causes the value of n to become quite large, especially for the sections of the inner column.

4.3 Shear loading

The shear failure parameters are obtained from the detailed models loaded in shear. The Coulomb shear failure criterion, based on stresses normal to the bed joint, describe the shear failure in the EMM. This means that only the shear failure of the bed-joint has to be analysed. The required parameters that describe the Coulomb friction are the cohesion, friction angle and fracture energy. In order to find these, several models should be created where different values of compressive loads are applied, in addition to the shear load. This will provide different combinations of shear stresses and compressive stresses. Therefore, three different models have been analysed for each section, with compressive stresses of 0.5 MPa, 1 MPa and 2 MPa.

The compressive load is placed on the top face (orange load), pointing in the negative z direction. The bottom is supported in x and z, while the back of the plates are supported in y, which prevents any out of plane deformations. The support in x at the top is required for the prescribed deformation load. This is the green load, which can be seen at the top left of the structure. This load causes the top face of the structure to be displaced in the positive x-direction. In addition, tyings were added to the top face of the structure for the translation in z. In the figures below, it can be seen which node was selected as master node for the tyings. This ensures that the top face will remain straight throughout the analysis.

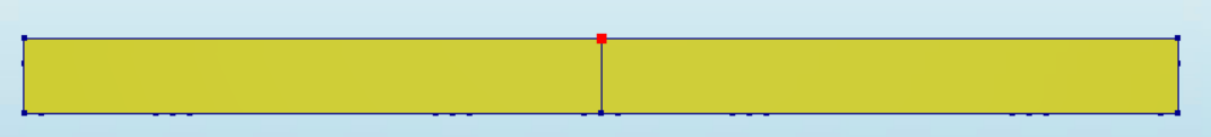

Figure 4.13: Position of master node used for the tyings at the top face

The results of OS3_det_shear_small and IS1_det_shear_small (see appendix A for the explanation of the model names) are given below. For the results of the other sections, see appendix B. The force displacement curve shows the results of the three different models for each section. As mentioned, the only difference between the models is the magnitude of the compression load. A figure including the stress-strain curves of both models is also presented, where the compressive load (σ) is 0.5 MPa.

a)

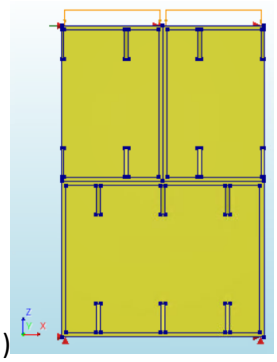

c)

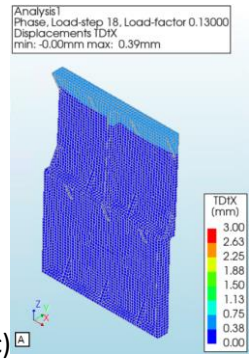

d)

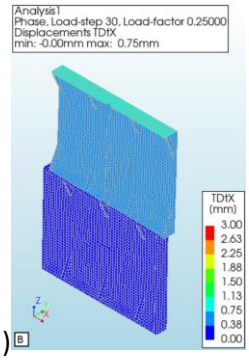

b)

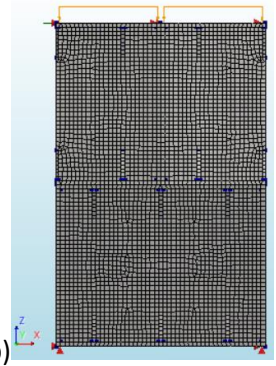

e)

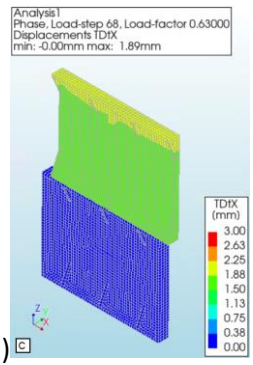

f)

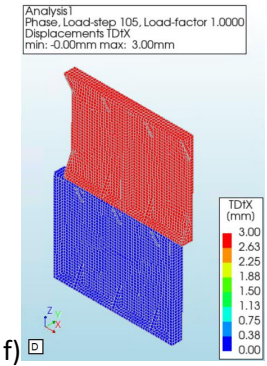

g)

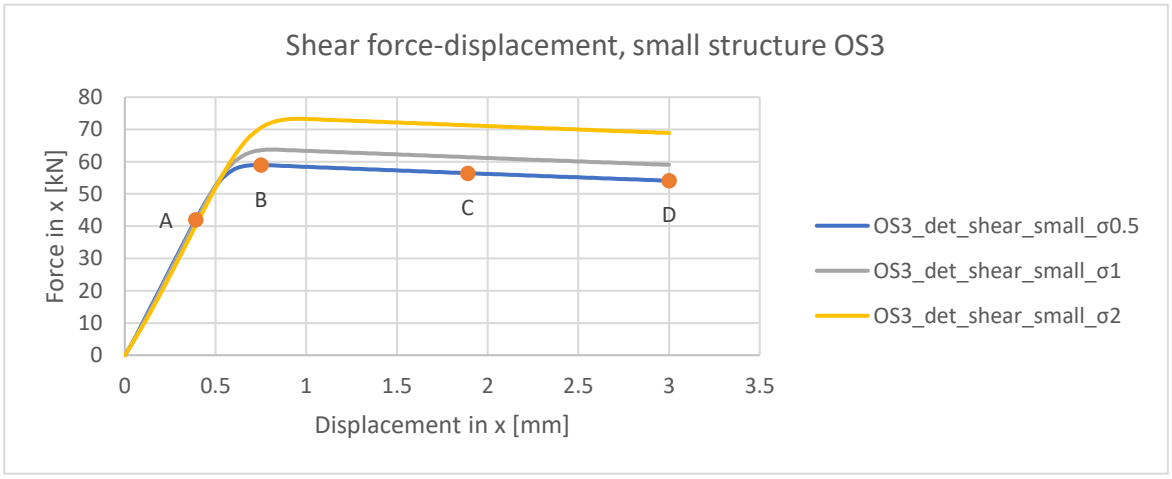

h)

Average element size [mm]		20x20
Number of elements	HX24L	4505
	PY15L	1145
	TE12L	856
	TP18L	242
	Q24IF	344
Total number of nodes		10402

i)

Load	Compression		Translation	
Iteration method	Newton-Raphson		Newton-Raphson	
Convergence norms	Force	Displacement	Force	Displacement
Convergence tolerances	0.01	0.01	0.01	0.01
Step size	0.2(5)		0.01(100)	
Maximum number of iterations per step	100		100	
All norms satisfied	No		No	

Figure 4.14: Results of finite element analysis OS3_det_shear_small_σ0.5, σ1 & σ2. a-i: structure (a), finite element mesh (b), displacement at point A (c), displacement at point B (d), displacement at point C (e), displacement at point D (f), force-displacement curve (g), overview elements and nodes (h), overview iterative scheme (i)

a) b)

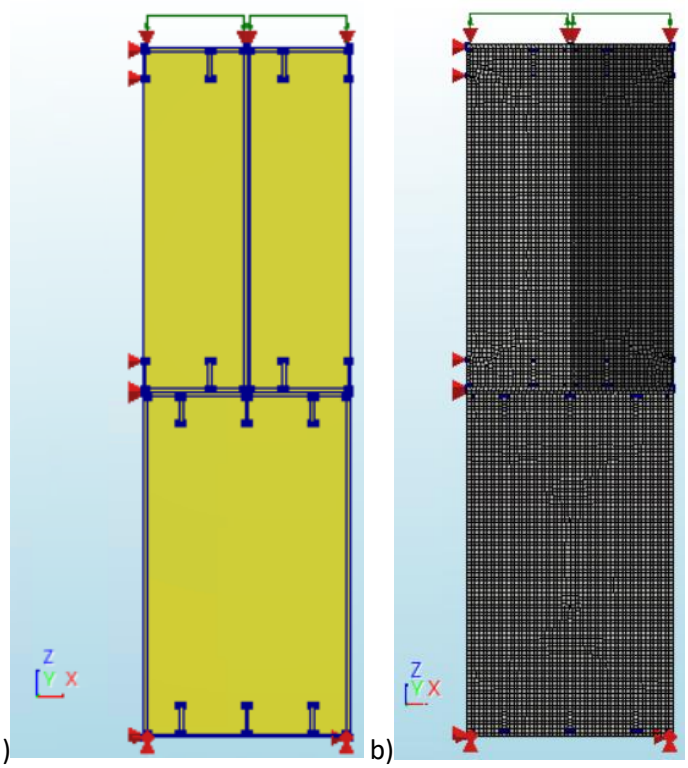

c)

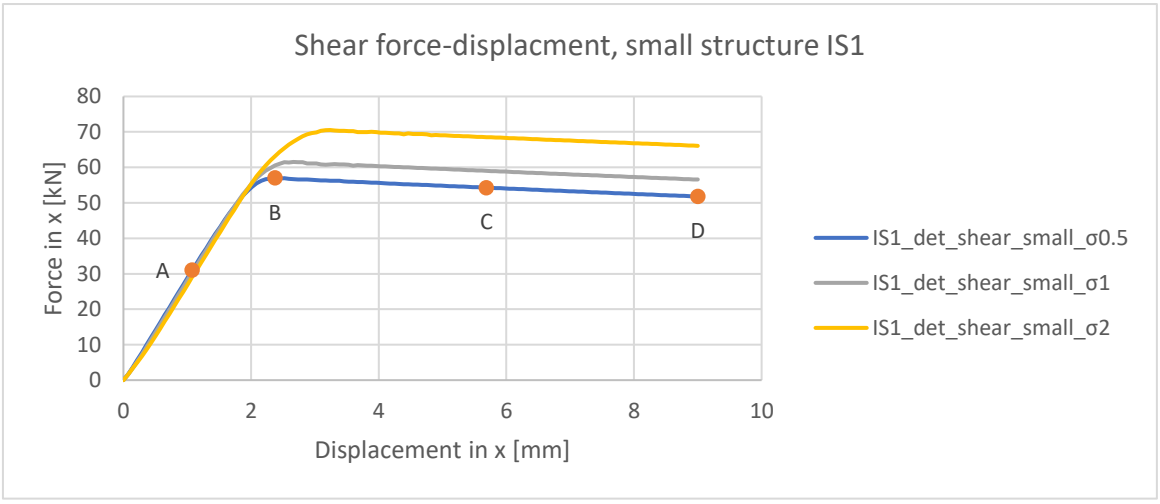

d)

Average element size [mm]		20x20
Number of elements	HX24L	10982
	PY15L	520
	TE12L	384
	TP18L	140
	Q24IF	564
Total number of nodes		23182

e)

Load	Compression		Translation	
Iteration method	Newton-Raphson		Newton-Raphson	
Convergence norms	Force	Displacement	Force	Displacement
Convergence tolerances	0.01	0.01	0.01	0.01
Step size	0.2(5)		0.01(100)	
Maximum number of iterations per step	100		100	
All norms satisfied	No		No	

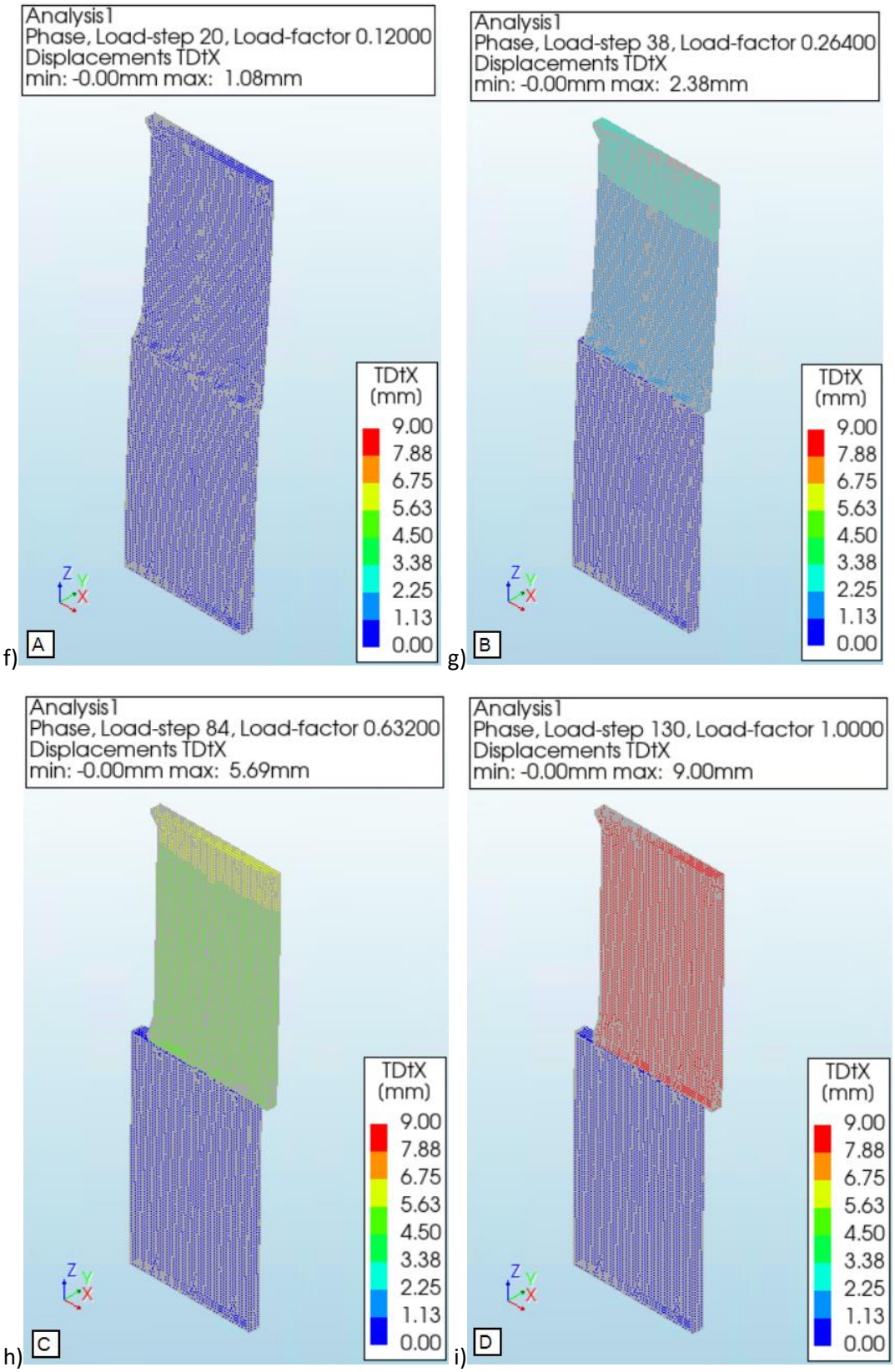

Figure 4.15: Results of finite element analysis IS1_det_shear_small_σ0.5, σ1 & σ2. a-i: structure (a), finite element mesh (b), force-displacement curve (c), overview elements and nodes (d), overview iterative scheme (e), displacement at point A (f), displacement at point B (g), displacement at point C (h), displacement at point D (i)

The shear stress here is equal to the average shear stress in the plate, not including the flanges. It is calculated as the horizontal force divided by the surface area of the plates. The shear strain is equal to the deformation in the loading direction, divided by the height of the structure.

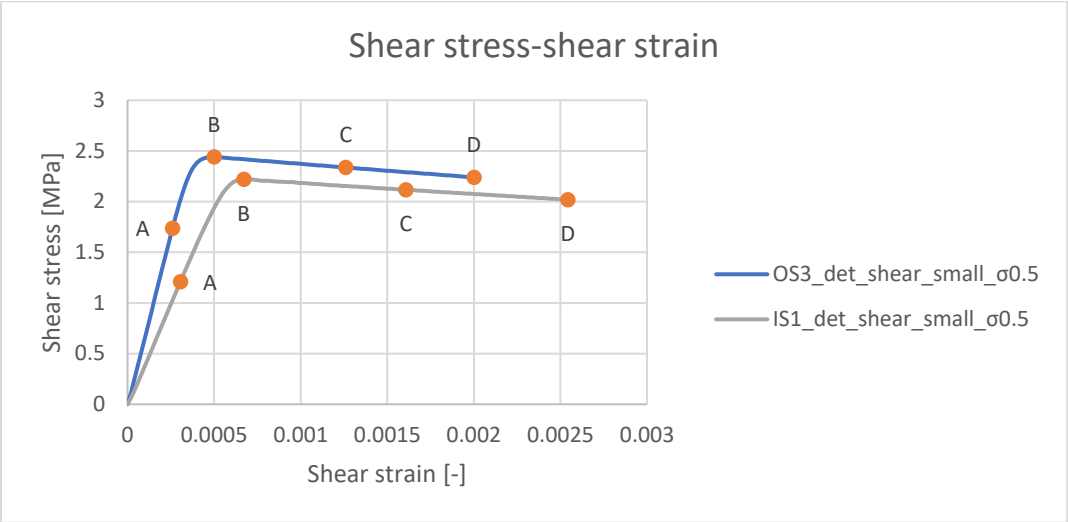

Figure 4.16: Stress-strain curves from shear models OS3_det_shear_small_σ0.5 & IS1_det_shear_small_σ0.5

The highlighted points A-D are determined as follows: point B shows the peak force and point D is where the displacement load has been fully applied. The displacement in point A is equal to half the displacement in point B, while the displacement in point C is equal to half the displacement in point D. From the force-displacement curve, it is clear that when the different compressive stresses are increased, the peak force becomes higher. From the contour plots, it is clear that the interfaces are disconnected, but the interface will still have some residual strength. This is caused by the friction in the interface. It can be observed that this residual force remains quite high after the peak force has been reached. As mentioned, the input fracture energy had to be quite high to ensure convergence in the analysis. This is the reason the residual force remains so high. From the stress-strain curves, it can be observed that the shapes of the curve is the same for both the models of OS3 and IS1. The stiffness and strength are higher for section OS3, which is caused by the difference in plate size and the number of bolts per connection. For the models of the outer column, a displacement load of 3 mm was applied, while a displacement of 9 mm was applied for the inner column models. This is why the total shear strain is larger for the model of IS1 compared to the model of OS3.

The peak stress can be determined from the curves to find the relation to the compressive stress. The peak stress is the maximum average stress that occurs in the analysis of the structure, which is highlighted as point B in the stress-strain curves presented above. From the relation between the peak stress (τ) and the compressive stress (σ), the cohesion (c) and friction angle (ϕ) can be determined. The formula that describes this relation is:

$$\tau = c + \sigma * \tan(\varphi)$$

A small diagram can be made to show the different values for the peak stress and residual stress related to the values for the compressive stress. A linear relation can be found for these points to predict the shear stress for different values of σ. From the relation of the peak stress to the compressive stress, it is possible to determine the cohesion and friction angle. The graphs for OS3 and IS1 are presented below. In the graphs, the formula that describes the relation between the peak stress and the compressive stress is also given.

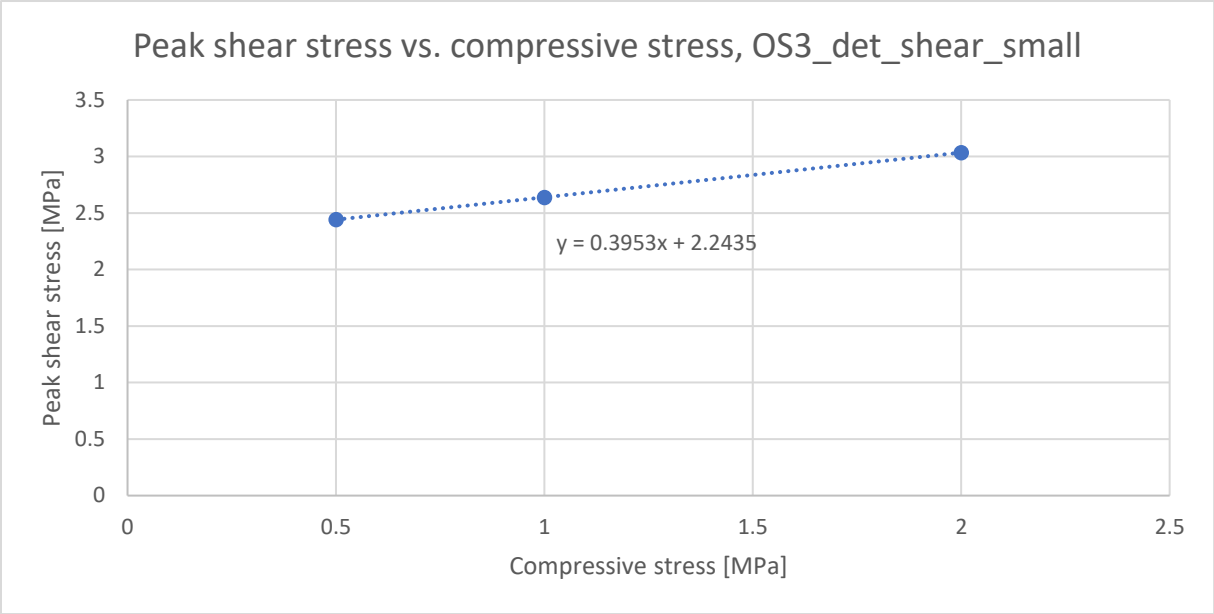

Figure 4.17: Diagram of peak shear stress vs. compressive stress, OS3_det_shear_small

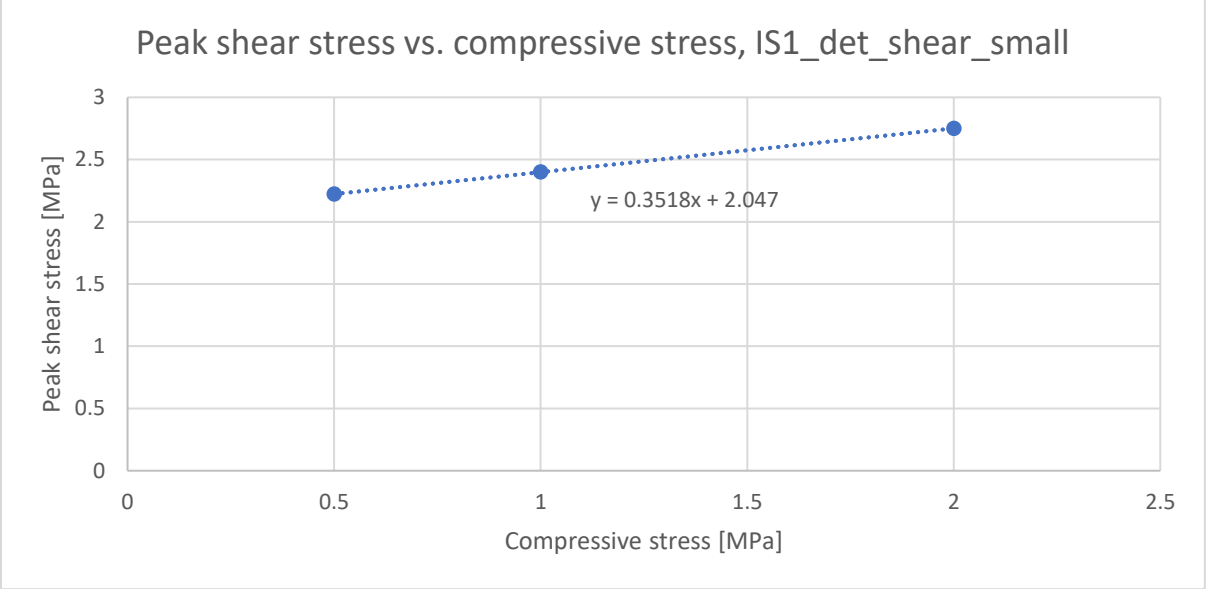

Figure 4.18: Diagram of peak shear stress vs. compressive stress, IS1_det_shear_small

As the formula is in the form $y = ax + b$, the friction angle can be found from $\tan^{-1}$(a), while the cohesion is simply equal to b. The fracture energy in shear usually follows from the area of the curve, but it can be seen that the residual force remains very high. This is the result of requiring a minimum value for the parameter in the analysis. As the input fracture energy is very high, the output fracture energy is also very high and cannot be determined accurately for the shear models without greatly increasing the total shear displacement load. As a result, it is chosen to use the same value as for the fracture energy in compression. The fracture energy values from the compression models are quite high, and will ensure high residual forces in the equivalent EMM shear models. Finally, the shear modulus (G) can be determined from the force-displacement curves, as it is the stiffness of the linear-elastic part. The values for all different sections are given below.

Table 4.10: Shear failure parameters obtained from results of detailed models

Section	Friction angle [rad]	Cohesion [MPa]	Fracture energy shear [N/mm]	G-modulus [MPa]
OS1	0.378	1.518	304.66	6915.2
OS2	0.376	1.832	345.11	6829.0
OS3	0.376	2.244	437.38	6534.4
IS1	0.338	2.047	612.30	3899.2
IS2	0.356	1.861	611.42	3093.2
IS3	0.313	2.556	791.86	2633.1

There are a few things of importance to notice here. It is observed that the output values of the friction angle are quite close to the input value of 0.38 rad. Also, for the G-modulus, the values are much lower for the inner column sections. This is caused by the ratio of height/width of the structure, which is much higher for these sections compared to the outer column sections.

5 Verification and calibration of EMM parameters

All the required input parameters for the EMM have been determined from the detailed models of the small plate structures. The obtained parameters will now be used in equivalent EMM models, where the EMM is used as the material model of the structure. The analysis that was performed on the detailed models of the small structures will now be performed on equivalent EMM models of these structures. The results of the detailed and equivalent models can be compared, in order to find the differences and similarities in the structural behaviour. First, the goal is to verify that the equivalent models where the calculated EMM parameters are used, provide similar results as the detailed models. Next, from the differences that are discovered between the results, it is attempted to calibrate the EMM input parameters to increase the similarity of the results.

5.1 Bed-joint tension and compression loading

In this section, the input parameters for compression and tension related to the bed-joint models will be verified. By comparing the results, it becomes clear whether using the calculated input parameters in a model where the EMM is used, provide the same results as the detailed models. There is a reason why compression and bed-joint tension are part of the same section here. For almost all input parameters, there is one value that can be used, but there are a few exceptions. The most important is the E-modulus in y-direction. Two values were determined: one from the bed-joint tension model ($E_{y,tension}$) and one from the compression model ($E_{y,compression}$). It can be chosen to use one of the values, or to take the average of the two. The result of using $E_{y,tension}$ is examined first.

The first step is to analyse the bed-joint models in tension. As the EMM is now used, the models simply consist of a polygon sheet of the same dimensions as used in the detailed model. The thickness of the plate is used and the geometry of the flanges and stiffeners is no longer part of the structure. However, their effect on the structural behaviour is part of the input parameters that were determined from the detailed models. The exact same analysis is performed as on the detailed model. This means the boundary conditions and loads are the same as the detailed model where the bed-joint is loaded in tension. For the boundary conditions, this means the left side is supported in x and the bottom is supported in y and z. The support in z at the top only acts as a reference for the prescribed deformation load, which is in the positive z direction. The results of OS3_eqEMM_ten_bed_small_$E_{y,tension}$_$G_{ft,bed}$ (see appendix A for the explanation of the model names) are given below. In addition, the stress-strain curve of the equivalent EMM model is compared to the curve of the detailed model.

a)

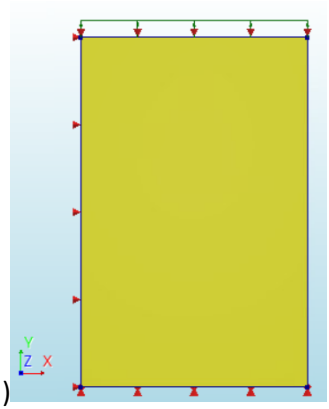

c)

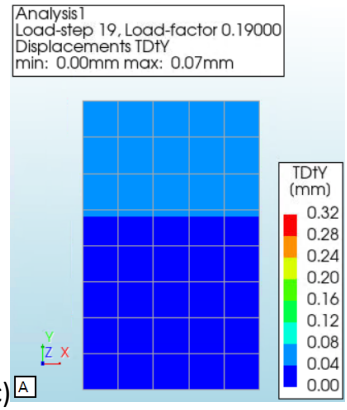

d)

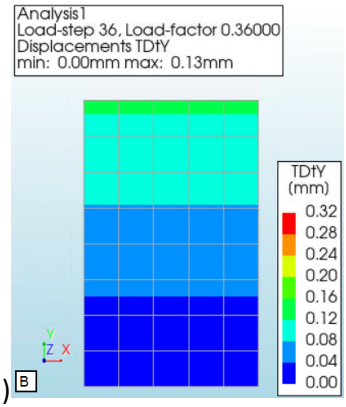

b)

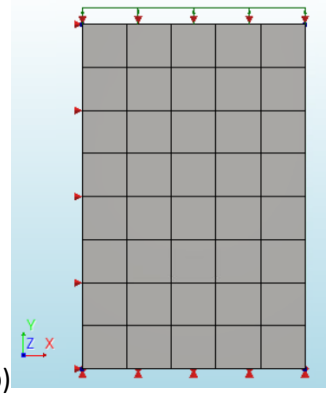

e)

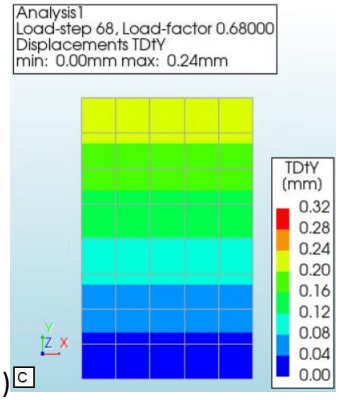

f)

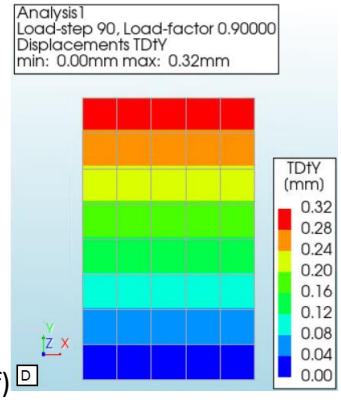

g)

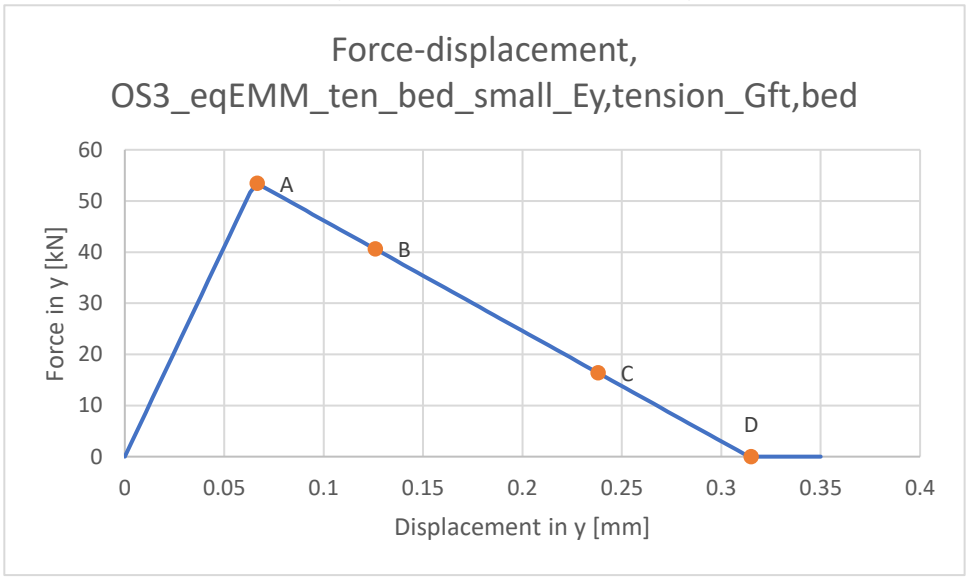

h)

Average element size [mm]		194x187.5
Number of elements	Q20SH	40
Total number of nodes		54

i)

Iteration method	Secant (Quasi-Newton)	
Convergence norms	Displacement	Force
Convergence tolerances	0.01	0.01
Step size	0.01(100)	
Maximum number of iterations per step	100	
All norms satisfied	No	

Figure 5.1: Results of finite element analysis OS3_eqEMM_ten_bed_small_$E_{y,tension}$_$G_{ft,bed}$. a-i: structure (a), finite element mesh (b), displacement at point A (c), displacement at point B (d), displacement at point C (e), displacement at point D (f), force-displacement curve (g), overview elements and nodes (h), overview iterative scheme (i)

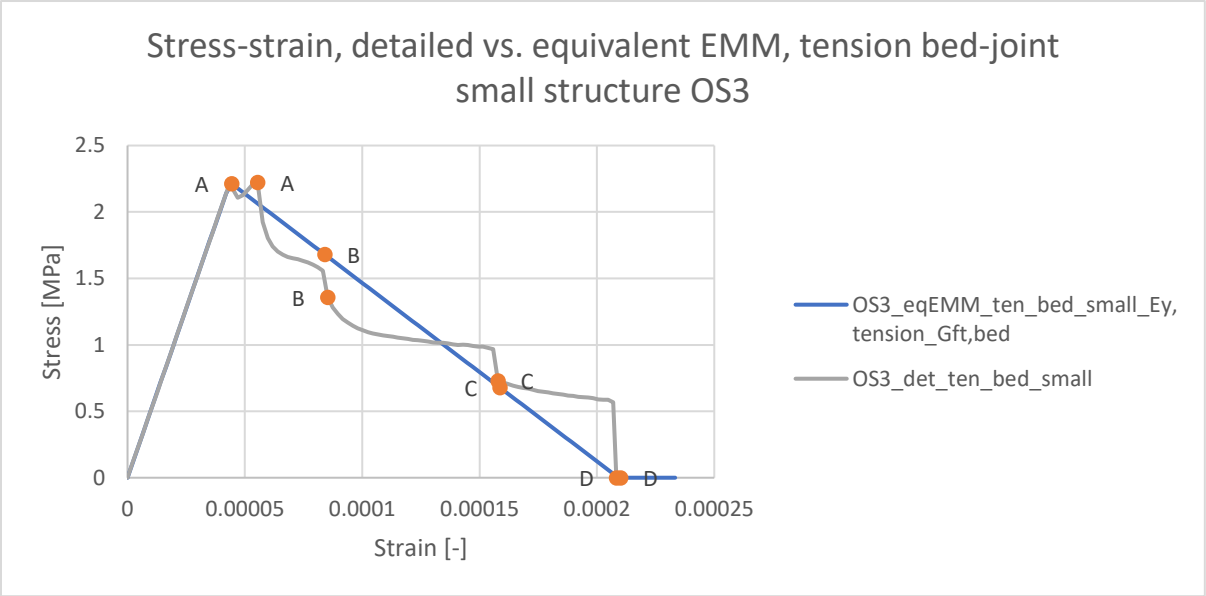

Figure 5.2: Stress-strain curves from tension bed-joint models OS3_eqEMM_ten_bed_small_Ey,tension_Gft,bed & OS3_det_ten_bed_small

The points A-D of the equivalent EMM model were determined as follows: point A is where the peak force occurs and point D shows the displacement where the force becomes 0 kN. The points B and C were chosen such that the displacement is equal to the displacement of points B and C in the results of OS3_det_ten_bed_small. By choosing these four points, it is clear to see the differences between the structural behaviour. It is clear that the linear elastic parts of the curves are an exact match, which is expected as $E_{y,tension}$ was used as input. As the peak forces are the same, the bed-joint strength has been verified. In the Engineering Masonry Model, the force will linearly go to 0 after the peak force has been reached. This is the reason that the curves are not an exact match after reaching the peak force. The forces in points B and C are therefore not the same for the two models. The contour plots of the displacements at the point of failure (D) are given in the figure below.

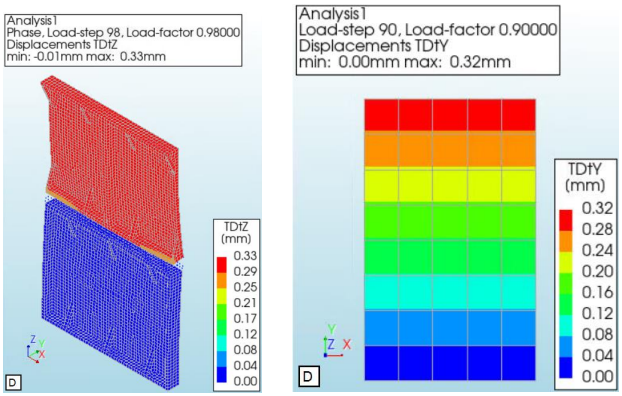

Figure 5.3: Vertical displacements at point of failure (D), tension bed-joint detailed (left) and equivalent EMM model (right), section OS3

It is clear to see that the failure mode is different than for the detailed models in tension. In the detailed models, the failure occurs at the joints and the deformations in the plates remain small. In the equivalent EMM model, the displacements are uniformly distributed.

The same comparison can be made for the compression models, where $E_{y,tension}$ will be used for E_y. The results of OS3_eqEMM_comp_small_$E_{y,tension}$ are given below, after which a comparison between the stress-strain curves of the detailed and equivalent EMM models is presented.

a)

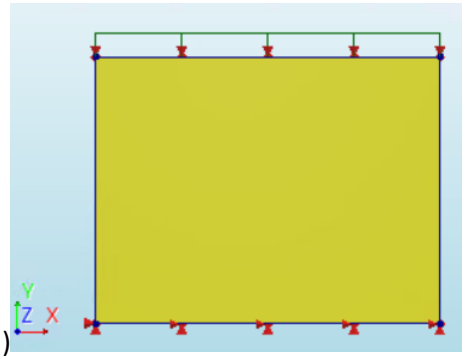

c)

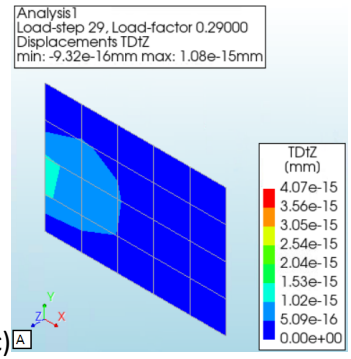

d)

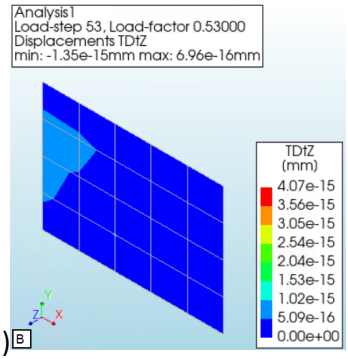

b)

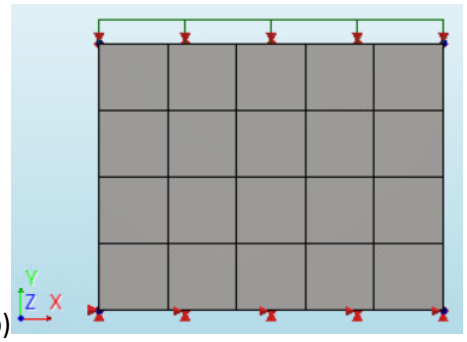

e)

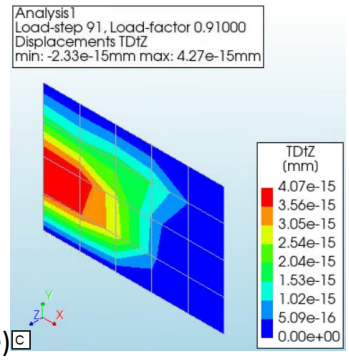

f)

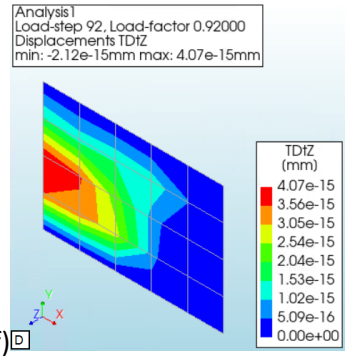

g)

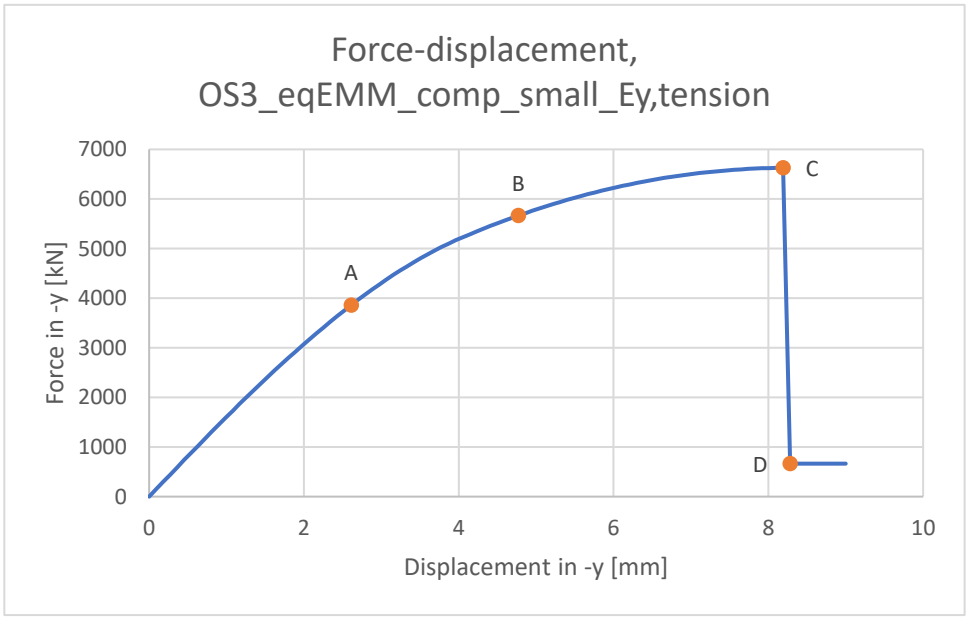

h)

Average element size [mm]		194x187.5
Number of elements	Q20SH	20
Total number of nodes		30

i)

Iteration method	Secant (Quasi-Newton)	
Convergence norms	Displacement	Force
Convergence tolerances	0.01	0.01
Step size	0.01(100)	
Maximum number of iterations per step	100	
All norms satisfied	No	

Figure 5.4: Results of finite element analysis OS3_eqEMM_comp_small_$E_{y,tension}$. a-i: structure (a), finite element mesh (b), displacement at point A (c), displacement at point B (d), displacement at point C (e), displacement at point D (f), force-displacement curve (g), overview elements and nodes (h), overview iterative scheme (i)

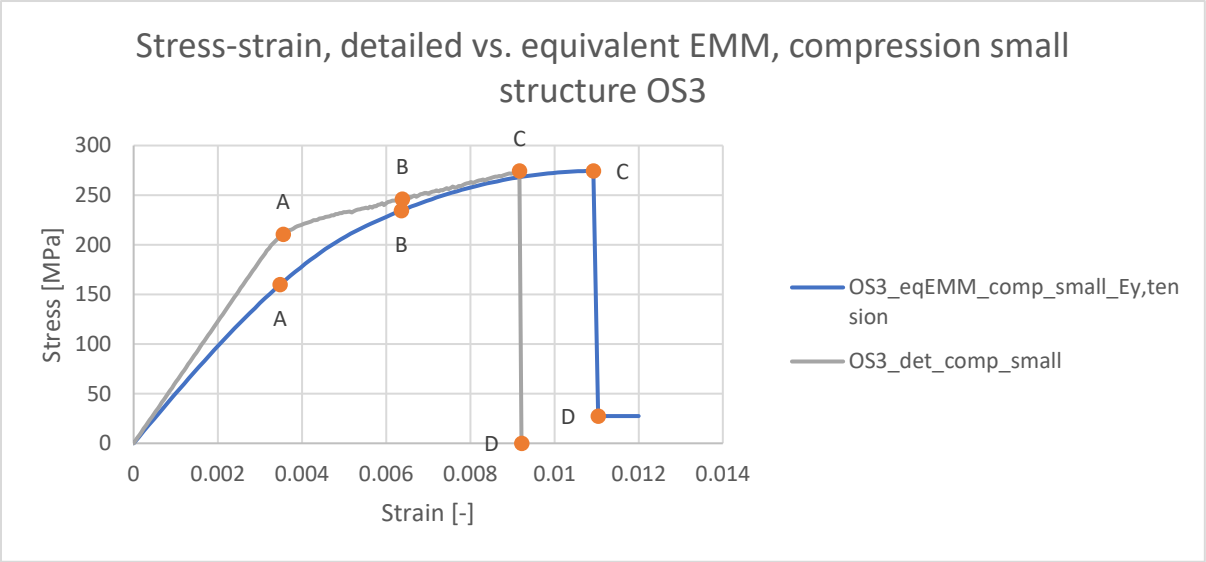

Figure 5.5: Stress-strain curves from compression models OS3_eqEMM_comp_small_$E_{y,tension}$ & OS3_det_comp_small

The points A-D were chosen as follows: points A and B of the equivalent EMM models have the same displacement as points A and B of the detailed model. Point C is where the peak force occurs and point D is where the force reaches the residual value. In the detailed compression model, the contour plots of the out of plane displacements were presented, as they showed the buckling pattern of the structure. The out of plane displacements are given here as well, but it is clear that the displacement values are almost 0 mm, even in points C and D. This shows that the failure mode of the equivalent EMM model is not the same as in the detailed models. It can also be observed that the residual force of the equivalent EMM model is equal to 0 N. In the Engineering Masonry Model, the resultant force will be equal to 10% of the peak force, while in reality the resultant force should be equal to 0 N. This is part of the settings of the EMM, so it cannot be changed. This is an important difference to keep in mind when the EMM will be used in a model of the lighthouse. The contour plots of the out of plane displacements are given in the figure below for the point where the peak force occurs.

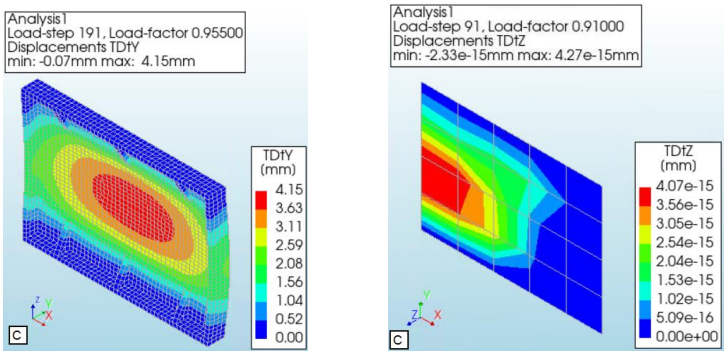

Figure 5.6: Out of plane displacements at point of peak force (C), compression detailed (left) and equivalent EMM model (right), section OS3

Similar as for the tension models, it is clear that the failure modes of the detailed and equivalent EMM models are quite different. There is an out of plane displacement of 4 mm in the detailed model, while the out of plane displacements in the equivalent EMM model are negligible. It shows that the plate buckling that is observed in the detailed model does not occur in the equivalent EMM model.

The stress-strain diagram shows that there is quite a difference in the ultimate strain of the two models. As $E_{y,tension}$ is lower than the actual E-modulus that was obtained from the detailed model in compression, the curve of the equivalent EMM model has a much lower path to the maximum compressive force. As value of the factor to strain, n (which is based on $E_{y,compression}$), is also quite large, the ultimate displacement is larger for the equivalent EMM model. It can be concluded that the impact of using $E_{y,tension}$ in the compression model results different stress-strain curves. As the input stiffness for the EMM model is lower than the stiffness found in the detailed compression model, the displacement at failure is much higher for the EMM models. Using $E_{y,tension}$ for E_y will give very good results for the bed-joint model loaded in tension, but not for the model loaded in compression. If $E_{y,compression}$ is used instead, the curves of the compression model will give an (almost) exact match, while the bed-joint tension models will not match well. The best solution is to use the average value of the two:

$$E_y = (E_{y,tension} + E_{y,compression})/2$$

When using this as the input value for E_y, the other parameters should be adjusted slightly as well, otherwise the curves will still be too different from those of the detailed models. For the bed-joint tension models of the outer column plates, the E now becomes higher. This means that, in order to get the peak force at the same displacement, the bed-joint strength should be increased. This result can be obtained by multiplying the initially found value of the bed-joint strength with a factor $E_y/E_{y,tension}$. To ensure that the ultimate displacement will be the same as in the EMM model where $E_{y,tension}$ was used, the fracture energy in tension should also be multiplied with this factor. The same procedure should be followed for the compression models. Here, the input value for E_y is lower for than the stiffness in the detailed model. The factor to strain (n) and the fracture energy in compression will therefore be multiplied by $E_y/E_{y,compression}$. This will cause the values to become lower, such that failure will occur at the same displacement again. For the plates of the inner column, the new E_y is higher than $E_{y,compression}$ and lower than $E_{y,tension}$. This means multiplying the tensile properties with $E_y/E_{y,tension}$ results in lower values for the bed-joint strength and fracture energy in tension. The factor to strain (n) and the fracture energy in compression will be multiplied by $E_y/E_{y,compression}$, which means their value increases.

By applying the adjusted input parameters to the models, a new analysis can be performed to observe the differences again. This has been done for both sections OS3 and IS1. The results of OS3_eqEMM_ten_bed_small_$E_{y,average}$_$G_{ft,bed}$, IS1_eqEMM_ten_bed_small_$E_{y,average}$_$G_{ft,bed}$, OS3_eqEMM_comp_small_$E_{y,average}$ and IS1_eqEMM_comp_small_$E_{y,average}$ are presented in the figures below. After that, figures are presented which include the stress-strain curves of the equivalent EMM model and their corresponding detailed model. The points A-D are chosen in the same way as the equivalent bed-joint tension and compression models that were presented above. As the failure in compression is not the same in the equivalent EMM models compared to the detailed models, showing the out of plane deformations does not provide any information on the failure mode. It is therefore chosen to show the contour plots of the vertical displacements instead, which are the displacements in y-direction for these models.

a)

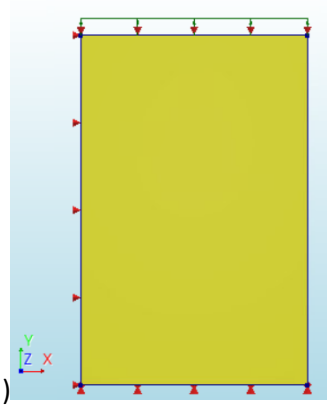

b)

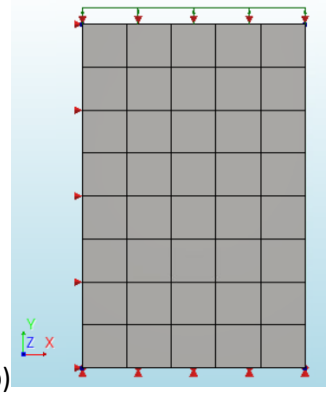

c)

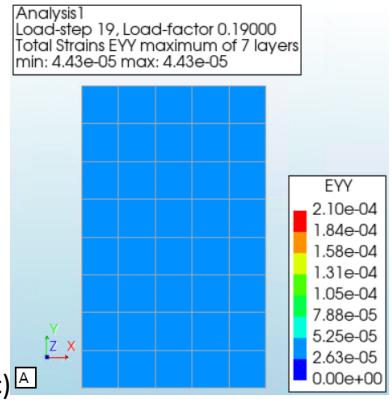

d)

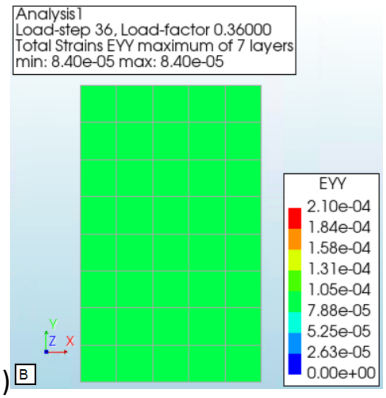

e)

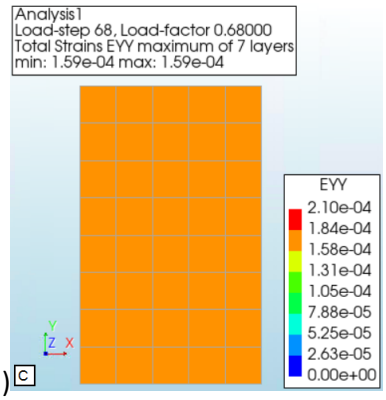

f)

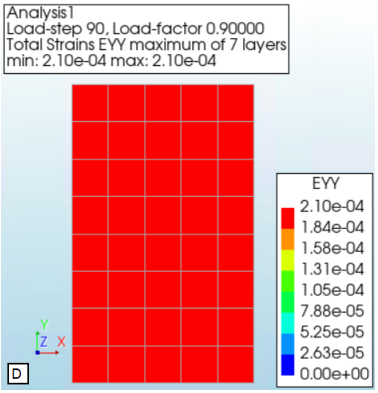

g)

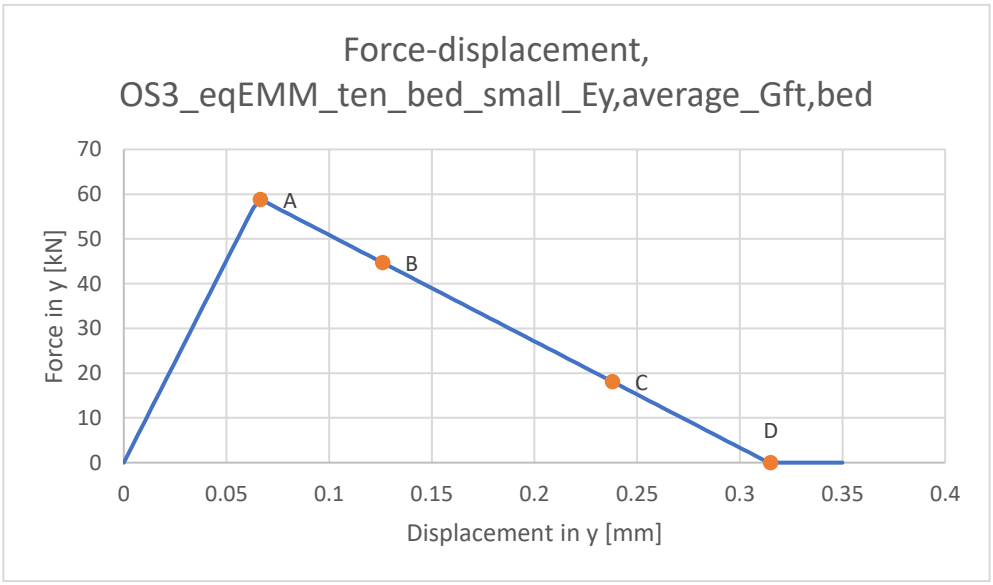

h)

Average element size [mm]		194x187.5
Number of elements	Q20SH	40
Total number of nodes		54

i)

Iteration method	Secant (Quasi-Newton)	
Convergence norms	Displacement	Force
Convergence tolerances	0.01	0.01
Step size	0.01(100)	
Maximum number of iterations per step	100	
All norms satisfied	No	

Figure 5.7: Results of finite element analysis OS3_eqEMM_ten_bed_small_$E_{y,average}$_$G_{ft,bed}$. a-i: structure (a), finite element mesh (b), strain at point A (c), strain at point B (d), strain at point C (e), strain at point D (f), force-displacement curve (g), overview elements and nodes (h), overview iterative scheme (i)

a) b)

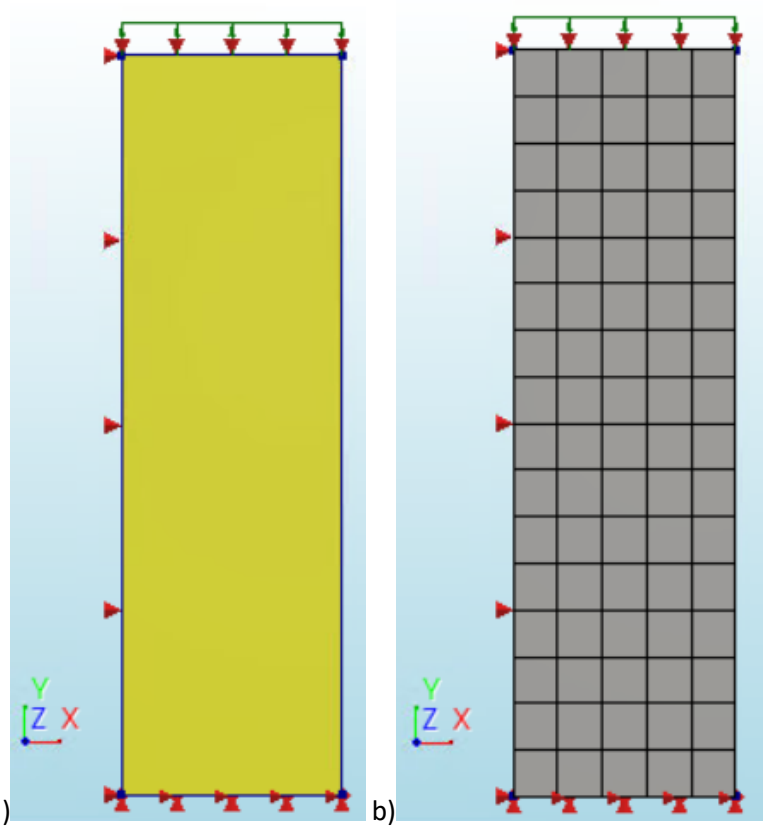

c)

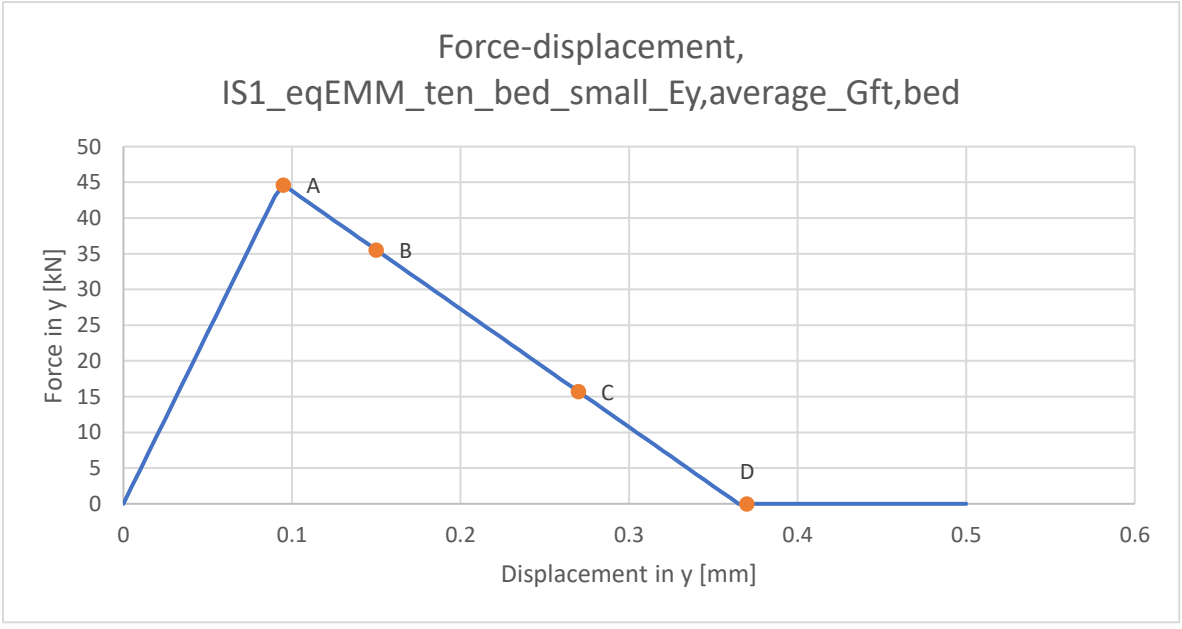

h)

Average element size [mm]		210.2x221.25
Number of elements	Q20SH	80
Total number of nodes		102

i)

Iteration method	Secant (Quasi-Newton)	
Convergence norms	Displacement	Force
Convergence tolerances	0.01	0.01
Step size	0.01(100)	
Maximum number of iterations per step	100	
All norms satisfied	No	

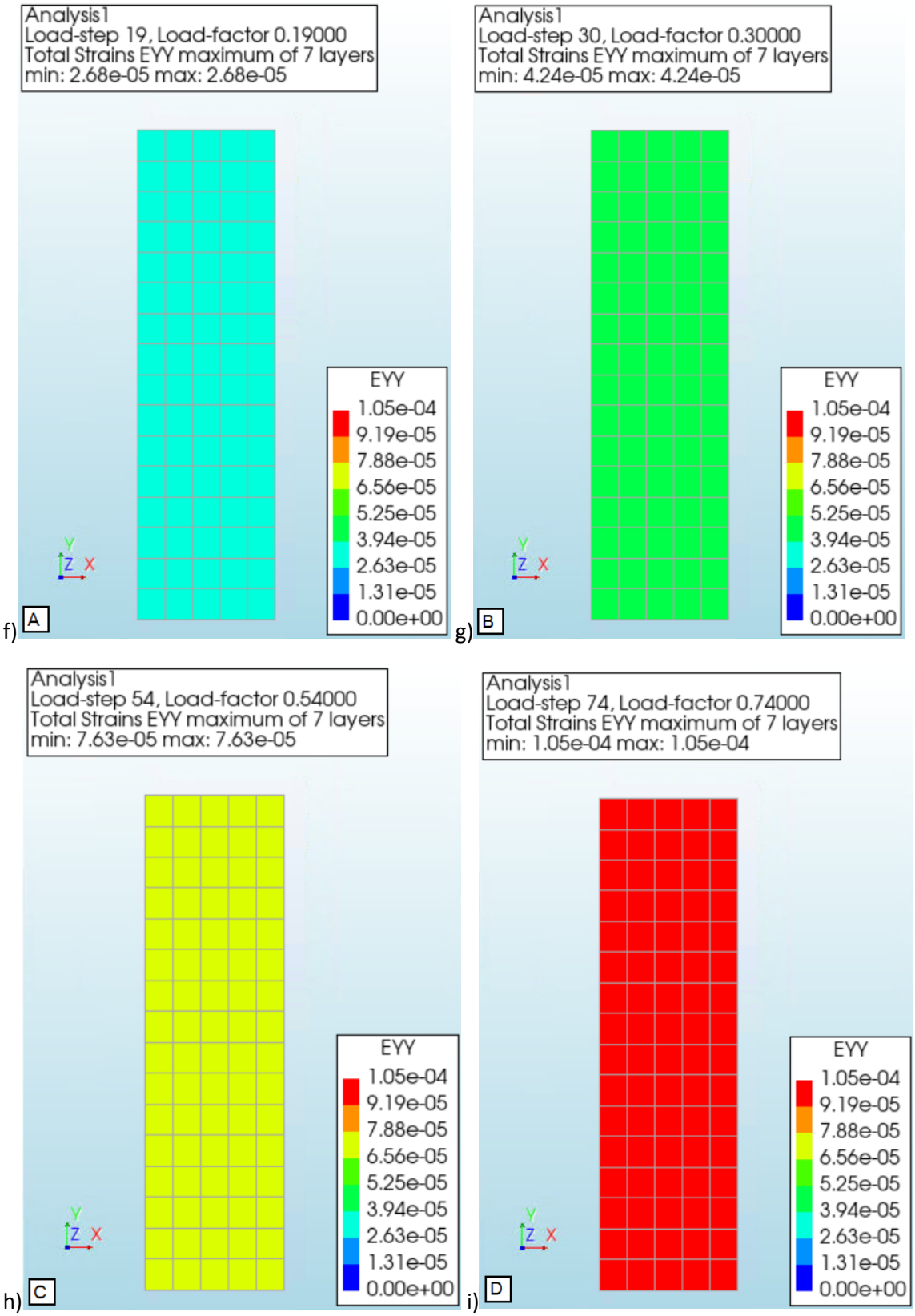

Figure 5.8: Results of finite element analysis IS1_eqEMM_ten_bed_small_$E_{y,average}$_$G_{ft,bed}$. a-i: structure (a), finite element mesh (b), force-displacement curve (c), overview elements and nodes (d), overview iterative scheme (e), strain at point A (f), strain at point B (g), strain at point C (h), strain at point D (i)

a) 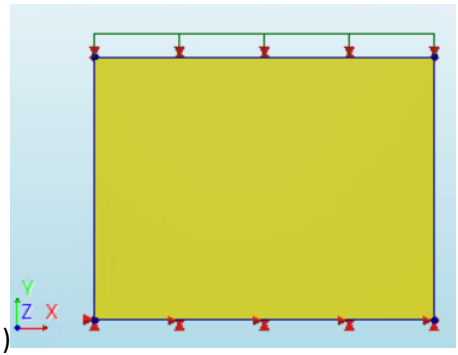

c) 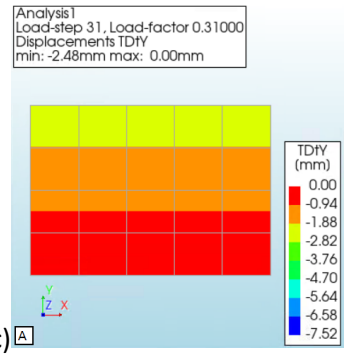

d) 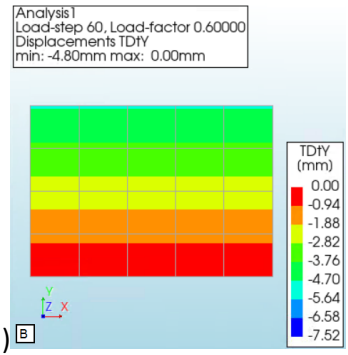

b) 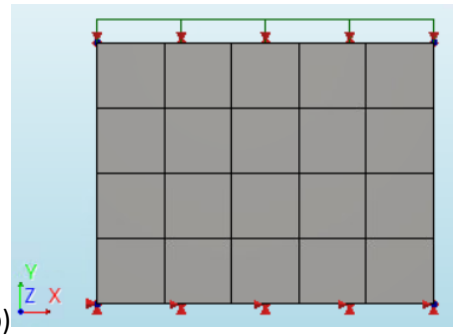

e) 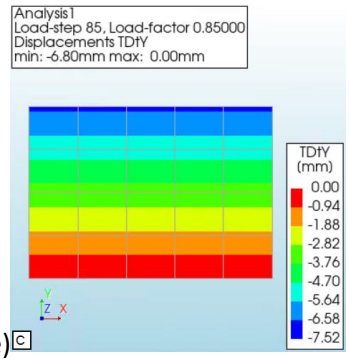

f) 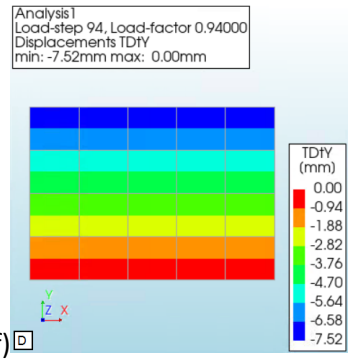

g) 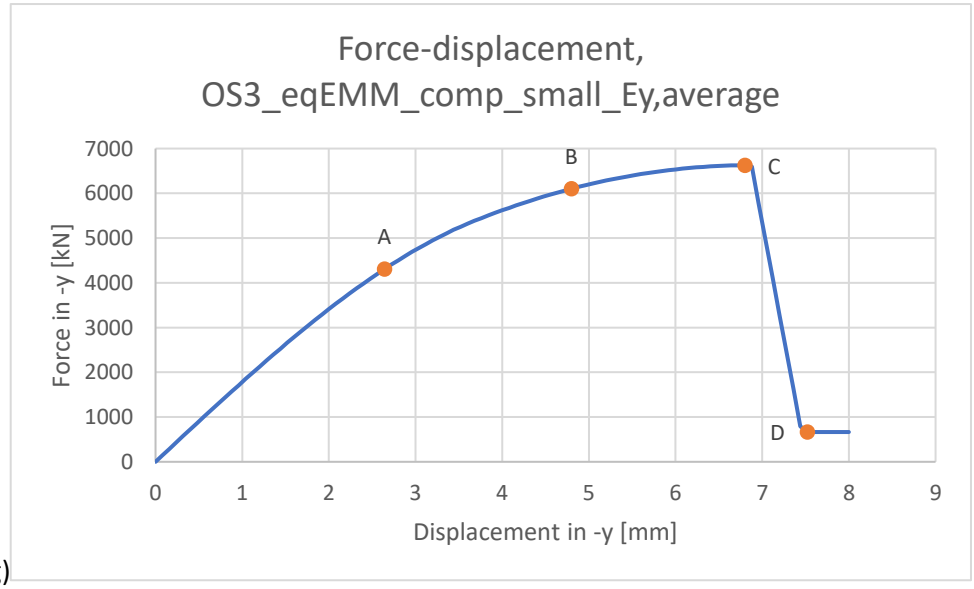

h)

Average element size [mm]		194x187.5
Number of elements	Q20SH	20
Total number of nodes		30

i)

Iteration method	Secant (Quasi-Newton)	
Convergence norms	Displacement	Force
Convergence tolerances	0.01	0.01
Step size	0.01(100)	
Maximum number of iterations per step	100	
All norms satisfied	No	

Figure 5.9: Results of finite element analysis OS3_eqEMM_comp_small_$E_{y,average}$. a-i: structure (a), finite element mesh (b), displacement at point A (c), displacement at point B (d), displacement at point C (e), displacement at point D (f), force-displacement curve (g), overview elements and nodes (h), overview iterative scheme (i)

a)

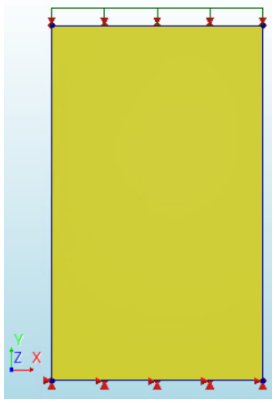

c)

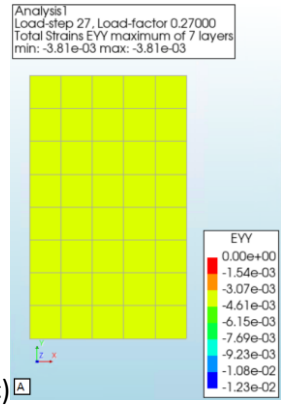

d)

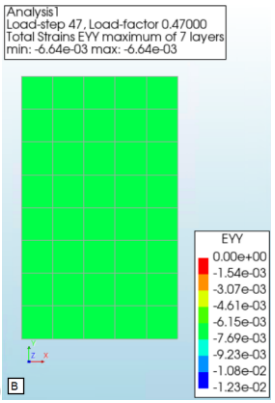

b)

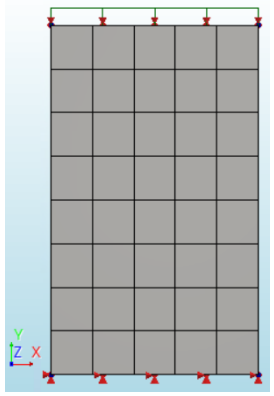

e)

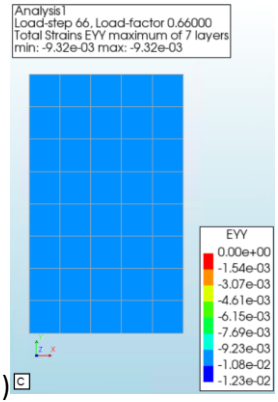

f)

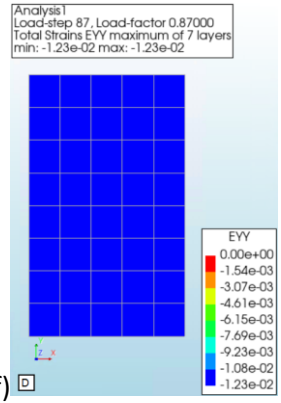

g)

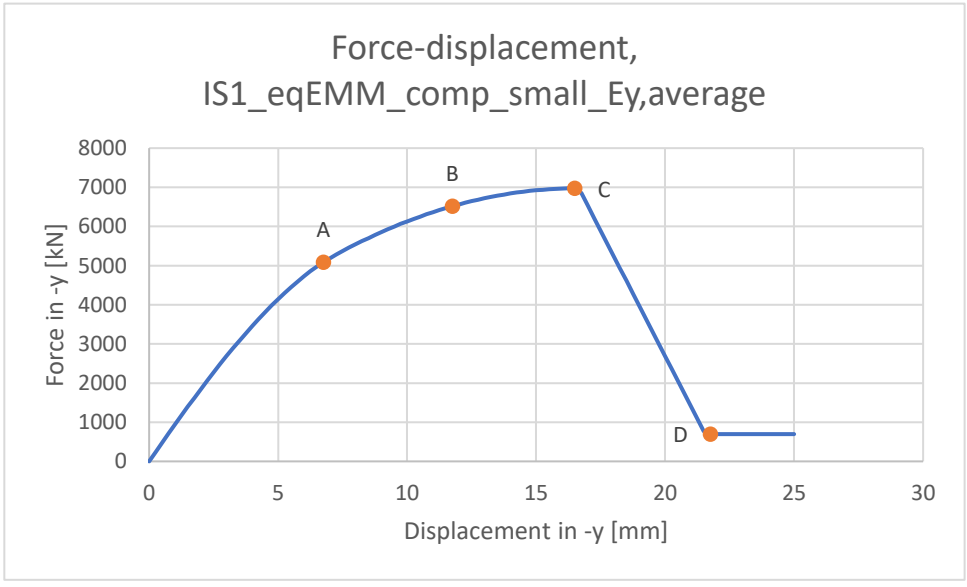

h)

Average element size [mm]		210.2x221.25
Number of elements	Q20SH	40
Total number of nodes		54

i)

Iteration method	Secant (Quasi-Newton)	
Convergence norms	Displacement	Force
Convergence tolerances	0.01	0.01
Step size	0.01(100)	
Maximum number of iterations per step	100	
All norms satisfied	No	

Figure 5.10: Results of finite element analysis IS1_eqEMM_comp_small_$E_{y,average}$. a-i: structure (a), finite element mesh (b), strain at point A (c), strain at point B (d), strain at point C (e), strain at point D (f), force-displacement curve (g), overview elements and nodes (h), overview iterative scheme (i)

In figures 5.7 and 5.8, the results of the models loaded in tension are presented. It was chosen to show the vertical strains in the contour plots for the tension models this time. It can be observed that the strains are equal throughout the entire plate, for all load steps in the analysis. Now it is even more clear how the tensile load results in uniformly distributed failure in the structure.

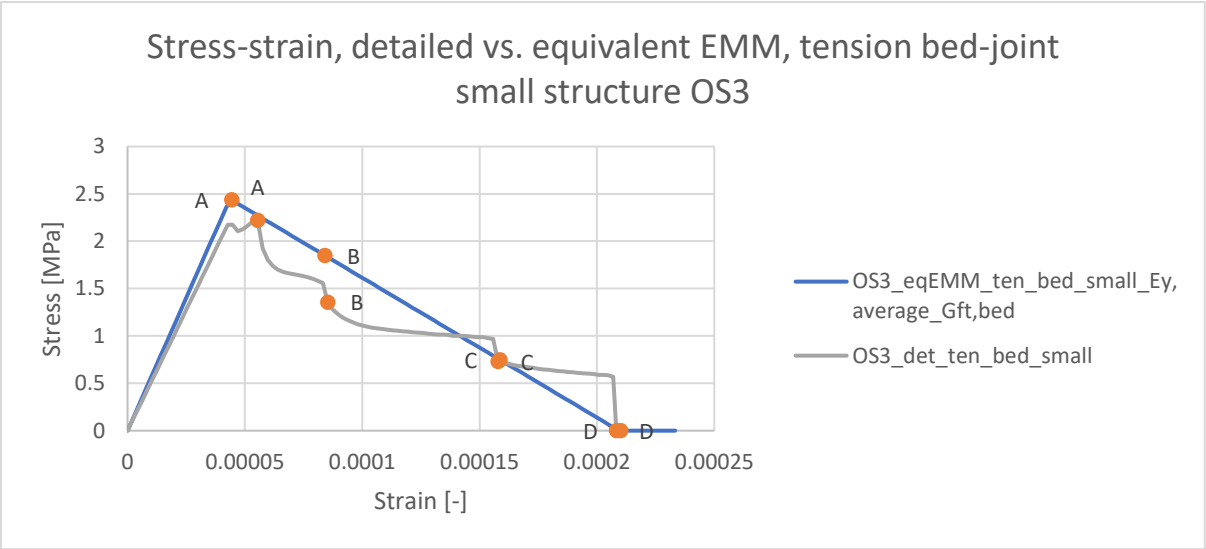

Figure 5.11: Stress-strain curves from tension bed-joint models OS3_eqEMM_ten_bed_small_$E_{y,average}$_$G_{ft,bed}$ & OS3_det_ten_bed_small

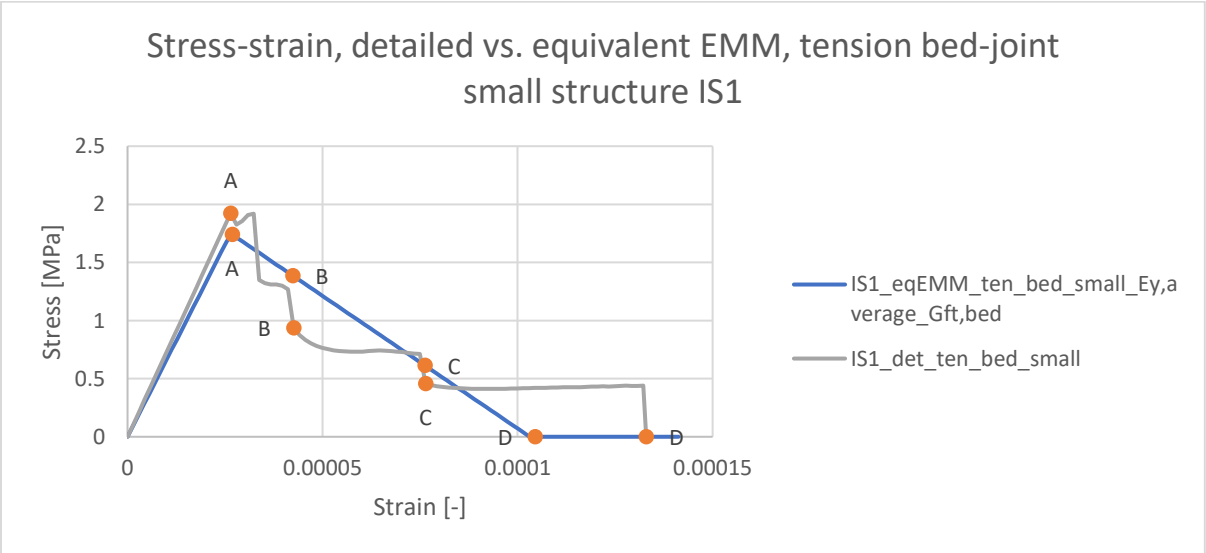

Figure 5.12: Stress-strain curves from tension bed-joint models IS1_eqEMM_ten_bed_small_$E_{y,average}$_$G_{ft,bed}$ & IS1_det_ten_bed_small

When the stress-strain curves of the updated equivalent EMM models, loaded with bed-joint tension, are compared to the curves of the detailed models, it is clear there are now some small differences between the curves. The peak stresses are slightly different, as a result of using $E_{y,average}$ instead of $E_{y,tension}$. Furthermore, it is also clear that there is quite a difference in the ultimate displacement between the models of section IS1. This will be explored more in the following section.

Previously, the out of plane displacements were shown in the contour plots of the equivalent EMM model loaded in compression. As they were negligible, it was chosen to show the vertical displacements in figure 5.9. Similar as in for the models loaded in tension, the displacements are uniformly distributed in the structure. Figure 5.10 shows the vertical strains in the contour plots, which again show very similar results as for the models loaded in tension. The strains are equal throughout the entire structure in every load step of the analysis. The failure modes of tension and compression in the equivalent EMM models is very similar. However, both loading conditions result in different failure modes in the equivalent EMM models when they are compared to the failure modes of the detailed models.

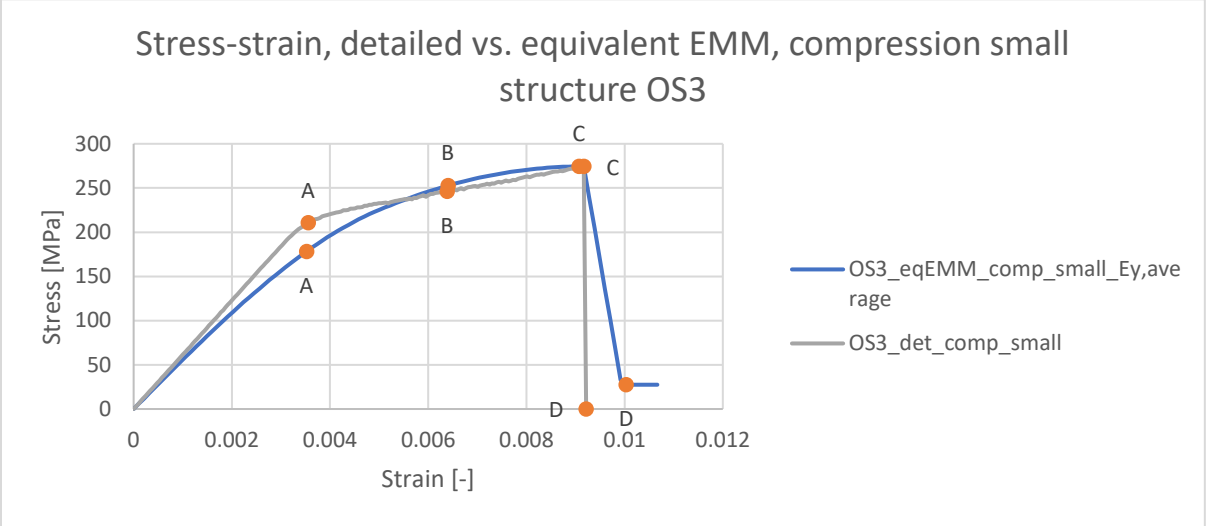

Figure 5.13: Stress-strain curves from compression models OS3_eqEMM_comp_small_$E_{y,average}$ & OS3_det_comp_small

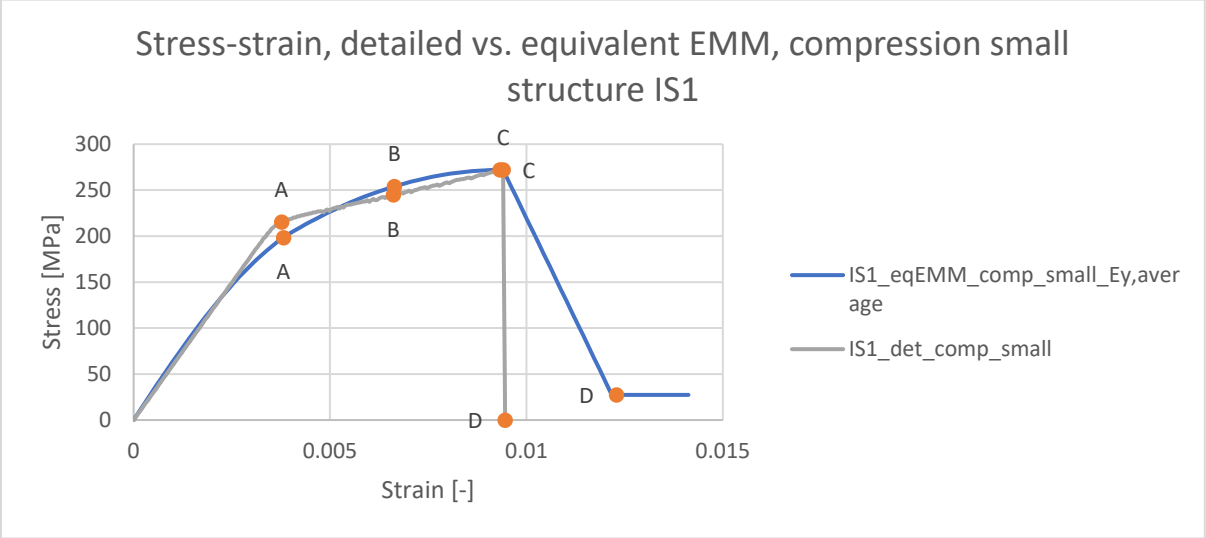

Figure 5.14: Stress-strain curves from compression models IS1_eqEMM_comp_small_$E_{y,average}$ & IS1_det_comp_small

For the models in compression, it can be observed that the peak stresses are now occurring at almost the exact same displacement. After that, the curve of the equivalent model will gradually reach the residual force value, instead of instantly dropping to 0 N. This means the ultimate displacement is still larger for the equivalent EMM models. However, it is clear that the curves of the compression models are now a much better match. It is clear that using the average value for E_y and adjusting the other parameters provides better results, as now the bed-joint tension and compression models give very close matching force-displacement curves.

5.2 Head-joint tension loading

The head-joint models loaded in tension will be verified next. This verification is much easier, as compression failure in this direction is not considered. The loads that will be included in the model of the lighthouse are self-weight and wind, so failure in normal direction of the head-joints is very unlikely, which is the reason only tensile failure is considered for the head joints. This means E_x in the EMM models will simply be equal to $E_{x,tension}$. However, there is still one issue, which is the fracture energy in tension. The values of the bed-joint and head-joint are different, but only one value can be used. In the previous section, $G_{ft,bed}$ was used for the fracture energy in tension. This value will also be used for the models here. Again, the equivalent EMM models consist of a polygon sheet of the same dimensions as used in the detailed model. The same boundary conditions are used as in the detailed models, so the left side is supported in x & y and the bottom is supported in z. The support in x at the right side acts as a reference for the prescribed deformation load, which is in the positive x direction.

The results of OS3_eqEMM_ten_head_small_$G_{ft,bed}$ and IS1_eqEMM_ten_head_small_$G_{ft,bed}$ are presented in appendix C (see appendix A for the explanation of the model names). The figures in the appendix show the force-displacement curve and the contour plots of points A-D. Figures are presented below which include the stress-strain curves of the equivalent EMM model and their corresponding detailed model.

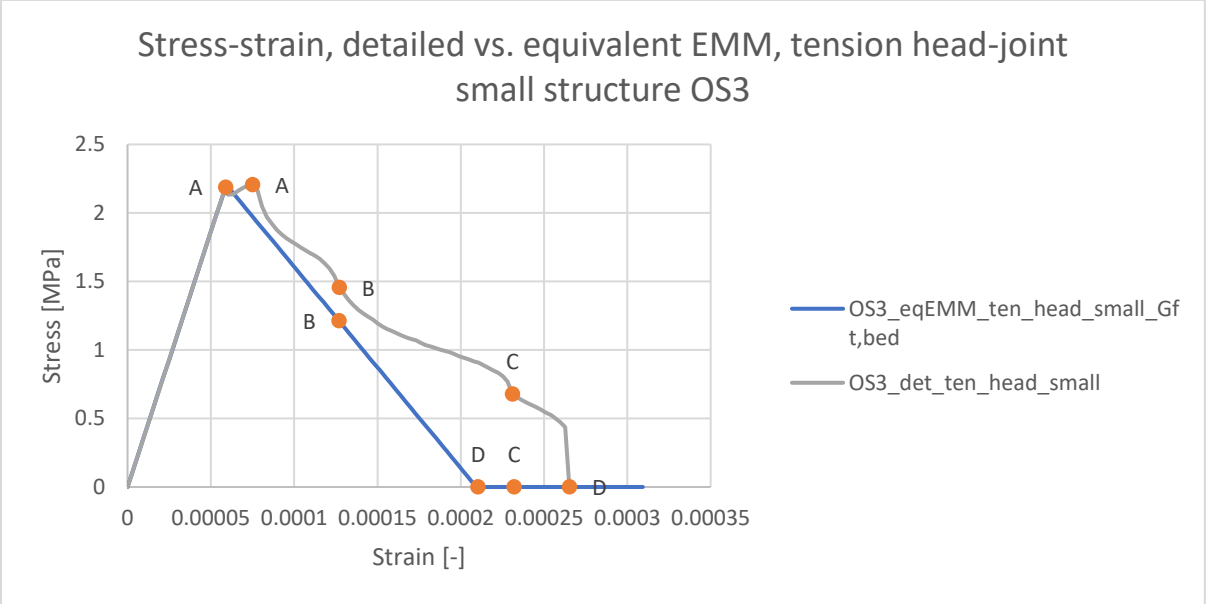

Figure 5.15: Stress-strain curves from tension head-joint models OS3_eqEMM_ten_head_small_$G_{ft,bed}$ & OS3_det_ten_head_small

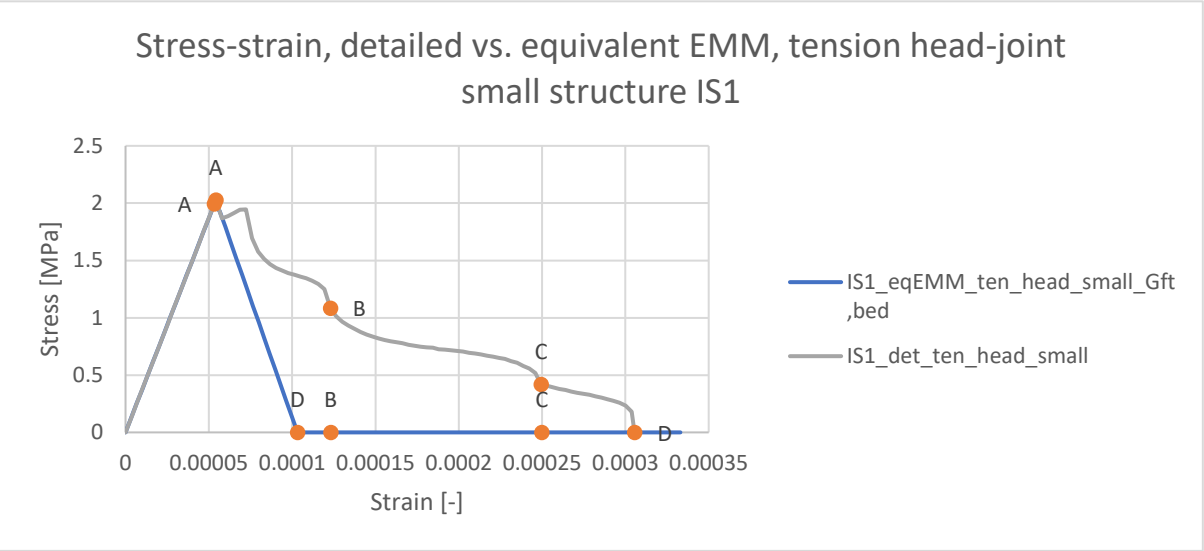

Figure 5.16: Stress-strain curves from tension head-joint models IS1_eqEMM_ten_head_small_$G_{ft,bed}$ & IS1_det_ten_head_small

The points A-D of the equivalent EMM models were determined as follows: point A is where the peak force occurs and point D shows the displacement where the force becomes 0 kN. The points B and C were chosen such that the displacement is equal to the displacement of points B and C in the results of the corresponding detailed model. As the input for E_x is equal to $E_{x,tension}$, the stiffness of the EMM models is exactly the same as the stiffness of the detailed models. As a result of having the same linear elastic behaviour, the peak force occurs at the same displacement value for both the EMM and the detailed models. This also means that the correct value for the head-joint strength is being used.

However, after the peak force has been reached, the curves do not match that well anymore. As the fracture energy $G_{ft,bed}$ was used in the models, the ultimate displacement is quite different in the equivalent EMM models. As a result, the point D occurs much sooner in the equivalent EMM models compared to the detailed models. As the points B and C are based on displacement values that were observed in the detailed models, the point D even occurs before B and/or C here. This shows that the used input parameters do not provide very good results here.

If the fracture energy of the head-joint tension models would have been used instead, the ultimate displacement of the EMM model would have matched much better. Similar to the E-modulus in y, an average value should be used of the 2 cases. Therefore, the fracture energy in tension will be based on the fracture energy obtained from the head-joint model, and the fracture energy obtained from the compression and bed-joint model (as calculated in the previous section). The new input value will be used in both the head-joint tension and the bed-joint tension models, as this will impact both of these load cases. The results of OS3_eqEMM_ten_head_small_$G_{ft,average}$, IS1_eqEMM_ten_head_small_$G_{ft,average}$, OS3_eqEMM_ten_bed_small_$E_{y,average}$_$G_{ft,average}$ and IS1_eqEMM_ten_bed_small_$E_{y,average}$_$G_{ft,average}$ are presented in appendix C (see appendix A for the explanation of the model names). Figures are presented below which include the stress-strain curves of the updated equivalent EMM model and their corresponding detailed model.

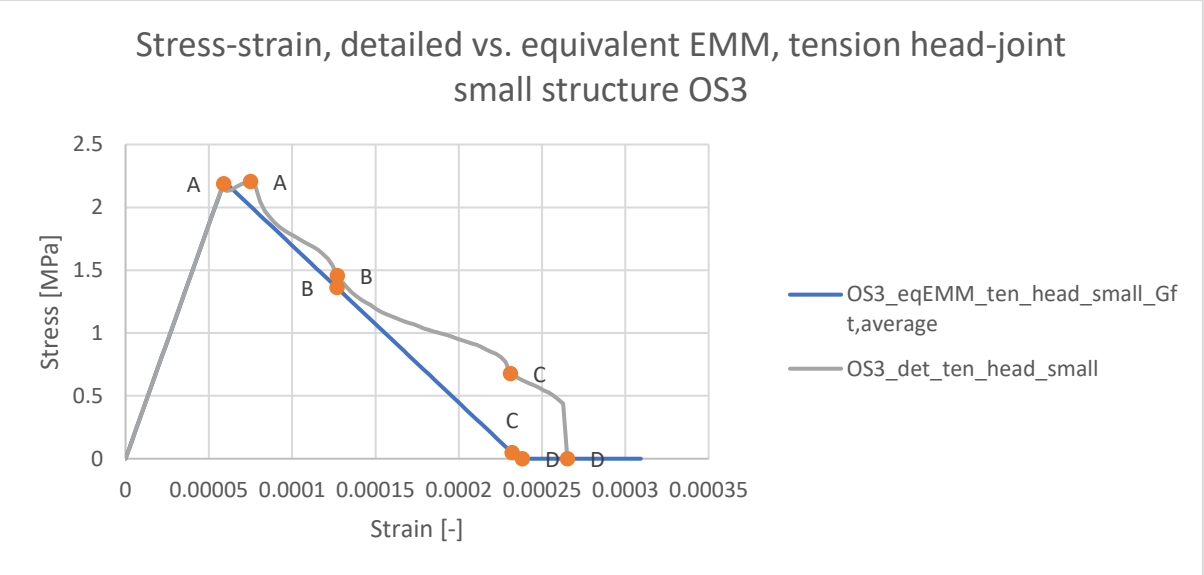

Figure 5.17: Stress-strain curves from tension head-joint models OS3_eqEMM_ten_head_small_$G_{ft,average}$ & OS3_det_ten_head_small

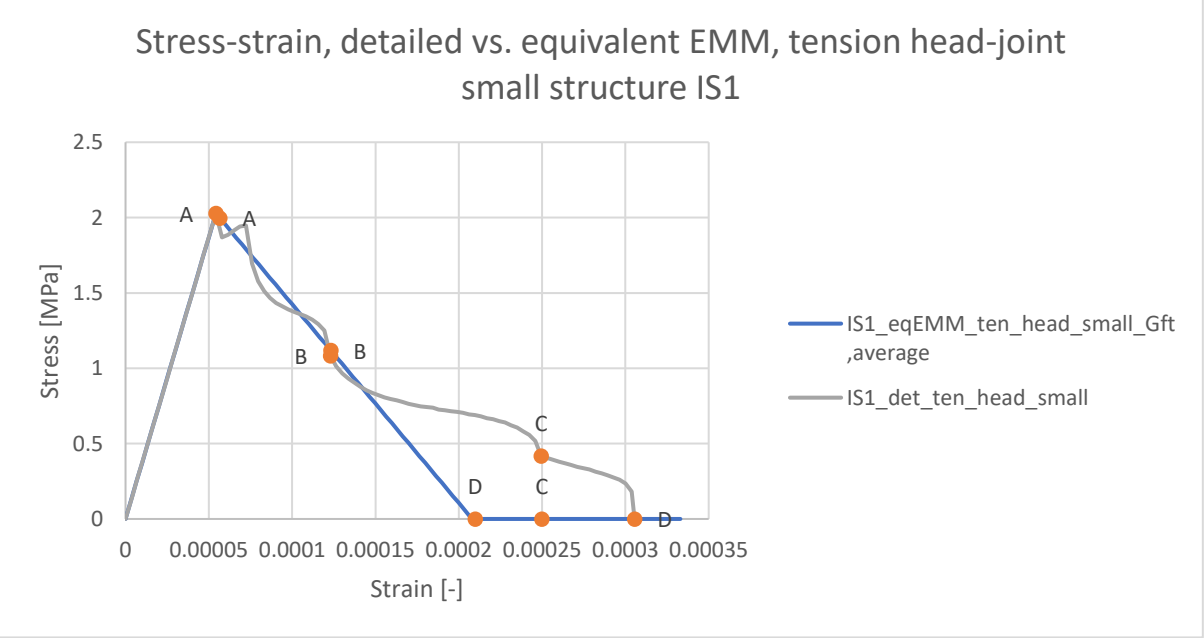

Figure 5.18: Stress-strain curves from tension head-joint models IS1_eqEMM_ten_head_small_$G_{ft,average}$ & IS1_det_ten_head_small

As a result of changing the fracture energy to the average value, the curves of the head-joint tension models give a much better match now. The ultimate displacement values are still lower for the equivalent EMM models, but the difference is much smaller now. The forces in the points B and C in the equivalent models are also much closer to the forces in those points in the detailed models.

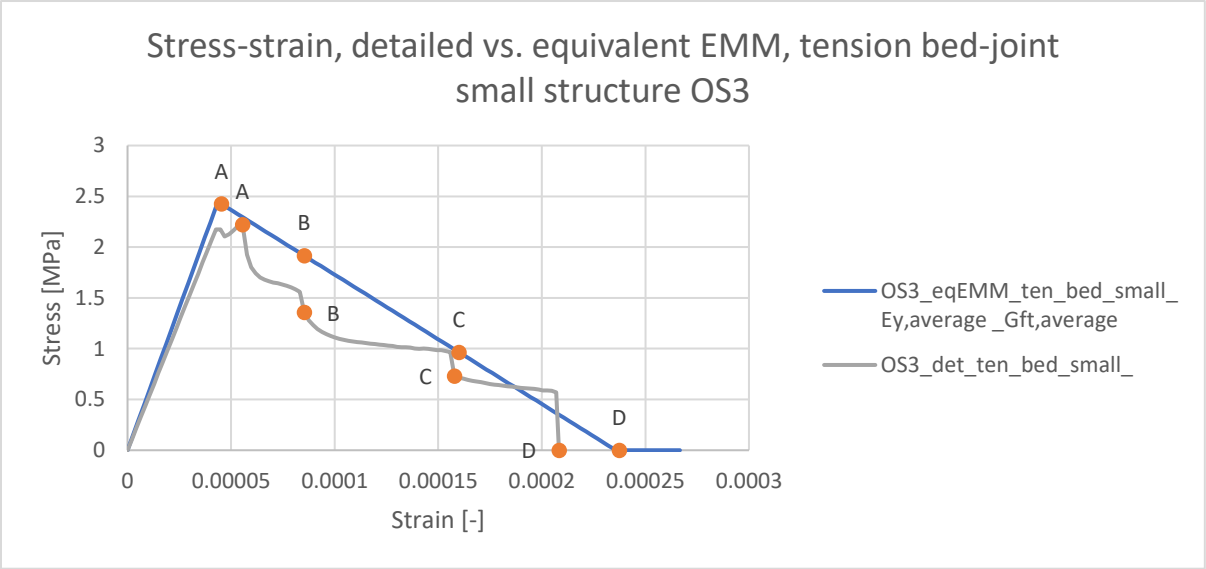

Figure 5.19: Stress-strain curves from tension bed-joint models OS3_eqEMM_ten_bed_small_$E_{y,average}$_$G_{ft,average}$ & OS3_det_ten_bed_small

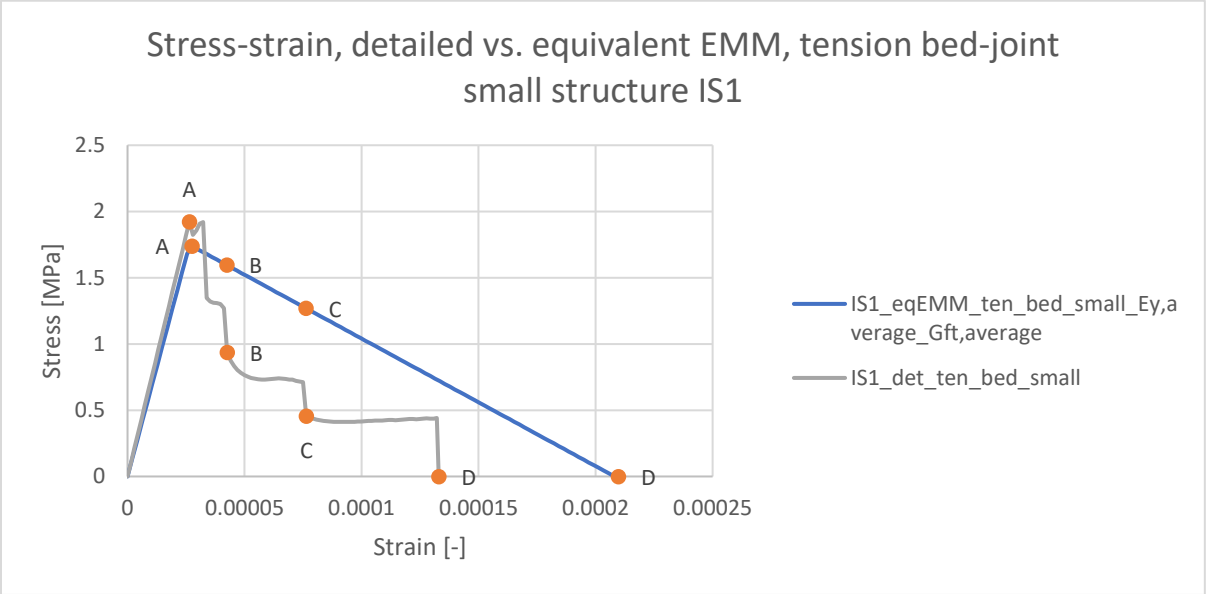

Figure 5.20: Stress-strain curves from tension bed-joint models IS1_eqEMM_ten_bed_small_$E_{y,average}$_$G_{ft,average}$ & IS1_det_ten_bed_small

As the fracture energy was also changed in the bed-joint models, the curves of the bed-joint tension equivalent EMM models have become slightly less similar as the curves of the detailed models. This mostly shows in the ultimate displacement of the equivalent EMM models, which has become larger. In the previous section, when $G_{ft,bed}$ was used for the fracture energy, it was observed for the models of section IS1 that the ultimate displacement of the equivalent EMM model was much lower than that of the detailed model. Now the average value was used, the ultimate displacement of the equivalent EMM model is now even larger than that of the detailed model. This shows that the value of the fracture energy has quite a large impact on the ultimate displacement.

5.3 Shear loading

Finally, the shear failure parameter should be verified. Equivalent EMM models will be created again, in which the boundary conditions are the same as in the detailed models. First, to ensure that the structure is loaded in pure shear, a mesh which consists of only 1 element is used in the equivalent EMM model. This means that the element size is equal to 2 times the plate size. Only the case where the compressive stress equals 0.5 MPa is considered for the verification of the parameters. The results of IS1_eqEMM_shear_small_σ0.5_one_el and IS1_eqEMM_shear_small_σ0.5_one_el are presented below (see appendix A for the explanation of the model names). After that, figures are presented which contain the stress-strain curves of the equivalent EMM model and their corresponding detailed model. The contour plots that are given in the presentation of the results of the models show the displacements in horizontal direction (x), which was also the case for the detailed models.

The points A-D have been determined as follows: point B is where the peak force occurs and point D is where the displacement load is fully applied. Points A and C are chosen such that the displacement in the equivalent EMM model is equal to the displacement in the corresponding detailed model.

a)

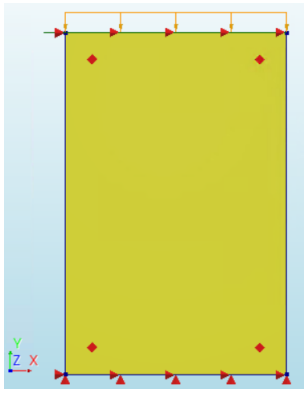

c)

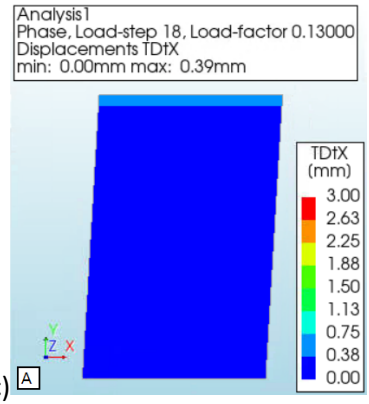

d)

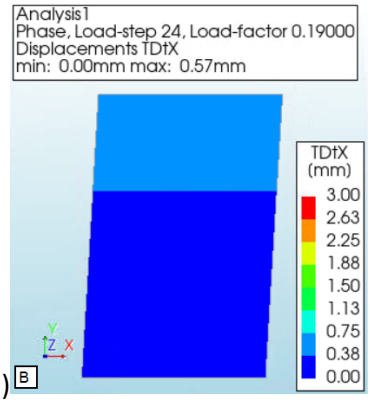

b)

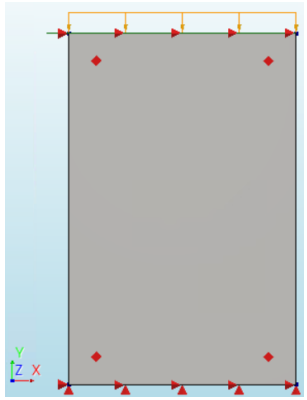

e)

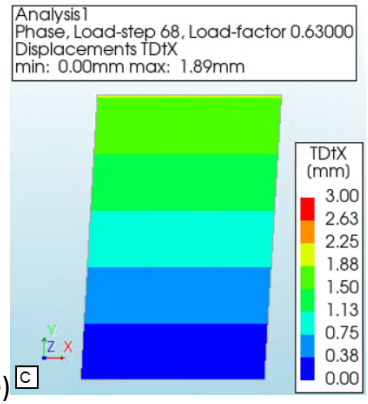

f)

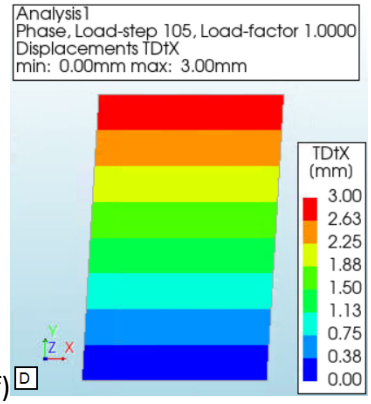

g)

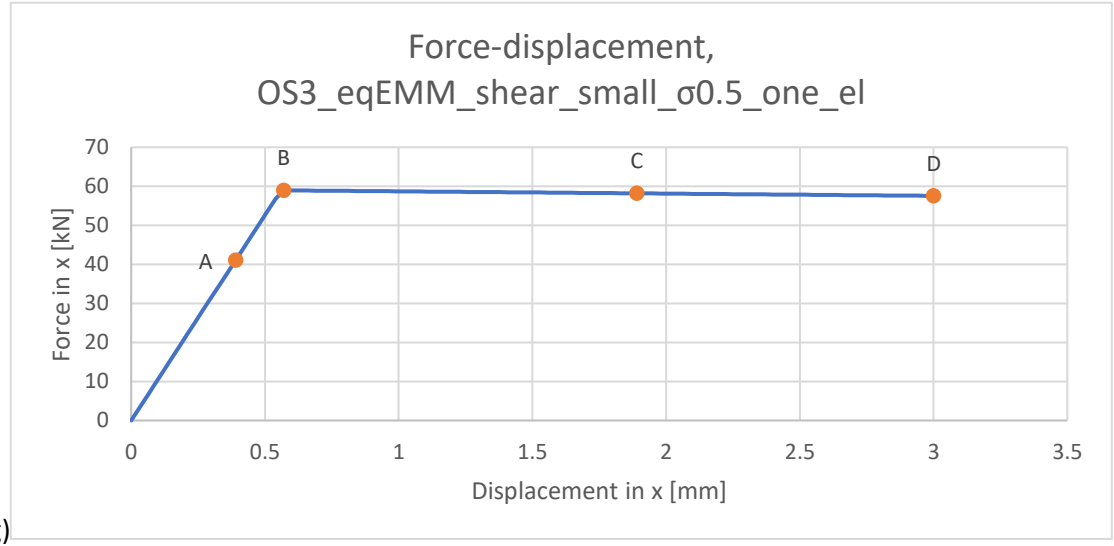

h)

Average element size [mm]		970x1500
Number of elements	Q20SH	1
Total number of nodes		4

i)

Load	Compression		Translation	
Iteration method	Secant (Quasi-Newton)		Secant (Quasi-Newton)	
Convergence norms	Force	Displacement	Force	Displacement
Convergence tolerances	0.01	0.01	0.01	0.01
Step size	0.2(5)		0.01(100)	
Maximum number of iterations per step	100		100	
All norms satisfied	No		No	

Figure 5.21: Results of finite element analysis OS3_eqEMM_shear_small_σ0.5_one_el. a-i: structure (a), finite element mesh (b), displacement at point A (c), displacement at point B (d), displacement at point C (e), displacement at point D (f), force-displacement curve (g), overview elements and nodes (h), overview iterative scheme (i)

a) b)

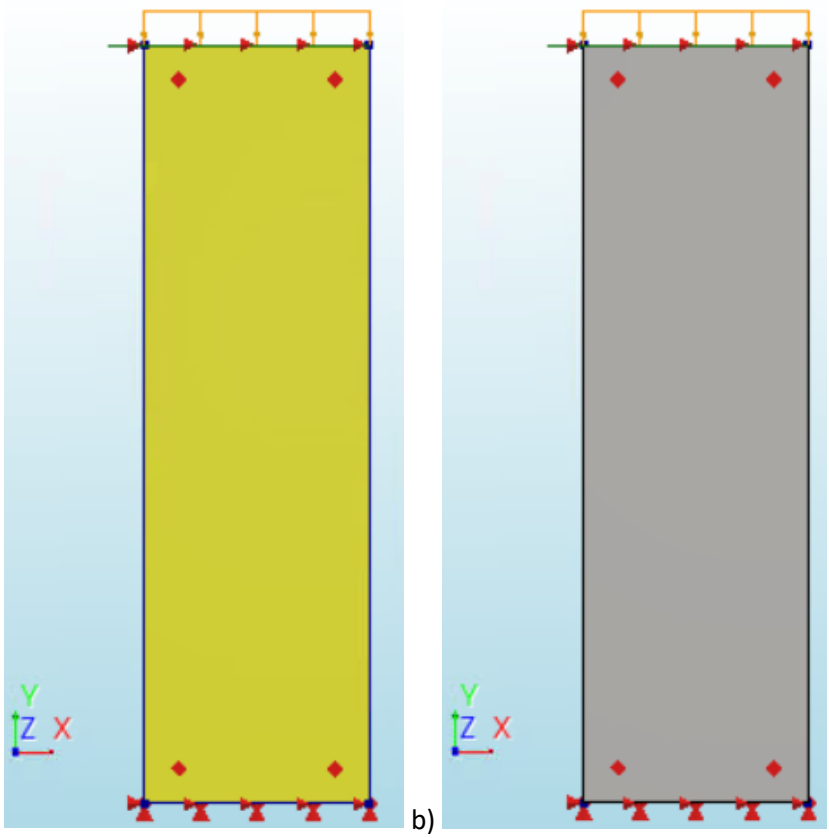

c)

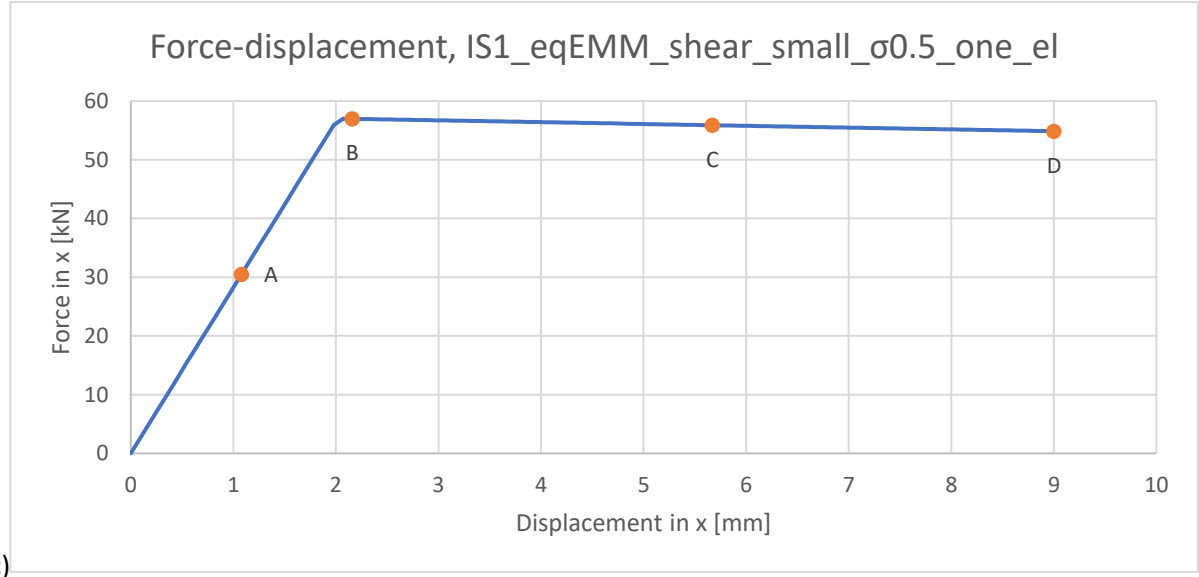

h)

Average element size [mm]		1051x3540
Number of elements	Q20SH	1
Total number of nodes		4

i)

Load	Compression		Translation	
Iteration method	Secant (Quasi-Newton)		Secant (Quasi-Newton)	
Convergence norms	Force	Displacement	Force	Displacement
Convergence tolerances	0.01	0.01	0.01	0.01
Step size	0.2(5)		0.01(100)	
Maximum number of iterations per step	100		100	
All norms satisfied	No		No	

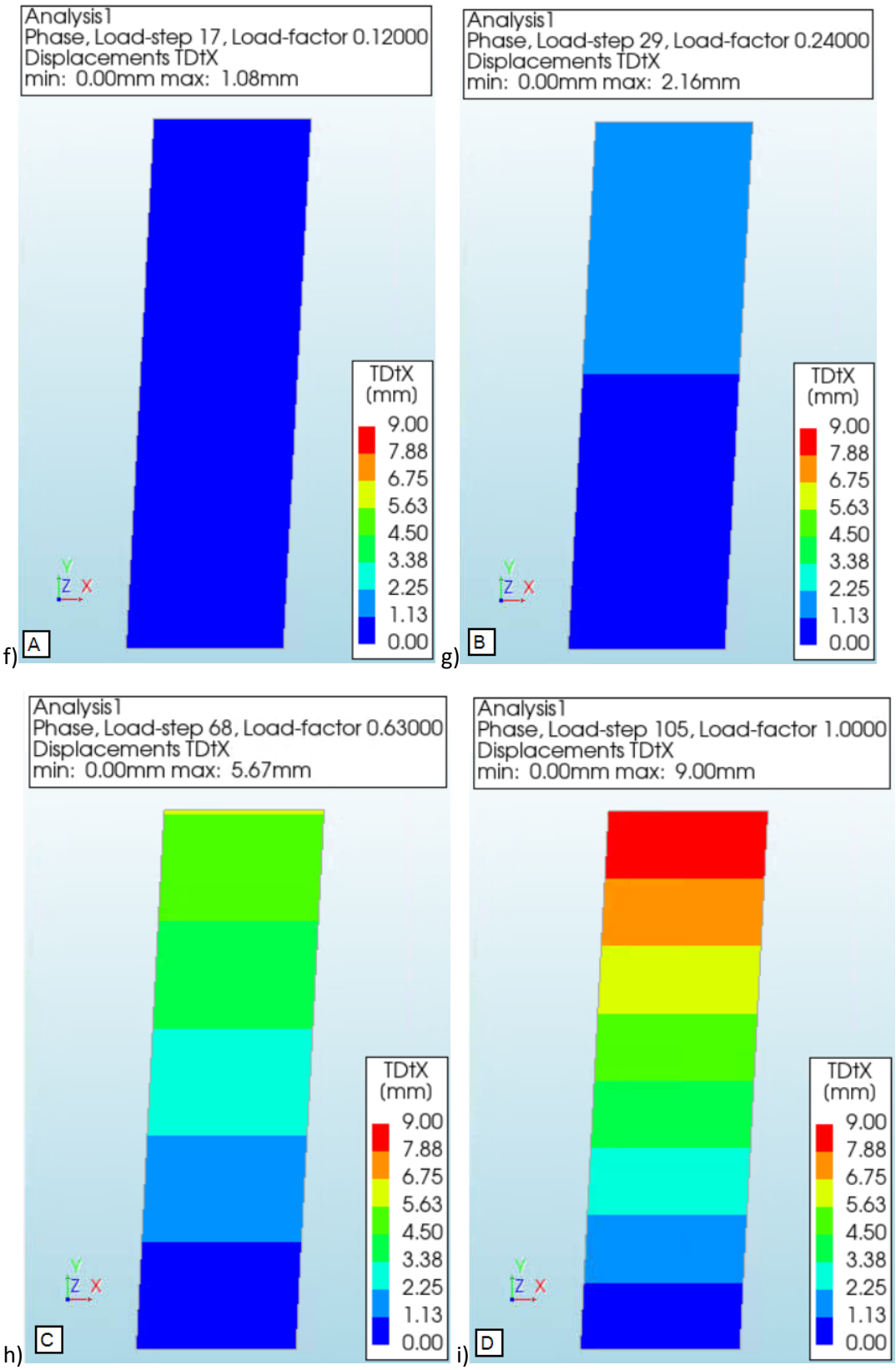

Figure 5.22: Results of finite element analysis IS1_eqEMM_shear_small_σ0.5_one_el. a-i: structure (a), finite element mesh (b), force-displacement curve (c), overview elements and nodes (d), overview iterative scheme (e), displacement at point A (f), displacement at point B (g), displacement at point C (h), displacement at point D (i)

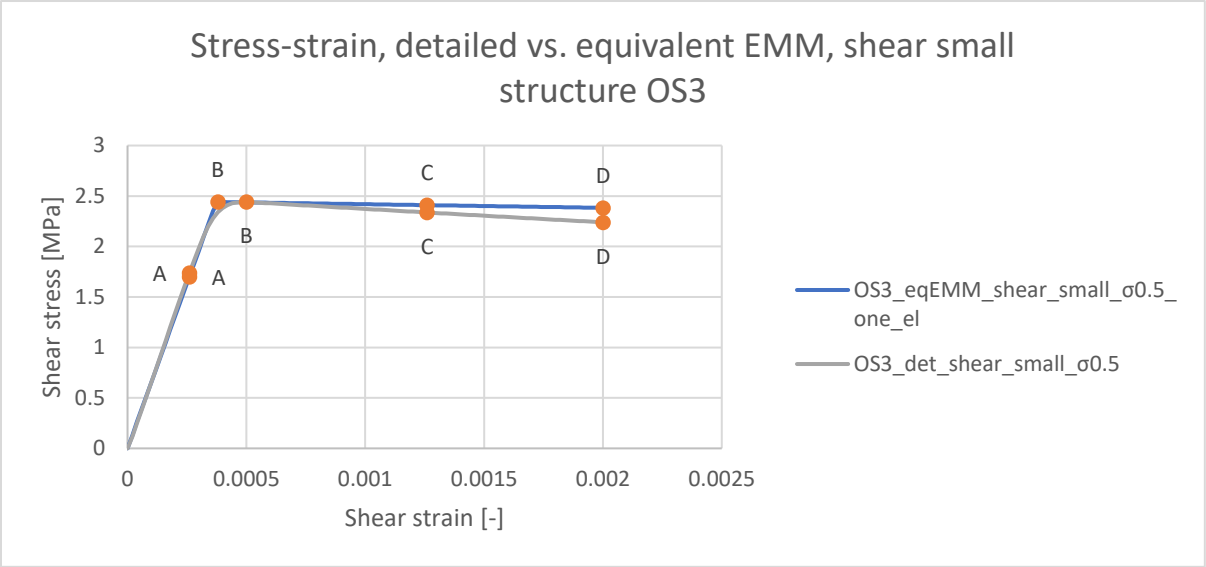

Figure 5.23: Stress-strain curves from shear models OS3_eqEMM_shear_small_σ0.5_one_el & OS3_det_shear_small_σ0.5

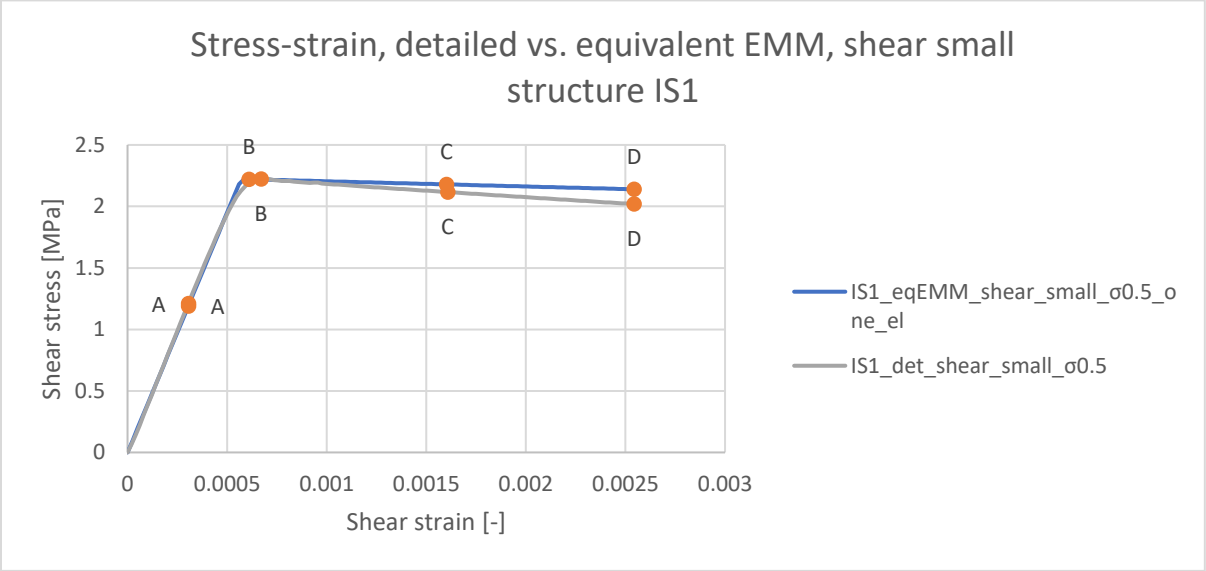

Figure 5.24: Stress-strain curves from shear models IS1_eqEMM_shear_small_σ0.5_one_el & IS1_det_shear_small_σ0.5

As mentioned, by using only one element for the structure, it is loaded in pure shear. It can be seen that the displacement at the peak is not exactly the same for the models, but it is still very close. Another difference between the curves is that the residual force of the detailed models is slightly lower than in the equivalent models. As the input value of the fracture energy in shear is quite high, the residual force is also quite high. In this case, even higher as the residual force of the detailed models. The points A and C of the curves almost coincide exactly as well. It is clear that the obtained input parameters provide good results when one element is used for the structure. Using one element allows the verification of the shear failure parameters, but using smaller elements will provide more realistic results, as this causes the model to be no longer loaded in pure shear, but also bending. The results of OS3_eqEMM_shear_small_σ0.5_mult_el and IS1_eqEMM_shear_small_σ0.5_mult_el are presented below. After that, figures are presented which contain the stress-strain curves of the equivalent EMM model and their corresponding detailed model. For the models of multiple elements, it was chosen to show the vertical strains in the contour plots.

a)

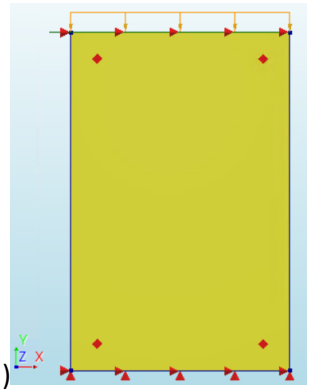

c)

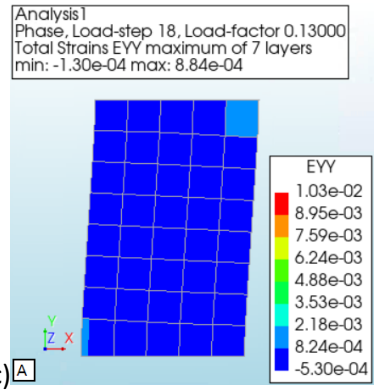

d)

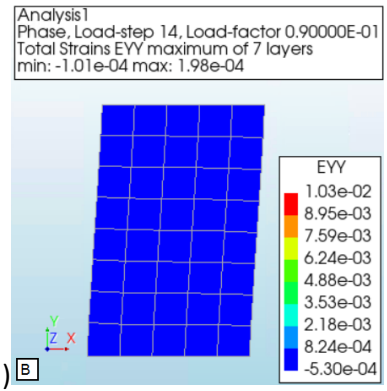

b)

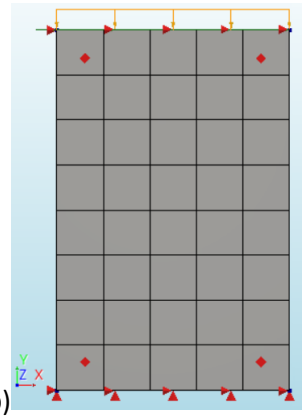

e)

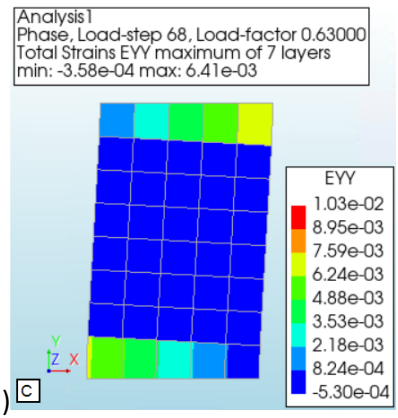

f)

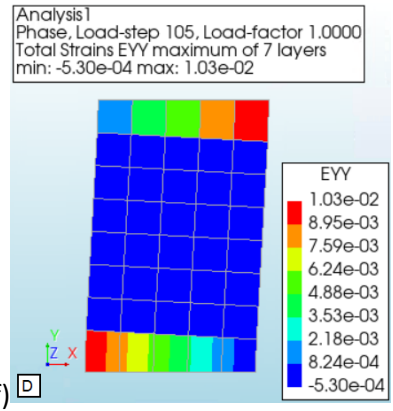

g)

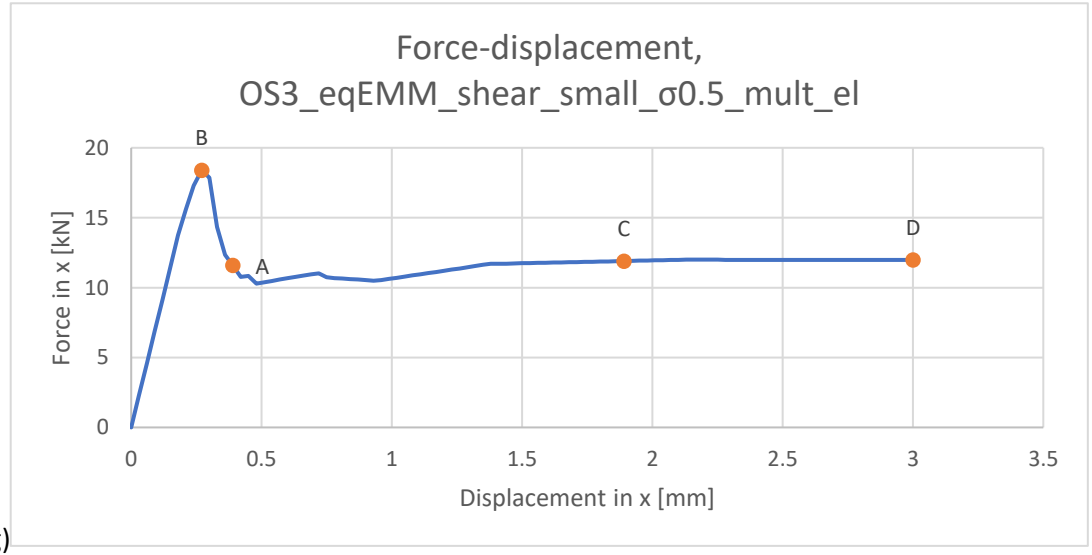

h)

Average element size [mm]		194x187.5
Number of elements	Q20SH	40
Total number of nodes		54

i)

Load	Compression		Translation	
Iteration method	Secant (Quasi-Newton)		Secant (Quasi-Newton)	
Convergence norms	Force	Displacement	Force	Displacement
Convergence tolerances	0.01	0.01	0.01	0.01
Step size	0.2(5)		0.01(100)	
Maximum number of iterations per step	100		100	
All norms satisfied	No		No	

Figure 5.25: Results of finite element analysis OS3_eqEMM_shear_small_σ0.5_mult_el. a-i: structure (a), finite element mesh (b), strain at point A (c), strain at point B (d), strain at point C (e), strain at point D (f), force-displacement curve (g), overview elements and nodes (h), overview iterative scheme (i)

a) b)

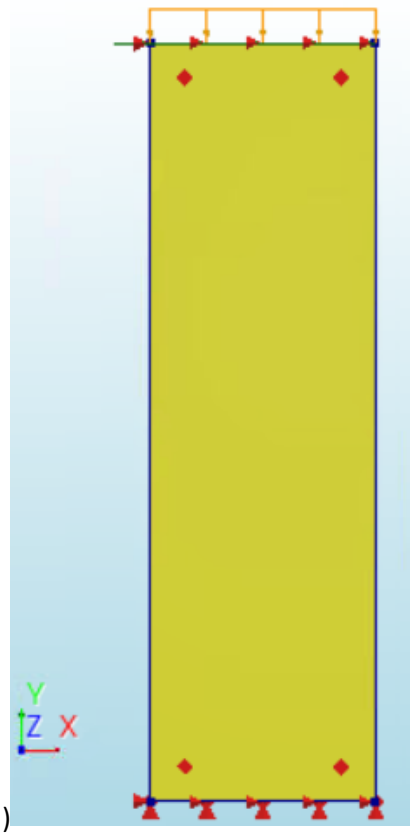

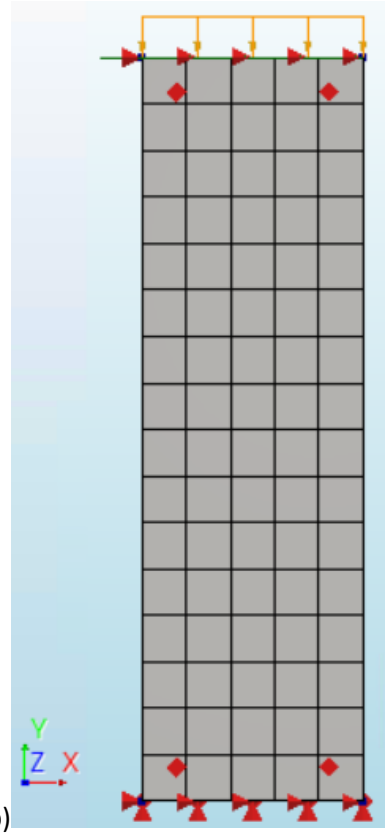

c)

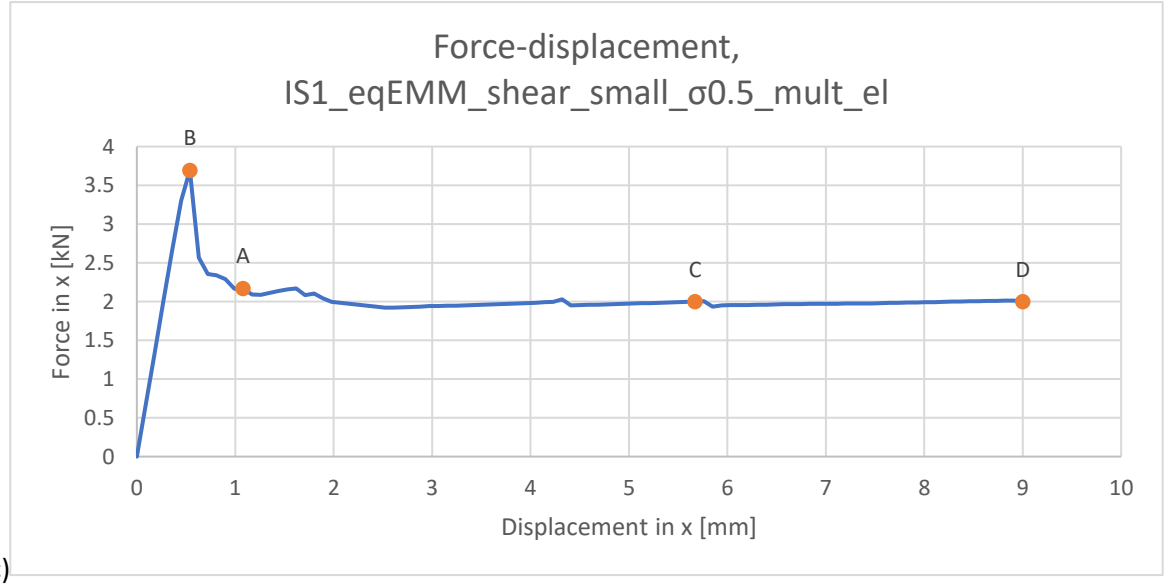

h)

Average element size [mm]		210.2x221.25
Number of elements	Q20SH	80
Total number of nodes		102

i)

Load	Compression		Translation	
Iteration method	Secant (Quasi-Newton)		Secant (Quasi-Newton)	
Convergence norms	Force	Displacement	Force	Displacement
Convergence tolerances	0.01	0.01	0.01	0.01
Step size	0.2(5)		0.01(100)	
Maximum number of iterations per step	100		100	
All norms satisfied	No		No	

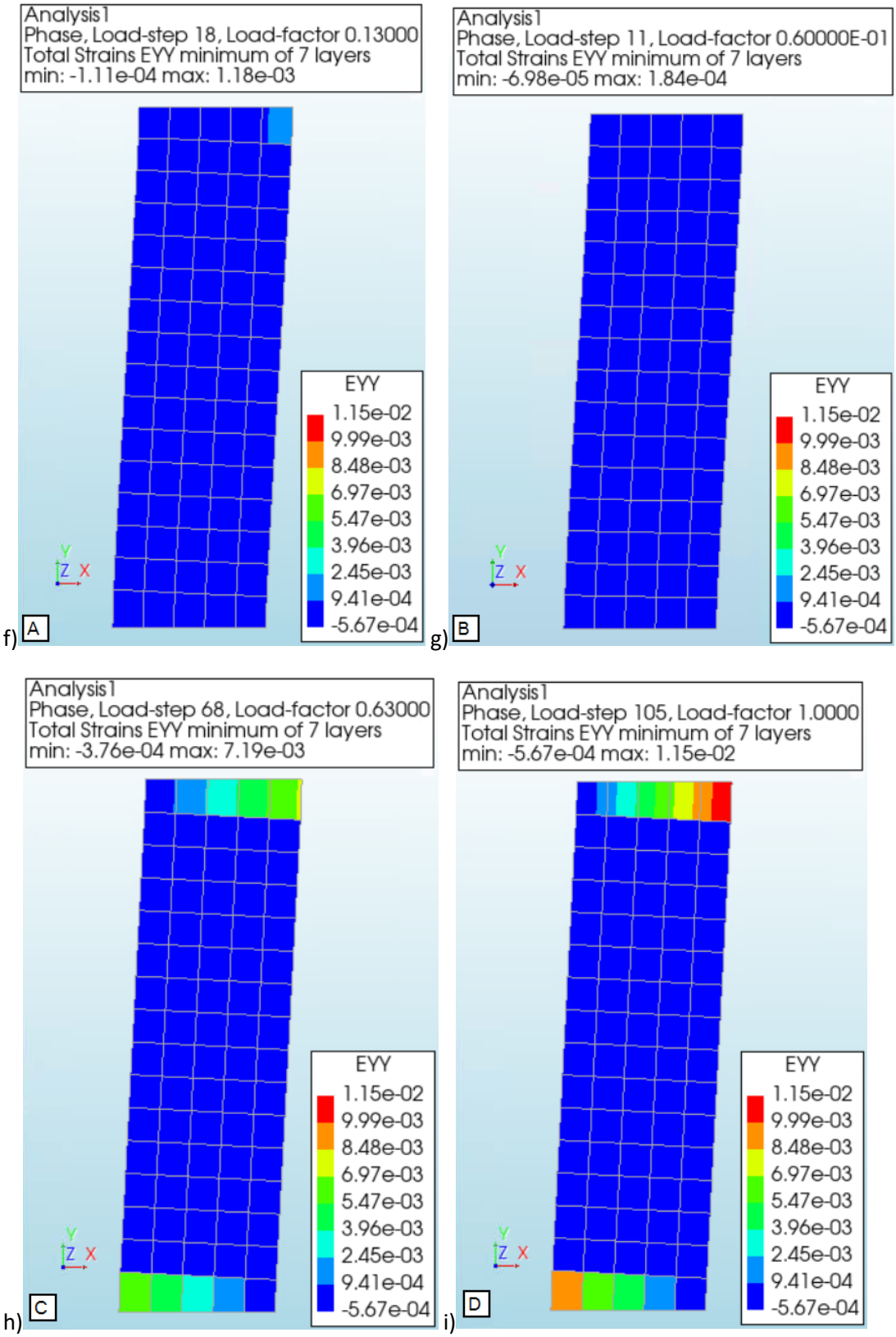

Figure 5.26: Results of finite element analysis IS1_eqEMM_shear_small_σ0.5_mult_el. a-i: structure (a), finite element mesh (b), force-displacement curve (c), overview elements and nodes (d), overview iterative scheme (e), strain at point A (f), strain at point B (g), strain at point C (h), strain at point D (i)

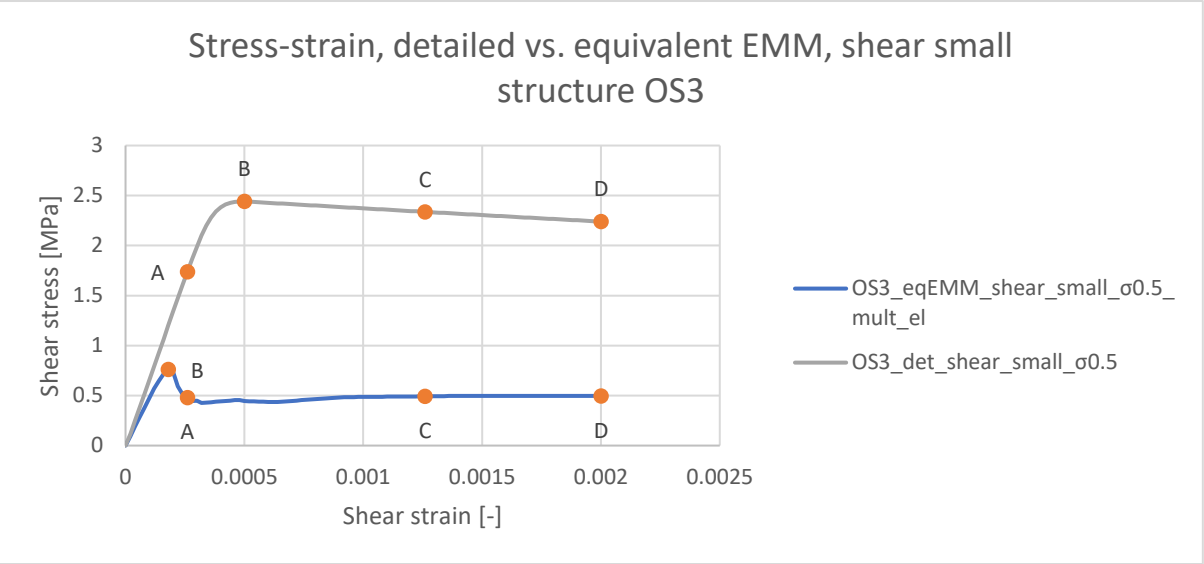

Figure 5.27: Stress-strain curves from shear models OS3_eqEMM_shear_small_σ0.5_mult_el & OS3_det_shear_small_σ0.5

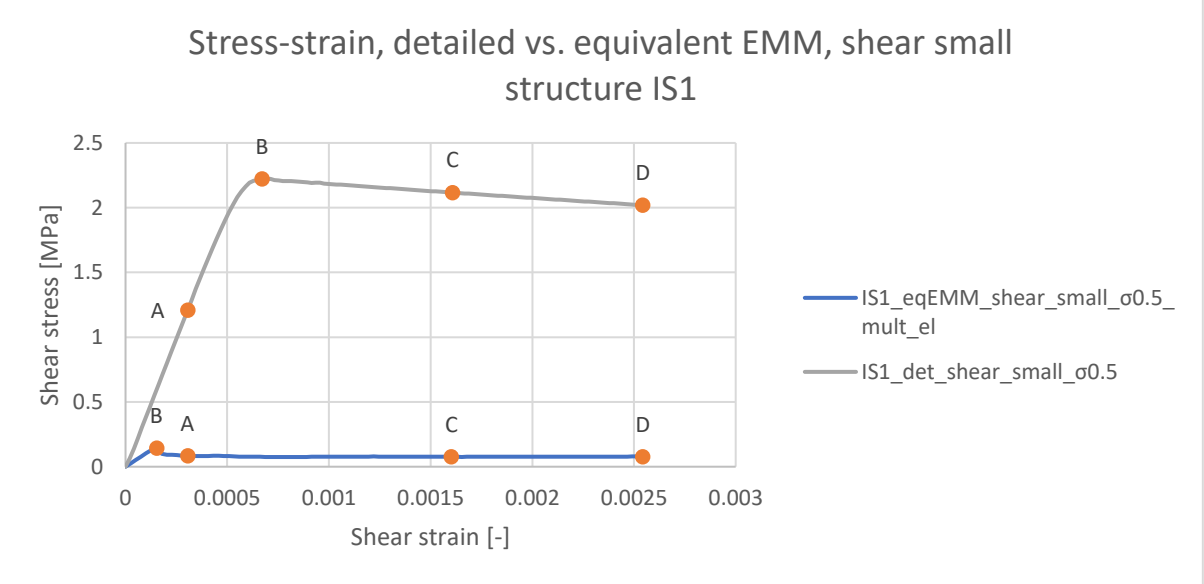

Figure 5.28: Stress-strain curves from shear models IS1_eqEMM_shear_small_σ0.5_mult_el & IS1_det_shear_small_σ0.5

Due to bending of the plates, tensile stresses in y-direction will develop as rotation of the plate is prevented. As the tensile strength of the material is quite low, the stresses will exceed the strength quite easily. As the tensile stresses exceed the tensile strength of the material, cracks will start to appear, which is clearly visible in the contour plots where the vertical strain is shown. This already happens for small shear displacements, which is why the peak force (point B) is much lower and occurs much sooner than in the detailed models. As point A is based on a displacement value of the detailed models, point B will occur before point A in the equivalent EMM models. From the results of the equivalent EMM model with one element, it can be concluded that the input parameters are correct. However, when a smaller mesh is used, it is clear that the behaviour of the equivalent EMM model does not match the behaviour of the detailed model when loaded in shear. It is important to keep this in mind when the EMM will be used in a model of the lighthouse. In the figure below, the failure modes of the different models loaded in shear are presented for section OS3.

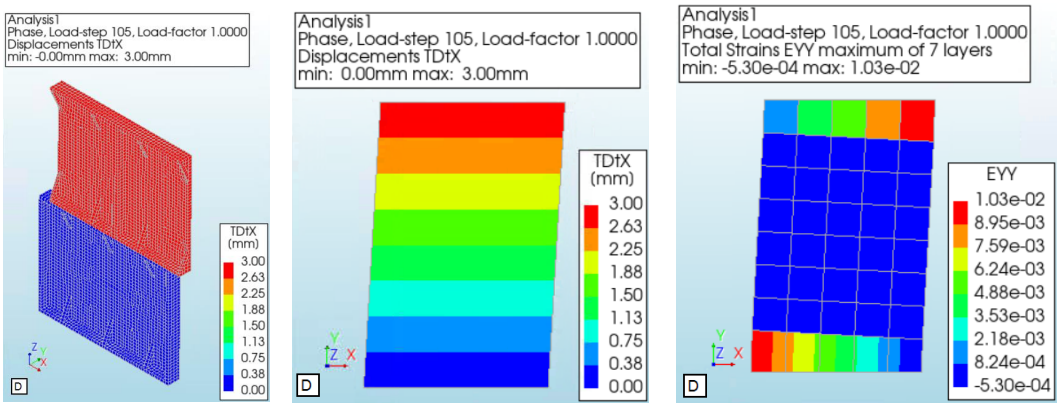

Figure 5.29: Failure mode at point D in shear for detailed model (left), equivalent EMM model with 1 element (middle) and equivalent EMM model with multiple elements (right), section OS3

From the contour plots that are given, it is clear to see the differences between the failure modes. The detailed models shows shear failure, but the failure is focused at the bed-joint. The equivalent EMM model with 1 element is loaded in pure shear, which results in uniformly distributed horizontal displacements in the structure. The model with multiple elements also experiences bending, which results in tensile stresses in the structure. As they exceed the strength of the material, cracks start to form.

5.4 Overview parameters for all sections

All required EMM parameters have been obtained by analysing detailed models of small structures. After using them in equivalent EMM models and comparing the results, it was determined which parameters were correct, and which parameters had to be calibrated. The calibrated parameters are: the E-modulus in y-direction, bed-joint tensile strength, angle between cracks, compressive strength and the factor to strain at compressive strength. The resultant values of the parameters are given in the tables below, where each table provides the parameters of a specific category.

Table 5.1: Elasticity parameters

Section	E-modulus in x-direction [MPa]	E-modulus in y-direction [MPa]	G-modulus [MPa]
OS1	47916.2	51292.1	6915.2
OS2	46164.9	53167.1	6829.0
OS3	37234.6	56117.4	6534.4
IS1	37385.0	66131.9	3899.2
IS2	32389.3	64973.7	3093.2
IS3	28253.3	71675.2	2633.1

Table 5.2: Cracking parameters

Section	Bed-joint tensile strength [MPa]	Head-joint tensile strength [MPa]	Fracture energy in tension [N/mm]	Angle between cracks [rad]
OS1	1.832	1.706	0.0457	0.241
OS2	2.059	2.079	0.0541	0.289
OS3	2.447	2.206	0.0778	0.369
IS1	1.749	2.028	0.0555	0.700
IS2	2.031	2.426	0.1292	0.774
IS3	2.812	2.714	0.2522	0.858

Table 5.3: Crushing parameters

Section	Compressive strength [MPa]	Fracture energy in compression [N/mm]	Factor to strain at compressive strength	Unloading factor
OS1	236.12	345.02	1.486	0
OS2	251.32	383.82	1.659	0
OS3	274.43	477.62	1.875	0
IS1	272.04	551.36	2.287	0
IS2	283.74	578.36	2.263	0
IS3	311.12	710.90	2.543	0

Table 5.4: Shear failure parameters

Section	Friction angle [rad]	Cohesion [MPa]	Fracture energy shear [N/mm]
OS1	0.378	1.518	345.02
OS2	0.376	1.832	383.82
OS3	0.376	2.244	477.62
IS1	0.338	2.047	551.36
IS2	0.356	1.861	578.36
IS3	0.313	2.556	710.90

6 Analysing the size effect

In the previous chapter, it was verified that by using the (adjusted) obtained EMM parameters in equivalent models, similar results are obtained as from the analyses of the detailed models. However, this verification only states that the parameters provide the correct output for those specific structures. The structure of the lighthouse consists of many more plates, so it should be checked if and how the obtained parameters will be affected by increasing the size of the structure that is analysed with an equivalent EMM, while using the input EMM parameters that are obtained from detailed models of small structures. Slightly larger models will be created, consisting of an assembly of multiple plates and connections. The force-displacement curves of those models will show how the parameters might be influenced by this size effect. The results of this section will provide an answer to the second sub-question.

6.1 Tension loading

Now that all the obtained EMM parameters have been verified for those specific models, the next step is to increase the size of the structure and see if the obtained EMM parameters still provide similar results. The size of the structure will be increased such that it consists of an assembly of multiple plates and the structure will therefore also include multiple joints. The final step of this study is to analyse a model in which the complete lighthouse structure is present. Therefore, the size of the structures that will be analysed is determined by using the lighthouse as a reference.

In width, the sections will still be equal to the size of 1 plate. As discussed earlier in the report, the outer column has the shape of a hexadecagon, where each side is has the width of 1 plate. It is therefore the most logical size to use for the section width. For the height, the floor height shall be used. The floors will provide stability and strength to the structure, so failure is most likely to happen within the floor height. The section height is therefore equal to 4 times the plate height for the sections of the outer column and 2 times the plate height for the inner column sections.

For the tensile models, this means only a few structures have to be increased in size and analysed again. The head-joint models already had the width of one plate. As the section width is not increased, these results are still valid for the determination of the tension parameters for loads in this direction. For the bed-joint models, only the models of the outer sections have to be increased. The models of the inner sections were 2 plates in height, which is already equal to the floor height. The bed-joint models of the outer sections will be increased from 2 to 4 plates in height. Again, a tensile displacement will be applied on the top face in the normal direction to the bed-joint, which will introduce forces in this direction. The left side is supported in x and the bottom is supported in y and z. The support in z at the top is required for the prescribed deformation load, which is in the positive z direction. The results of OS3_det_ten_bed_large (see appendix A for the explanation of the model names) are presented below. For the results of the other sections, see appendix C. Additionally, a figure is presented which contains the stress-strain curves of the large detailed model and the small detailed model of section OS3.

a) b)

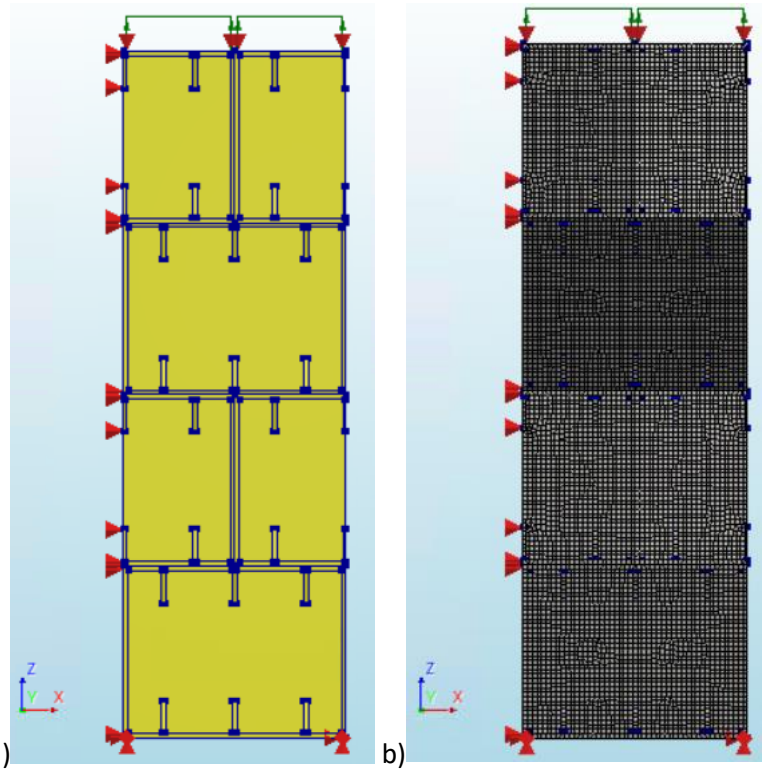

c)

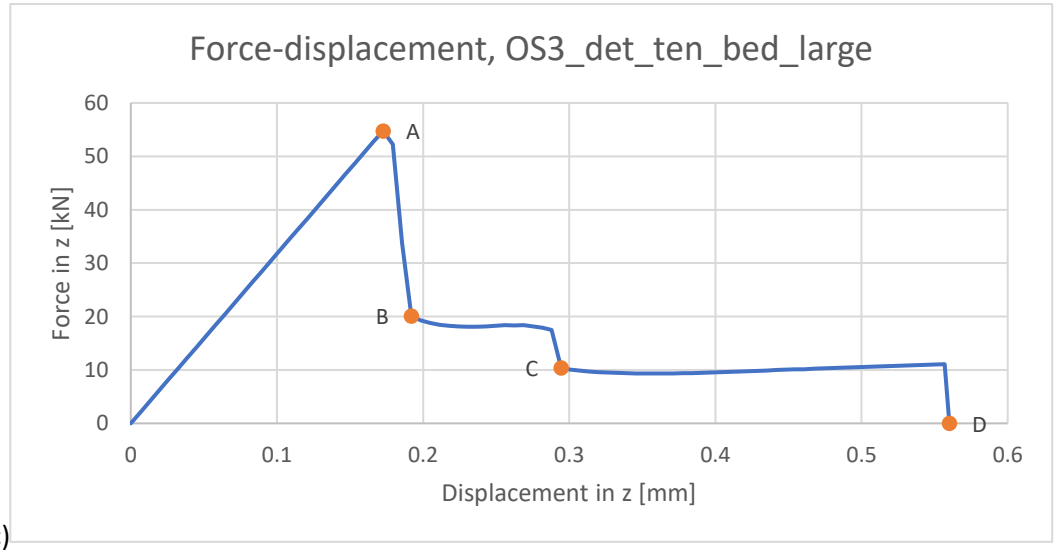

d)

Average element size [mm]		20x20
Number of elements	HX24L	9136
	PY15L	1715
	TE12L	1204
	TP18L	410
	Q24IF	880
Total number of nodes		20609

e)

Iteration method	Newton-Raphson	
Convergence norms	Displacement	Force
Convergence tolerances	0.01	0.01
Step size	0.01(100)	
Maximum number of iterations per step	100	
All norms satisfied	No	

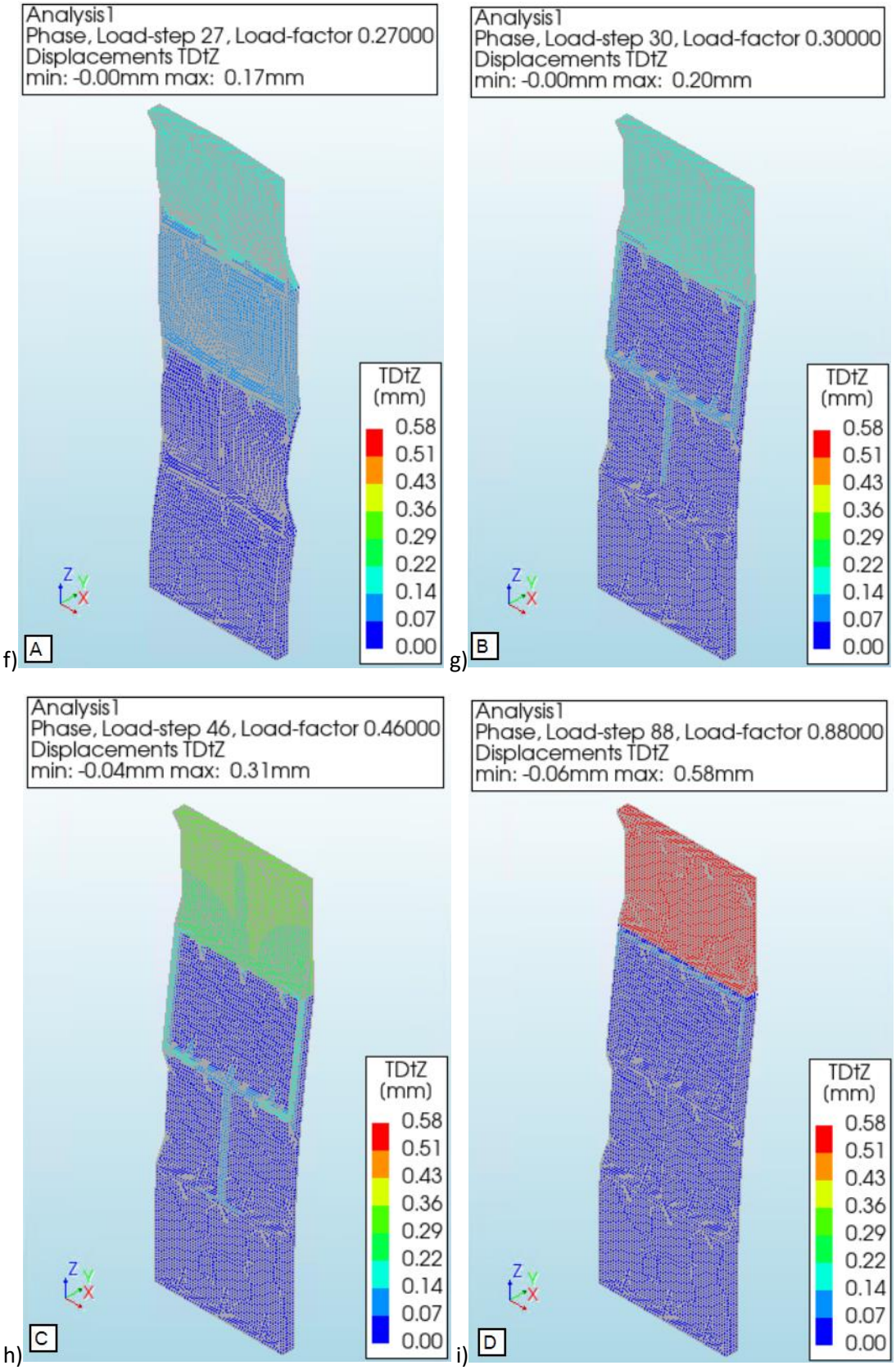

Figure 6.1: Results of finite element analysis OS3_det_ten_bed_large. a-i: structure (a), finite element mesh (b), force-displacement curve (c), overview elements and nodes (d), overview iterative scheme (e), displacement at point A (f), displacement at point B (g), displacement at point C (h), displacement at point D (i)

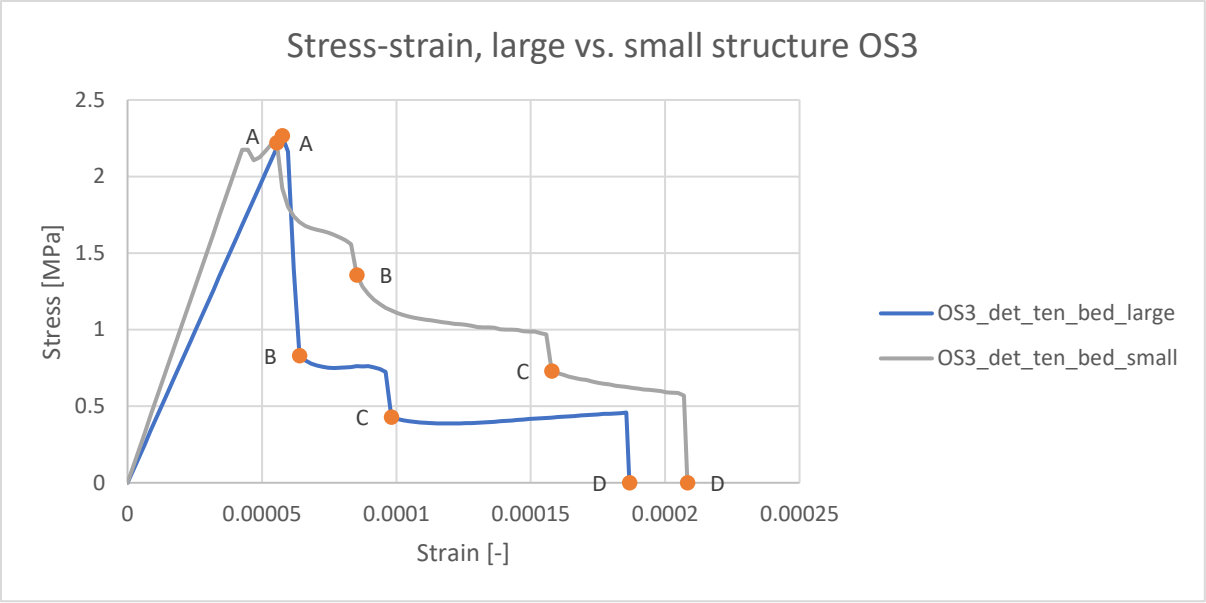

Figure 6.2: Stress-strain curves from tension bed-joint models OS3_det_ten_bed_large & OS3_det_ten_bed_small

The points A-D are chosen in the same way as for the small detailed model: point A is where the peak force occurs, point D where the ultimate displacement occurs and at points B and C there is a sudden drops in the force. It can be observed here that the models are actually very similar. The peak stress is almost exactly the same, but there are some small differences in the stiffness and the ultimate strain. This is what was expected, as the joints are exactly the same in both models, so both have the exact same tensile strength. From the contour plots, it is also clear that the failure mode is the same as what was observed in the small detailed model OS3_det_ten_bed_small, which was analysed in section 4.1. The figure below shows the vertical displacements in point D for both structures.

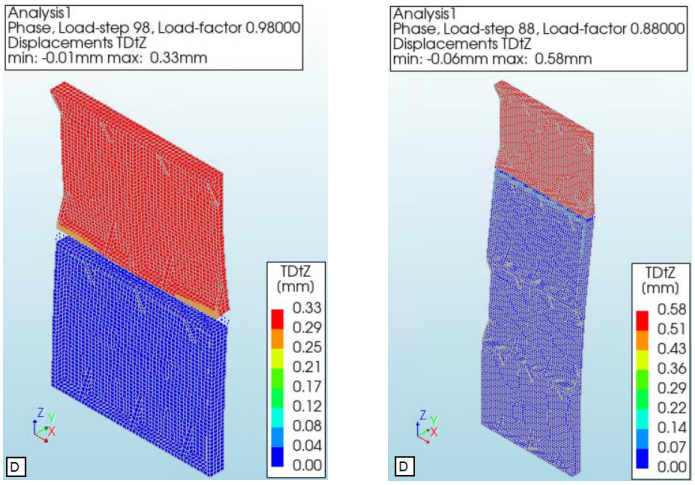

Figure 6.3: Vertical displacements at point D, tension bed-joint models small structure (left) and large structure (right), section OS3

Now, an equivalent EMM model of the large structure can be analysed where all boundaries and loads are the same as in the detailed model. The parameters of section 5.4 will be used, which are based on the results of the small models. This will show if the obtained parameters will still provide good results when the structure size is increased. The results of OS3_eqEMM_ten_bed_large_ sq1_parameters are presented in the figure below (see appendix A for the explanation of the model names). Additionally, a figure is presented that contains the stress-strain curves of the equivalent EMM model and the detailed model.

a) b)

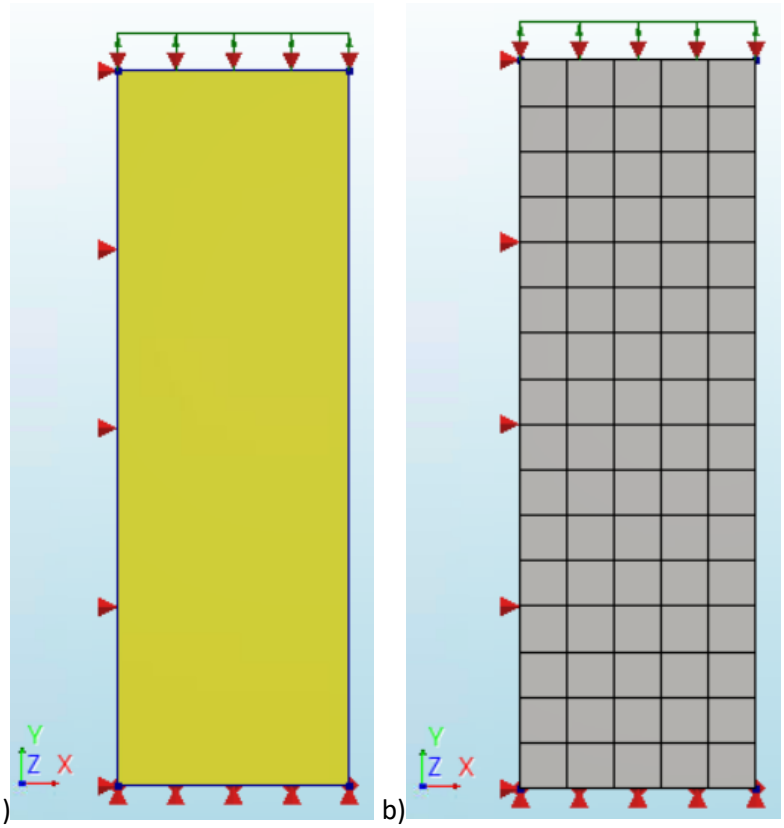

c)

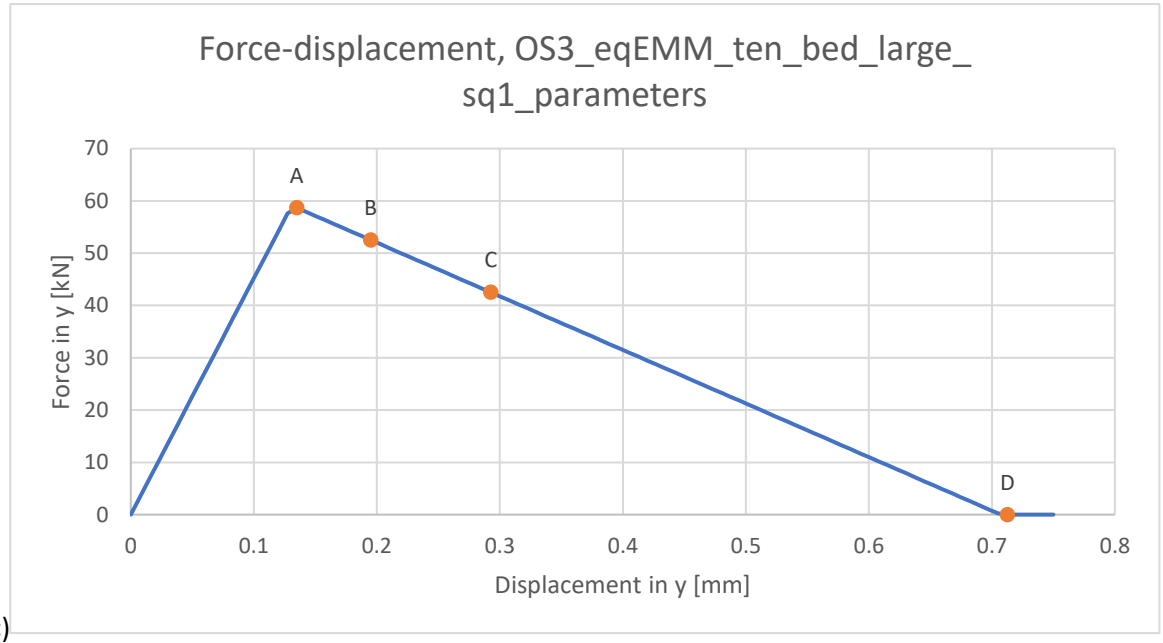

d)

Average element size [mm]		194x187.5
Number of elements	Q20SH	80
Total number of nodes		102

e)

Iteration method	Secant (Quasi-Newton)	
Convergence norms	Displacement	Force
Convergence tolerances	0.01	0.01
Step size	0.01(100)	
Maximum number of iterations per step	100	
All norms satisfied	No	

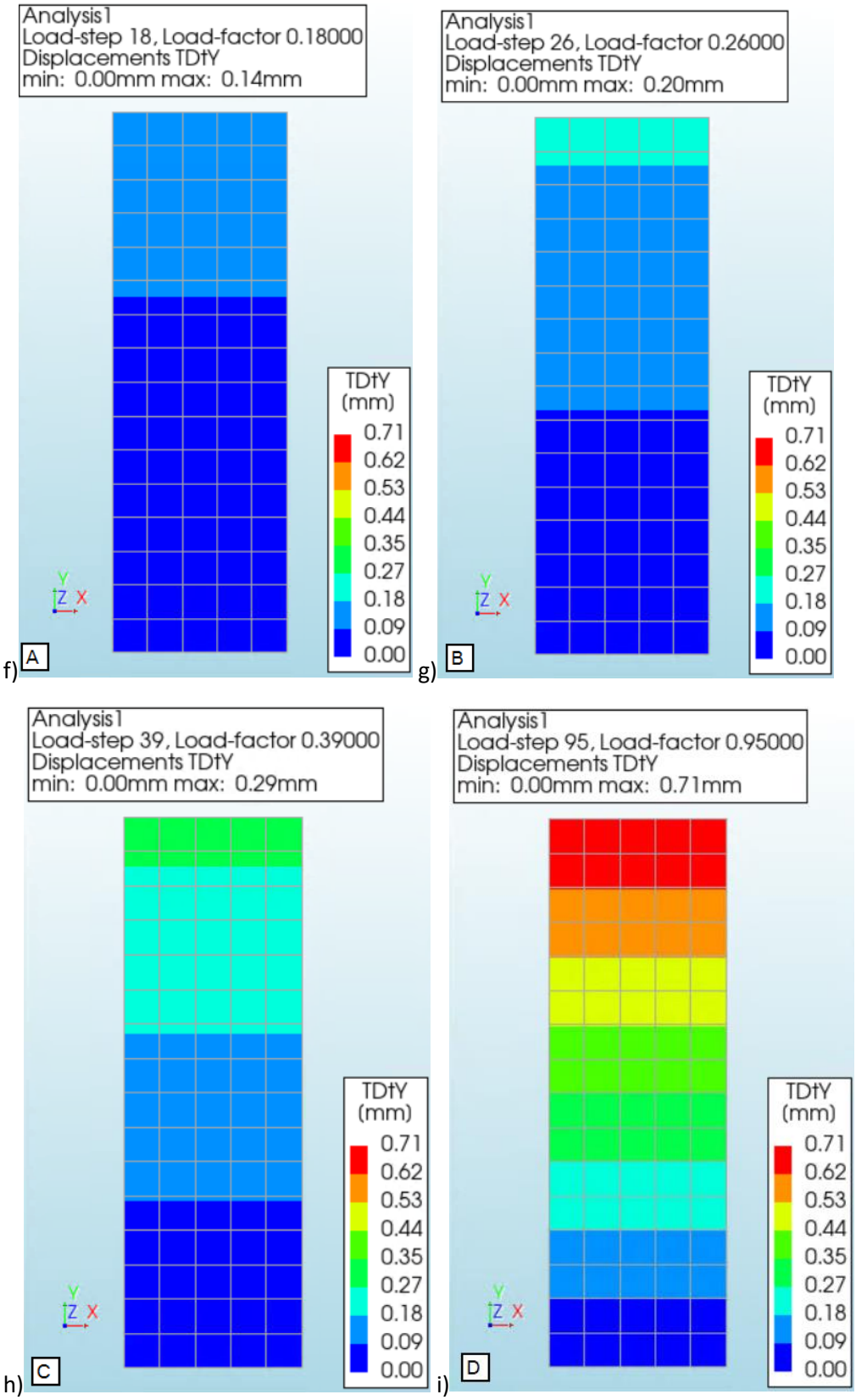

Figure 6.4: Results of finite element analysis OS3_eqEMM_ten_bed_large_sq1_parameters. a-i: structure (a), finite element mesh (b), force-displacement curve (c), overview elements and nodes (d), overview iterative scheme (e), displacement at point A (f), displacement at point B (g), displacement at point C (h), displacement at point D (i)

From the contour plots that are presented, it is clear that the failure modes of the equivalent EMM models loaded in tension are the same for the small and large structures when the EMM is used.

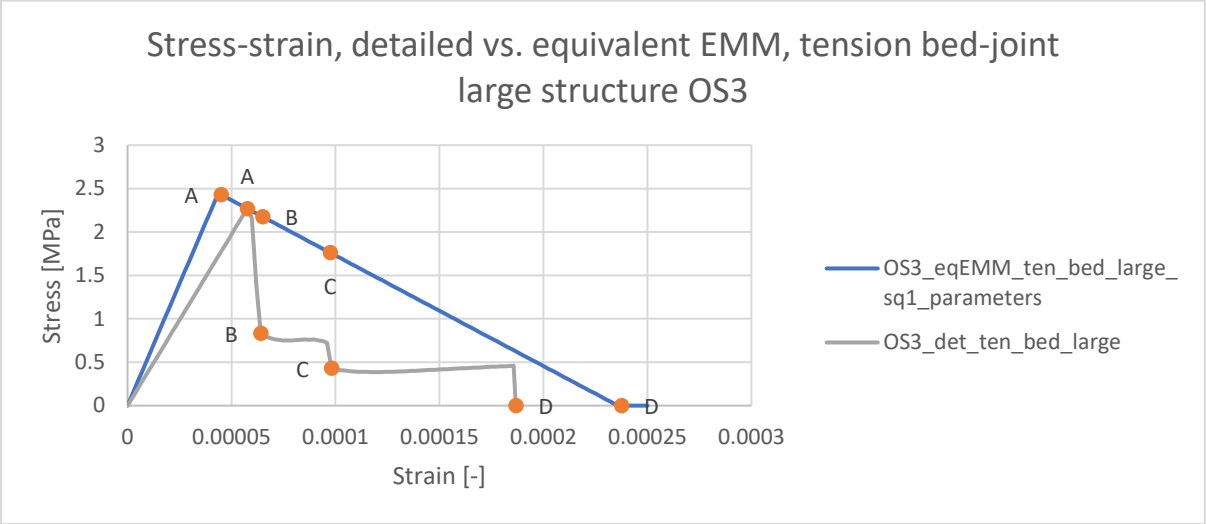

Figure 6.5: Stress-strain curves from tension bed-joint models OS3_eqEMM_ten_bed_large_sq1_parameters & OS3_det_ten_bed_large

The points A-D of the equivalent EMM model were determined in the same way as for the equivalent EMM model of the small structures: point A is where the peak force occurs and point D shows the displacement where the force becomes 0 kN. The points B and C were chosen such that the displacement is equal to the displacement of points B and C in the results of OS3_det_ten_bed_large.

From the figure of the stress-strain curves, it is clear that the results of the models match quite well, but there are some small differences. The stiffness of the detailed model is slightly lower than that was used in the equivalent EMM model. The maximum tensile stress is slightly lower as well, but as explained in the previous chapter, the bed-joint strength was adjusted, as the average of $E_{y,tension}$ and $E_{y,compression}$ was used for E_y. For the case of section OS3, it meant that the bed-joint strength was increased, thus the maximum tensile force is expected to be slightly higher. As $G_{ft,average}$ was used for the fracture energy, this also results in a slightly larger ultimate displacement in the equivalent EMM model. It is clear that the EMM parameters that are related to the bed-joint tension failure of the outer sections should be adjusted slightly. The new parameters will provide more accurate results for the EMM models of the larger structure and are also expected to provide better results when used in the final model of the lighthouse. An overview of the final EMM parameters will be provided in section 6.4 of this chapter.

6.2 Compression loading

For compression, only a single plate was analysed for all sections in the previous chapter. In this chapter, the structure size will be increased such that the height of the structure matches the floor height. The structures of the outer section will consist of 4 plates in height, while the structures of the inner sections will have a height of 2 plates. The bottom of the structure is supported in x, y and z, while the top is supported in y. The top face will also be supported in z to function as a reference for the prescribed deformation load, which displaces the top face in the negative z-direction. The results of OS3_det_comp_large and IS1_det_comp_large are presented in the figures below (see appendix A for the explanation of the model names). In the results, the contour plots of the out of plane displacements will be given, as they clarify how the structure will fail. For the results of the other sections, see appendix C. Additionally, figures will be presented which contain the stress-strain curves that result from the detailed models of the large and small structure of that section.

a) b)

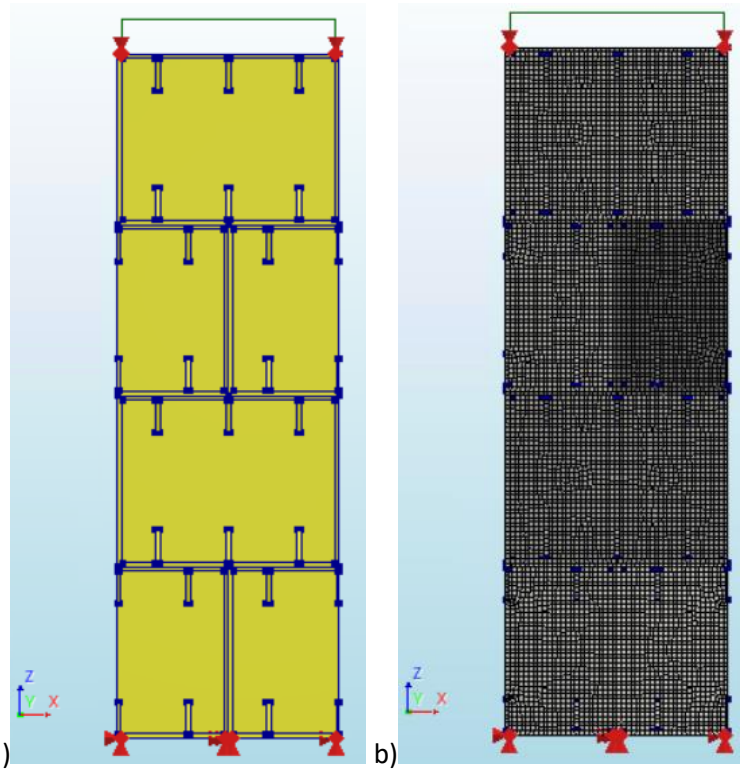

c)

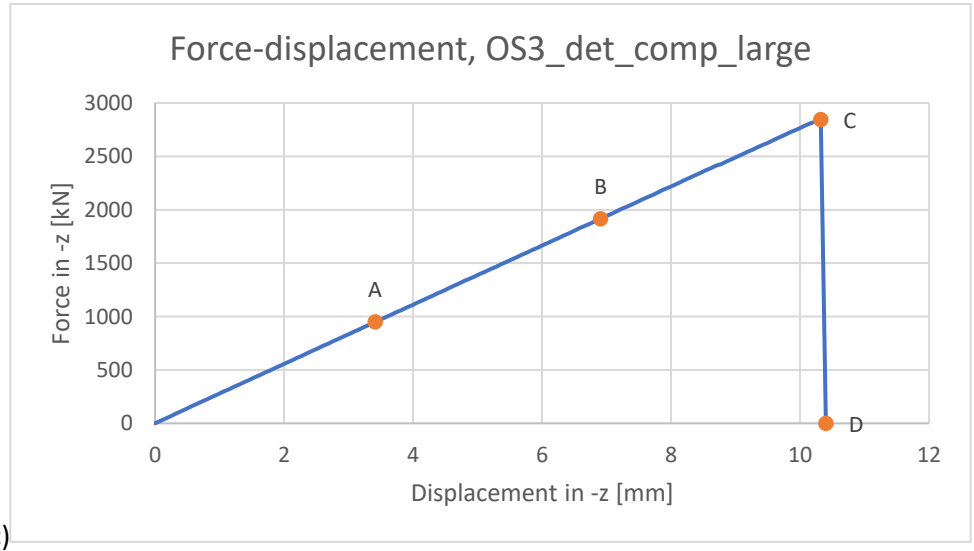

d)

Average element size [mm]		20x20
Number of elements	HX24L	9165
	PY15L	1624
	TE12L	1125
	TP18L	395
	Q24IF	880
Total number of nodes		20590

e)

Iteration method	Newton-Raphson	
Convergence norms	Displacement	Force
Convergence tolerances	0.01	0.01
Step size	0.00625(160)	
Maximum number of iterations per step	100	
All norms satisfied	No	

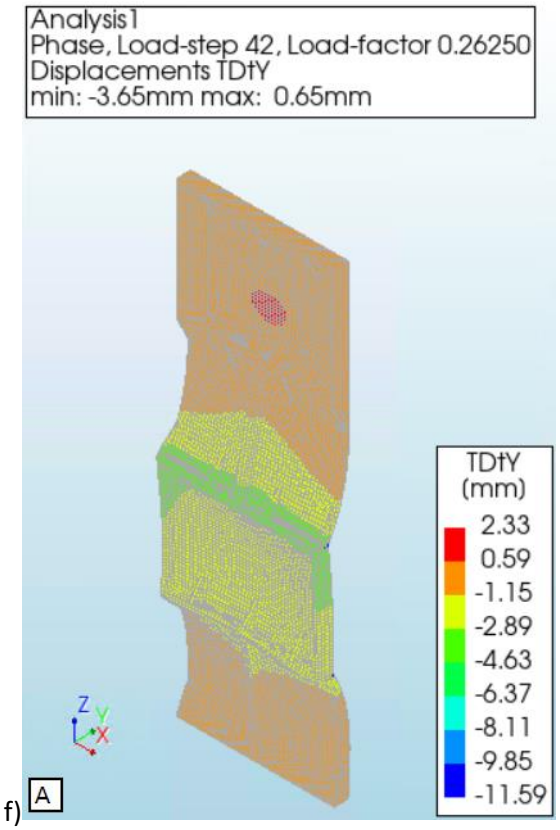

f)

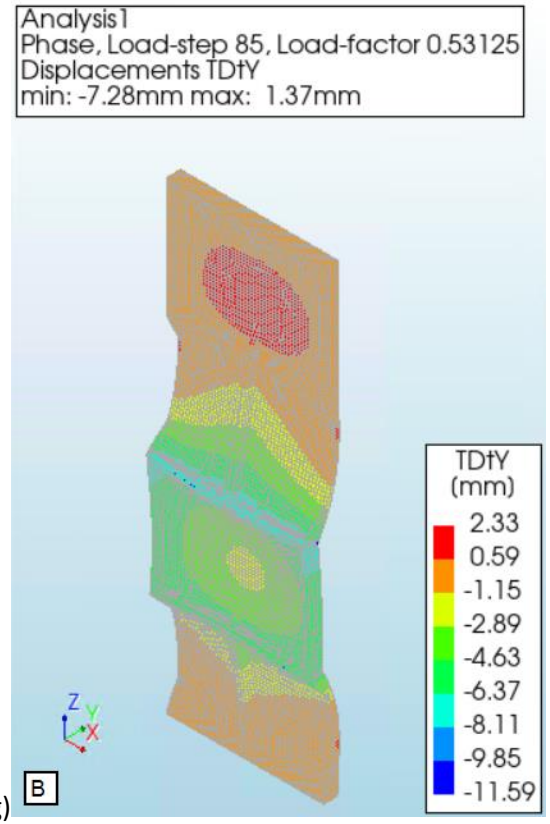

g)

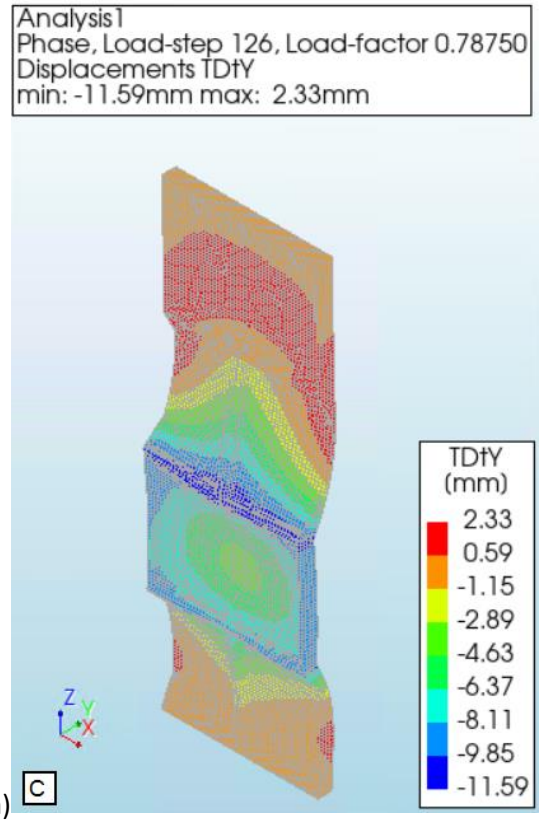

h)

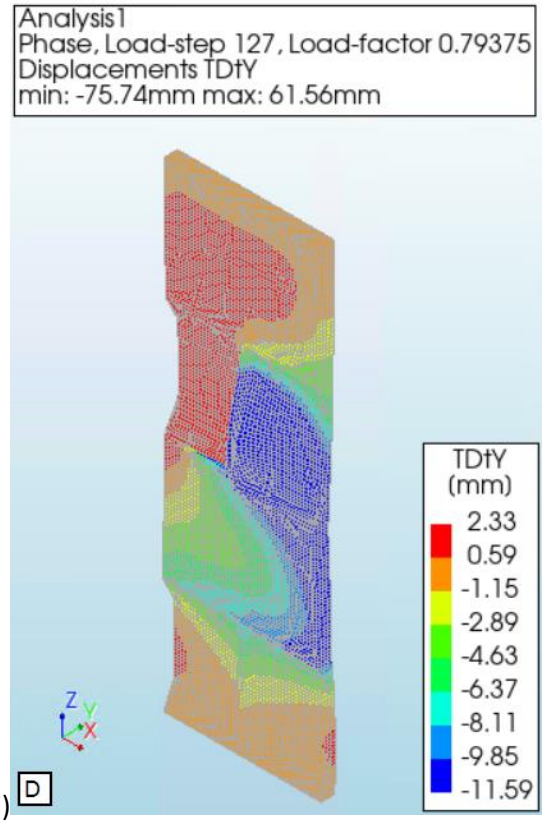

i)

Figure 6.6: Results of finite element analysis OS3_det_comp_large. a-i: structure (a), finite element mesh (b), force-displacement curve (c), overview elements and nodes (d), overview iterative scheme (e), displacement at point A (f), displacement at point B (g), displacement at point C (h), displacement at point D (i)

a) b)

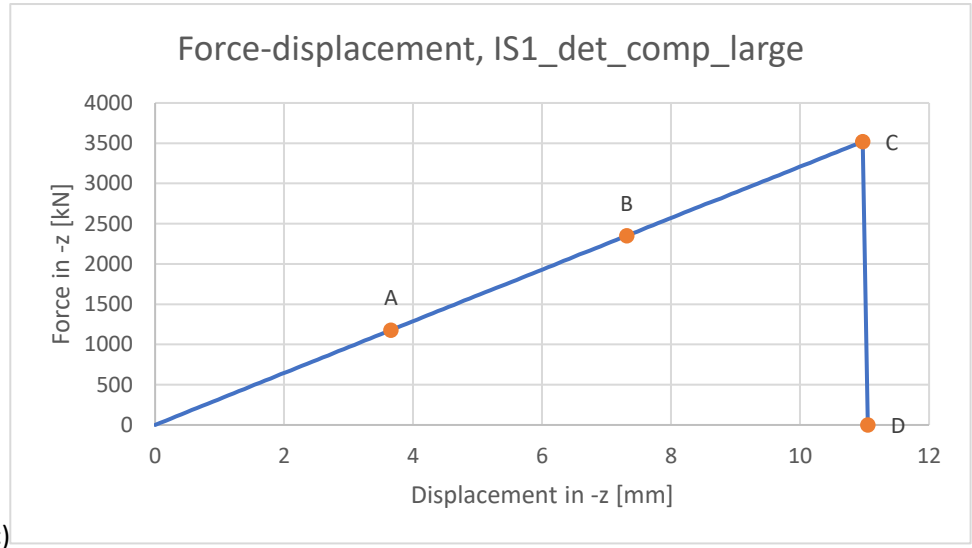

c)

Average element size [mm]		20x20
Number of elements	HX24L	11010
	PY15L	449
	TE12L	272
	TP18L	125
	Q24IF	564
Total number of nodes		23163

d)

Iteration method	Newton-Raphson	
Convergence norms	Displacement	Force
Convergence tolerances	0.01	0.01
Step size	0.00625(160)	
Maximum number of iterations per step	100	
All norms satisfied	No	

e)

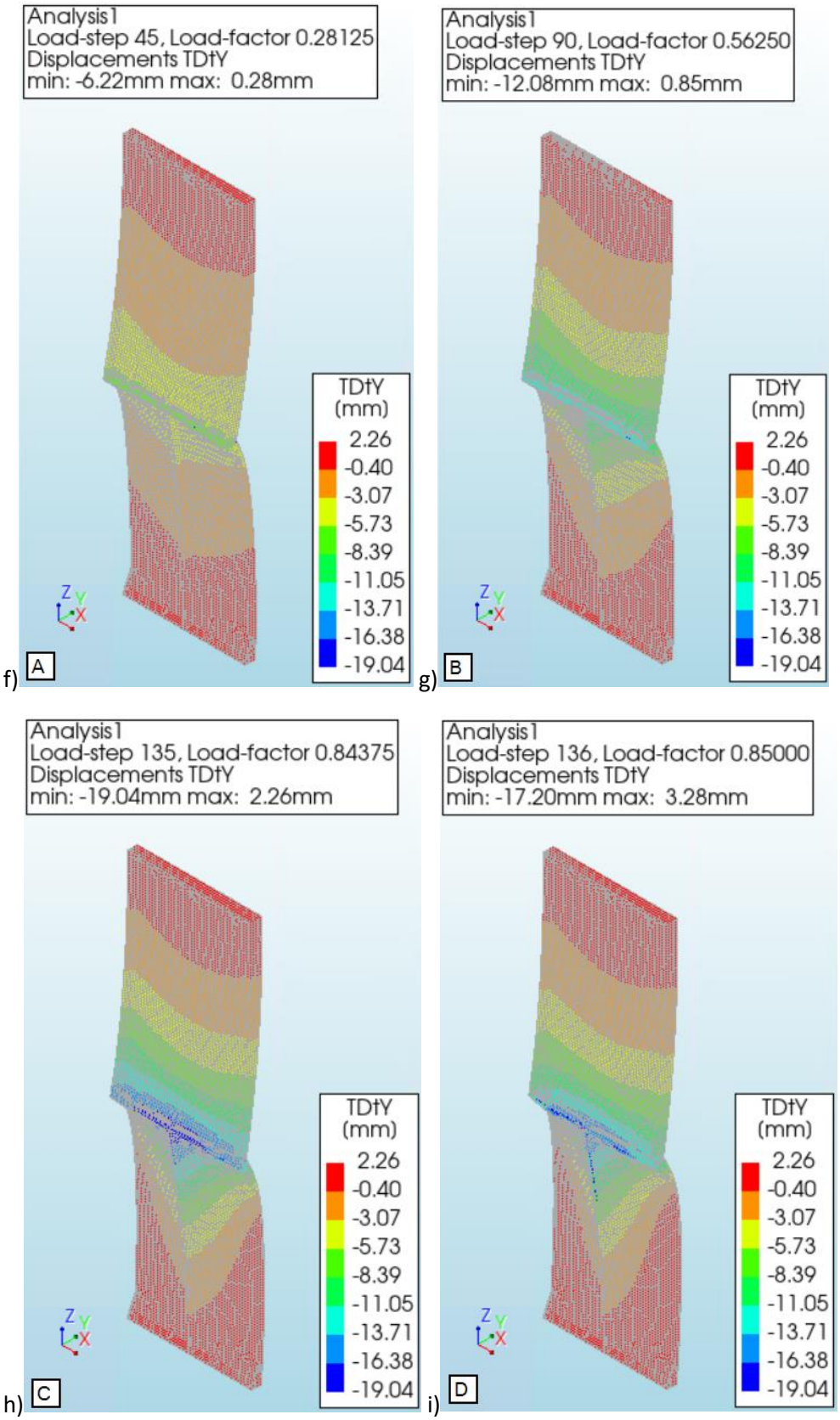

Figure 6.7: Results of finite element analysis IS1_det_comp_large. a-i: structure (a), finite element mesh (b), force-displacement curve (c), overview elements and nodes (d), overview iterative scheme (e), displacement at point A (f), displacement at point B (g), displacement at point C (h), displacement at point D (i)

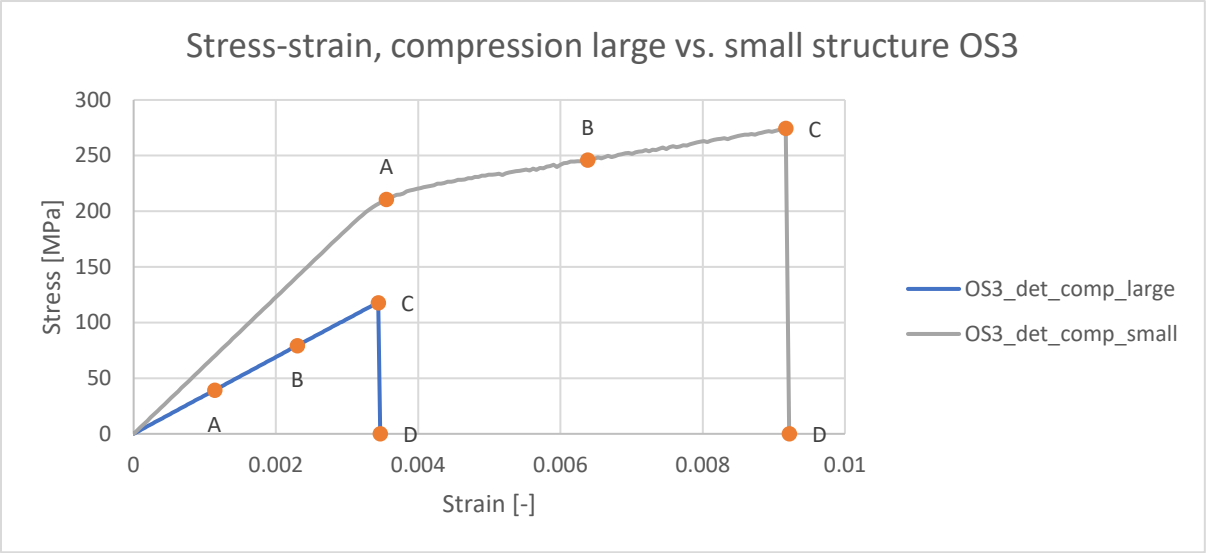

Figure 6.8: Stress-strain curves from compression models OS3_det_comp_large & OS3_det_comp_small

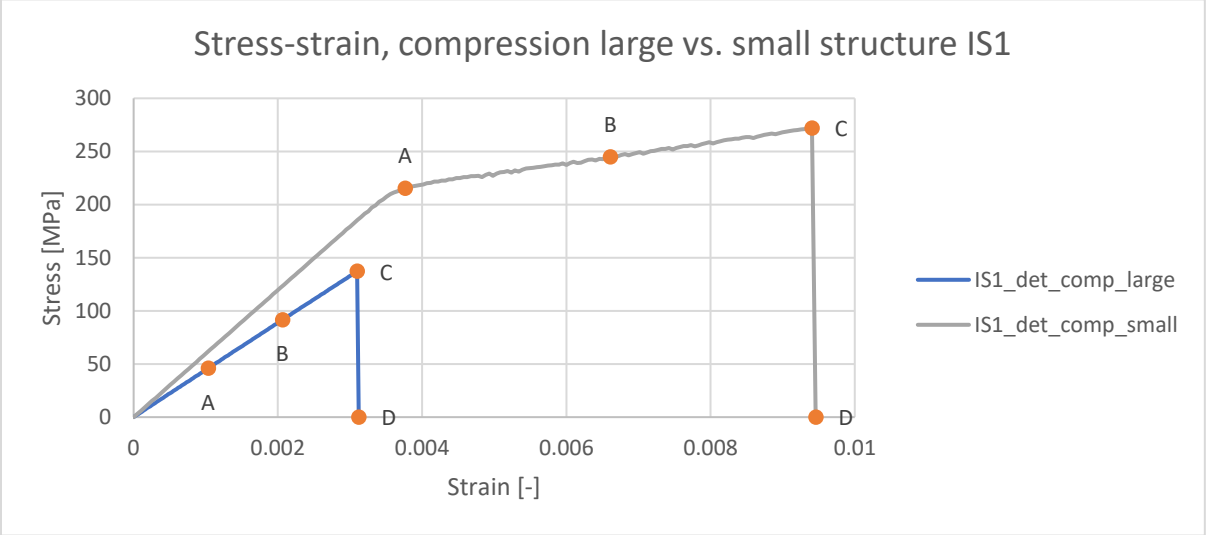

Figure 6.9: Stress-strain curves from compression models IS1_det_comp_large & IS1_det_comp_small

The points A-D of the large detailed models are chosen as follows: point C is where the peak force occurs and point D is where the force becomes 0 kN. Points A and B are located at 1/3 and 2/3 of the ultimate displacement. From the stress-strain curves, it is clear that the peak stress is much lower for the larger structures. As the large structures are much less stable than a single plate, this structure is expected to fail at a lower compressive force, as buckling occurs faster. In reality, the structure will be less prone to buckling as there will be plates on both sides. This means the buckling stresses will actually slightly higher. However, the supports on the sides are not considered here, which results in a more conservative value for the compressive strength. It can also be seen that the curve is still in linear-elastic region when failure occurs. As a result, the fracture energy is much lower and the value of n will be very close to 1. The contour plots of the out of plane displacements at point C of the detailed models (small and large structure) of section OS3 are presented in the figure below.

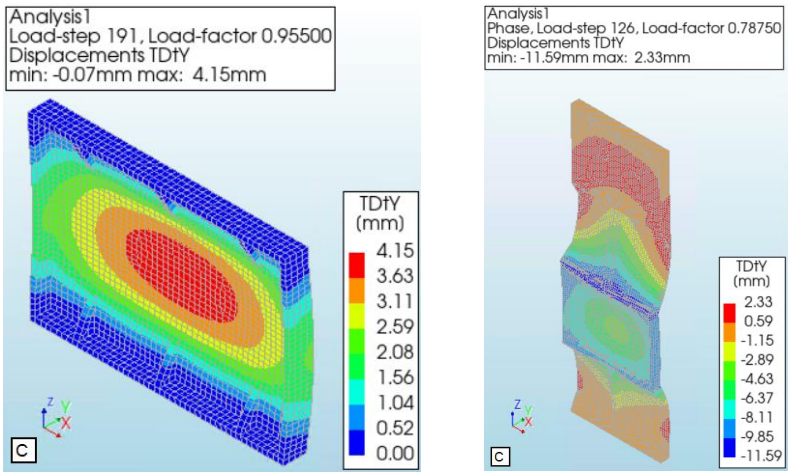

Figure 6.10: Out of plane displacements at point C, detailed model small structure (left) and large structure (right), section OS3

It is clear that for both models, the failure is related to the large out of plane displacements. However, the large structure is much more unstable due to the larger height. As a result, failure occurs at a much lower value of the average plate stress.

Similar as for the tensile models, the EMM parameters from chapter 5.4 can now be used in an equivalent EMM model of the large structure. A comparison can then be made to see if the results are still similar when the size of the structure is increased. The results of OS3_eqEMM_comp_large_ sq1_parameters and IS1_eqEMM_comp_large_ sq1_parameters are presented below (see appendix A for the explanation of the model names). Additionally, figures are presented that contain the stress-strain curves of the equivalent EMM model of the large structure and their corresponding detailed model.

a) b)

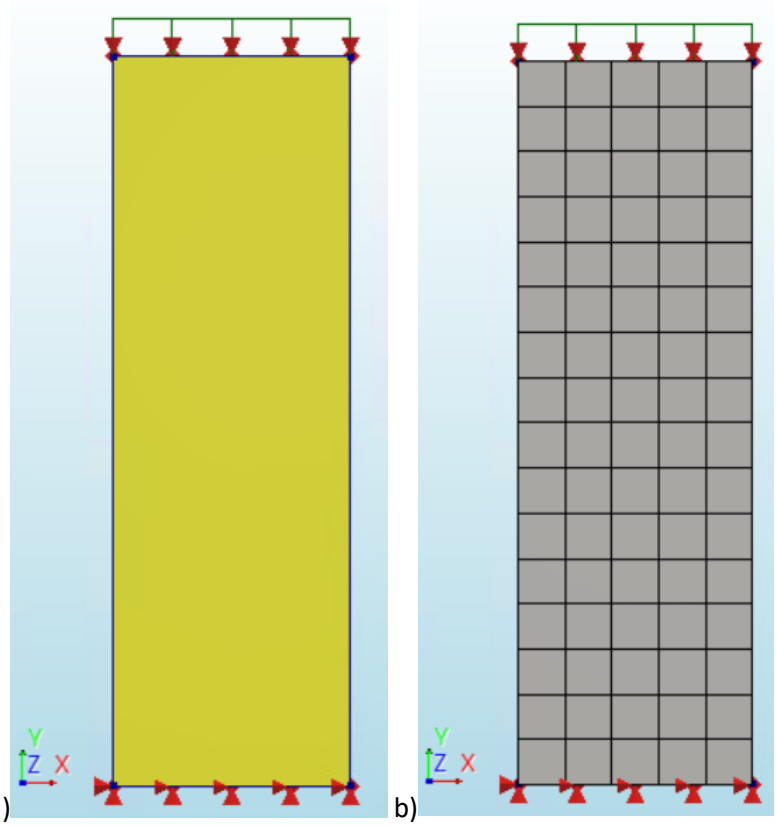

c)

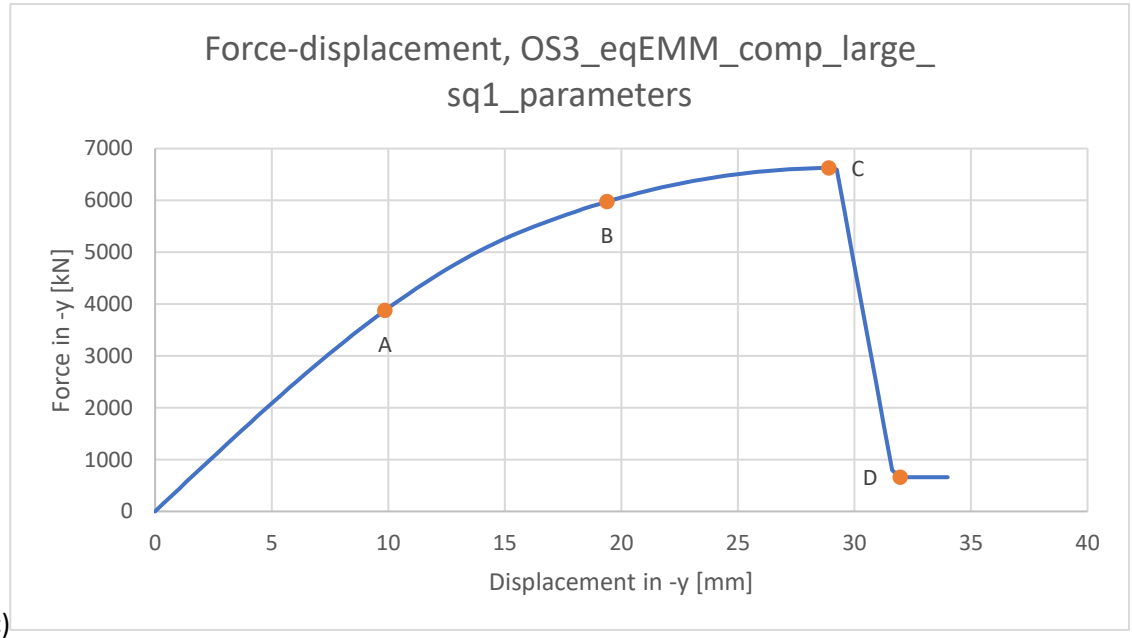

d)

Average element size [mm]		194x187.5
Number of elements	Q20SH	80
Total number of nodes		102

e)

Iteration method	Secant (Quasi-Newton)	
Convergence norms	Displacement	Force
Convergence tolerances	0.01	0.01
Step size	0.01(100)	
Maximum number of iterations per step	100	
All norms satisfied	No	

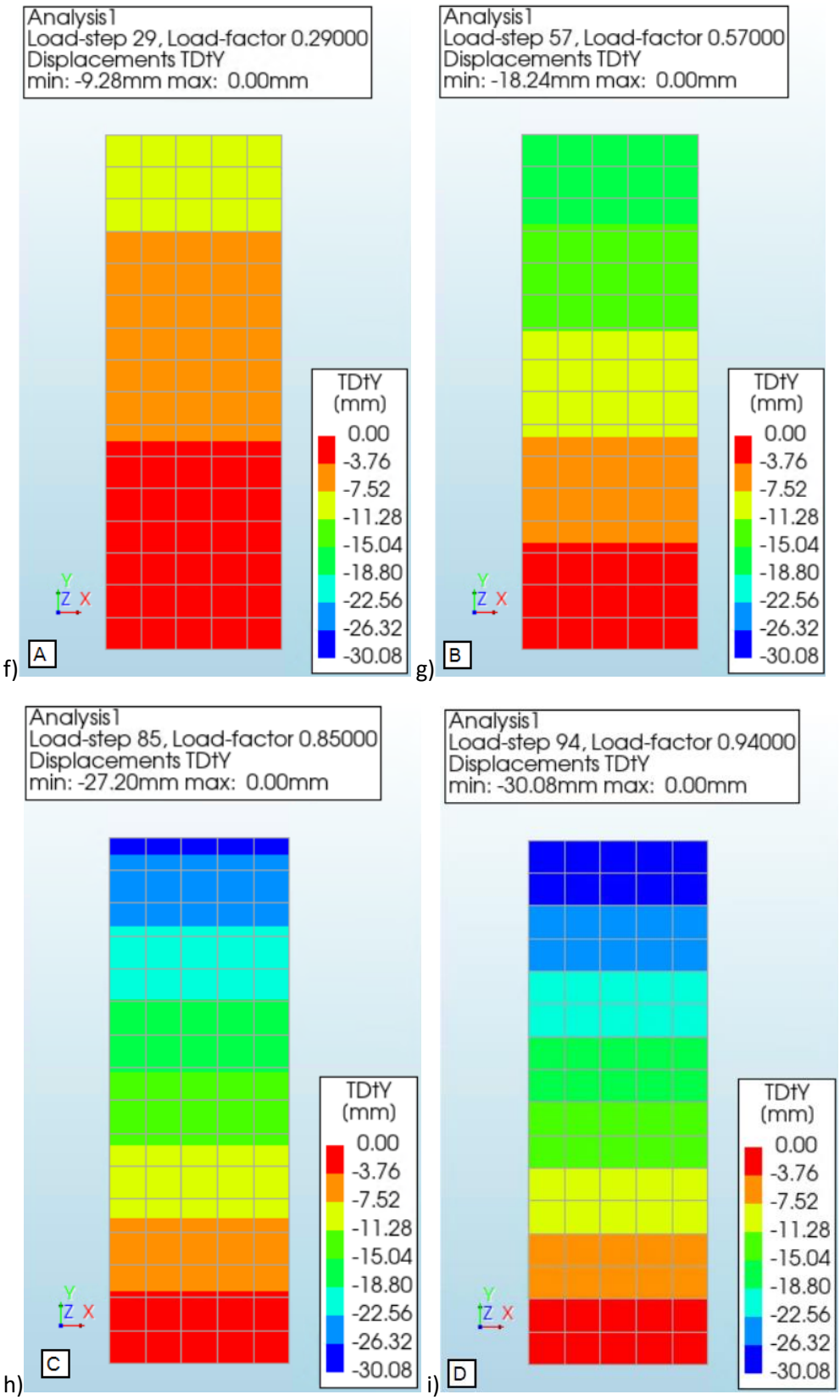

Figure 6.11: Results of finite element analysis OS3_eqEMM_comp_large_ sq1_parameters. a-i: structure (a), finite element mesh (b), force-displacement curve (c), overview elements and nodes (d), overview iterative scheme (e), displacement at point A (f), displacement at point B (g), displacement at point C (h), displacement at point D (i)

a) b)

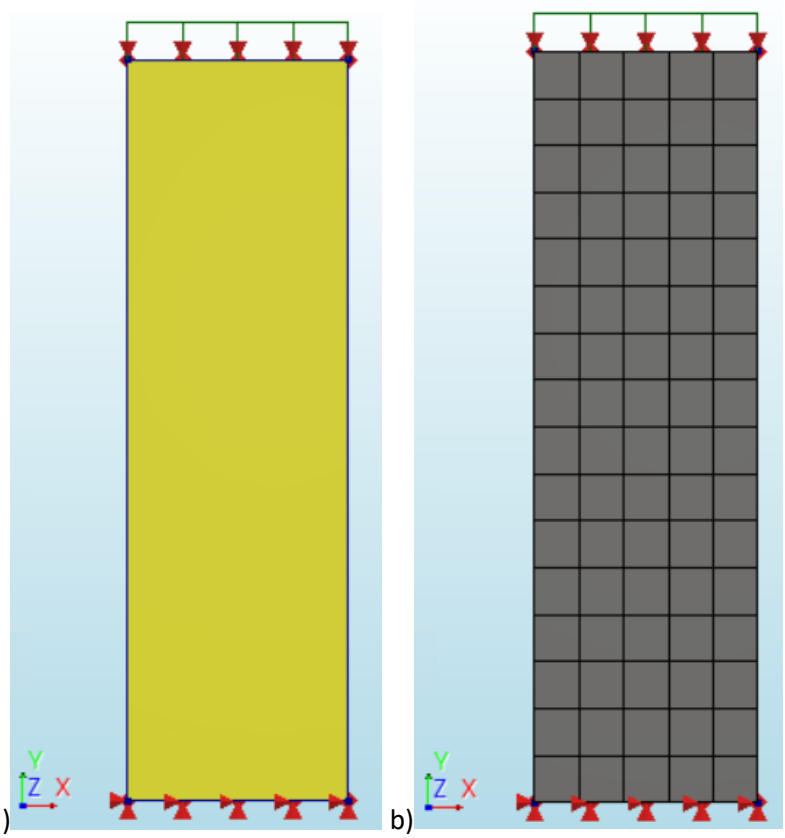

c)

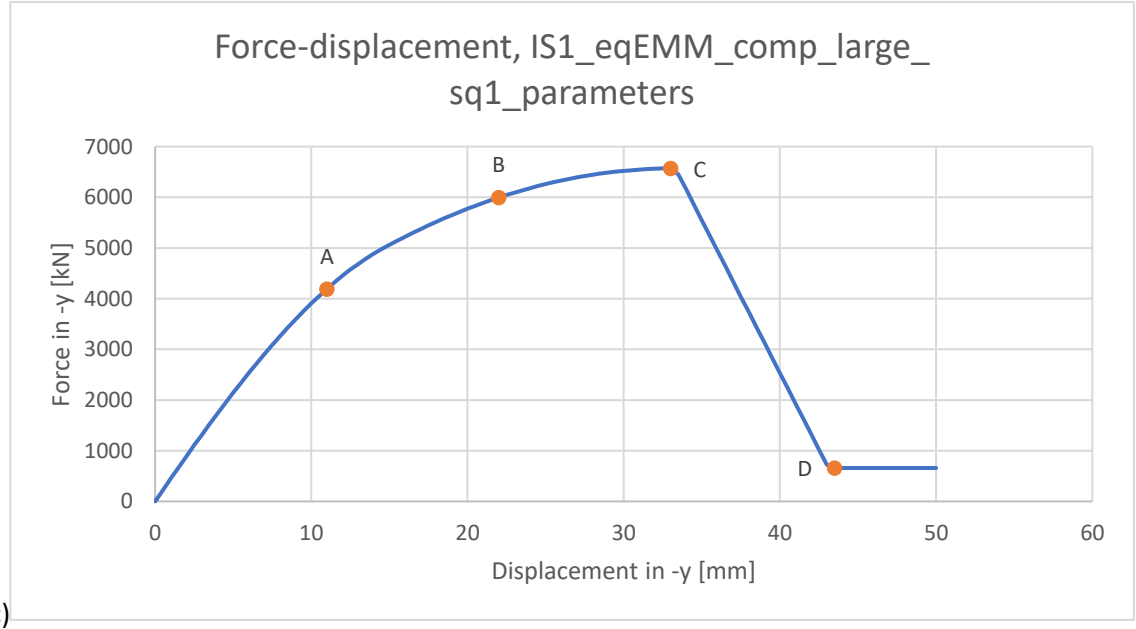

h)

Average element size [mm]		210.2x221.25
Number of elements	Q20SH	80
Total number of nodes		102

i)

Iteration method	Secant (Quasi-Newton)	
Convergence norms	Displacement	Force
Convergence tolerances	0.01	0.01
Step size	0.01(100)	
Maximum number of iterations per step	100	
All norms satisfied	No	

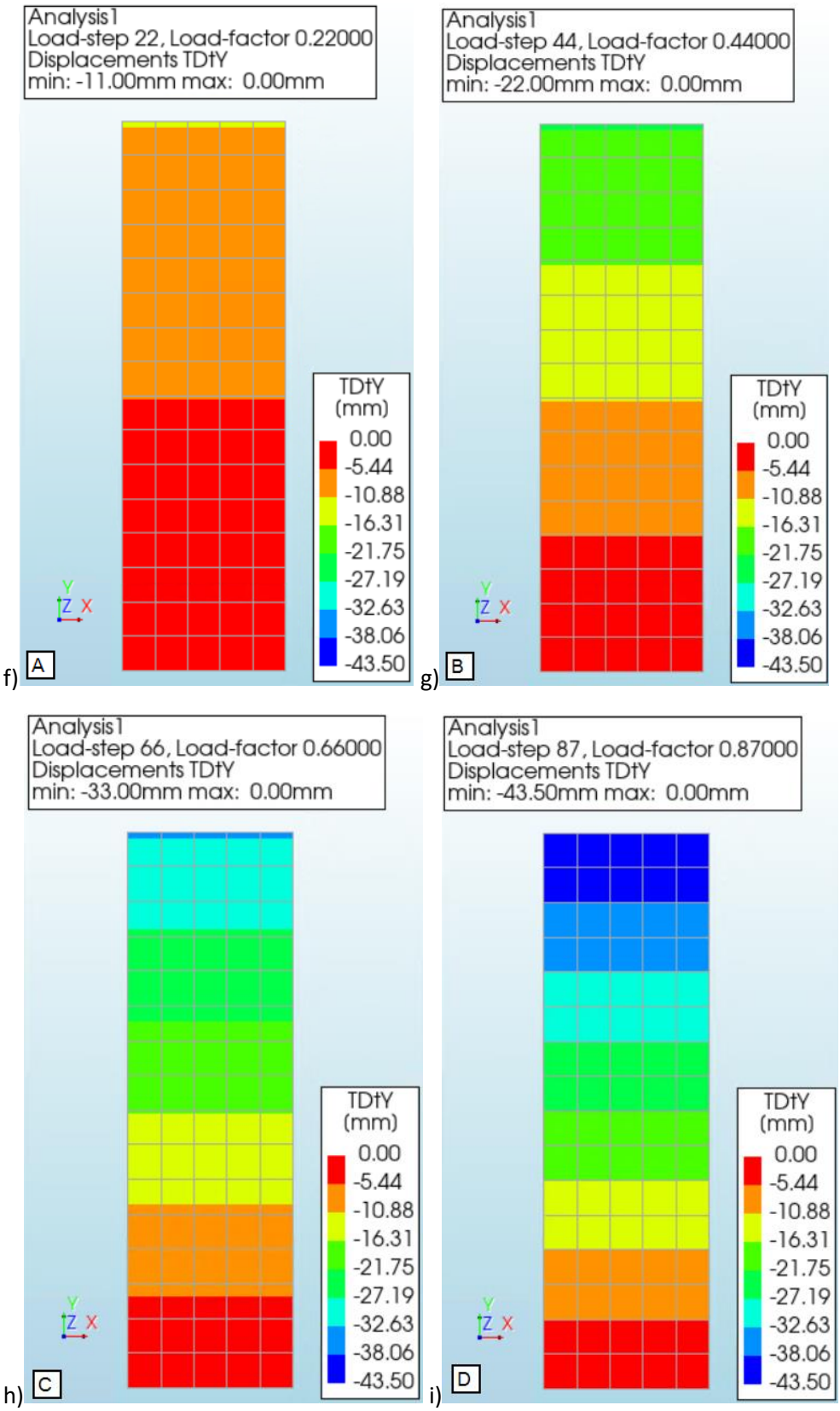

f) g) h) i)

Figure 6.12: Results of finite element analysis IS1_eqEMM_comp_large_sq1_parameters. a-i: structure (a), finite element mesh (b), force-displacement curve (c), overview elements and nodes (d), overview iterative scheme (e), displacement at point A (f), displacement at point B (g), displacement at point C (h), displacement at point D (i)

The same conclusion can be made as for the tension models: from the contour plots that are presented, it is clear that the failure modes of the equivalent EMM models loaded in compression are the same for the small and large structures when the EMM is used.

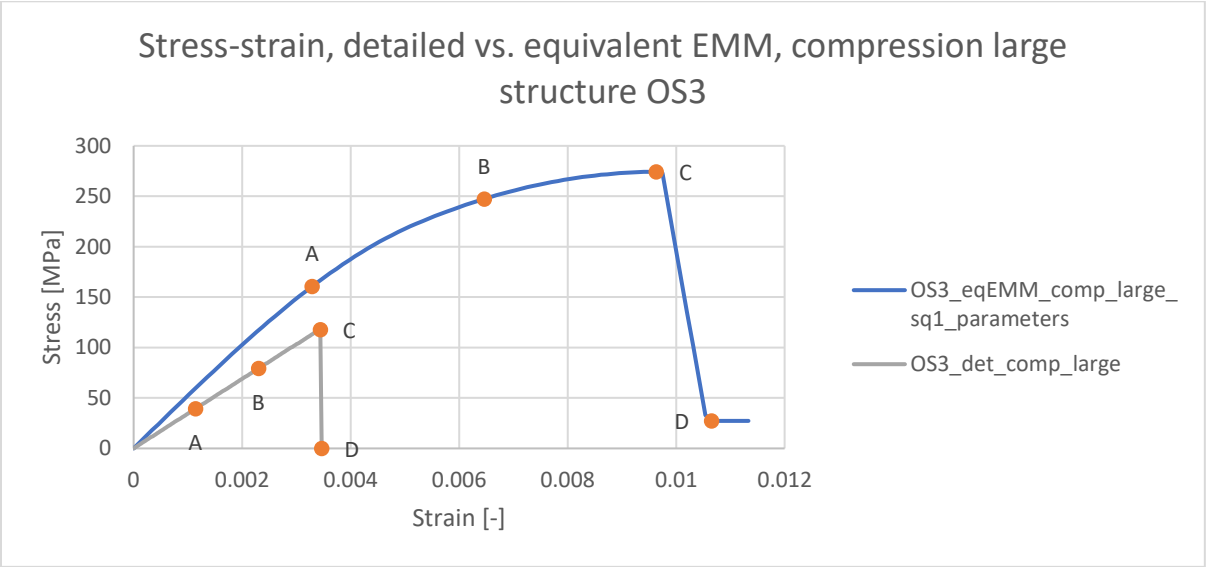

Figure 6.13: Stress-strain curves from compression models OS3_eqEMM_comp_large_sq1_parameters & OS3_det_comp_large

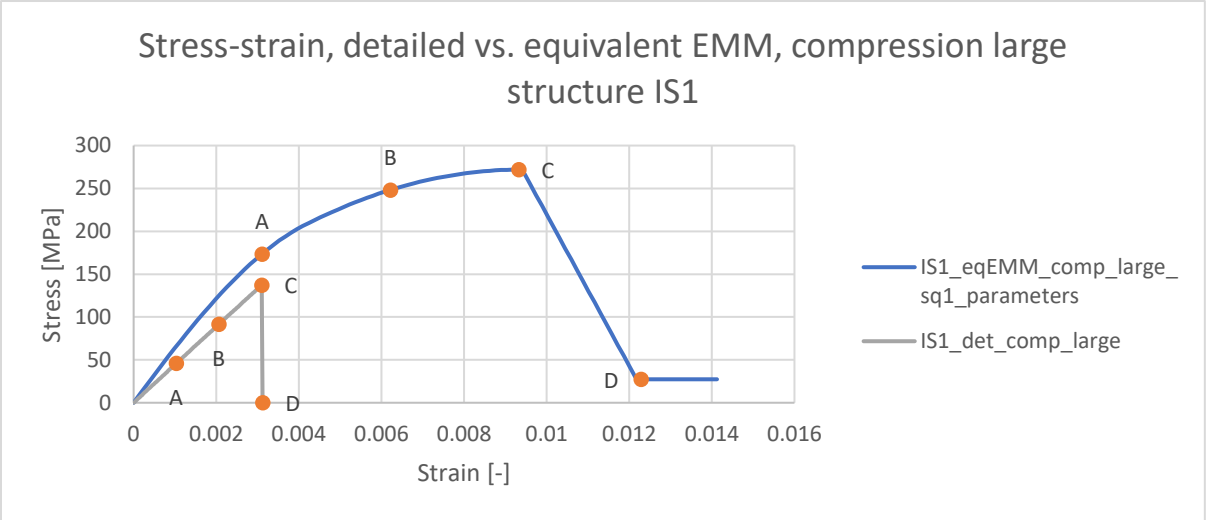

Figure 6.14: Stress-strain curves from compression models IS1_eqEMM_comp_large_sq1_parameters & IS1_det_comp_large

The points A-D are chosen in almost the exact same way as for the detailed models of the large structure: point C is where the peak force occurs and point D is where the force becomes 0 kN. Points A and B are located at 1/3 and 2/3 of the displacement in point C. It is clear that the stress-strain curves of the detailed and equivalent EMM models of the large structures are very different, but this is what can be expected, as the input parameters are based on the results of the small detailed models. Since the results of the large detailed models are not very similar to the results of the small detailed models, the results are expected to be different here as well. As the failure of the large detailed model occurs much sooner, the ultimate displacement is much lower as in the equivalent EMM model. It is clear that the cracking parameters need to be adjusted for all sections when they are used in large structures. An overview of the final EMM parameters will be provided in section 6.4 of this chapter.

6.3 Shear loading

For shear, the situation is slightly different than for the other loading types. Shear failure is often paired with bending failure, which was also the case for the structures that were analysed in the previous chapters. In order to reduce the amount of bending, the ratio of width/height minimally needs to be increased. If the structure has a very small width, rotating of the plates cannot be prevented in the structure. However, when a larger width is used, the rotation is prevented by the plates besides them. To obtain a larger width/height ratio, the section width has to be increased here. It is chosen to use 3 plates in width for the outer column sections, while 6 plates shall be used for the inner column sections, such that the ratio of width/height is larger than 1 for all structures. When only 3 plates in width are used for the inner column sections, the ratio is still lower than 1. The ratios of all sections, based on the plate width and height, are given in the table below.

Table 6.1: Ratio width/height for assembly structures used in shear models

Section	**Ratio width/height**
OS1	3.05
OS2	2.53
OS3	1.94
IS1	1.78
IS2	1.53
IS3	1.30

The shear models are still two plates in height, but the width has been increased. The bottom of the structure is supported in x and z, while the back of the plates are supported in y. The support in x at the top is required for the prescribed deformation load, which is the green load. This load causes the top face of the entire structure to be displaced in the positive x-direction. Again, tyings were added to the top face of the structure for the translation in z, to ensure that this face remains straight.

Similar as before, three different models will be analysed per section. The compressive stresses that are applied to the models are 0.5, 1 and 2 MPa. The results of OS3_det_shear_large and IS1_det_shear_large are presented in the figures below (see appendix A for the explanation of the model names). For the results of the other sections, see appendix C. Additionally, figures are presented which contain the stress-strain curves that result from the detailed models of the large and small structure of both sections. In the results of IS1_det_shear_large, it can be observed that the contour plots are slightly different than for the other models. As the mesh is very small and the structure quite large, the mesh lines have been turned off in the plots. When the lines were visible, it was not possible to see the colours in the contour plots.

a)

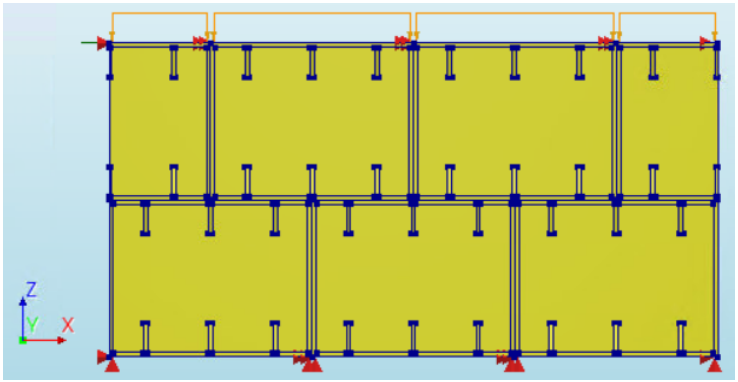

b)

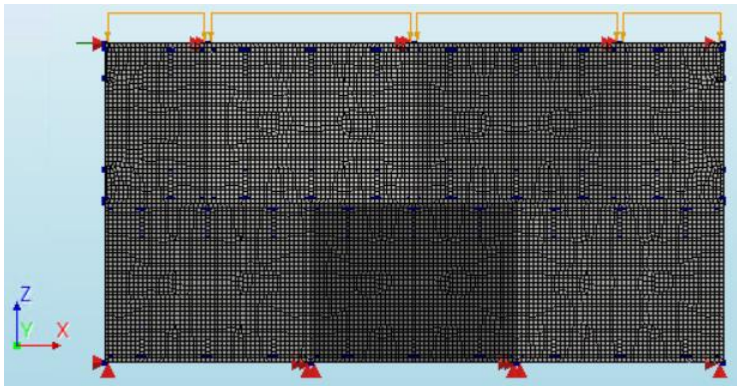

c)

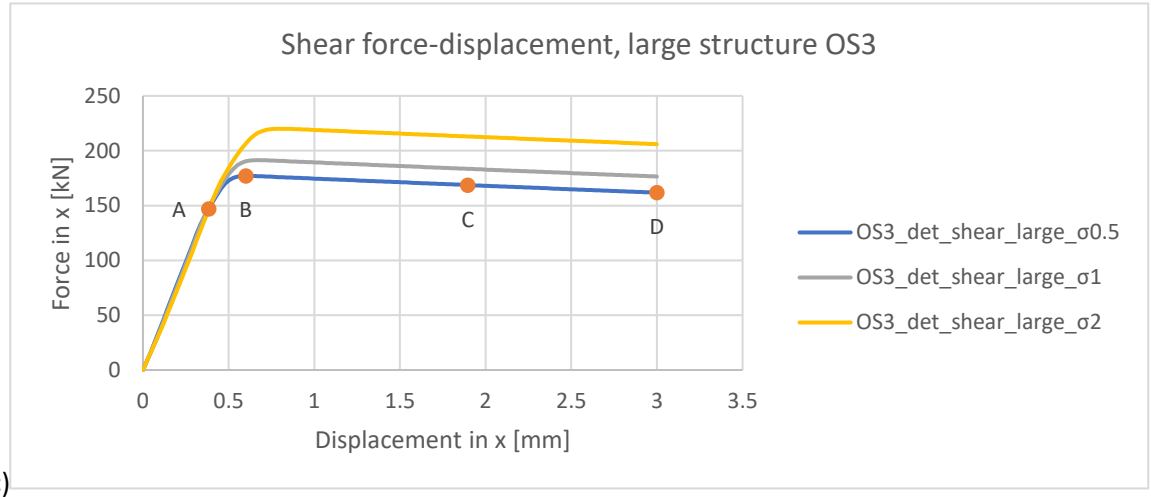

d)

Average element size [mm]		20x20
Number of elements	HX24L	13395
	PY15L	3438
	TE12L	2581
	TP18L	908
	Q24IF	1336
Total number of nodes		30951

e)

Load	Compression		Translation	
Iteration method	Newton-Raphson		Newton-Raphson	
Convergence norms	Force	Displacement	Force	Displacement
Convergence tolerances	0.01	0.01	0.01	0.01
Step size	0.2(5)		0.008(125)	
Maximum number of iterations per step	100		100	
All norms satisfied	No		No	

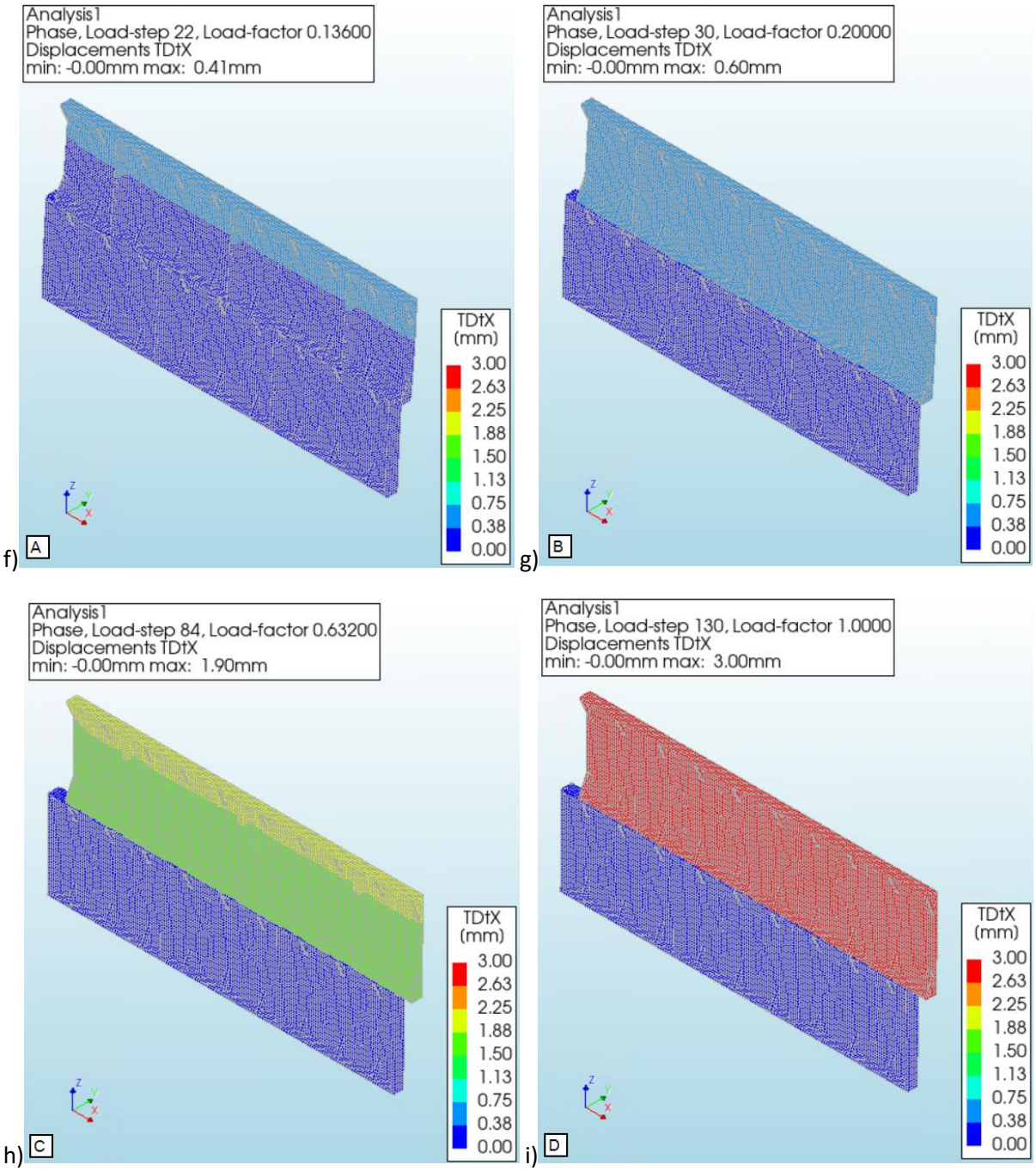

Figure 6.15: Results of finite element analysis OS3_det_shear_large_σ0.5, σ1 & σ2. a-i: structure (a), finite element mesh (b), force-displacement curve (c), overview elements and nodes (d), overview iterative scheme (e), displacement at point A (f), displacement at point B (g), displacement at point C (h), displacement at point D (i)

a)

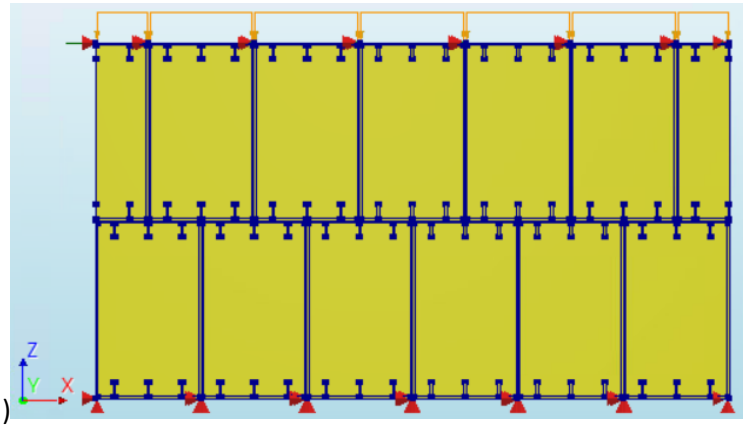

b)

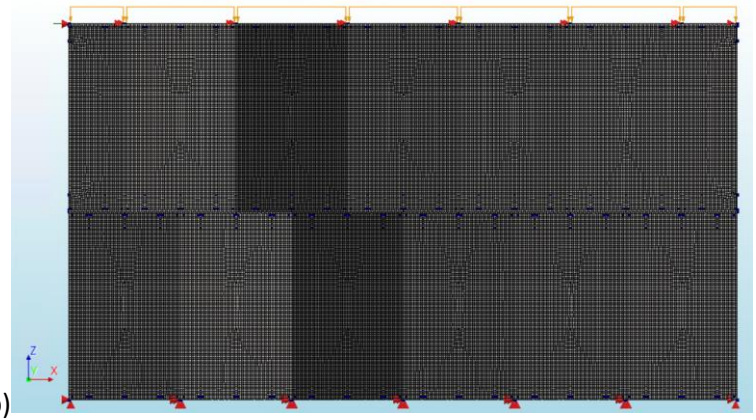

c)

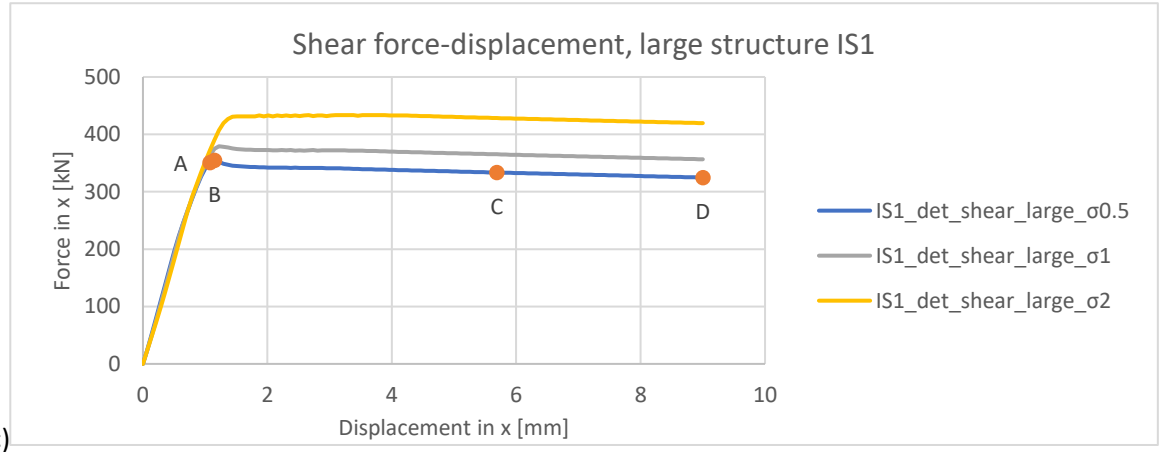

d)

Average element size [mm]		20x20
Number of elements	HX24L	66523
	PY15L	770
	TE12L	437
	TP18L	664
	Q24IF	5164
Total number of nodes		137658

e)

Load	Compression		Translation	
Iteration method	Newton-Raphson		Newton-Raphson	
Convergence norms	Force	Displacement	Force	Displacement
Convergence tolerances	0.01	0.01	0.01	0.01
Step size	0.2(5)		0.008(125)	
Maximum number of iterations per step	100		100	
All norms satisfied	No		No	

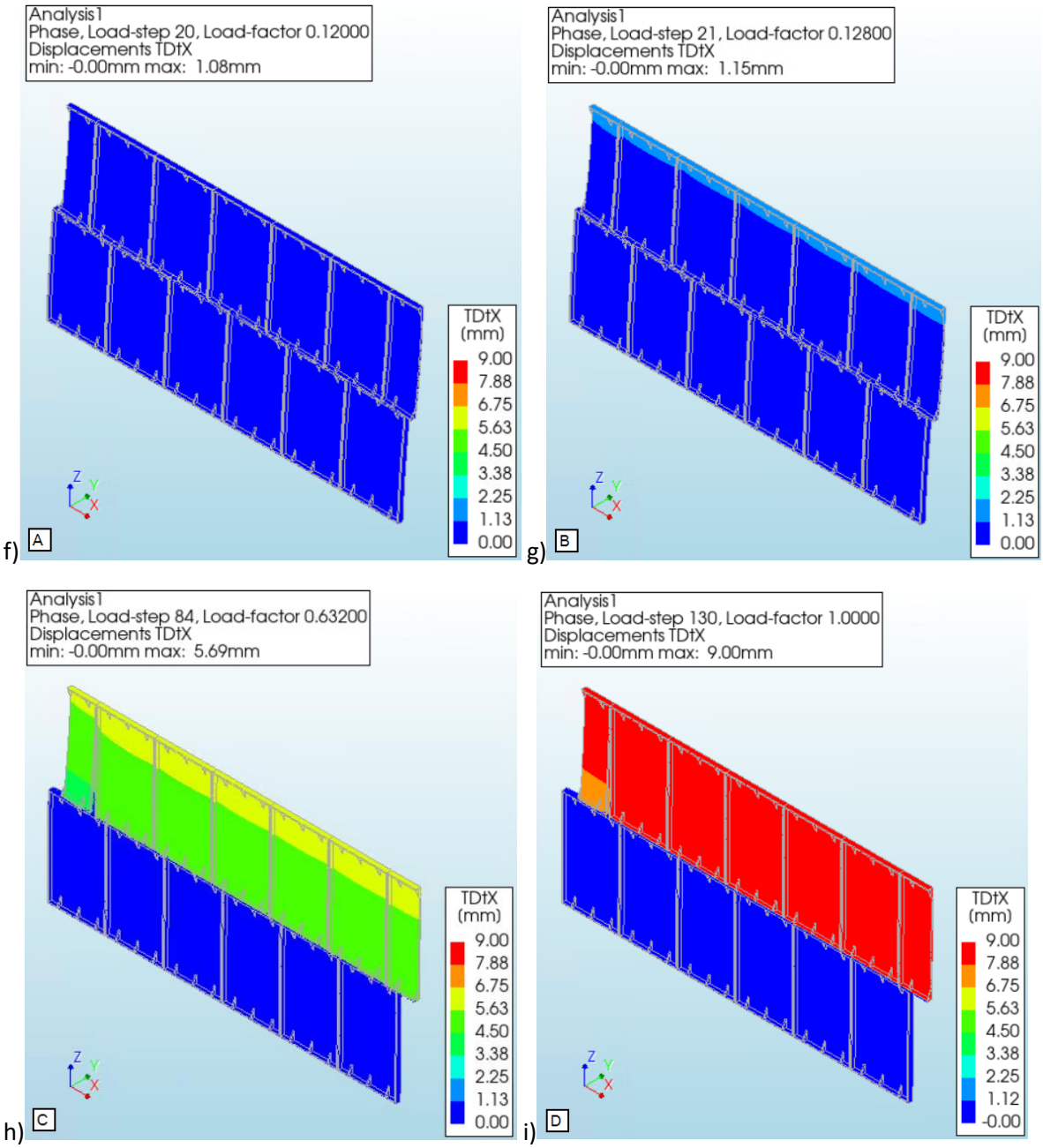

Figure 6.16: Results of finite element analysis IS1_det_shear_large_σ0.5, σ1 & σ2. a-i: structure (a), finite element mesh (b), force-displacement curve (c), overview elements and nodes (d), overview iterative scheme (e), displacement at point A (f), displacement at point B (g), displacement at point C (h), displacement at point D (i)

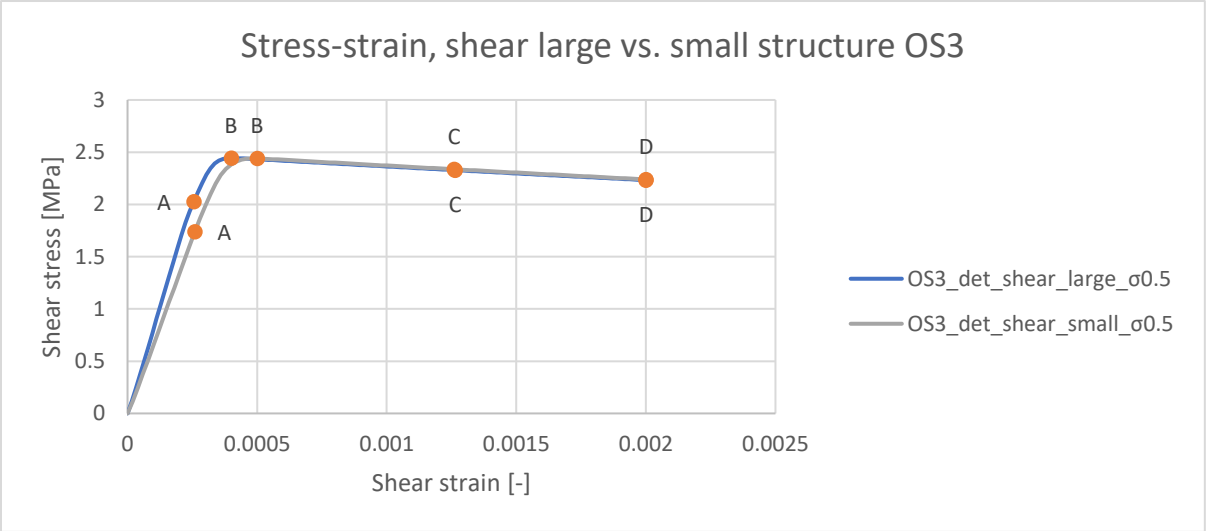

Figure 6.17: Stress-strain curves from shear models OS3_det_shear_large_σ0.5 & OS3_det_shear_small_σ0.5

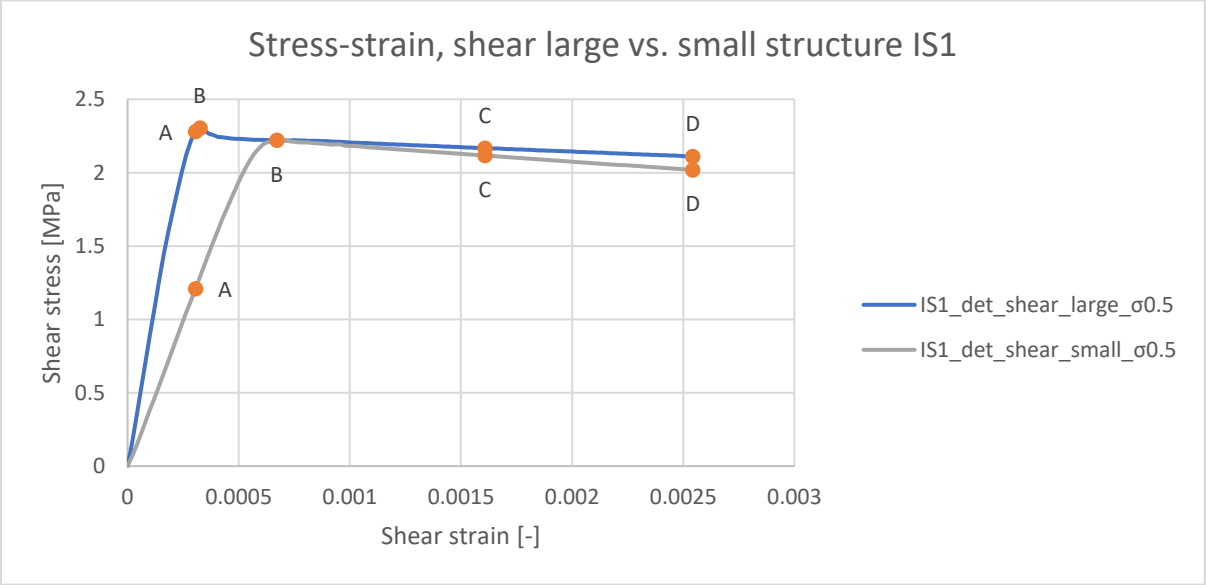

Figure 6.18: Stress-strain curves from shear models IS1_det_shear_large_σ0.5 & IS1_det_shear_small_σ0.5

The points A-D of the large structures were chosen as follows: point B is where the peak force occurs and point D is where the displacement load is fully applied. Points A and C are chosen such that the strain matches the strain in points A and C of the small detailed models. From the curves, it is clear that the results of OS3 are very similar, besides a small difference in stiffness. As the width/height ratio of the small structure was already quite high, there was only a small amount of bending in the failure mode. By increasing the ratio, the failure is more related to shear, which results in a slightly higher shear modulus. For section IS1, the difference in shear modulus is more significant. Also, it is observed that the maximum shear stress is quite a bit higher for the large structure. Both are the result of increasing the width/height ratio, as this eliminates bending from the failure mode. The figure below shows the horizontal displacements in point D for the small and large detailed models of section OS3.

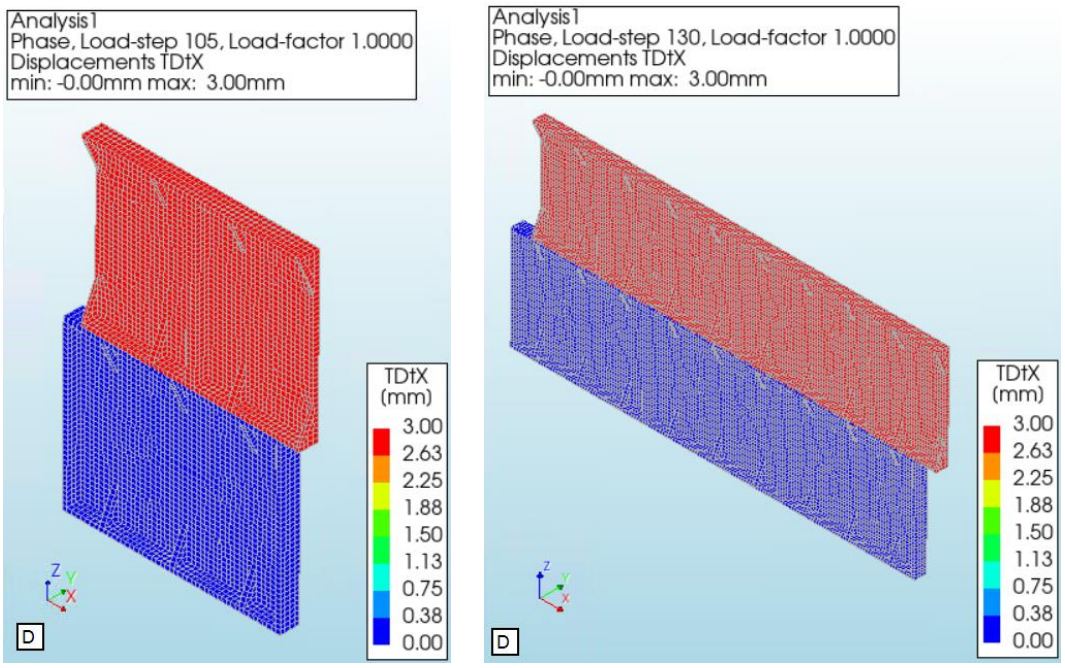

Figure 6.19: Horizontal displacements in point D, detailed models small structure (left) and large structure (right), section OS3

From the figures of the contour plots, it is clear that the behaviour of the structures is still very similar. However, from the stress-strain diagrams it is clear that the bending is mostly eliminated from the failure mode of the large structure, which results in a slightly higher stiffness.

Now, equivalent EMM models of the large structure will be analysed, in which the EMM parameters of chapter 5.4 are applied. First, only 1 element is used in the equivalent EMM model to ensure pure shear failure. The results of IS1_eqEMM_shear_large_σ0.5_one_el and IS1_eqEMM_shear_large_σ0.5_one_el are presented below (see appendix A for the explanation of the model names. Additionally, figures are presented which contain the stress-strain curves that result from the equivalent EMM models and their corresponding detailed model.

a)

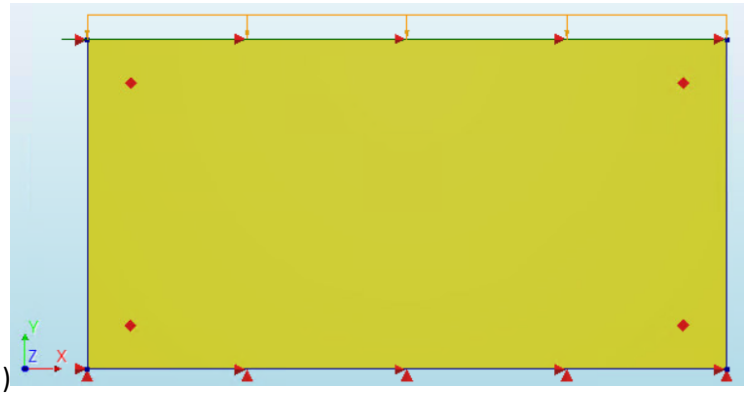

b)

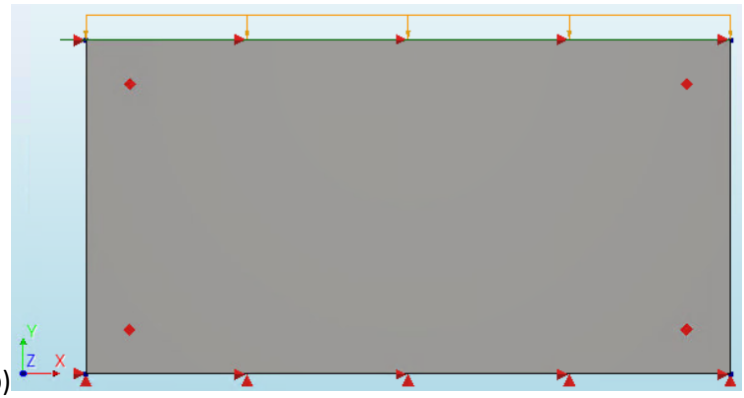

c)

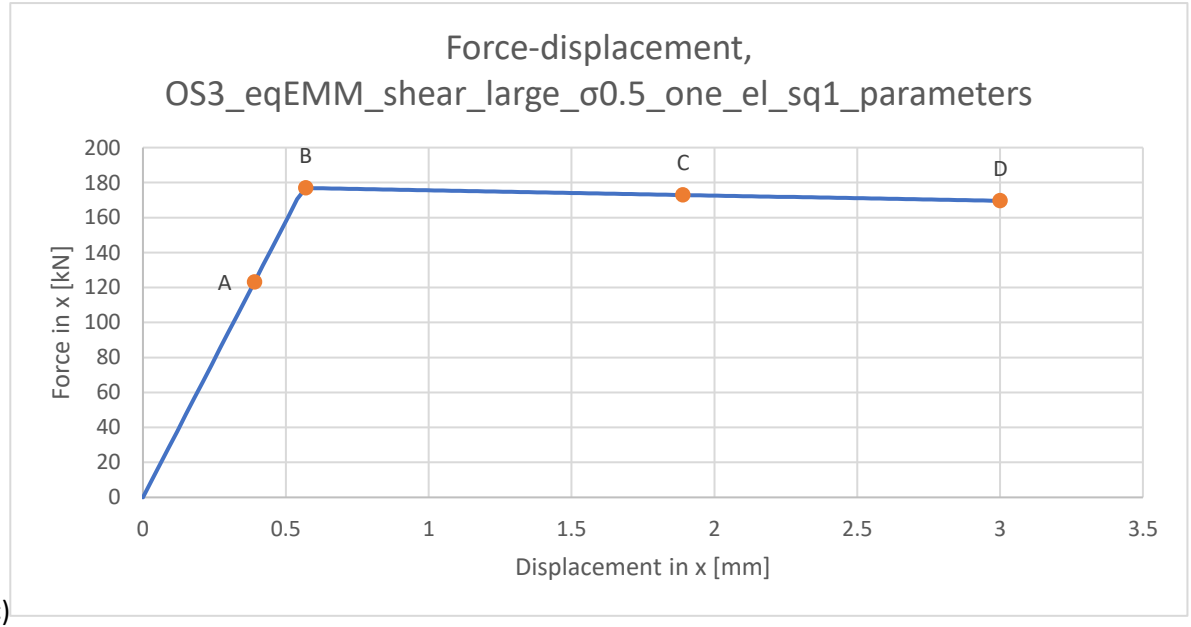

h)

Average element size [mm]		2910x1500
Number of elements	Q20SH	1
Total number of nodes		4

i)

Load	Compression		Translation	
Iteration method	Secant (Quasi-Newton)		Secant (Quasi-Newton)	
Convergence norms	Force	Displacement	Force	Displacement
Convergence tolerances	0.01	0.01	0.01	0.01
Step size	0.1(10)		0.01(100)	
Maximum number of iterations per step	100		100	
All norms satisfied	No		No	

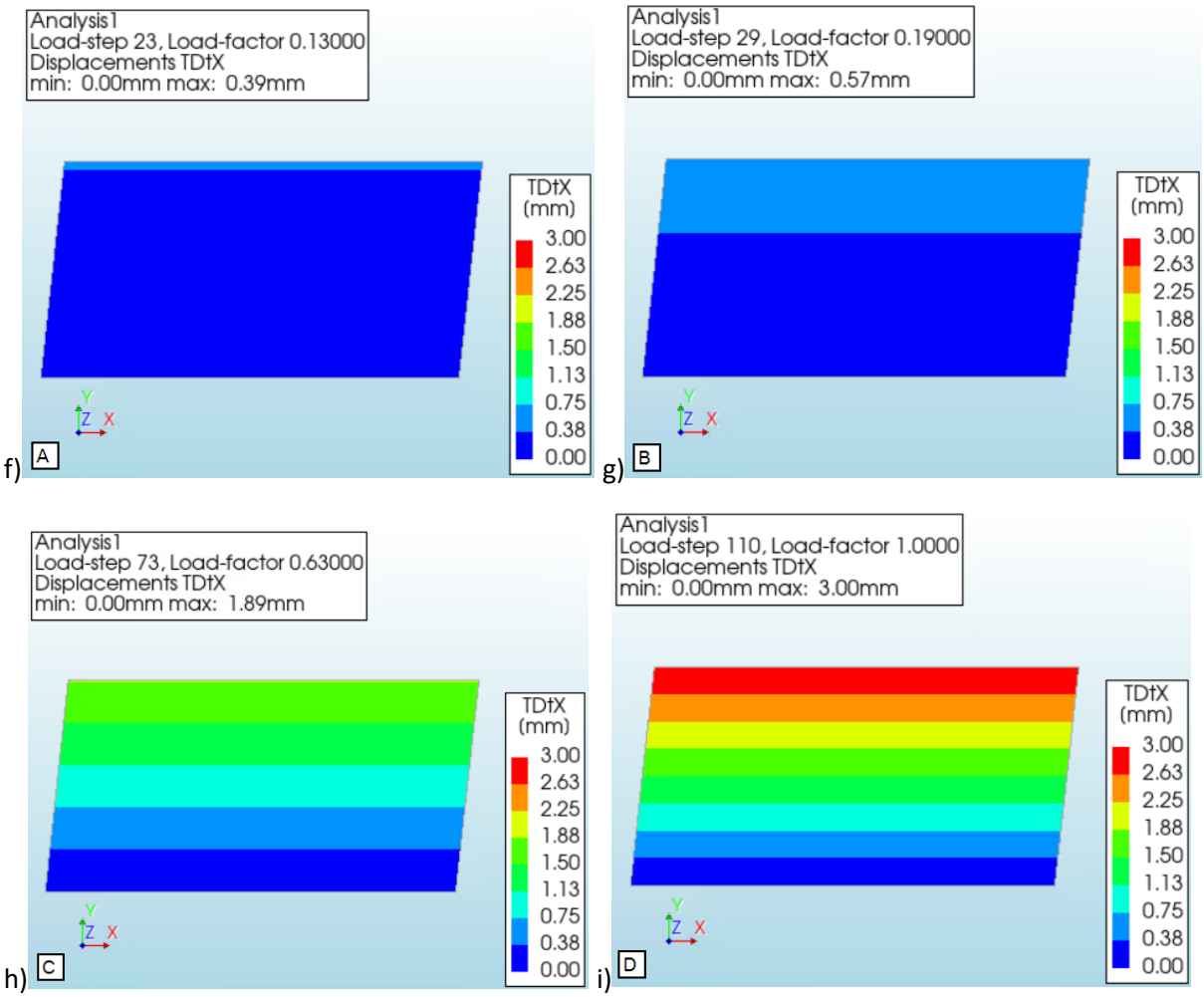

Figure 6.20: Results of finite element analysis OS3_eqEMM_shear_large_σ0.5_one_el_sq1_parameters. a-i: structure (a), finite element mesh (b), force-displacement curve (c), overview elements and nodes (d), overview iterative scheme (e), displacement at point A (f), displacement at point B (g), displacement at point C (h), displacement at point D (i)

a)

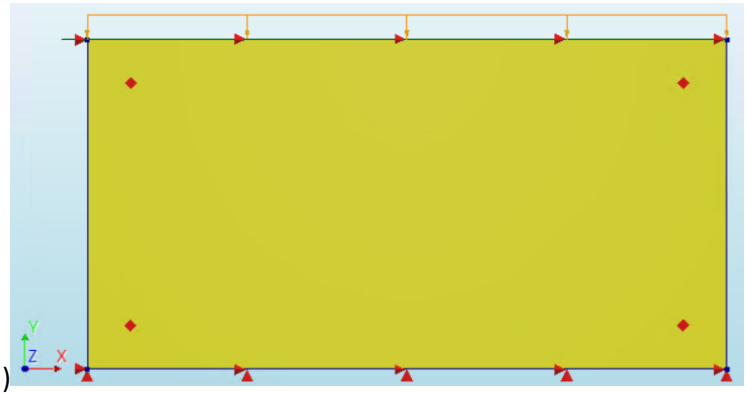

b)

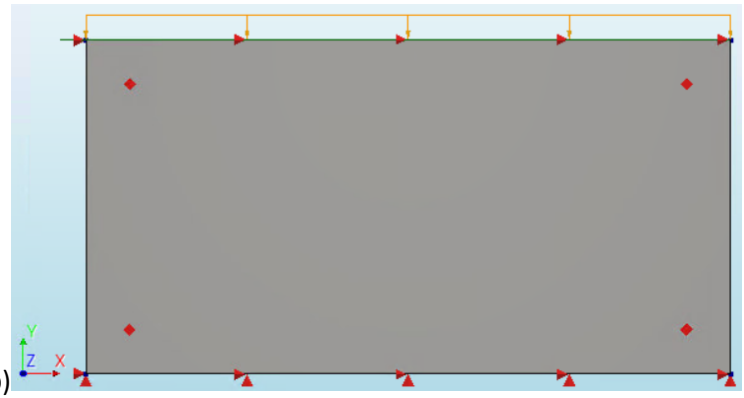

c)

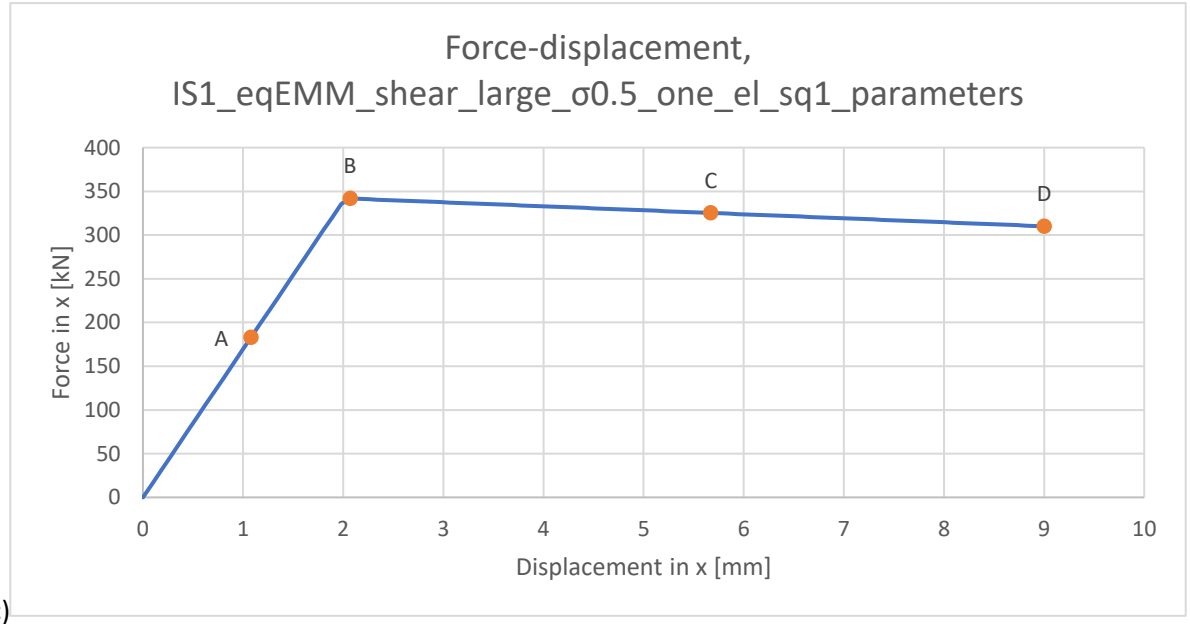

h)

Average element size [mm]		6306x3540
Number of elements	Q20SH	1
Total number of nodes		4

i)

Load	Compression		Translation	
Iteration method	Secant (Quasi-Newton)		Secant (Quasi-Newton)	
Convergence norms	Force	Displacement	Force	Displacement
Convergence tolerances	0.01	0.01	0.01	0.01
Step size	0.1(10)		0.01(100)	
Maximum number of iterations per step	100		100	
All norms satisfied	No		No	

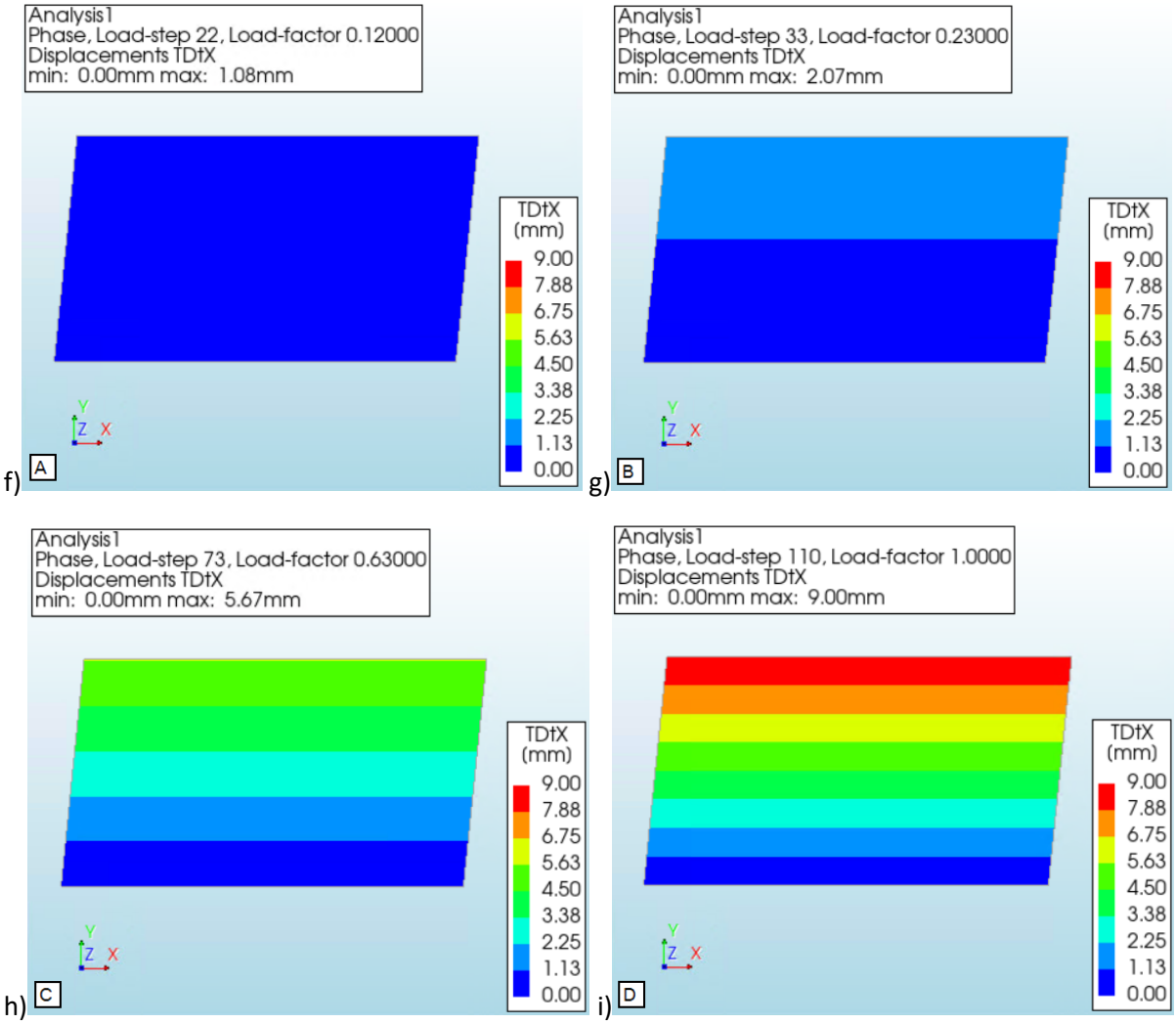

Figure 6.21: Results of finite element analysis IS1_eqEMM_shear_large_σ0.5_one_el_sq1_parameters. a-i: structure (a), finite element mesh (b), force-displacement curve (c), overview elements and nodes (d), overview iterative scheme (e), displacement at point A (f), displacement at point B (g), displacement at point C (h), displacement at point D (i)

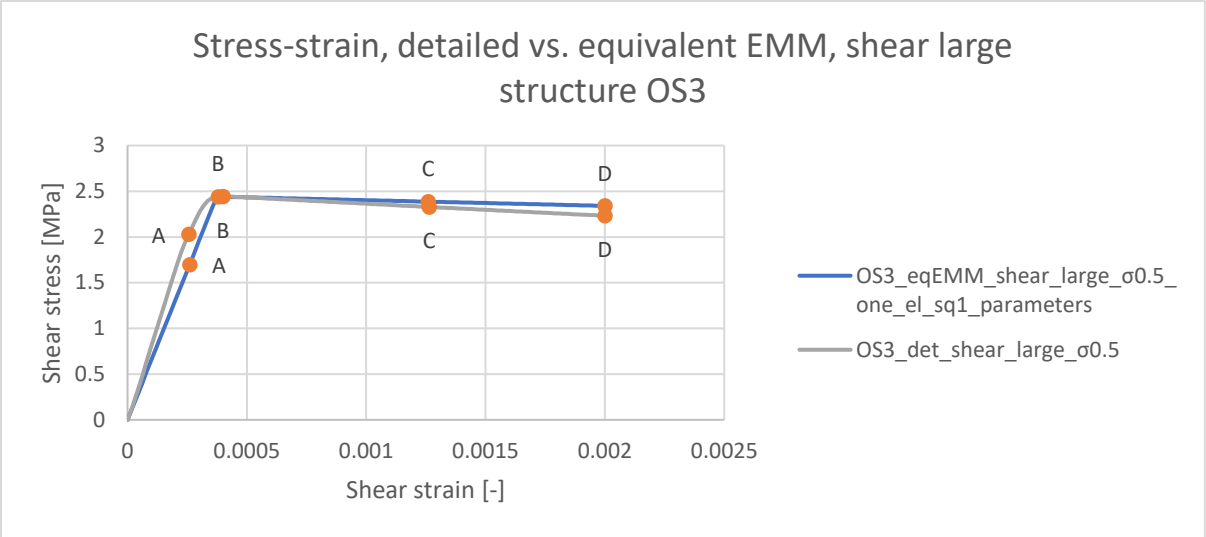

Figure 6.22: Stress-strain curves from shear models OS3_eqEMM_shear_large_σ0.5_one_el_sq1_parameters & OS3_det_shear_large_σ0.5

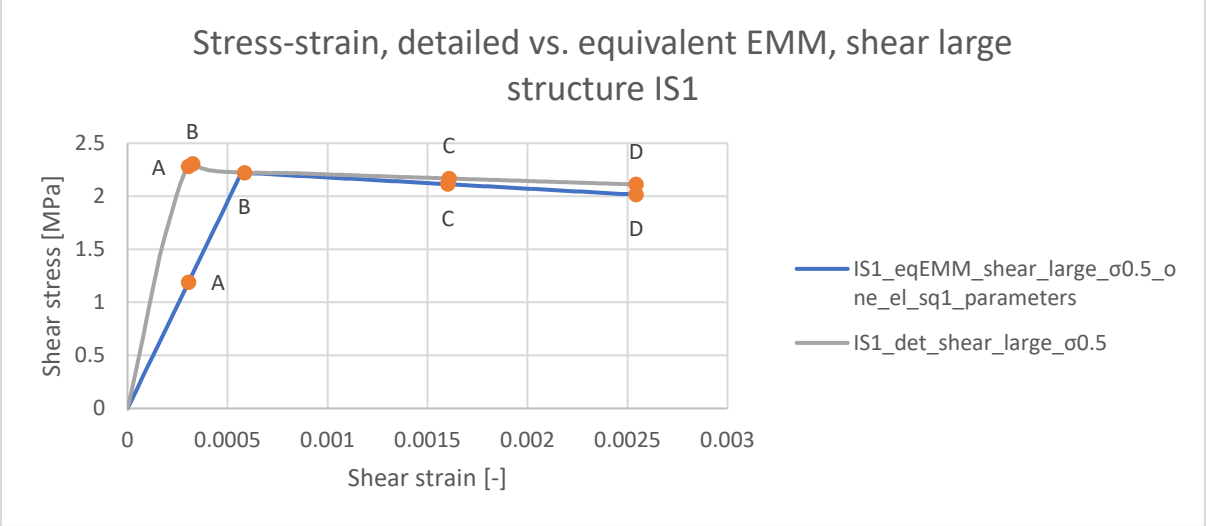

Figure 6.23: Stress-strain curves from shear models IS1_eqEMM_shear_large_σ0.5_one_el_sq1_parameters & IS1_det_shear_large_σ0.5

The points A-D for the equivalent models have been chosen as follows: point B is where the peak force occurs and point D where the displacement load has been fully applied. Points A and C are located at the same displacements as points A and C of the large detailed model. In the previous chapter, it became clear from the curves that the used parameters provide quite good results when compared to the results of the small detailed models. As the detailed models of the large structure are slightly different, it is expected that the results of the equivalent EMM models are slightly different for the large structures as well. Again, the curves of section IS1 are quite different, as the EMM parameters are based on the failure mode of the small structure, which included quite some bending. Even though there are some small differences, the equivalent EMM models which consist of one element are still quite similar to the detailed models. However, as mentioned before, more elements should be used to get a more realistic structural behaviour. The results of the models OS3_eqEMM_shear_large_σ0.5_mult_el_sq1_parameters and OS3_eqEMM_shear_large_σ0.5_mult_el_sq1_parameters are presented below (see appendix A for the explanation of the model names). Additionally, figures are presented which contain the stress-strain curves that result from the equivalent EMM models and their corresponding detailed model.

a)

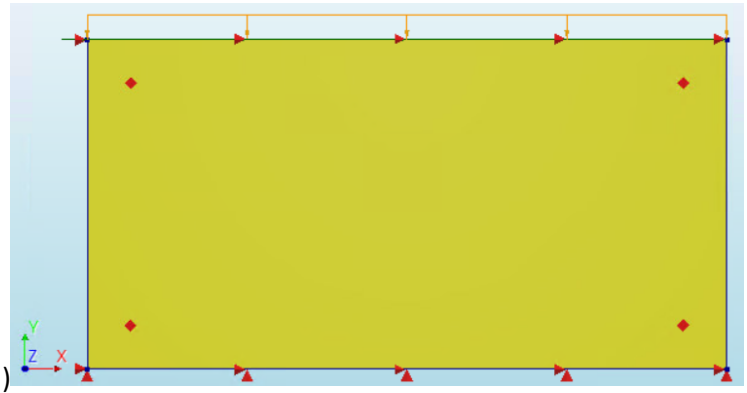

b)

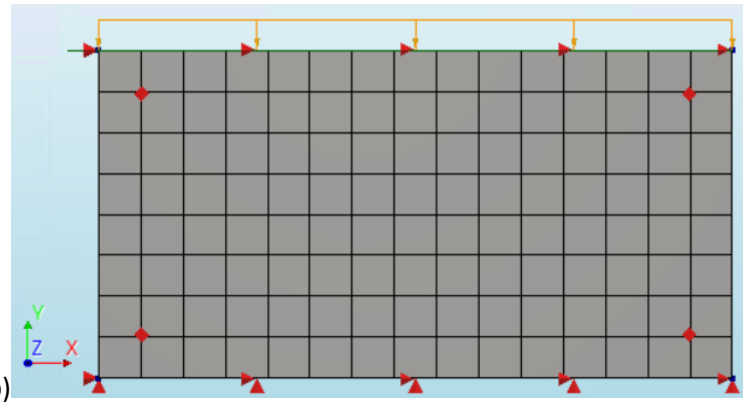

c)

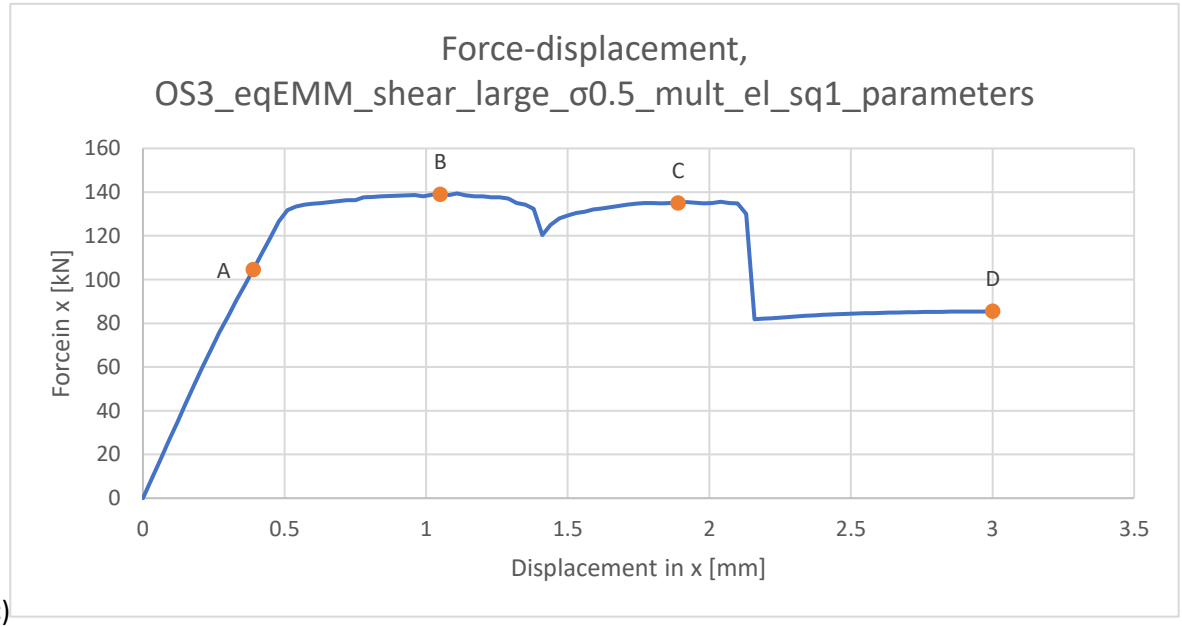

h)

Average element size [mm]		194x187.5
Number of elements	Q20SH	120
Total number of nodes		144

i)

Load	Compression		Translation	
Iteration method	Secant (Quasi-Newton)		Secant (Quasi-Newton)	
Convergence norms	Force	Displacement	Force	Displacement
Convergence tolerances	0.01	0.01	0.01	0.01
Step size	0.1(10)		0.01(100)	
Maximum number of iterations per step	100		100	
All norms satisfied	No		No	

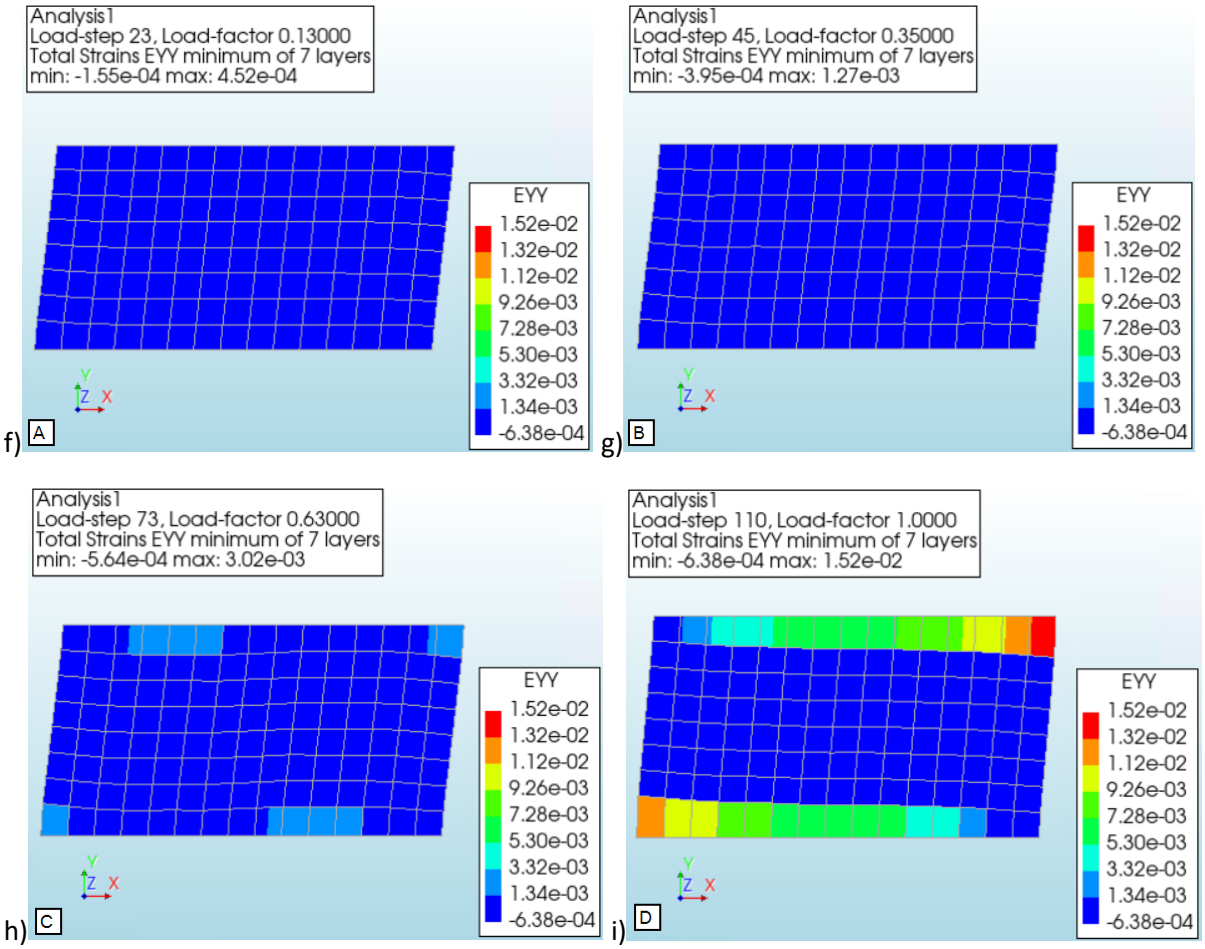

Figure 6.24: Results of finite element analysis OS3_eqEMM_shear_large_σ0.5_mult_el_sq1_parameters. a-i: structure (a), finite element mesh (b), force-displacement curve (c), overview elements and nodes (d), overview iterative scheme (e), strain at point A (f), strain at point B (g), strain at point C (h), strain at point D (i)

a)

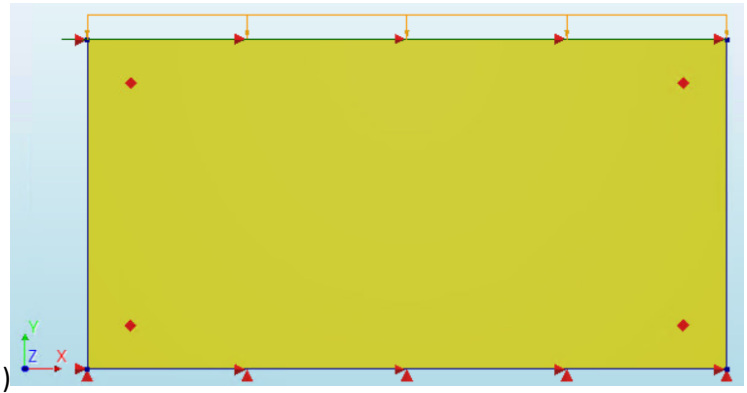

b)

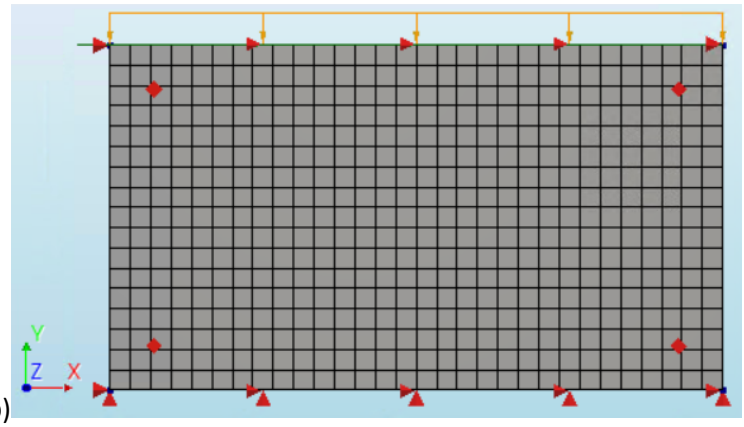

c)

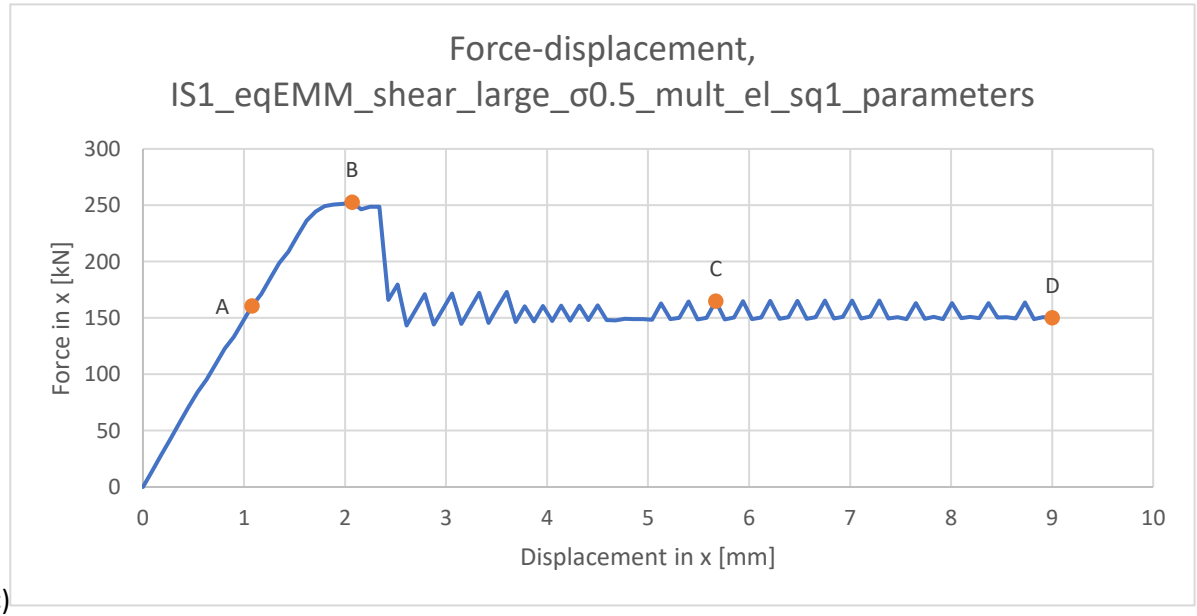

h)

Average element size [mm]		210.2x221.25
Number of elements	Q20SH	510
Total number of nodes		558

i)

Load	Compression		Translation	
Iteration method	Secant (Quasi-Newton)		Secant (Quasi-Newton)	
Convergence norms	Force	Displacement	Force	Displacement
Convergence tolerances	0.01	0.01	0.01	0.01
Step size	0.1(10)		0.01(100)	
Maximum number of iterations per step	100		100	
All norms satisfied	No		No	

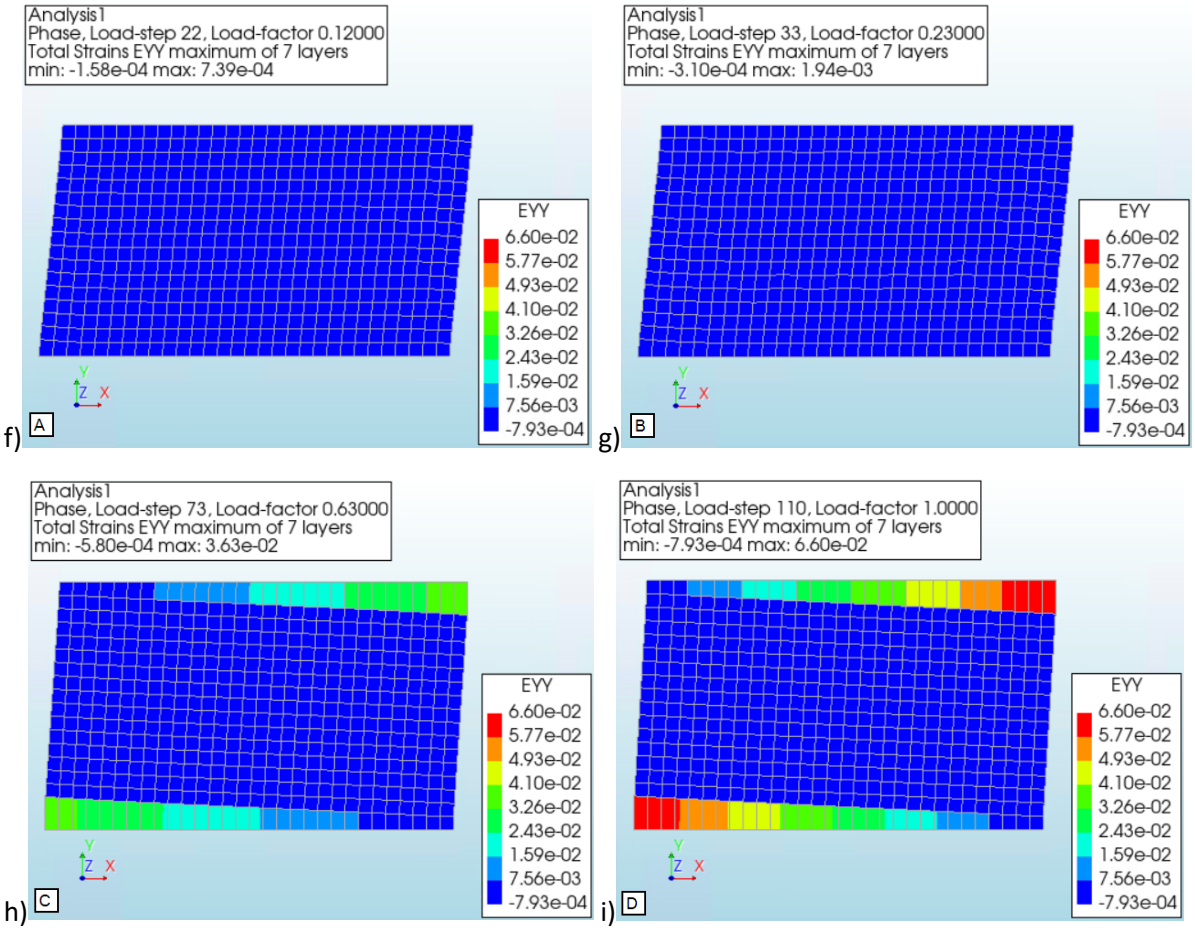

Figure 6.25: Results of finite element analysis IS1_eqEMM_shear_large_σ0.5_mult_el_sq1_parameters. a-i: structure (a), finite element mesh (b), force-displacement curve (c), overview elements and nodes (d), overview iterative scheme (e), strain at point A (f), strain at point B (g), strain at point C (h), strain at point D (i)

The failure modes of the equivalent EMM models loaded in shear are the same for the large structures as for the small structures. Again, the model of 1 element shows uniform failure, while the model with multiple elements shows cracking due to tension.

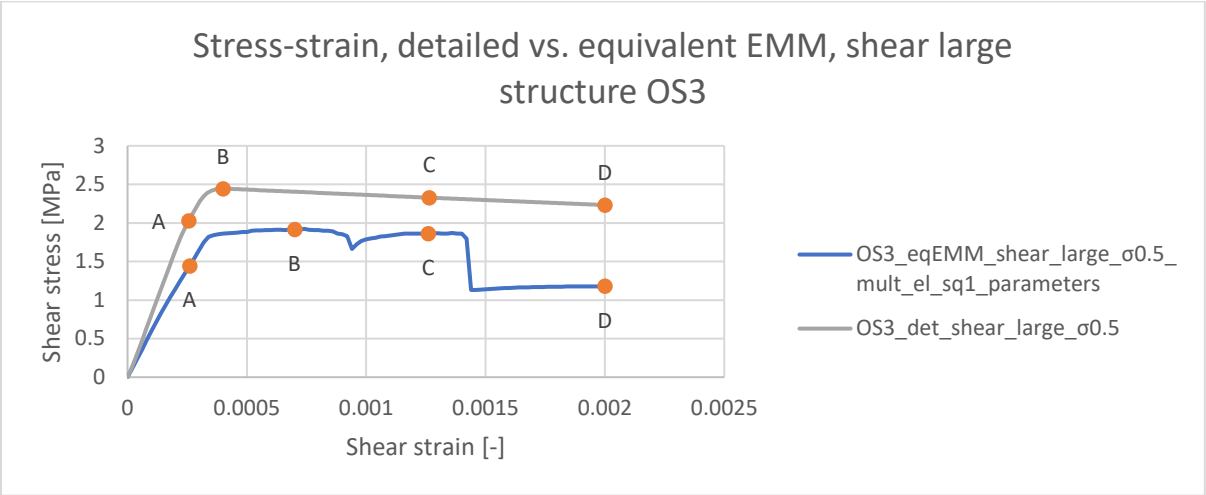

Figure 6.26: Stress-strain curves from shear models OS3_eqEMM_shear_large_σ0.5_mult_el_sq1_parameters & OS3_det_shear_large_σ0.5

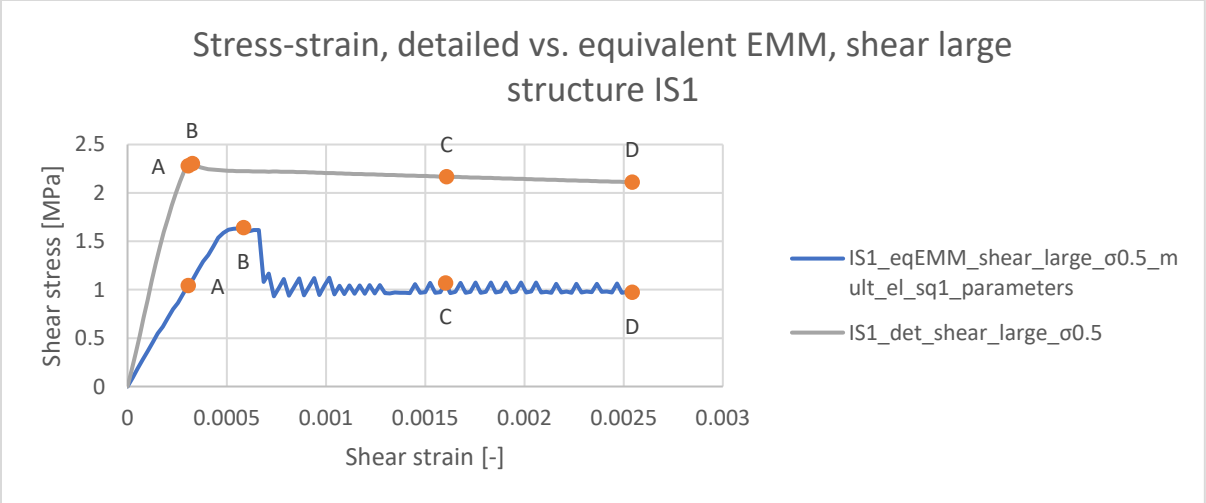

Figure 6.27: Stress-strain curves from shear models IS1_eqEMM_shear_large_σ0.5_mult_el_sq1_parameters & IS1_det_shear_large_σ0.5

In chapter 5, it was clear that using multiple elements resulted in having different F-D curves for the equivalent EMM model. However, by increasing the ratio of width/height and eliminating the bending aspect from the failure mode, the tensile stresses in the structure are much lower than before. This means that for small displacements, the equivalent EMM model now provides more accurate results. It is clear that the shear stiffness is still slightly lower, as well as the maximum shear stress, However, for small displacements, the curves are not too different. After the peak shear stress has been reached, the curve becomes a bit unstable due to some cracks that start to appear. However, all analysis results were still fully converging. It can be concluded that using multiple elements in the equivalent EMM model of the large structure gives reasonably accurate results, as long as the displacements remain within the linear-elastic regime. It is expected that the shear displacements in the final model will remain linear-elastic, which suggests the results that will be obtained in chapter 7 will include a good approximation of the shear behaviour. The EMM parameters will be calibrated to match the failure modes slightly better. The final parameters will be provided in section 6.4.

6.4 Overview final EMM parameters for all sections

All parameters have now been determined for the section size that corresponds to the floor height and the width of 1 plate. The same calibration has been performed here as in the previous chapter, as average values of the E-modulus in y-direction and the fracture energy in tension provide a better balance between the results of different loading types. The tables below contain all the relevant parameters that are required to use as input for the EMM. These are the parameters that will be used in the final model, which contains the entire structure of the lighthouse.

Table 6.2: Final elasticity parameters

Section	E-modulus in x-direction [MPa]	E-modulus in y-direction [MPa]	G-modulus [MPa]
OS1	47916.2	30038.0	7509.6
OS2	46164.9	31763.0	7823.9
OS3	37234.6	37114.1	7856.1
IS1	37385.0	58703.2	8485.2
IS2	32389.3	56001.4	7259.9
IS3	28253.3	63804.9	7234.8

As the stiffness of the larger structures was lower than in the small structures, especially in compression, the values for E_y have been lowered. Also, the shear modulus values are now more similar for all sections, as a result of increasing the width/height ratio of the structure. This ensured that the failure of the structure was caused by shear, not by a combination of bending and shear.

Table 6.3: Final cracking parameters

Section	Bed-joint tensile strength [MPa]	Head-joint tensile strength [MPa]	Fracture energy in tension [N/mm]	Angle between cracks [rad]
OS1	1.416	1.706	0.0320	0.241
OS2	1.573	2.079	0.0392	0.289
OS3	2.132	2.206	0.0609	0.369
IS1	1.552	2.028	0.0539	0.700
IS2	1.751	2.426	0.1254	0.774
IS3	2.504	2.714	0.2472	0.858

Due to the calibration of the E-modulus in y-direction and the fracture energy in tension, the bed-joint strength has also been calibrated.

Table 6.4: Final crushing parameters

Section	Compressive strength [MPa]	Fracture energy in compression [N/mm]	Factor to strain at compressive strength	Unloading factor
OS1	101.98	76.178	1.181	0
OS2	72.65	32.774	1.186	0
OS3	117.77	59.115	1.084	0
IS1	137.21	85.968	1.325	0
IS2	107.01	50.106	1.299	0
IS3	94.53	35.565	1.321	0

The compressive strength values are now significantly lower than before. By increasing the size of the structure, the stability greatly decreased, which caused failure of the structures at a much lower compressive force. This also results in much lower values for the fracture energy. In addition, as the F-D curves are now only in the linear-elastic part, the values of n are much closer to 1 than before.

Table 6.5: Final shear failure parameters

Section	Friction angle [rad]	Cohesion [MPa]	Fracture energy shear [N/mm]
OS1	0.378	1.519	76.178
OS2	0.378	1.831	32.774
OS3	0.376	2.247	59.115
IS1	0.329	2.130	85.968
IS2	0.375	1.870	50.106
IS3	0.373	2.658	35.565

As mentioned before, by increasing the width/height ratio of the structure, the failure due to shear was enforced instead of having failure due to a combination of bending and shear. This results in output friction angles which are almost equal to the input friction angle of 0.38 rad. The values of cohesion are almost the same as before for the outer column sections. As the small structures already had quite a large width/height ratio, the failure in those models was already very close to pure shear. As this was not the case for the small structures of the inner column sections, the cohesion values that were obtained from the results of the large structures are slightly higher than the values obtained from the smaller models. By reducing the amount of bending of the plates, the maximum allowable shear force has been increased.

6.5 Final comparison detailed & equivalent EMM models

All required EMM parameters have been obtained and the necessary calibrations have been applied. Before using the values as input in such a large structure as the lighthouse, it is important to know what differences can be expected between the results of the equivalent EMM models and detailed models. For sections OS3 and IS1, a final comparison between the detailed and equivalent EMM models will be given. The models that were presented in this chapter, which are the assemblies of plates (large structures), will be analysed for this comparison. For all load cases, the results of the equivalent EMM models for sections OS3 and IS1 will be presented in appendix E. The figures that are presented here contain the stress-strain curves that result from the equivalent EMM models and their corresponding detailed model. First, the bed-joint tension load case is analysed. The models that are analysed are OS3_eqEMM_ten_bed_large_ final_parameters andIS1_eqEMM_ten_bed_ small_ final_parameters (see appendix A for the explanation of the model names).

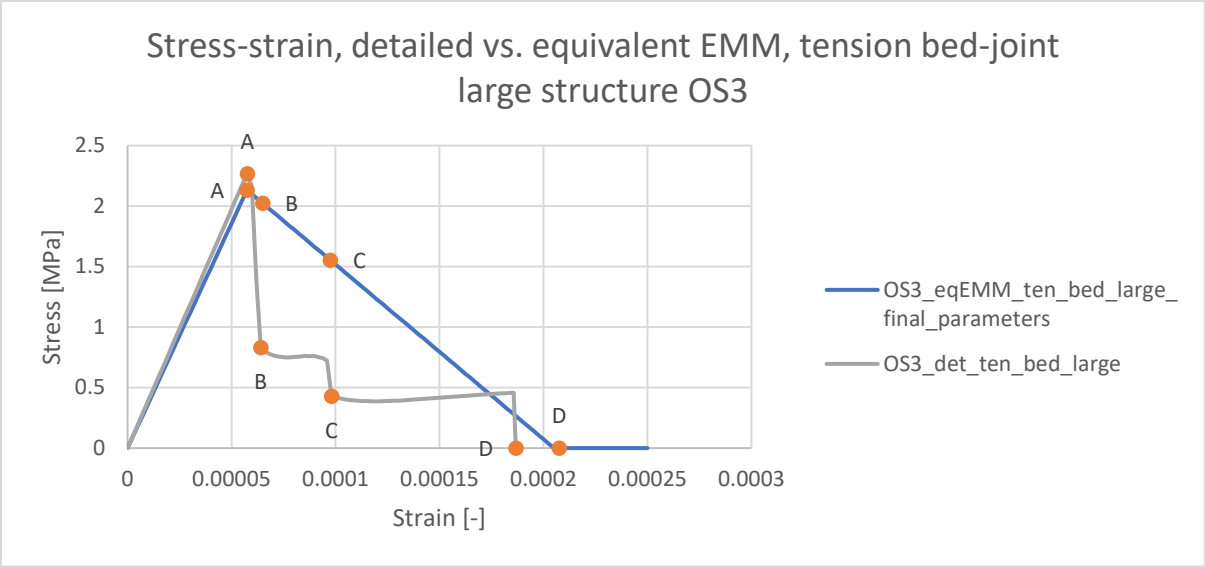

Figure 6.28: Stress-strain curves from tension bed-joint models OS3_eqEMM_ten_bed_large_final_parameters & OS3_det_ten_bed_large

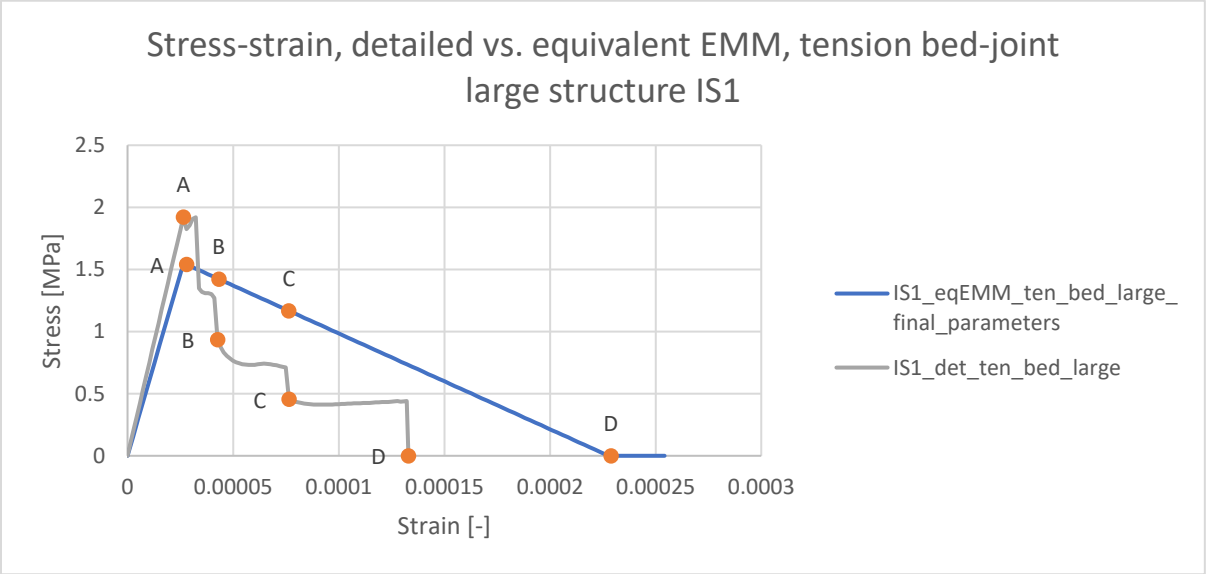

Figure 6.29: Stress-strain curves from tension bed-joint models IS1_eqEMM_ten_bed_large_final_parameters & IS1_det_ten_bed_large

From the comparison between the final equivalent EMM models and the detailed models, it is clear that the linear-elastic behaviour of the models is very similar. The stiffness of the models is almost the same, but the peak stresses are slightly different. In addition, after the peak stress, the curves are a quite different. As mentioned before, the curve linearly goes to 0 kN in the EMM, which is not the case in the detailed models, where the curves goes to 0 kN with some sudden drops due to disconnecting of the interface. For some column sections, the ultimate displacements of the models are quite similar, but the stress-strain figure of section IS1 shows that there is quite a large difference between the equivalent EMM and the detailed model. Therefore, it is expected that when the obtained EMM parameters are used in a model of the lighthouse, the structural behaviour can be accurately modelled for the linear-elastic region. Once the stresses exceed the strength, the model will likely become less accurate. Next, the tension head-joint models OS3_eqEMM_ten_head_small_final_parameters and IS1_eqEMM_ten_head_small_final_parameters are analysed (see appendix A for the explanation of the model names).

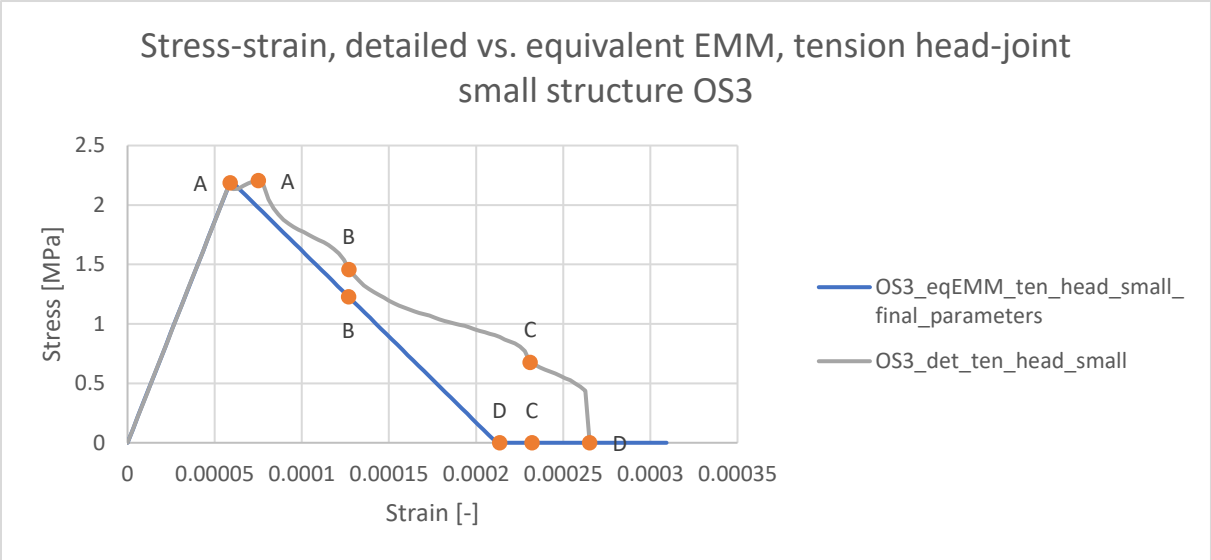

Figure 6.30: Stress-strain curves from tension head-joint models OS3_eqEMM_ten_head_small_final_parameters & OS3_det_ten_head_small

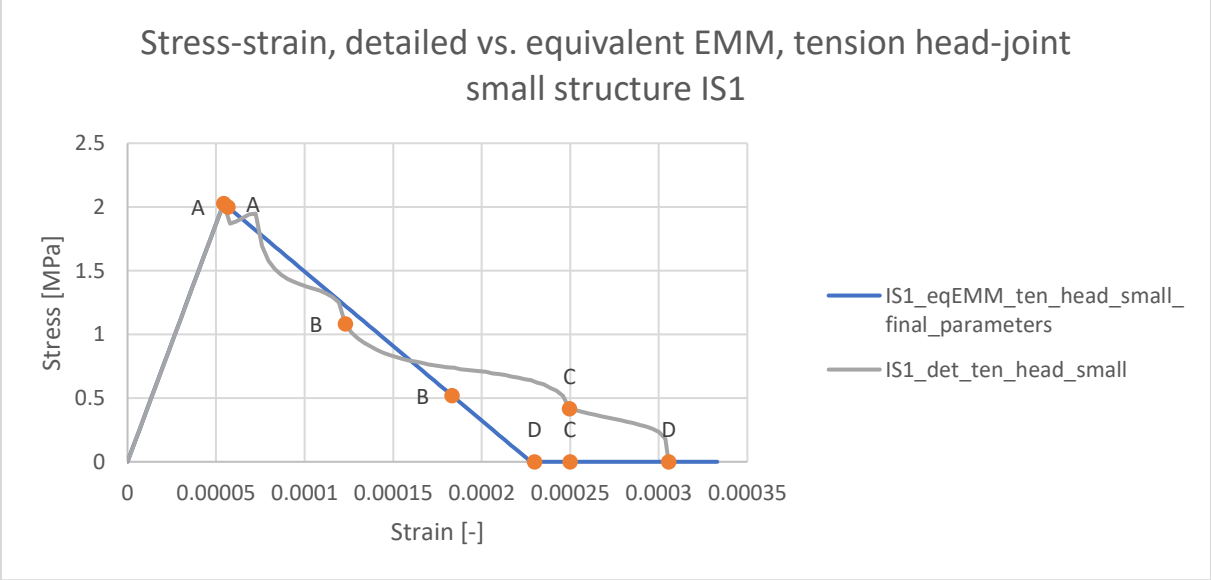

Figure 6.31: Stress-strain curves from tension head-joint models IS1_eqEMM_ten_head_small_final_parameters & IS1_det_ten_head_small

From the final comparison of the head-joint models, it is clear that the same conclusion can be made as for the bed-joint tension models. It is clear that the linear-elastic behaviour of the models is very similar, but when the stresses exceed the strength, there is quite a difference between the stress-strain curves. The linear-elastic parts of the curves seem even more accurate for the head-joint tension models, as it is observed that the stiffnesses of the models are exactly the same and the peak stresses are also very close. However, there is quite a difference between the ultimate displacement that can be reached. Therefore, the same conclusion as for the bed-joint tension loading can be made: it is expected that when the obtained EMM parameters are used in a model of the lighthouse, the structural behaviour can be accurately modelled for the linear-elastic region. However, when the stresses exceed the strength, the model will likely become less accurate. Next, the compression models OS3_eqEMM_comp_large_final_parameters and IS1_eqEMM_comp_large_final_parameters are analysed (see appendix A for the explanation of the model names).

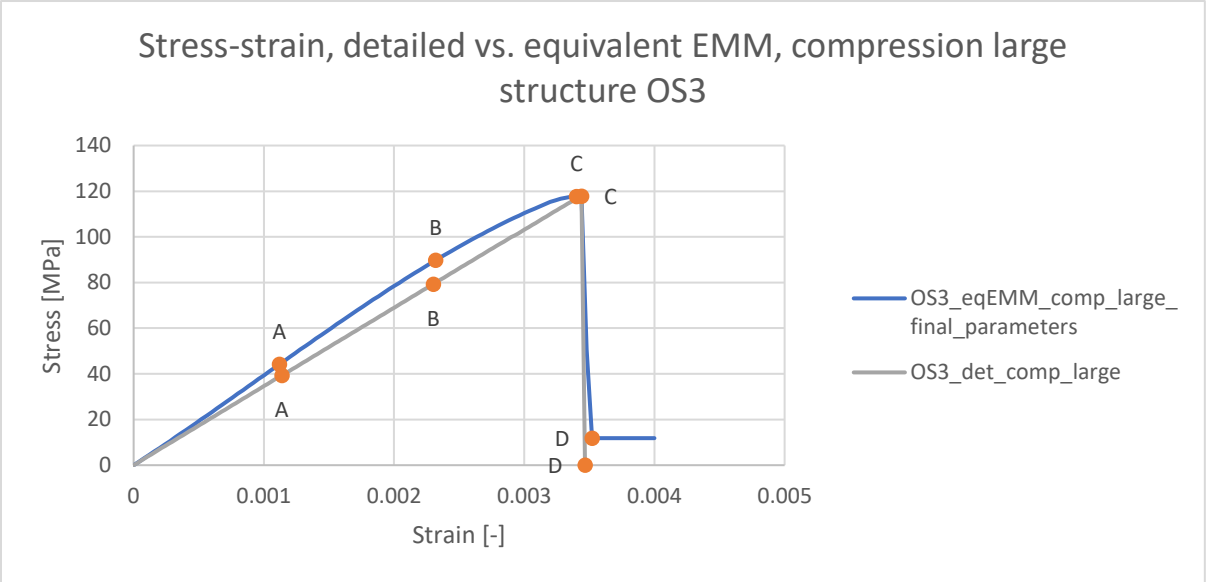

Figure 6.32: Stress-strain curves from compression models OS3_eqEMM_comp_large_final_parameters & OS3_det_comp_large

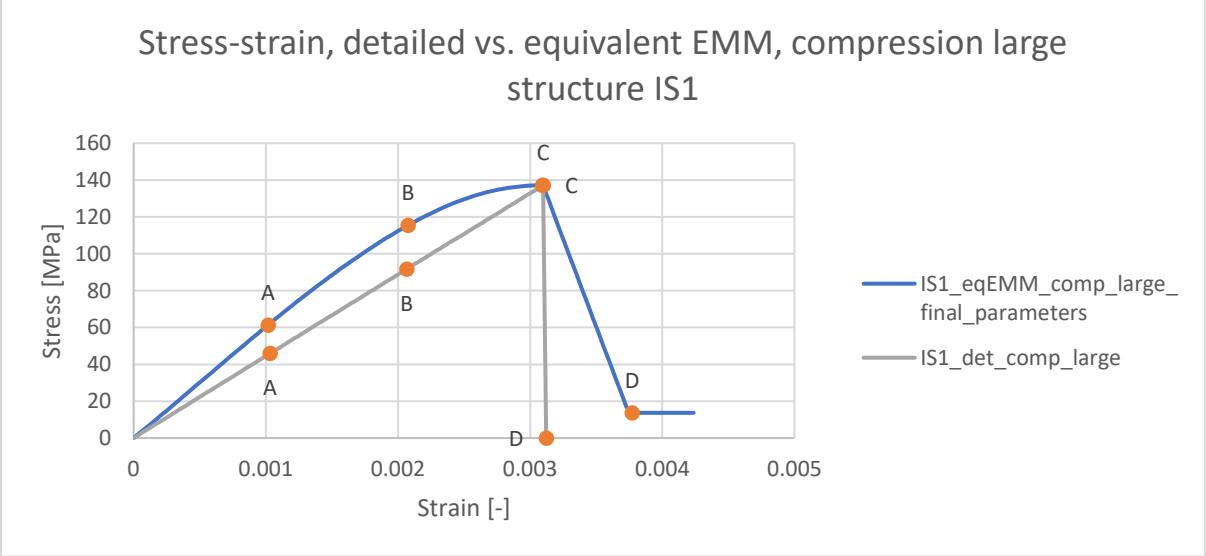

Figure 6.33: Stress-strain curves from compression models IS1_eqEMM_comp_large_final_parameters & IS1_det_comp_large

From the comparison of the stress-strain curves, it is clear that the results of the equivalent EMM model are quite accurate. As the factor to strain is not equal to 1, the curve of the equivalent EMM model is not fully linear. This results in slightly higher stresses compared to the detailed models. Another difference between the models, which has already been discussed, is that there will be a residual strength in compression in the EMM, which means the stresses will not reduce to 0 MPa. Therefore, for the compressive behaviour of the lighthouse, it can be expected that the differences between an equivalent EMM model and a detailed model will be very similar. Only after the peak stress has been reached, the equivalent EMM model will still have a residual strength, which will allow the displacements to become very large very quickly. This will likely cause the model to become unstable very quickly as well. Finally, the shear models OS3_eqEMM_shear_large_σ0.5_mult_el_final_parameters and IS1_eqEMM_shear_large_σ0.5_mult_el_final_parameters are analysed (see appendix A for the explanation of the model names).

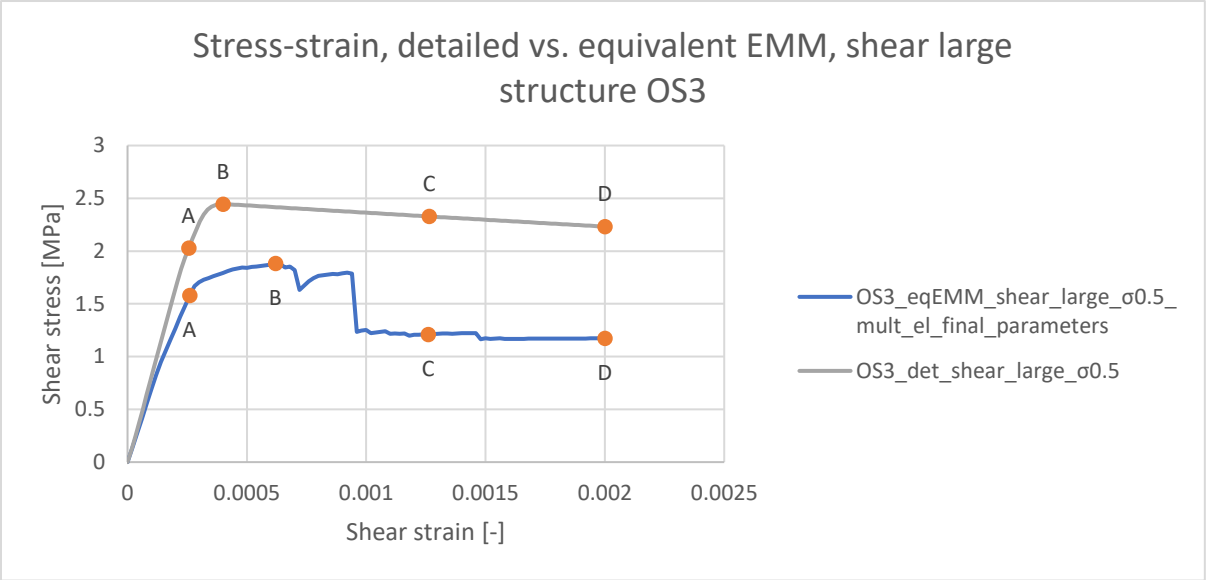

Figure 6.34: Stress-strain curves from shear models OS3_eqEMM_shear_large_σ0.5_mult_el_final_parameters & OS3_det_shear_large_σ0.5

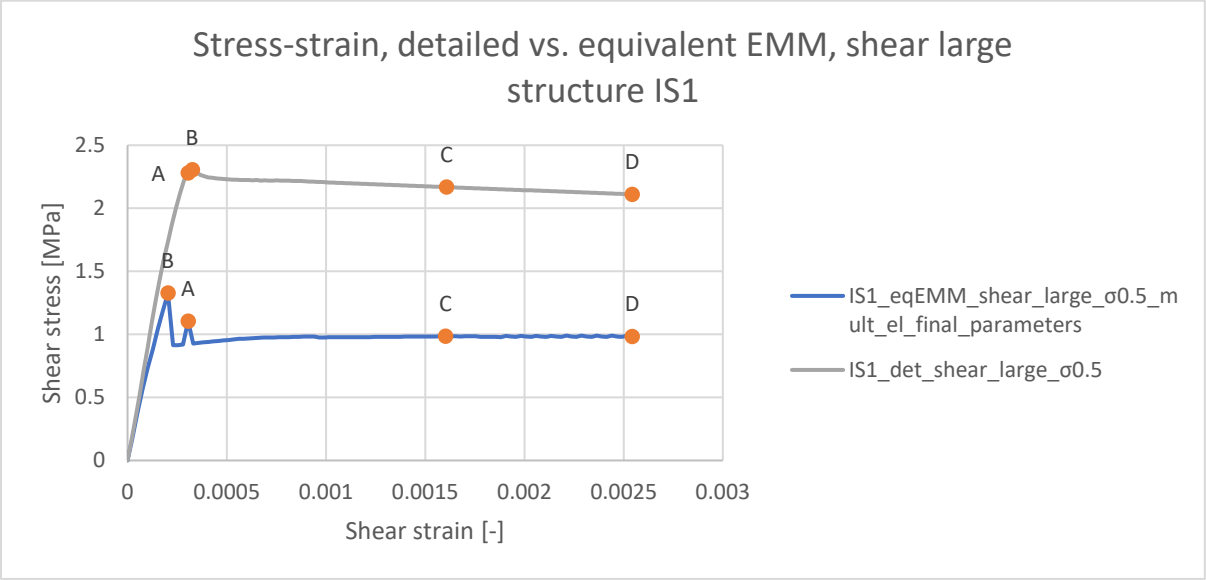

Figure 6.35: Stress-strain curves from shear models IS1_eqEMM_shear_large_σ0.5_mult_el_final_parameters & IS1_det_shear_large_σ0.5

From the final comparison of the shear models, it can be seen that for small displacements, the results of the equivalent EMM model are quite similar to the results of the detailed model. After the final adjustments, the stiffness of the model is now much more accurate as well. After the peak shear stress has been reached, it seems that some cracks that start to appear. This shows in the fact that the peak shear stress is much lower in the equivalent EMM models. Additionally, the residual stresses are also much lower in the equivalent EMM models. Therefore, it can be expected that when the final parameters are used in an equivalent EMM model of the lighthouse, the shear behaviour will be quite similar to that of a detailed lighthouse model, when the shear displacements remain small. Once the shear displacements start to increase, the results will likely become less accurate.

7 Analysis of equivalent EMM lighthouse model

Now, the equivalent EMM model of the lighthouse will be defined and analysed. The input parameters for the EMM have been determined in the previous chapter, where the size effect has been taken into account. An analysis is performed which shows the structural behaviour of the lighthouse when loaded by self-weight and wind. By comparing the results of the analyses to the results of the analysis of the detailed model of PT Structural, an answer to the final sub-question is obtained. In addition, an analysis is made to show the compressive structural behaviour of the lighthouse, by increasing the gravitational acceleration, causing the self-weight load to be multiplied by a load factor of 20.

7.1 Model definitions

First, the geometry of the lighthouse in the model has to be defined. The outer column has a diameter of 10.5 meters at the bottom and 3.9 meters at the top. The inner column starts at a diameter of 3 meters, and ends at 1.5 meters at the top. The top and bottom are connected linearly, which means the diameter decreases linearly as the height increases. In reality, the thickness of the plates will also decrease linearly with the height of the lighthouse. However, as discussed before, both columns were divided into three sections, where each section has its own thickness. Each section also has its own set of input parameters, as presented in section 6.4. The next thing to consider is that there are 17 floors in the lighthouse. The floors connect the two columns and have a major influence on the structural stability of the lighthouse. The behaviour of the floors is not something that will be studied here, so only the effect of the floors on the columns is implemented in the model. This can be achieved by adding tyings to the columns at the height of every floor level. The tyings ensure that the columns will have equal translations in the x- and z-directions (horizontal) at the floor level, which is the global effect of the presence of the floors. This allows to leave the floor structures out of the model, which means no unnecessary extra elements, so the running time of the analysis is reduced a bit more. However, by modelling the floors in this way, the local effect of the floors is not implemented in the model. The table below provides an overview of the heights at which a floor is present. Additionally, the radius of the inner and outer columns at every floor level is given.

Table 7.1: Overview of floor heights and the corresponding inner and outer column radius

Floor	**Height [m]**	**r_{outer} [m]**	**r_{inner} [m]**
1	3.80	5.02	1.44
2	7.40	4.81	1.39
3	10.95	4.60	1.33
4	14.45	4.39	1.28
5	17.85	4.19	1.23
6	21.25	3.99	1.18
7	24.55	3.79	1.13
8	27.85	3.59	1.08
9	31.10	3.40	1.03
10	34.30	3.21	0.98
11	37.50	3.02	0.93
12	40.60	2.84	0.89
13	43.70	2.65	0.84
14	46.75	2.47	0.80
15	49.75	2.29	0.75
16	52.75	2.11	-
17	55.50	1.95	-

As the inner column only has a height of 49.75 m and floors number 16 and are placed at larger height, there is no inner column radius provided for these floors. In addition, the height of the structure in the model is only 55.5 meters, while the actual height of the lighthouse is 63.45 meters. This is due to the fact there is a chamber at the top, which is where the light is located. Similar to the floors, the chamber will not be present in the model, as the main focus of the analysis is on the inner and outer columns of the lighthouse. However, the presence of the chamber will be taken into account when determining the magnitude of the relevant forces, self-weight and wind. Regarding the boundary conditions of the structure, the bottom of both columns are supported in x, y and z. An overview of the elements and nodes of the model is given in the table below.

Table 7.2: Overview of elements and nodes of thesis model

Average element size [mm]		200x200
Number of elements	Q20SH	36882
	T15SH	161
Total number of nodes		37100

The total number of nodes for the model of the entire lighthouse is equal to 37100. In chapter 6.3, the model of IS1_det_shear_large was analysed. This model consisted of 12 plates and contained a total of 137658 nodes. In the EMM model, regular curved shell elements are used, which allows a much larger element size to be used, the total amount of elements and nodes is decreased significantly, which results in a much shorter running time for the finite element analysis. The model of the lighthouse and the finite element mesh are presented in the figure below.

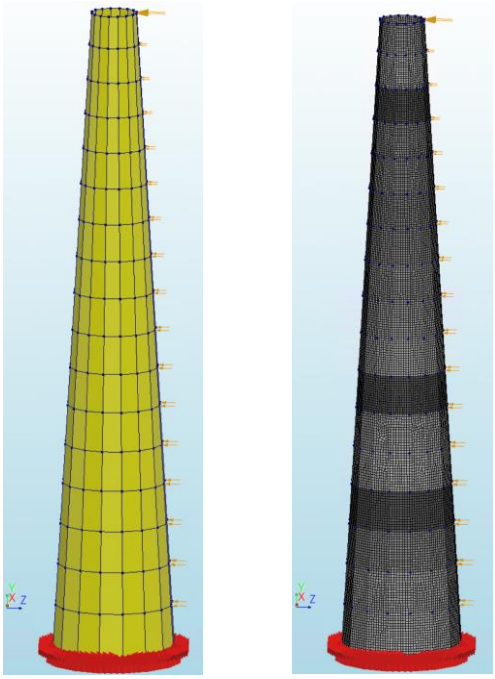

Figure 7.1: Finite element structure of thesis model (left) and finite element mesh of thesis model (right)

7.2 Calculation of the forces

There are two forces that will be applied to the lighthouse: self-weight and wind load. The combination of these forces is considered in the report of PT Structural Design & Analysis. In addition, part of their study was to determine the maximum wind velocity at which there are no vertical tensile stresses in the outer column of the lighthouse. In order to compare the static analysis of both models, the same load combination of self-weight and wind will be applied here. The calculations of those forces are provided in this section.

The self-weight will be applied by giving the each column section a mass density. The report 'De bouwwijze van de gietijzeren vuuroten te Kijkduin' states the following about the self-weight of the different parts of the lighthouse: The outer column plates weighed a total of 352.500 kg, the inner column plates 66700 kg, and the floors 73500 kg. The spiral staircase weighed 11100 kg, and including all other components such as the entrance door, windows, balustrade, etc., the entire delivery involved 506100 kg of cast iron. This means the other components (door, windows, balustrade, etc.) had a total weight of 2300 kg (Suchtelen, 1978).

Note that the weight of the top chamber is also included in the numbers above. The actual weight of the chamber itself was not found in any literature, so the total weight will not be applied as a force on top, but will be equally divided over each section. The calculation of the weight per section will be based on the volume of the section. The volume of a full plate can be determined by adding the volumes of the flanges, stiffeners and the plate itself. The stiffeners are triangular and each have a volume of $0.5 * 140 * 60 * 20 = 84000$ mm^3. The flanges have a thickness of 20 mm and a width of 60 mm and are present over the entire edge of the plate. The volume of one plate is then multiplied by the number of plates in the section. The number of plates per section can easily be determined when looking at the number of floors per section. For the outer column sections, there are 4 layers of plates per floor, and 16 plates per layer. The inner column sections only have 2 layers of plates per floor and 8 plates per layer. This means there are 64 plates per floor for the outer column sections and 16 plates per floor for the inner column sections. The relevant dimensions of the plates and the total volume of each section is given in the tables below.

Table 7.3: Plate dimensions and volumes

Section	h [m]	t [m]	b [m]	$n_{stiffeners}$	V_{plate} [m^3]	n_{floors}	$V_{section}$ [m^3]
OS1	0.885	0.0332	1.802	5	0.36	6	23.09
OS2	0.8125	0.0290	1.368	4	0.19	5	12.17
OS3	0.750	0.0249	0.970	3	0.14	6	8.70
IS1	1.770	0.0244	1.051	3	0.32	6	5.05
IS2	1.624	0.0234	0.830	2	0.19	5	3.01
IS3	1.532	0.0206	0.662	2	0.11	4	1.69

The total volume of the outer column is equal to 43.96 m^3, while the inner column has a volume of 9.75 m^3. By using the ratio $V_{section}/V_{column}$ and multiplying this with the weight of the column, the total weight of the plates per section is determined. Next, it will be determined how the weight of the floors, stairs and other components must be divided over the column sections. This will be determined by calculating the area of each floor and looking at which section each floor is placed. The area of the floors can be calculated by using the radii of the columns, which are provided in the previous section. The area of the floor is equal to $\pi * (r_{outer}^2 - r_{inner}^2)$. For every floor that is connected to both columns, it is assumed that the weight will be equally carried by the outer and inner columns. The floor area per section can now be determined. If this is divided by the total floor

area, a ratio is obtained which can be multiplied by the total floor weight to obtain the floor weight per section. The same ratio is then multiplied with the weight of the stairs and the other components to obtain the weight of those parts per section. By dividing the total weight of the section by its volume, the mass density can finally be obtained. All relevant values are given in the table below.

Table 7.4: Resultant mass density values per section

Section	Weight of plates [kg]	Weight of floors [kg]	Weight of stairs + other [kg]	Total weight [kg]	Mass density [kg/m3]	Mass density [T/mm3]
OS1	185157.26	20891.91	3808.87	209858.04	9087.34	9.087E-09
OS2	97605.31	9882.37	1801.68	109289.37	8977.52	8.978E-09
OS3	69737.43	7519.61	1370.92	78627.96	9039.89	9.040E-09
IS1	34524.94	20891.91	3808.87	59225.72	11735.71	1.174E-08
IS2	20617.14	9882.37	1801.68	32301.20	10718.21	1.072E-08
IS3	11557.92	4431.82	807.98	16797.71	9942.66	9.943E-09

The second load to be calculated is the wind load. The same calculation method will be applied as in the report of PT Structural Design & Analysis. The followed the rules that are described in the code NEN-EN 1991-1-4 + A1 + C2:2011/NB:2019. Many different factors are involved in determining the wind load, but since the same values will be used as the company PT Structural Design & Analysis used, the relevant factors to calculate the force can be taken from their report. As mentioned, part of their study was to find the maximum wind velocity at which there are no vertical tensile stresses in the outer column of the lighthouse. From their research, a value of 18.3 m/s was found. In the Eurocode, a velocity of 29.5 m/s is used to determine the maximum wind load. In the analysis here, the maximum wind load (based on v = 29.5 m/s) will be applied in very small steps. By analysing the results for every step, it is possible to find both the maximum wind velocity at which there are no vertical tensile stresses in the outer column and the maximum wind velocity at which the structure will fail.

Essentially, only 2 parameters have to be used from their report, which are the peak velocity pressure $q_p(z)$, which depends on the height z, and the factor $c_{p0,h}$, which is the pressure coefficient at height z. PT Structural Design & Analysis determined these values at every meter, and applied a force at every meter as well. In this study, a simplified approach will be used where the forces will only be applied at every floor level. Through linear interpolation, the values for $q_p(z)$ can be determined for every floor level. As the lighthouse is actually 63.45 meters high, there will also be forces acting on the structure above the columns. Therefore, $q_p(z)$ will also be determined for a height of 64 meters, and the resulting force will be applied at the top of the lighthouse. As the force is translated to a lower point, the difference in the resulting bending moment from the force should also be taken into account.

Next, the values of $c_{p0,h}$ can simply be obtained from the report of PT Structural Design & Analysis, as only three different values are used by them. The final required parameter is the area over which the peak velocity pressure acts, which will be equal to the area between two floors. In addition, the resulting bending moment at the bottom of the structure due to the forces can be determined. The values are given in the table below for all relevant heights. The value of b represents the width of the column at the height z.

Table 7.5: Wind loads at different heights

z [m]	b [m]	$q_p(z)$ [m]	$c_{p0,h}$ [-]	A [m^2]	F_{wind} [kN]	M_{wind} [kNm]
64.00	3.900	2.214	0.71	33.150	52.11	3335.03
55.50	3.900	2.163	0.71	11.175	17.16	952.45
52.75	4.227	2.142	0.72	13.216	20.38	1075.18
49.75	4.584	2.119	0.72	14.286	21.79	1084.13
46.75	4.941	2.101	0.72	15.622	23.63	1104.50
43.70	5.303	2.077	0.72	17.011	25.44	1111.71
40.60	5.672	2.046	0.72	18.154	26.74	1085.78
37.50	6.041	2.020	0.72	19.939	29.00	1087.45
34.30	6.421	1.992	0.72	21.156	30.34	1040.56
31.10	6.802	1.953	0.72	22.733	31.97	994.27
27.85	7.188	1.914	0.73	24.368	34.05	948.33
24.55	7.581	1.873	0.73	25.663	35.09	861.35
21.25	7.973	1.820	0.73	27.795	36.93	784.74
17.85	8.377	1.761	0.73	29.170	37.51	669.47
14.45	8.782	1.696	0.73	31.464	38.95	562.80
10.95	9.198	1.486	0.73	33.402	36.23	396.76
7.40	9.620	1.579	0.73	35.403	40.79	301.88
3.80	10.048	1.284	0.73	39.041	36.59	139.06

The force at every floor level can now be determined. In the model, the wind load will be applied by putting two forces on the edges of one side of the outer column. This causes the load to act perpendicularly to this side. The values of the forces that will be applied at every floor level, and the resulting bending moments per force, are given in the table below.

Table 7.6: Final wind load values applied at the floor height z

Wind force	z [m]	F/2 [kN]	M/2 [kNm]
w01	55.50	34.64	1922.27
w02	52.75	10.19	537.59
w03	49.75	10.90	542.06
w04	46.75	11.81	552.25
w05	43.70	12.72	555.86
w06	40.60	13.37	542.89
w07	37.50	14.50	543.73
w08	34.30	15.17	520.28
w09	31.10	15.98	497.13
w10	27.85	17.03	474.17
w11	24.55	17.54	430.67
w12	21.25	18.46	392.37
w13	17.85	18.75	334.74
w14	14.45	19.47	281.40
w15	10.95	18.12	198.38
w16	7.40	20.40	150.94
w17	3.80	18.30	69.53

The total wind force that is applied to the structure is equal to the sum of all F/2 values multiplied by 2, which is equal to 575 kN. The resulting bending moment at the bottom of the lighthouse due to the wind forces is 17093 kNm. The values of the forces that PT Structural Design & Analysis applied resulted in a total force of 560 kN and a bending moment of 16207 kNm. It is clear that the forces are quite similar, but the total force that is applied here is slightly higher. Also, since the total bending moment is already higher than in the PT report, it is not necessary to add an additional bending moment to compensate for the transfer of the load at 64 meters to 55.5 meters. Also, it was observed that the company PT Structural Design & Analysis has applied the load in the form of a pressure profile, see the figure below. This means at every side of the column, a positive or negative pressure is applied. In this study, the load application will consist of just two point loads at every floor, as can also be seen in the figure below. This means the local effects of the pressure differences caused by the wind will not really be visible here. However, the global effect of the wind load will be accurately modelled with the load application that was used here.

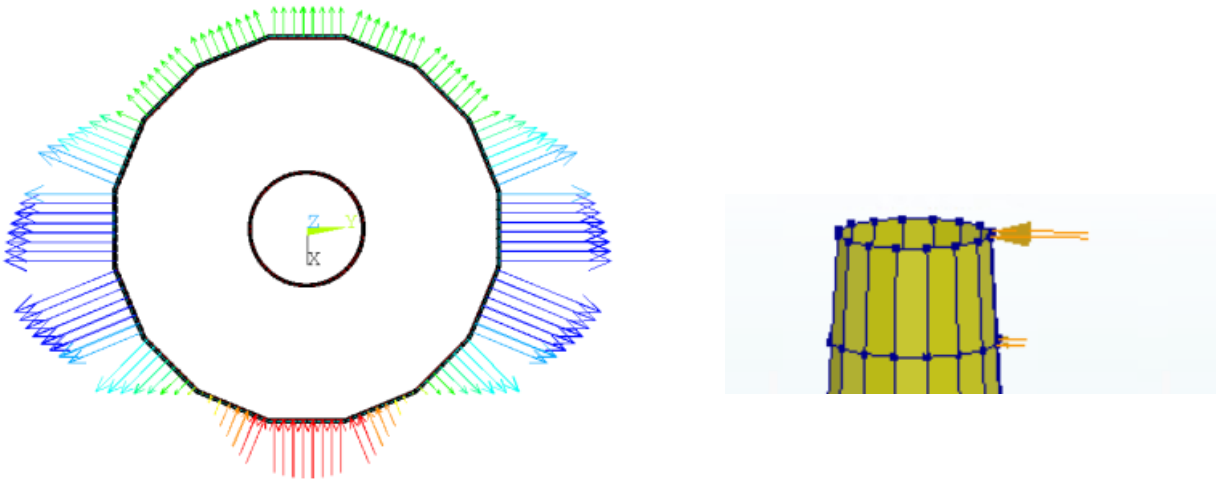

Figure 7.2: Pressure profile used to apply wind load in PT model (left) (PT Structural Design & Analysis bv, 2022) vs. wind load application in thesis model (right)

7.3 Results comparison thesis model and PT model

7.3.1 Dynamic analysis

In order to simplify the analysis of the differences and similarities between the models, the models will be referred to as follows: the detailed model of the company PT Structural Design & Analysis will be referred to as ‘PT model’, while the model which was created in this thesis, where the EMM is used, will be referred to as ‘thesis model’. The first analysis will be of the eigenfrequencies of the structure, which are the frequencies at which the structure will naturally start to vibrate. The values are heavily dependent on the mass and stiffness of the structure. The first three eigenfrequencies have been determined by DIANA. Eigenfrequencies 1, 2 and 3 can be observed in the figures below. The first three eigenfrequencies that PT Structural have determined for their model are also given, as well as a table which provides an overview of the eigenfrequency values.

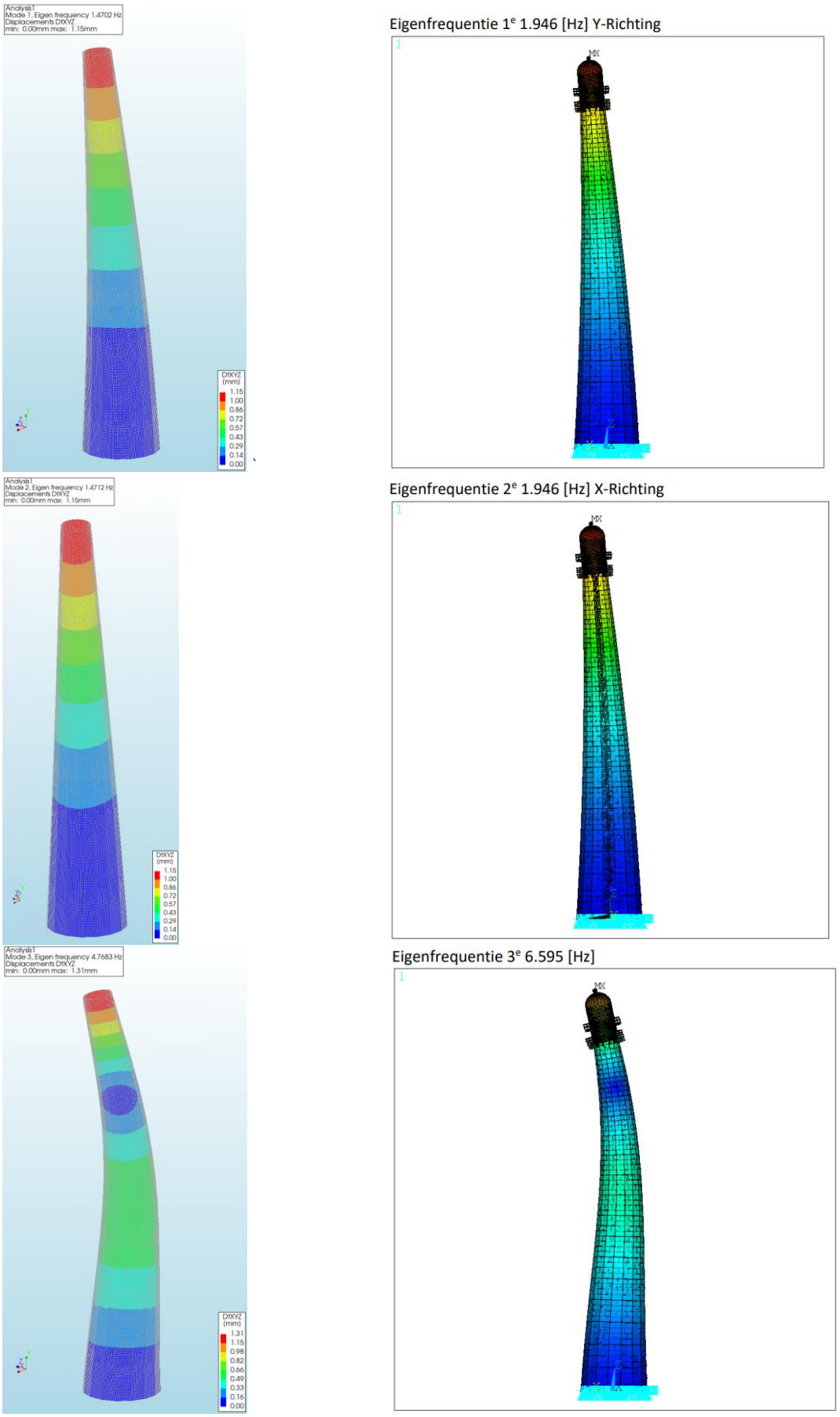

Figure 7.3: Eigenfrequencies 1 (top), 2 (middle) and 3 (bottom) of the thesis model (left) and the PT model (right)

Table 7.7: Eigenfrequencies 1, 2 and 3 of both models

Model	Eigenfrequency 1 [Hz]	Eigenfrequency 2 [Hz]	Eigenfrequency 3 [Hz]
Thesis model	1.470	1.471	4.768
PT model	1.946	1.946	6.595

The second eigenfrequency is (almost) exactly the same as the first value, as this results in the same structure shape, only displaced in a different direction. Furthermore, it is clear that the eigenfrequencies of the thesis model are a bit lower than those of the PT model. As mentioned, the eigenfrequencies of a structure are dependent on its mass and stiffness. The mass of the structure in the PT model was based on the same report as in this study, so the total mass of the structures should be quite similar. The main difference between the structures is in the way that they were modelled. In the thesis model, the structure has a height of only 55.5 meters, whereas the structure I the PT model has a total height of 63.45 meters. Higher structures are generally more flexible, which would decrease the eigenfrequency value. However, the way that the stiffness is applied to the structure is quite different for the thesis model. As an orthotropic continuum damage model is used, one stiffness value is used for the material of the structure, which combines the stiffness values of the cast iron and the connections. Additionally, the floors, flanges and stiffeners are not present in the thesis model. Even though their effect on the structure is incorporated in the input parameters that were used for the EMM, it seems that the total stiffness of the structure is lower here due to modelling choices that were made. Nevertheless, the values are still reasonably close and from the shape of the structures in the figures above, it is clear that the dynamic behaviour is quite similar.

7.3.2 Static analysis

The second part of the comparison between the PT model and the thesis model, explores the static analysis of the structures. The resultant stresses, strains and displacements that occur when the load combination of self-weight and wind is applied to the lighthouse will be analysed. As mentioned, PT analysed their structure after applying the load combination of self-weight and wind. After that, the wind velocity was lowered until a value was reached at which there were no vertical tensile stresses in the outer column of the lighthouse. A similar analysis will be performed on the thesis model.

At first, the self-weight load is applied to the structure, as this load is always present. After that, the maximum wind load will gradually be applied. This will be done in very small increments to enable acquiring accurate values of the wind loads and the associated wind velocities at some key points in the analysis. Figure 7.1 shows the geometry of the model and the mesh that is used. In this figure, the orange point loads represent the wind load that is applied to the structure. The self-weight load is applied in 25 steps, while 250 steps are used to apply the wind load. This results in a total of 275 load steps in the analysis. The iterative scheme of the loads is given in the table below.

Table 7.8: Iterative scheme of loads in thesis model

Load	Self-weight		Wind	
Iteration method	Secant (Quasi-Newton)		Secant (Quasi-Newton)	
Convergence norms	Force	Displacement	Force	Displacement
Convergence tolerances	0.01	0.01	0.01	0.01
Step size	0.04(25)		0.004(250)	
Maximum number of iterations per step	100		100	
All norms satisfied	No		No	

The figure below shows the vertical stresses (σ_{yy}) that occur at the bottom of the outer column, resulting from the self-weight load that is applied. The load application factor is used on the x-axis, which ranges from 0 to 1. At a load application factor of 0, no load is applied and at a load application factor of 1, the load is fully applied. This point is marked with the letter A.

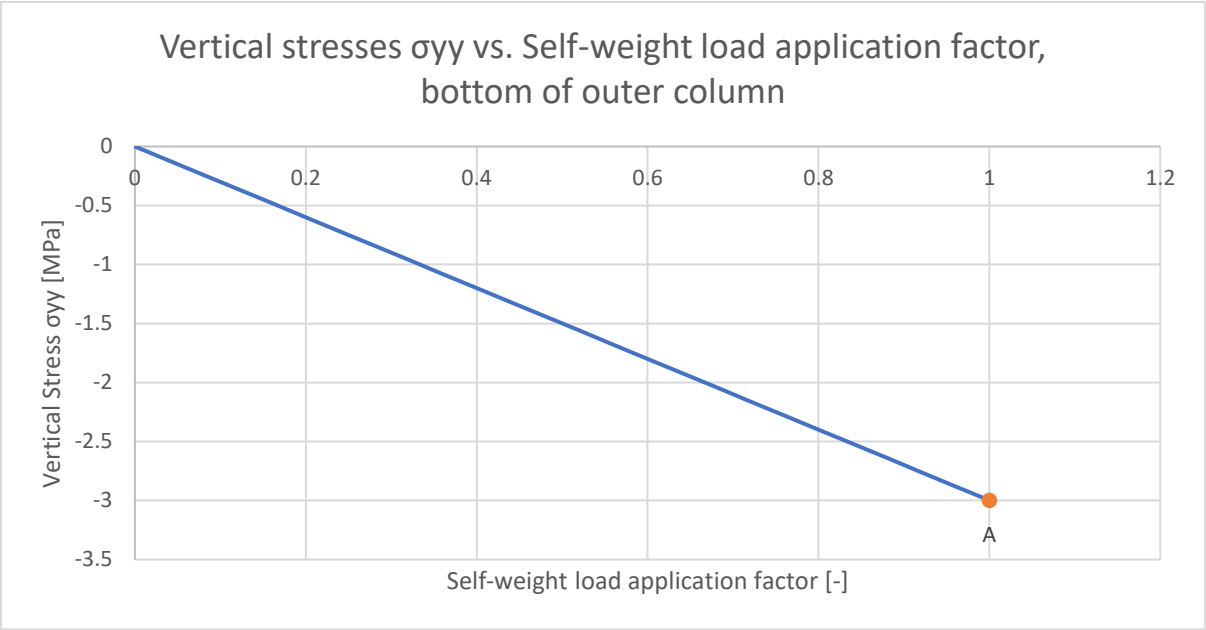

Figure 7.4: Vertical stress σ_{yy} vs. Self-weight load application factor, measured at a node at the bottom of the outer column, on the side at which the wind load is applied

The figure below shows the bottom of the lighthouse. In this figure, the orange arrows are the point loads of the wind load. The red dot, marked with a red circle as well, is the node where the vertical stresses were measured, which were shown in the previous figure. It can be seen that the node is on the side of where the wind load is applied. It was chosen to show the stresses in a node on this side, as the tensile stresses are the highest on this side due to the wind load.

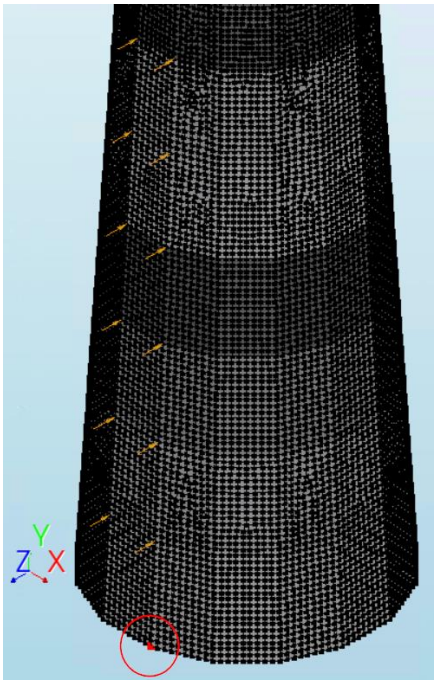

Figure 7.5: Node at the bottom of the lighthouse where the vertical stress σ_{yy} was measured

Now that the self-weight has been fully applied, the next step is to apply the wind load to the lighthouse. The figure below shows the vertical stresses (σ_{yy}) that occur at the bottom of the outer column, resulting from the wind load. The point starts from point A, as this is the point where the self-weight load is fully applied (as mentioned above).

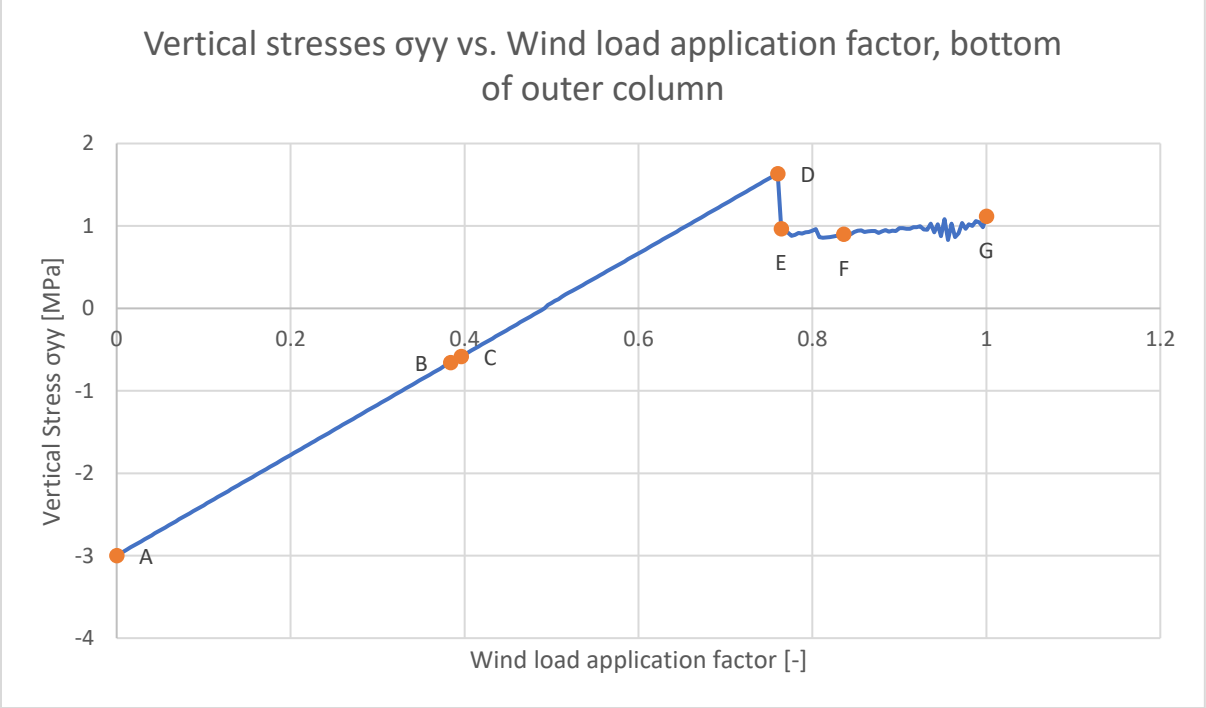

Figure 7.6: Vertical stress σ_{yy} vs. Wind load application factor, measured at a node at the bottom of the outer column, on the side at which the wind load is applied

Six points are highlighted in the figure, named A-G. Every point describes a key moment in the analysis. For example, point A is the point at which the self-weight load was fully applied (as mentioned above). For each point, an explanation will be provided with what is happening at this point and what makes this an important moment in the analysis. In addition, four contour plots of the lighthouse will be given for each point. This will include two plots of the vertical stresses (σ_{yy}), one plot of the vertical strains (ε_{yy}) and a plot of the displacements in z, as the wind load is applied in the negative z-direction. In the second plot, the tensile vertical stresses are marked with red.

Point A (load step 25): At this point, the self-weight load has been fully applied. No wind load is acting on the structure yet, so all stresses in the tower are due to its own mass. As a result, the vertical stresses in the column are evenly distributed, meaning they are equal at all sides for every value of y. The horizontal displacements are very minimal, as the self-weight only acts vertically.

Point B (load step 121): As mentioned, the wind load is slowly being applied in 250 load steps. In this specific load step, the wind load is applied with a load factor of 0.384, which means only 38.4% of the maximum wind load is applied yet. It can be determined that this corresponds to a total force of 221 kN. By adjusting the value of the wind velocity in the wind load calculation, the corresponding values of $q_p(z)$ can be obtained for all possible values of v_{wind}. Using the new values of $q_p(z)$, the total wind load at every wind velocity can be obtained. According to this calculation, a wind load of 221 kN occurs at a wind velocity of 18.3 m/s. PT Structural Analysis & Design determined that this is the maximum wind velocity at which there are (almost) no vertical tensile stresses in the outer column of the lighthouse. As mentioned, no clear limit was specified in the PT report for the acceptable tensile stresses, but from the curves that they present, it can be assumed that the maximum allowable

tensile stresses are 0.01 MPa. By looking at the contour plots that correspond to this load step, it is observed that all stresses are below 0.01 MPa in the outer column, so it can be concluded that a wind velocity of 18.3 m/s also results in (almost) no vertical tensile stresses in the outer column of the thesis model.

Point C (load step 122): After only one more load step, a total wind load of 223 kN is applied (load factor 0.388). From the contour plots below, it is clear that all vertical tensile stresses are still below 0.01 MPa. However, if the load is increased any further, tensile stresses that are larger than 0.01 MPa will start to appear. Therefore, it can be concluded that the load that is applied at point C is actually the maximum wind load at which there are (almost) no vertical tensile stresses in the outer column of the lighthouse, according to the thesis model. The wind load of 223 kN corresponds to a wind velocity of 18.4 m/s. This is only slightly higher than the maximum wind velocity that was determined by the company PT Structural Design & Analysis.

Point D (load step 215): The wind load on the structure keeps increasing, which means the tensile stresses also keep increasing. At point D, the tensile stresses in the outer column reach the tensile strength of the material. This means that the wind load that is applied here corresponds to the maximum allowable wind velocity the structure can withstand. As the wind load at this point equals 437 kN (load factor = 0.760), the maximum wind velocity the lighthouse is able to withstand is 25.7 m/s.

Point E (load step 216): In the previous point, the vertical stresses reached the tensile strength of the material. This happened at load step 215. Point E corresponds to the next load step, which is load step 216. In this step, the load is increased, but the stresses are not able to exceed the strength. For this reason, at the locations where the stresses are high, cracks will start to appear. The locations of the cracks can be seen in the contour plots of the vertical strains. Cracks will not visibly appear in DIANA, but the local displacements become very large. As a result, the local strains become very large as well. By looking at the maximum displacements in z, it can be seen that the top of the column has a displacement of 49.38 mm. In the previous load step, this was only 37.07 mm. This means the displacement has increased with more than 12 mm in 1 load step, which is clearly a result of the cracks in the column.

Point F (load step 234): In the next load steps, the stresses remain relatively constant. As the load keeps increasing, the existing cracks continue to grow and new cracks start to appear. As a result of the cracks, the horizontal displacements in z also increase rapidly. At some point, the program can no longer find converging results in the analysis as the cracks have grown too large. Point F is the point just before non-convergence, so the final converging load step is load step 234. At this point, the total wind load equals 480 kN, which corresponds to a wind velocity of 27 m/s.

Point G (load step 275): Even though the results are no longer converging, the wind load keeps increasing. Point G corresponds to the moment where the wind load has been fully applied. From the contour plots, it is clear why the program was not able to find converging results. The cracking has increased even more and as a result, the shape of the lighthouse has changed drastically. The displacement in z at the top of the column has increased to 5647 mm, which is more than 5.6 meters.

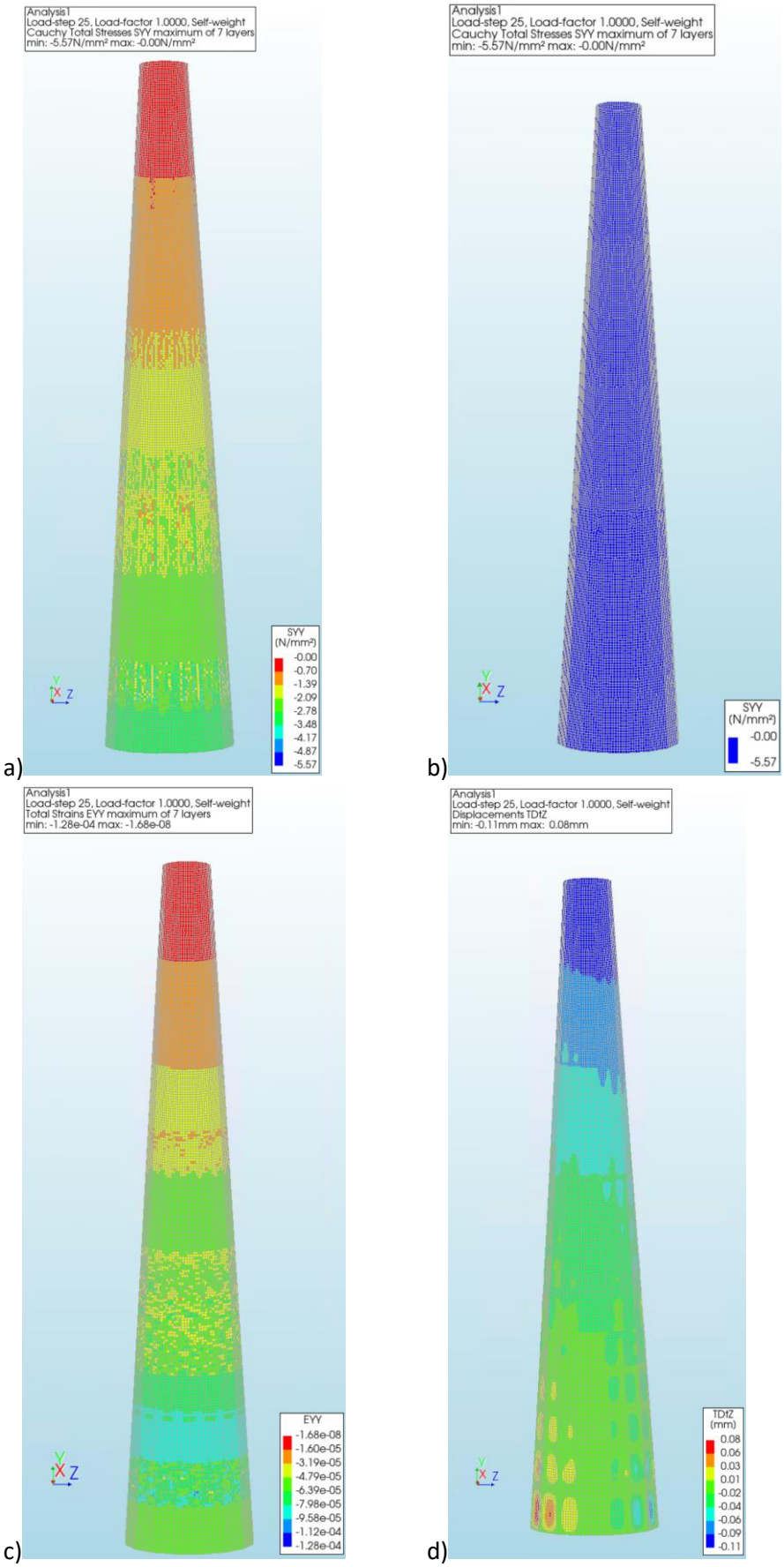

Figure 7.7: Contour plots of vertical stresses σ_{yy} (a and b), vertical strains ε_{yy} (c) and displacements in z (d), point A in analysis

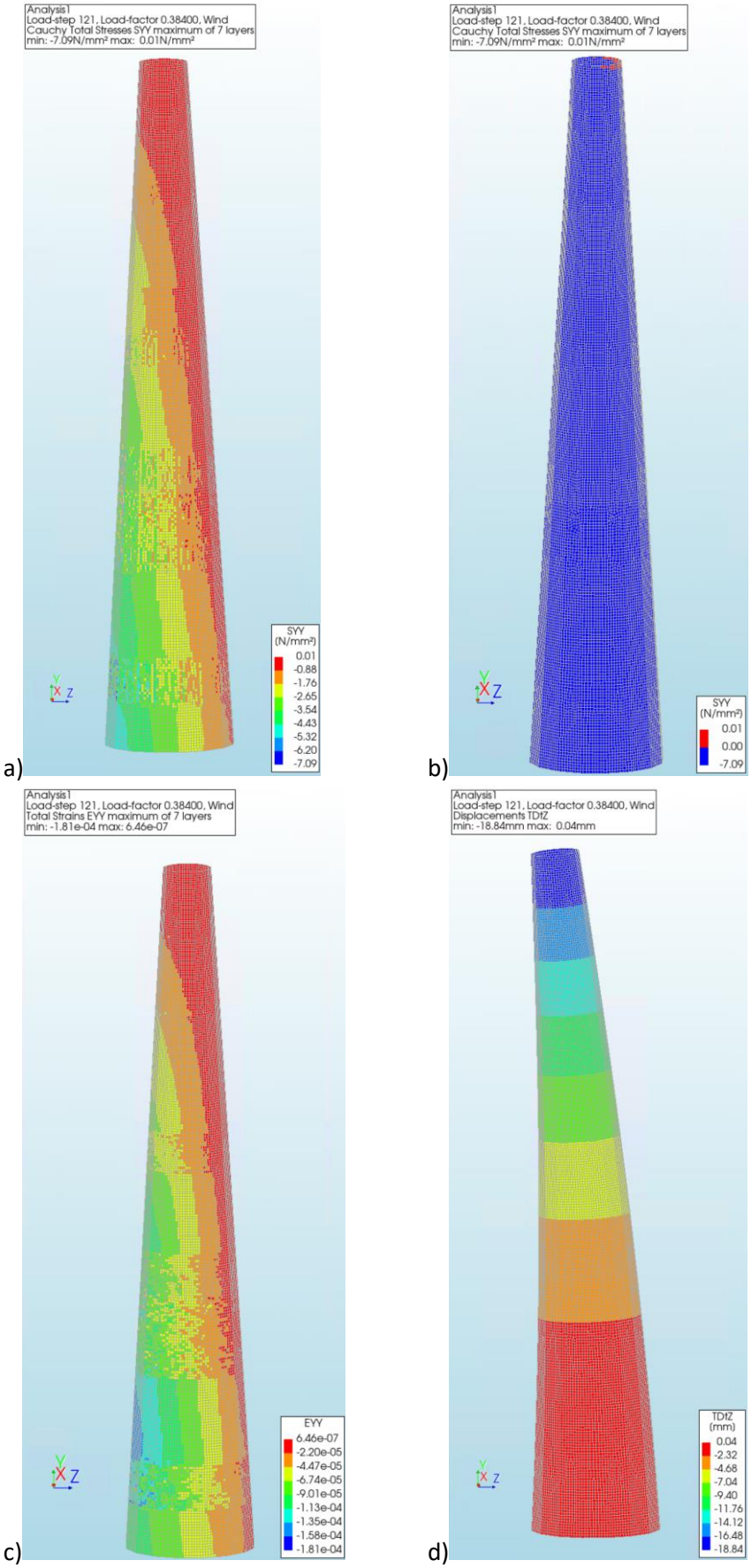

Figure 7.8: Contour plots of vertical stresses σ_{yy} (a and b), vertical strains ε_{yy} (c) and displacements in z (d), point B in analysis

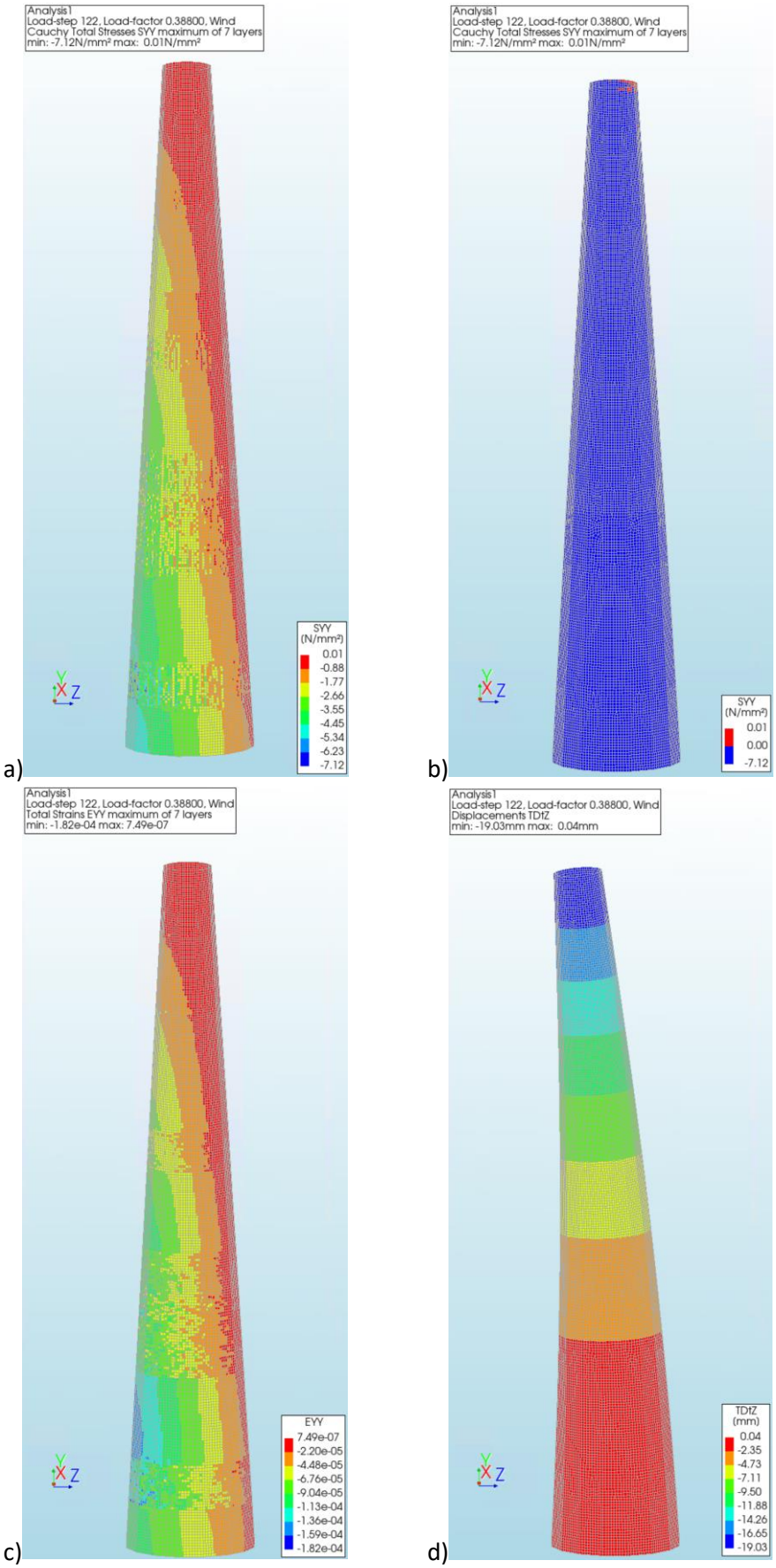

Figure 7.9: Contour plots of vertical stresses σ_{yy} (a and b), vertical strains ε_{yy} (c) and displacements in z (d), point C in analysis

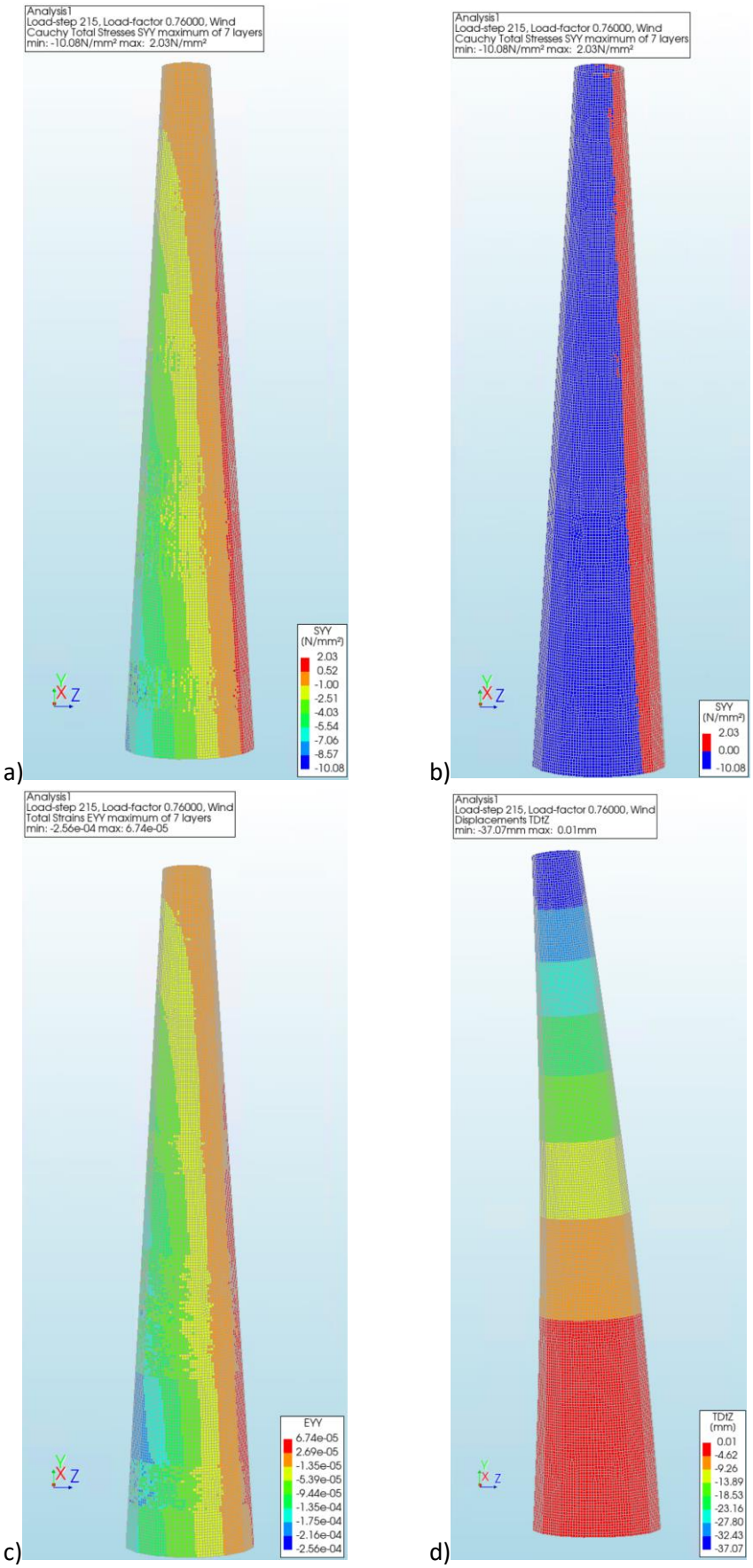

Figure 7.10: Contour plots of vertical stresses σ_{yy} (a and b), vertical strains ε_{yy} (c) and displacements in z (d), point D in analysis

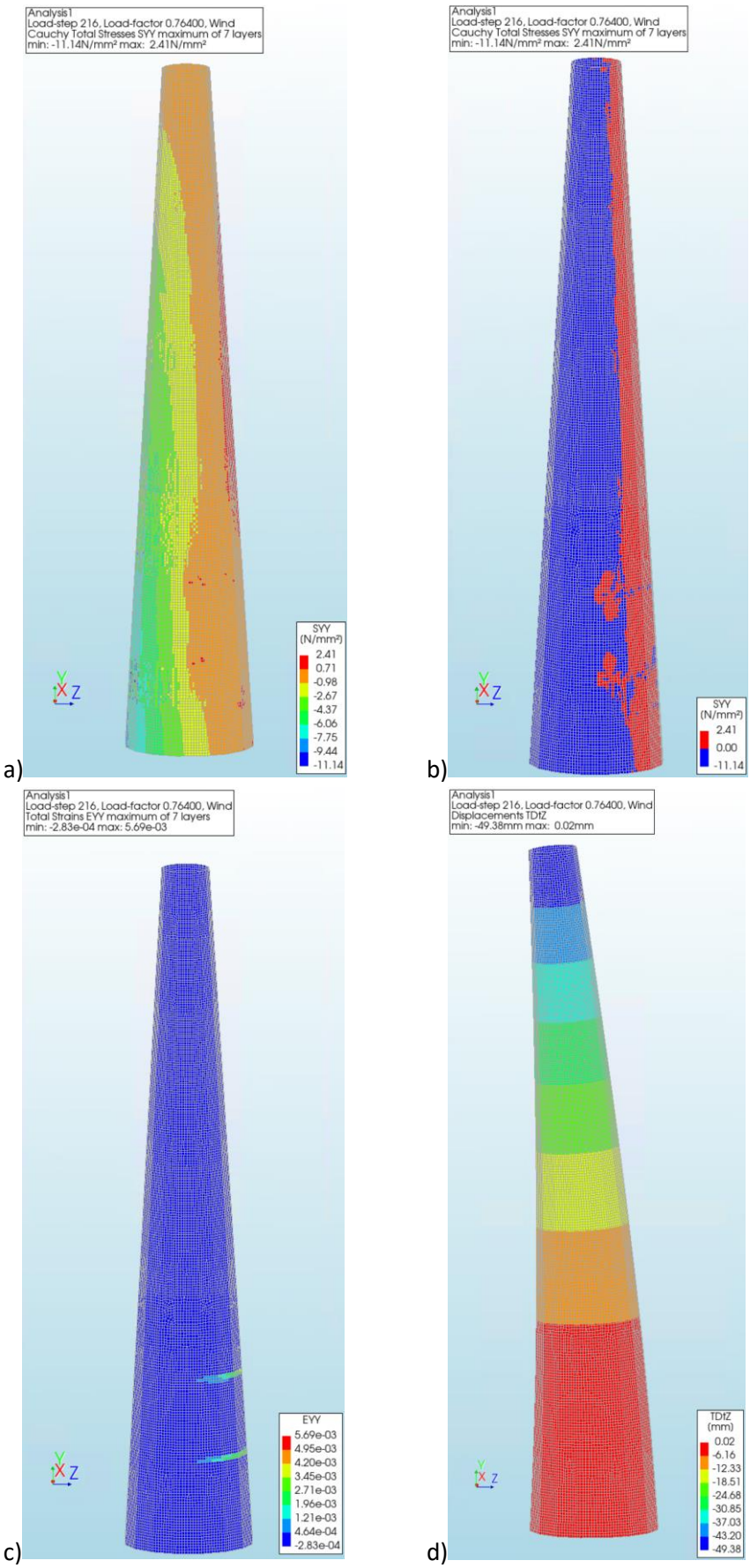

Figure 7.11: Contour plots of vertical stresses σ_{yy} (a and b), vertical strains ε_{yy} (c) and displacements in z (d), point E in analysis

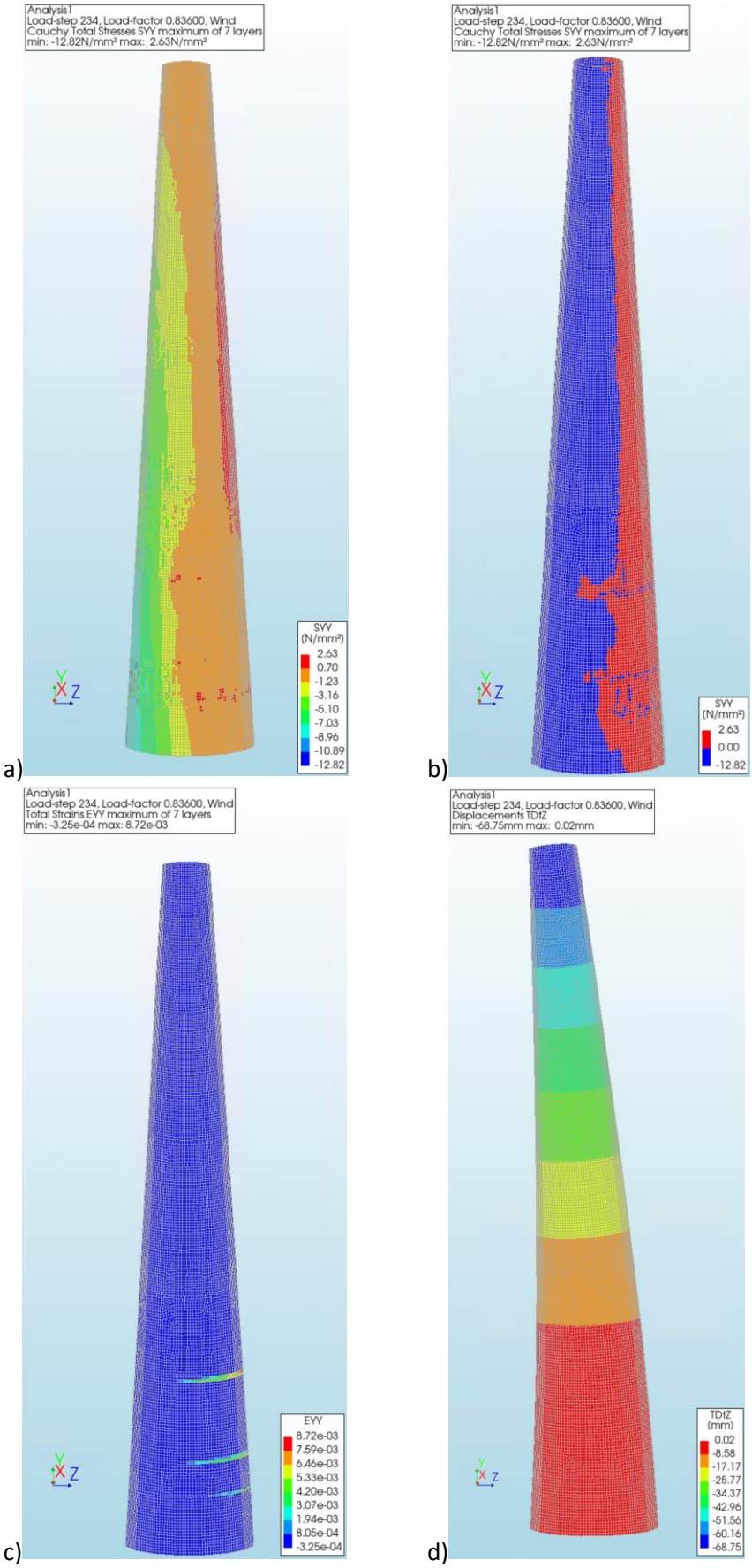

Figure 7.12: Contour plots of vertical stresses σ_{yy} (a and b), vertical strains ε_{yy} (c) and displacements in z (d), point F in analysis

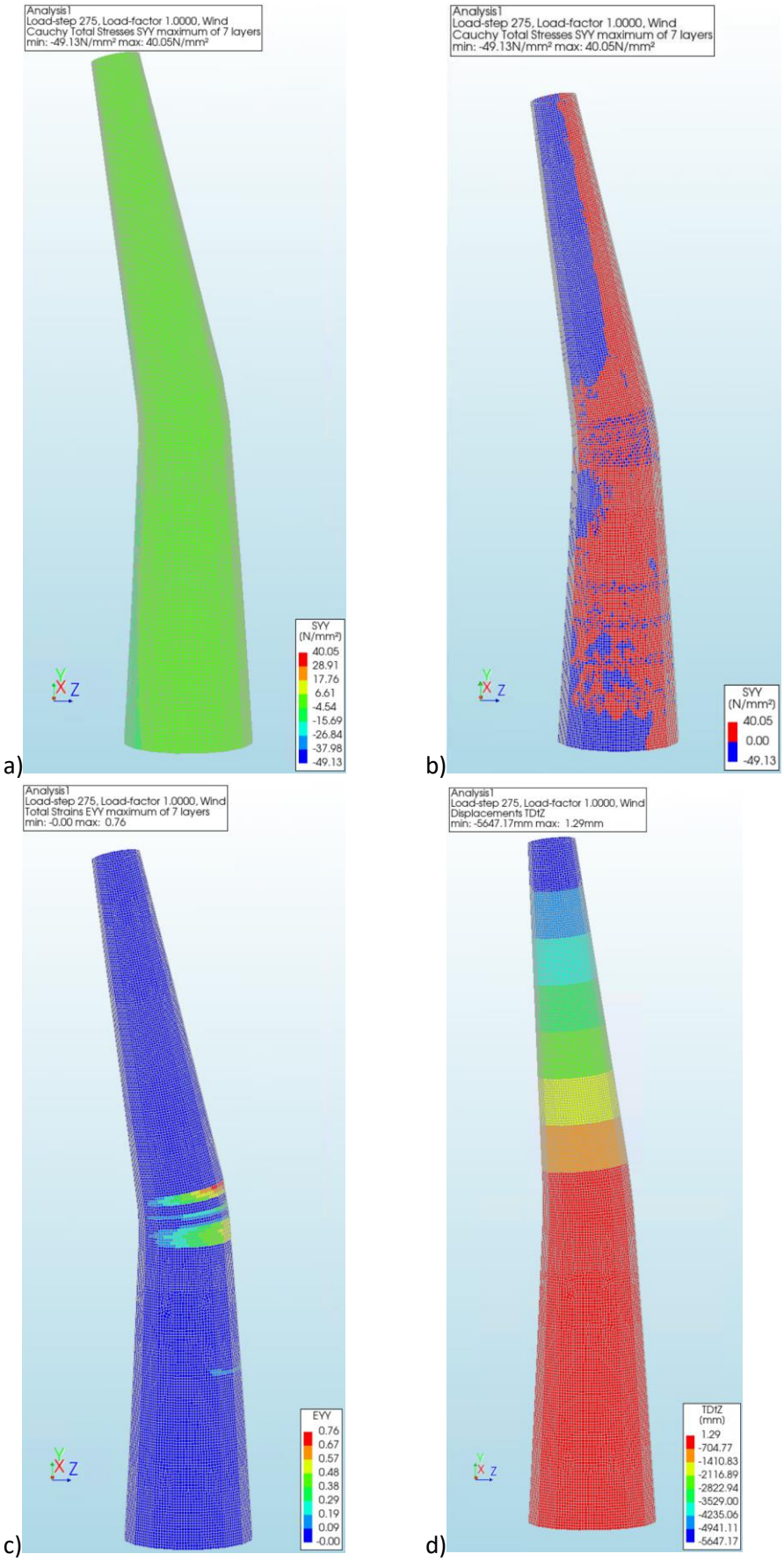

Figure 7.13: Contour plots of vertical stresses σ_{yy} (a and b), vertical strains ε_{yy} (c) and displacements in z (d), point G in analysis

A summary of the key points and the relevant factors is provided in the table below.

Table 7.9: Summary of key points in thesis model analysis

Point	Load-step	Load factors	F_{wind} [kN]	v_{wind} [m/s]	Description
A	25	Self-weight: 1 Wind: 0	-	-	Self-weight fully applied
B	121	Self-weight: 1 Wind: 0.384	221	18.3	Maximum wind velocity without vertical tensile stresses according to PT model
C	122	Self-weight: 1 Wind: 0.388	223	18.4	Maximum wind velocity without vertical tensile stresses according to the thesis model
D	215	Self-weight: 1 Wind: 0.760	437	25.7	Maximum vertical tensile stresses reached
E	216	Self-weight: 1 Wind: 0.764	439	25.8	First cracks start to appear
F	234	Self-weight: 1 Wind: 0.836	480	27.0	Last converging load step
G	275	Self-weight: 1 Wind: 1	575	29.5	Wind load fully applied (non-converging results)

From the analysis of the thesis model, a few things can be concluded. First of all, the behaviour of the thesis model matches the PT model quite well, as a very similar value was determined for the maximum wind velocity at which (almost) no vertical tensile stresses appear in the outer column. This was 18.4 m/s for the thesis model and 18.3 m/s for the PT model. This shows that when there are only linear-elastic deformations, using the EMM for this structure provides similar results as when a detailed model is used. However, when the stresses exceed the tensile strength, plastic deformations will appear and cracks will start to form in the structure. As a result, structural failure occurs at a wind velocity of 25.8 m/s. The PT model showed that structural failure will not occur, even at the maximum wind velocity of 29.5 m/s. In the equivalent EMM models loaded in pure tension, that were analysed in chapters 5 and 6, it is clear that similar results will be obtained as for detailed models loaded in pure tension. However, as the values of the bed- and head-joint tensile strengths that were obtained are quite low, tensile stresses which are larger than the tensile strength of the material can occur quite quickly, even when the structure is not loaded in pure tension. As only one material is used to model the plates and the connections, the stiffness and strength of the material is the same at every location. This is not the case in the detailed models, which has a large impact on the force distribution within the structure. It can be concluded that using an orthotropic continuum damage model, such as the EMM, will provide similar results as a detailed model, when there are only linear-elastic deformations in the structure. Once plastic deformations occur, the analysis of the thesis model quickly becomes unstable and the results are no longer accurate.

7.4 Analysis structural behaviour under large compressive force

Another analysis will be performed on the thesis model, where the gravitational acceleration will be increased by a factor of 20. Only the self-weight load will be applied, so the structure will be fully loaded in compression. By increasing the gravitational acceleration, the compressive stresses become very high which will shows what the structural behaviour of the model looks like when loaded with high compressive forces. The iterative scheme of the self-weight load that is applied in the model is presented in the table below.

Table 7.10: Iterative scheme of self-weight load in high gravity thesis model

Iteration method	Secant (Quasi-Newton)	
Convergence norms	Displacement	Force
Convergence tolerances	0.01	0.01
Step size	0.005(200)	
Maximum number of iterations per step	100	
All norms satisfied	No	

The figure below shows the geometry of the analysed structure and the mesh that is used. The green arrows are shown to give a visualisation of how the self-weight load is applied to the structure. The mesh is exactly the same as for the model that was analysed in the previous section. An overview of the elements and nodes was presented in table 7.2.

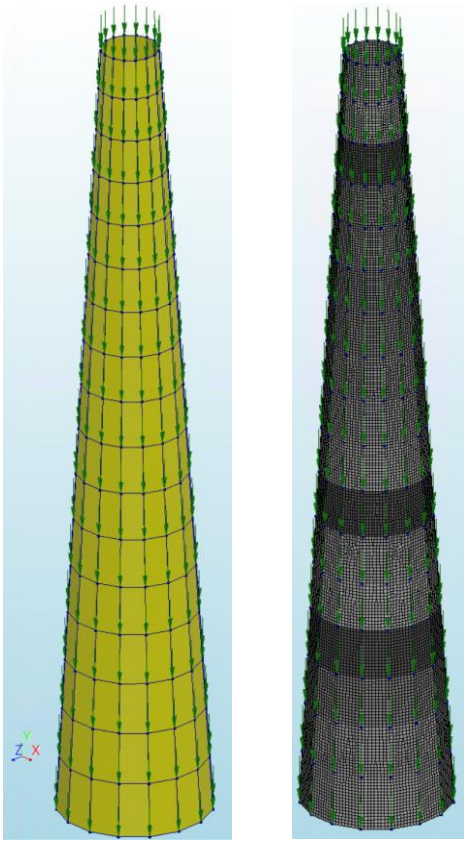

Figure 7.14: Geometry of analysed model (left) and the finite element mesh that was used (right)

The figure below shows the principal compressive stresses σ_3 compared to the load factor. The stresses σ_3 present the highest compressive stresses that will occur in the structure. The stresses were measured in a node of section OS2. As this section has a much lower compressive strength compared to the other column section, it is likely that the compressive stresses will exceed the compressive strength in this section before this can happen in different column sections. The node in which the stresses were measured was chosen as the node in which the largest peak compressive stress occurred. The load factor is related to the factor with which the gravitational acceleration is multiplied. This means a load factor of 1 shows the results of the self-weight application were g = 9.81 m/s^2.

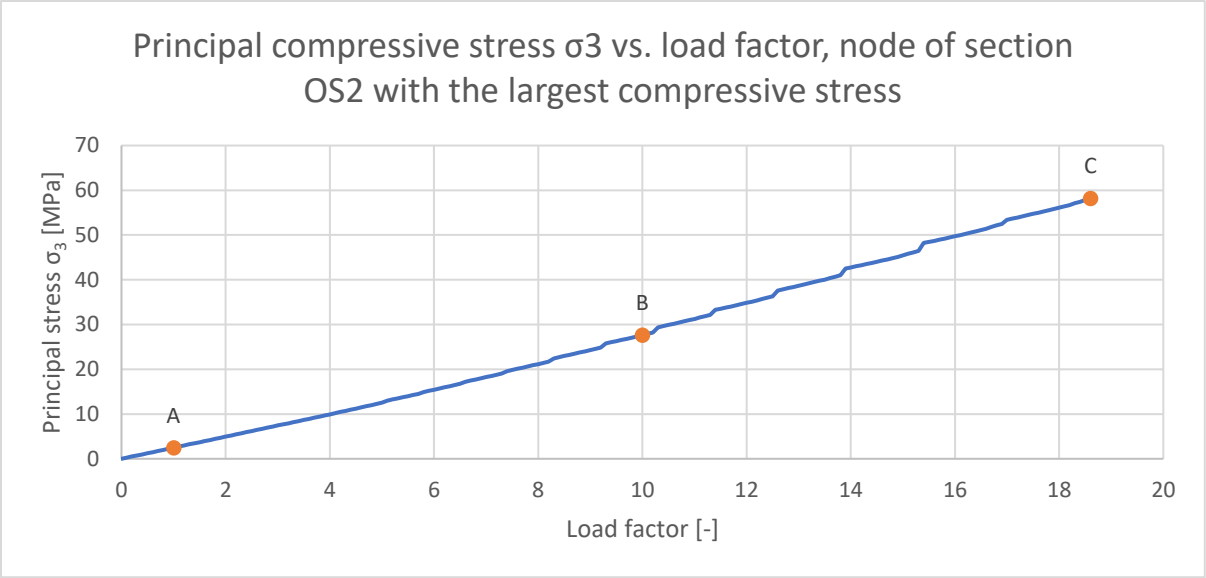

Figure 7.15: Principal stress σ_3 vs. load factor, node of section OS2 with the largest compressive stress

The figure below shows the bottom of the lighthouse. The red dot, marked with a red circle as well, is the node where the vertical stresses were measured, which were shown in the previous figure. This node is from section OS2 of the lighthouse. This node was chosen for showing the stresses, as the compressive stresses are closest to the compressive strength at this location.

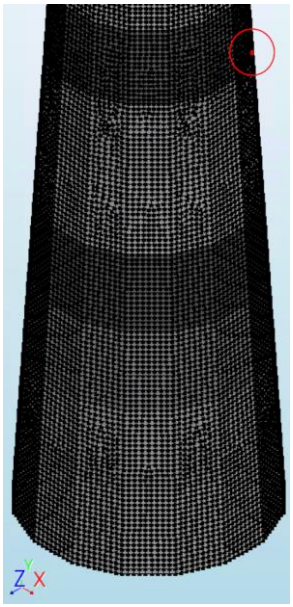

Figure 7.16: Node in section OS2 of the lighthouse where the principal stress σ_3 was measured

It can be observed that the compressive stresses will increase almost linearly when the load factor is increased. Three points are highlighted in the figure, named A-C. In these points, interesting load factors are applied. In point A, the load factor is equal to 1, which means the self-weight with the normal earth gravity. In point B, the load factor is equal to 10 and in the final point C, the load factor is equal to 18.6. It can be observed that point C is the final point of the curve, and no stresses are shown for higher load factors. When the load factor was increased to 18.7, the model became unstable and the results of the analysis diverged. For all three points, four contour plots of the lighthouse will be given: the principal stresses in vertical direction σ_3, the displacements in y (vertical), the displacements in x and the principal stresses σ_1.

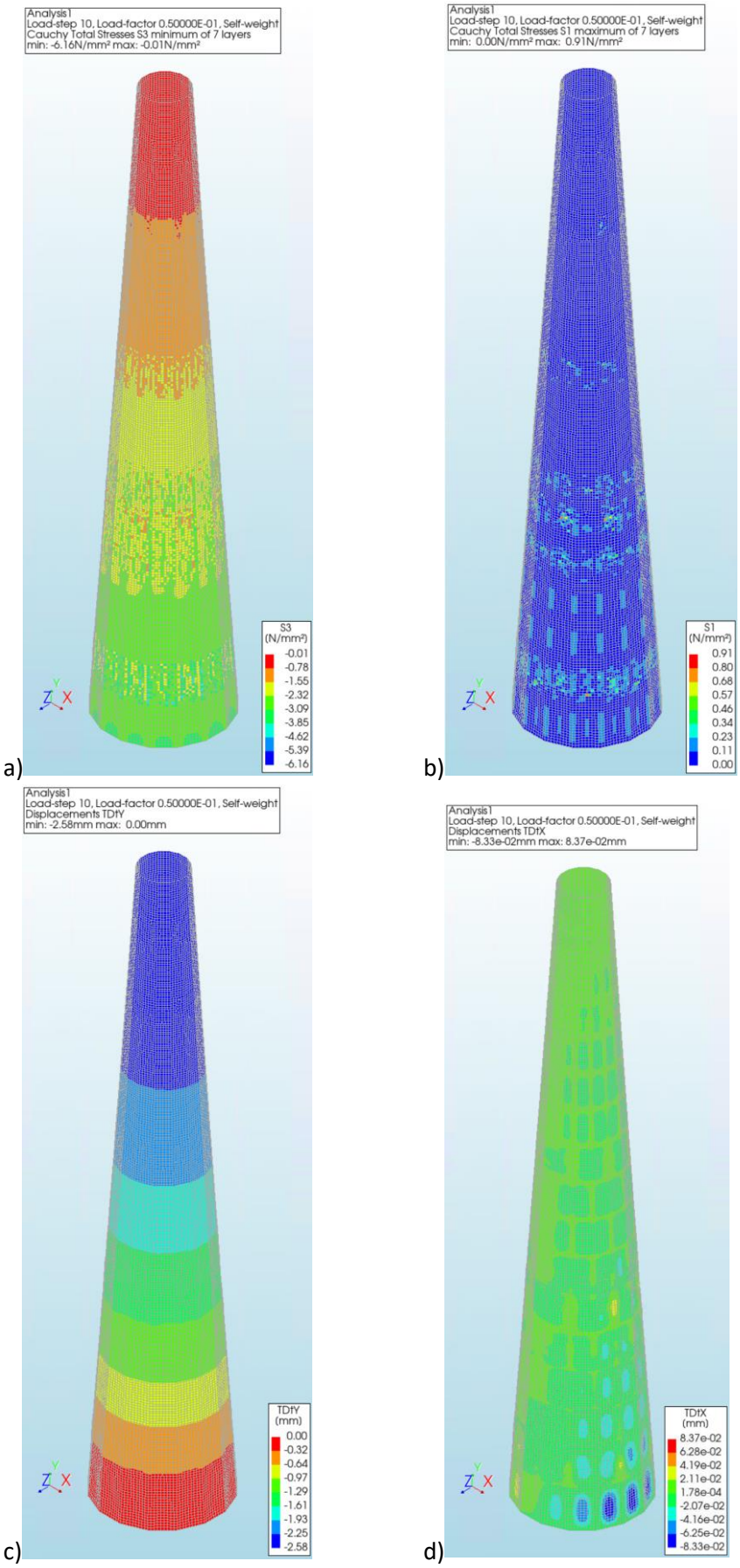

Figure 7.17: Contour plots of principal stresses in vertical direction σ_3 (a), principal stresses σ_1 (b), displacements in y (c) and displacements in x (d), point A in analysis

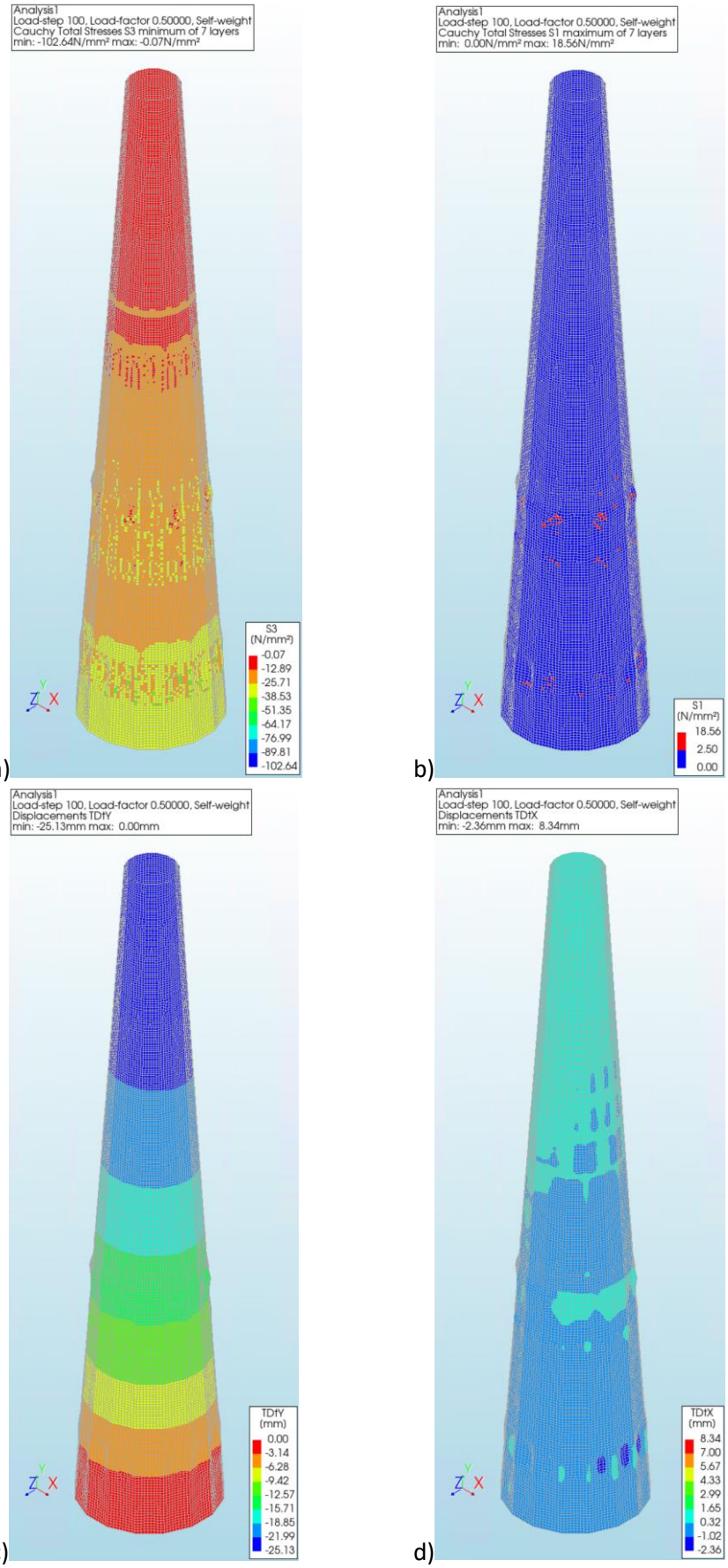

Figure 7.18: Contour plots of principal stresses in vertical direction σ_3 (a), principal stresses σ_1 (b), displacements in y (c) and displacements in x (d), point B in analysis

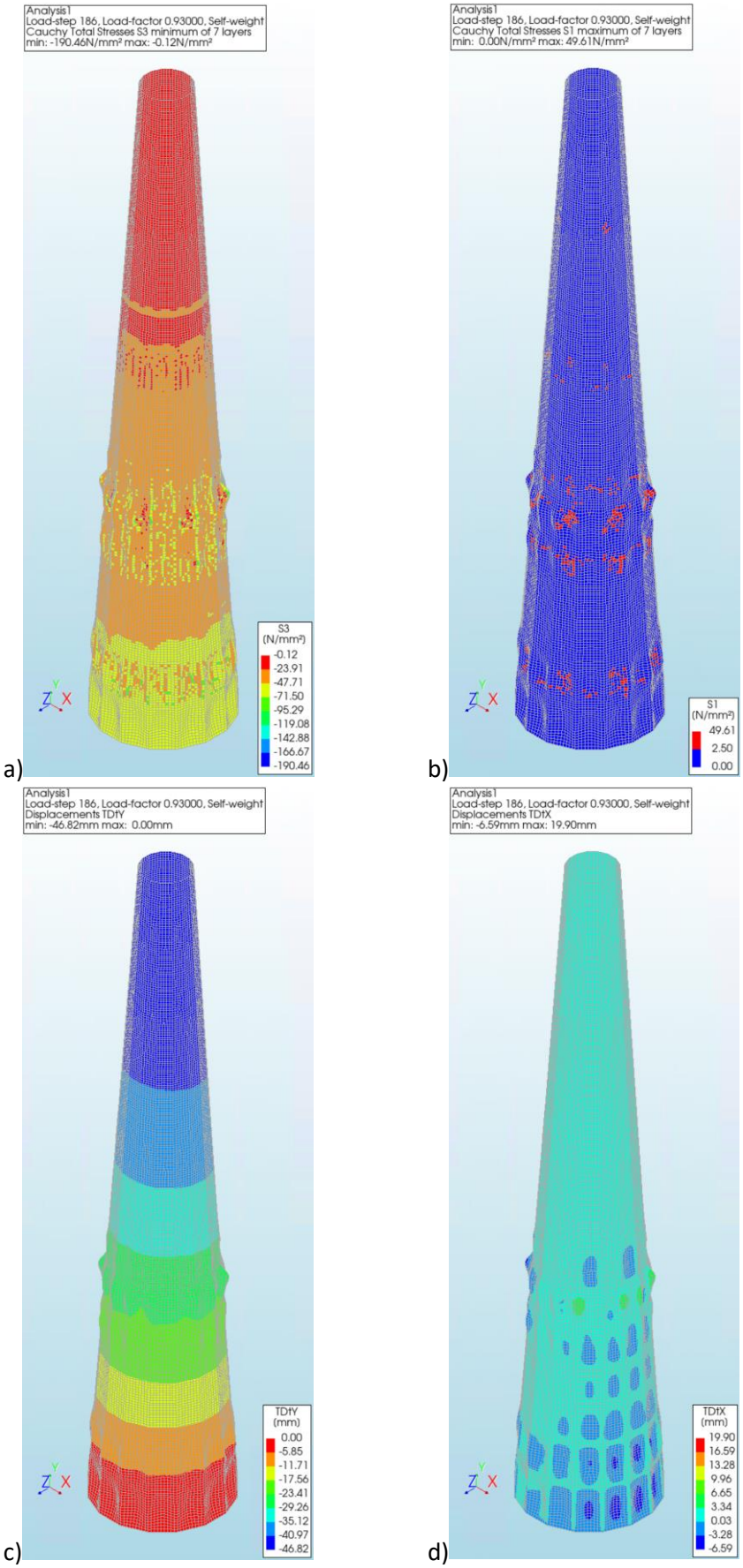

Figure 7.19: Contour plots of principal stresses in vertical direction σ_3 (a), principal stresses σ_1 (b), displacements in y (c) and displacements in x (d), point C in analysis

From the contour plots of the principal stresses in vertical direction σ_3, it can be observed how the compressive stresses keep increasing as the load is increased. The stresses are the highest at the bottom of the lighthouse, as those plates have to carry the weight of the entire structure. The displacements in y-direction are also gradually increasing during the analysis. In the final load step, the top of the lighthouse has a total vertical displacement of 46 mm. It is interesting to see that the out of plane displacements are also quite significant. As the load and the structure are both symmetrical, the displacements in x-direction are out of plane displacements for plates that are parallel to the xy-plane. In load step 186, the displacements in x are even 8 mm at some points. In the equivalent EMM models that were analysed in chapters 5 and 6, the models loaded in compression showed that the out of plane displacements were very close to 0 mm. The shape of lighthouse is most likely the reason for these large displacements. The columns linearly decrease in diameter, which means all plates are placed under an angle. As the self-weight load is applied in the y-direction, this will result in forces on the plates in local y- and z-directions. As a result of the out of plane displacements, tensile stresses will occur in the principal directions, σ_1 and σ_2. In the contour plots of the principal stresses σ_1, it was chosen to show where tensile stresses larger than 2.5 MPa appear, as the lowest input value of the joint strengths of the outer column is 2.206 MPa. This allows a clear overview of where the stresses exceed the tensile strength of the material. As a result, cracks start to appear in the model, and at some point the analysis becomes unstable. This happened when a load factor of 18.7 was applied to the model. As the failure mode of the model is not pure compression, the compressive stresses did not reach the compressive strength of the material.

It can be concluded that the behaviour of the structure loaded in compression is mostly as expected, as the compressive stresses will increase almost linearly. However, due to the fact that the plates are placed under an angle, the self-weight load results in forces in the local y- and z-directions of the plates. Out of plane displacements appear in the model, which results in tensile stresses. As the tensile strength of the material is quite low, the stresses will exceed the strength at a certain point. When this happens, cracks start to appear in the model and the force resistance of the structure will decrease quickly. As a result, a load factor of 18.7 caused the model to diverge in this case.

8 Conclusion

The research question of this project was:

How can an orthotropic continuum damage model be used to reduce the complexity of the structural analysis of a detailed finite element model for a cast iron plate structure?

By dividing the research question into three sub-questions, an answer to the question has been obtained. The following things can be concluded from the project:

- It is possible to obtain the input parameters that are required for an orthotropic continuum damage model, by creating detailed models of small plate structures, applying different displacement loads and analysing the force-displacement curves that result from the different load cases. In this project, the Engineering Masonry Model (EMM) was used, which covers tensile, shear and compressive failure modes. Therefore, the load cases that had to be considered for the detailed models of the small plate structures were tension, shear and compression
- By applying the obtained parameters in equivalent EMM models of the small plate structures and performing the exact same analyses on these models, the results of the detailed models can be compared to the results of the equivalent EMM models. From this comparison, it was concluded that the models mostly provided similar results, but some of the parameters had to be calibrated to increase the similarity of the equivalent EMM models
- When the size of the structure was increased, the failure modes became different for compression and shear, which resulted in quite a difference in strength and ultimate strain between the small and large structures. For the tension models, the failure mode remained the same but the stiffness of the structure was lower for the larger structures, which is caused by the difference in the ratio of plates/connections of the structure
- When the input parameters, that were obtained from the analyses of detailed models of small plate structures, were used in equivalent EMM models of the larger structures, it was observed that there were quite some differences in the analysis results. As the failure modes of the small structures were considered when obtaining the input parameters, and the failure modes of the large structures were not exactly the same for the load cases of compression and shear, the results of the equivalent EMM models were not very similar to the results of the detailed models for these load cases
- After calibrating the input parameters to match the failure modes of the large structures and using these new values in equivalent EMM models of the large structures, the comparison of the results showed that the results were mostly similar again. It can be concluded that the structure size is very important for the accuracy of the equivalent EMM models, as the failure mode might change when the structure size is increased
- After using the input parameters that were obtained from the results of the large detailed models in equivalent EMM models of the large structures, there were still some parameters that had to be calibrated to increase the similarity of the results. It can be concluded that, if this method is used to simplify the complexity of a detailed finite element model, one should use the obtained input parameters in equivalent models, as the comparison between the detailed models and equivalent models shows which parameters need to be calibrated and in what magnitude. From the results of this study, it is clear that parameters will have to be calibrated when different loading directions provide different values for certain input parameters. In this case, the tension and compression models resulted in calibration of several parameters, as there were multiple values for the E_y and $G_{f,tension.}$ As only one value could be used, the average value was used and the other relevant parameters were calibrated

- When the final input parameters were used in an orthotropic continuum damage model for the structure of lighthouse the 'Lange Jaap', it was concluded that very similar results were obtained as from the detailed model, as long as the stress values were low, such that only linear-elastic deformations occurred
- The maximum wind velocity at which (almost) no vertical tensile stresses occur in the lighthouse is equal to 18.4 m/s in the thesis model and 18.3 m/s in the PT model, which is almost exactly the same
- However, due to the low tensile strength of the material in the thesis model, the stresses exceeded the strength before the wind load was fully applied, which caused plastic deformations to occur. It can be concluded that once plastic deformations occur, the analysis of the thesis model quickly becomes unstable and the results are no longer accurate
- From the analysis of the high gravity thesis model, the behaviour of the structure loaded in compression was mostly as expected, as the compressive stresses increases almost linearly with the load factor. However, due to the fact that the plates are placed under an angle, the self-weight load results in out of plane displacements, which cause tensile stresses in the structure. It can be concluded that the low tensile strength of the orthotropic continuum damage model causes quite some problems in the analyses of the structure, as this allows cracks to form quite quickly, even when the tensile stresses are still relatively small

The answer to the main research question is as follows:

- When using an orthotropic continuum damage model, such as the EMM, only small detailed models of the unit structure size that include the most realistic failure modes have to be analysed, instead of a detailed model of the entire structure. It can be concluded that this can significantly reduce the total modelling time
- The geometry of the cast iron plate structure was simplified, as the flanges and stiffeners were not included in the model. As a result, it is possible to use regular curved shell elements instead of structural solids. This makes it very easy to create models of very large structures
- As regular curved shell elements were used, due to the simplification of the geometry, a much larger element size can be chosen which results in a much lower amount of elements and nodes compared to a detailed model. Fewer elements and nodes means the analysis time of the model becomes shorter. It can be concluded that using an orthotropic continuum damage model, such as the EMM, can significantly reduce the total running time of the analysis of large cast iron plate structures, as shell elements can be used

Finally, as the running time of the finite element model is reduced significantly when an orthotropic continuum damage model is used, it becomes very valuable to create such a model when many different analyses have to be performed, even though finding correct input parameters for the model might take some time. This aligns perfectly to the case study of the lighthouse structure, where the effectiveness of different kinds of strengthening solutions need to be studied. As mentioned, there is quite some damage to the structure and the strength of the structure no longer meets the requirements of the Eurocode. Many different analyses should be made of the lighthouse, where each model has a different strengthening solution applied. By using an orthotropic continuum damage model, the running time of the finite element model is reduced and making many different analyses of the finite element model can be achieved in a much shorter time period.

9 Recommendations

It is possible to use an orthotropic continuum damage model and it could eventually become a profitable method of modelling large plate structures. However, from the conclusion of this project, it is clear that there are still some limitations to modelling with this method, which have to be taken into account. The results of the thesis model show that when there are only linear-elastic deformations, the results of a finite element model in which an orthotropic continuum damage model is used for the cast iron plate structure, are very similar to the results of a detailed finite element model of the same structure.

As the maximum wind-load where there were almost no tensile stresses in the structure had to be found from the thesis model, all stresses were quite low, which resulted in linear-elastic deformations only. For these types of research questions, using an orthotropic continuum damage model can provide answers to the questions quickly due to the fast running time of the analysis. However, it also takes quite some time to convert all material properties of detailed models into input parameters of an orthotropic continuum damage model, as small detailed models still have to be analysed. The results of this project can be used to develop a method which speeds up this process. The total working time is equal to the time spent on obtaining the correct input parameters, creating the model, running time of the model and analysing the results. Only when the total working time becomes lower for the method in which an orthotropic continuum damage model is used compared to the regular method where a detailed model is used for the finite element model of the structure, it becomes profitable to use this method in the structural analysis.

When someone would like to use this method to analyse a similar structure as the cast iron plate structure of lighthouse that was analysed here, the following things are recommended:

- Only make detailed models of a unit structure size. The unit structure size should have the failure mode which is expected in the model of the entire structure. When comparing the structure size of the large detailed shear models and the head-joint tension models, it is clear that this unit structure size does not need to be the same for all load cases
- From the results of the equivalent EMM models, it is clear that adjustments are always necessary to some of the obtained parameters. To ensure a more accurate structural behaviour, it is recommended to make equivalent models of the unit structure size, before using the obtained input parameters in a finite element models of the entire structure. By testing the obtained input parameters for the orthotropic continuum damage model in equivalent EMM models, it becomes clear which parameters should be adjusted. As the equivalent EMM models are very easy to make and the running time of the analyses is very small, this can increase the accuracy of your model quite quickly
- In this study, the columns were divided into three sections, so a total of six different plate sizes had to be used in the detailed finite element models. The number of plate sizes that is considered when obtaining the input parameters, heavily impacts the total working time and the accuracy of the final model. When the working time is of higher importance, use only one or maybe just a few different plate sizes. When accuracy is of higher importance, use a larger amount of different plate sizes

It is also possible to obtain input parameters for the model in a different way. When the plates are very small, it might be possible to create real small structures and apply the different load cases in actual test set-ups. As the input parameters would then be based on the actual, real life behaviour of the structure, the input parameters that are obtained from these results will most likely result in even more accurate results when used in a finite element model.

Due to the simplification of the geometry, it was possible to use shell elements instead of structural solids, which resulted in much larger elements. This means two simplifications were made in the process of creating equivalent models of the cast iron plate structures, in the geometry and in the element type. A study can be performed to see what the effectiveness would be of just simplifying the geometry, by still using structural solids in the models. This would also show what the effect is of using shell elements instead of structural solids.

Additionally, in the equivalent EMM model of the lighthouse (thesis model), some more simplifications were made. The floors were modelled by using tyings between the columns, so only the global effect of the floors on the structure were included in the model. Also, the company PT Structural Analysis & Design used a pressure profile to apply the wind load, while point loads were used in the thesis model. For both simplifications, it could be studied how the results would change if the more complex situation was applied instead. This would mean the local effects are also included in the finite element model, which might have influence of the results of the analyses.

Finally, based on the finite element analysis results of the equivalent EMM lighthouse model, it is clear that tension is a large problem for the cast iron plates. Due to their low tensile strength and brittle behaviour in tension, cracks will start to form in the plates when tensile stresses appear and the structure quickly becomes unstable. As cracks have already started to form in the plates of lighthouse the Lange Jaap, it is recommended that the strengthening solution focuses on ensuring that tension will no longer appear in the plates. One way of doing this could be by introducing additional compressive stresses into the plates, by applying prestressing tendons to the structure. Prestressing is most commonly used in concrete structures, as concrete has a very low tensile strength. By applying compressive stress in advance, the amount of tensile stresses in the structure are reduced. However, it is also possible to apply similar stresses to existing structures by using prestressing tendons. From the equivalent EMM model of the lighthouse where the gravity was increased, it became apparent that these stresses should be in the local vertical direction of the plates, not the global vertical direction, otherwise tensile stresses still occur due to out of plane displacements. Therefore, it has to be ensured that the tendons are placed in the same line as the cast iron plates.

References

Beukers, A. (2022, March 14). Lange Jaap: world's 'oldest and tallest' iron lighthouse. Huisduinen.

CEN. (2005). *NEN-EN 1991-1-4: Eurocode 1: Actions on structures - Part 1-4: General actions - Wind actions.*

CEN. (2023). *NEN-EN 1561: Founding - Grey cast irons.*

Chiriatti, L., Mercado-Mendoza, H., Apedo, K. L., Fond, C., & Feugeas, F. (2019). *A study of bond between steel rebar and concrete under a friction-based approach.*

DIANA FEA bv. (2017). *DIANA FEA User's Manual.* DIANA FEA BV.

Harder, Q. (1875). Ijzeren kustlicht toren bij Kijkduin. Den Haag.

IECRT. (2010). *Vuurtoren Lange Jaap.* Rijswijk.

Lintsen, H. W., Bakker, M., Homburg, E., van Lente, D., Schot, J., & Verbong, G. (1993). *Geschiedenis van de techniek in Nederland.* Zutphen, Nederland: Walburg Pers.

Movares. (2023). *Bevindingen onderzoek ijzercementvoeg.*

Oostingh, J. (2012, November). De gietijzeren vuurtorens van IJmuiden. *Historisch Hoogovens*, p. 12.

PT Structural Design & Analysis bv. (2022). *RWS Scheurvorming Vuurtoren Lange Jaap Kijkduin, Den Helder.*

Rijkswaterstaat. (2020). *Vuurtoren Lange Jaap Kijkduin, Den Helder, Onderzoeksrapport Scheurvorming Vloeren.*

Schreppers, G., Garofano, A., Messali, F., & Rots, J. (2016). *DIANA validation report for masonry modelling. DIANA FEA report 2016-DIANA-R1601 TU Delft Structural Mechanics Report CM-2016-17.*

Suchtelen, H. v. (1978). *De bouwwijze van de gietijzeren vuurtoren te Kijkduin (Den Helder).*

TU Delft. (2021). CTB3330 : VERGEET-MIJ-NIETJES. Delft.

Veljkovic, M. (2021). CIE5122 - Lecture S12- 2021 Connections in WTT.

Vuurtoren Lange Jaap. (2025). Retrieved from Vuurtoren Lange Jaap: https://vuurtorenlangejaap.nl/#de-lange-jaap

A. List of names of all analysed models

In this report, results will be presented of many different finite element models. A table is presented below in order to have a clear overview of all models. The table provides a description of each model and how the model will be named. The names of the models are based on the column section, the type of model, the loading condition, the size of the structure and for some cases important input parameters are included in the name as well. The terms in the names were chosen such that they are relatively short, but it should also still be possible to deduce the most important properties of the model from the name. The different column sections are: IS1, IS2, IS3, OS1, OS2 and OS3. In the table below, OS3 is used as an example for the model names.

Table A.1: Overview of different model names and their description

Model description	**Model name**
Detailed model, loaded in tension on the head-joint, small structure	OS3_det_ten_head_small
Detailed model, loaded in tension on the bed-joint, small structure	OS3_det_ten_bed_small
Detailed model, loaded in compression, small structure	OS3_det_comp_small
Detailed model, loaded in shear, small structure, compressive stress in plate σ = 0.5 MPa	OS3_det_shear_small_σ0.5
Equivalent EMM model, loaded in tension on the bed-joint, small structure, where $E_{y,tension}$ and $G_{ft,bed}$ are used	OS3_eqEMM_ten_bed_small_$E_{y,tension}$_$G_{ft,bed}$
Equivalent EMM model, loaded in compression, small structure, where $E_{y,tension}$ is used	OS3_eqEMM_comp_small_$E_{y,tension}$
Equivalent EMM model, loaded in tension on the bed-joint, small structure, where $E_{y,average}$ and $G_{ft,bed}$ are used	OS3_eqEMM_ten_bed_small_$E_{y,average}$_$G_{ft,bed}$
Equivalent EMM model, loaded in compression, small structure, where $E_{y,average}$ is used	OS3_eqEMM_comp_small_$E_{y,average}$
Equivalent EMM model, loaded in tension on the head-joint, small structure, where $G_{ft,bed}$ is used	OS3_eqEMM_ten_head_small_$G_{ft,bed}$
Equivalent EMM model, loaded in tension on the head-joint, small structure, where $G_{ft,average}$ is used	OS3_eqEMM_ten_head_small_$G_{ft,average}$
Equivalent EMM model, loaded in tension on the bed-joint, small structure, where $E_{y,average}$ and $G_{ft,average}$ are used	OS3_eqEMM_ten_bed_small_ $E_{y,average}$ _$G_{ft,average}$
Equivalent EMM model, loaded in shear, small structure, compressive stress in plate σ = 0.5 MPa, where the mesh consists of one element	OS3_eqEMM_shear_small_σ0.5_one_el

Equivalent EMM model, loaded in shear, small structure, compressive stress in plate σ = 0.5 MPa, where the mesh consists of multiple elements	OS3_eqEMM_shear_small_σ0.5_mult_el
Detailed model, loaded in tension on the bed-joint, large structure	OS3_det_ten_bed_large
Equivalent EMM model, loaded in tension on the bed-joint, large structure, where EMM parameters of sub-question 1 (sq1) are used	OS3_eqEMM_ten_bed_large_ sq1_parameters
Detailed model, loaded in compression, large structure	OS3_det_comp_large
Equivalent EMM model, loaded in compression, large structure, where EMM parameters of sub-question 1 (sq1) are used	OS3_eqEMM_comp_large_ sq1_parameters
Detailed model, loaded in shear, large structure, compressive stress in plate σ = 0.5 MPa	OS3_det_shear_large_σ0.5
Equivalent EMM model, loaded in shear, large structure, compressive stress in plate σ = 0.5 MPa, where the mesh consists of 1 element and the EMM parameters of sub-question 1 (sq1) are used	OS3_eqEMM_shear_large_σ0.5_one_el_sq1_parameters
Equivalent EMM model, loaded in shear, large structure, compressive stress in plate σ = 0.5 MPa, where the mesh consists of multiple elements and the EMM parameters of sub-question 1 (sq1) are used	OS3_eqEMM_shear_large_σ0.5_mult_el_sq1_parameters
Equivalent EMM model, loaded in tension on the bed-joint, large structure, where the final EMM parameters are used	OS3_eqEMM_ten_bed_large_ final_parameters
Equivalent EMM model, loaded in tension on the head-joint, small structure (only one structure size will be analysed for head-joint tension models), where the final EMM parameters are used	OS3_eqEMM_ten_head_small_ final_parameters
Equivalent EMM model, loaded in compression, large structure, where the final EMM parameters are used	OS3_eqEMM_comp _large_ final_parameters
Equivalent EMM model, loaded in shear, large structure, compressive stress in plate σ = 0.5 MPa, where the mesh consists of multiple elements and the final EMM parameters are used	OS3_eqEMM_shear_large_σ0.5_ final_parameters

Detailed model of the full lighthouse, made by the company PT Structural Analysis & Design	PT model
Equivalent EMM model of the full lighthouse, created for this thesis, where the final EMM parameters are used, and the load combination of self-weight and wind is applied	Thesis model
Equivalent EMM model of the full lighthouse, created for this thesis, where the final EMM parameters are used, only the self-weight load is applied, and the gravitational acceleration is multiplied with a factor of 20 in the model to observe the behaviour after the compressive stresses exceed the compressive strength	High gravity thesis model

B. Results remaining detailed finite element models chapter 4

In this appendix, there are no contour plots in the results presentation, as the failure modes of these structures are identical to those of the structures of sections OS3 & IS1.

a) b)

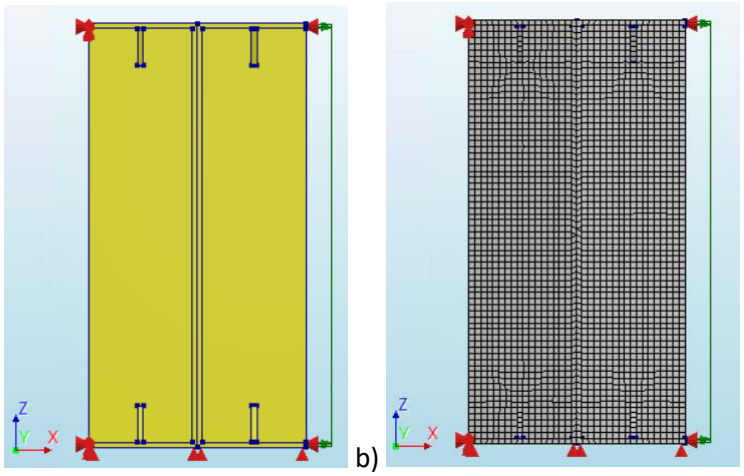

c)

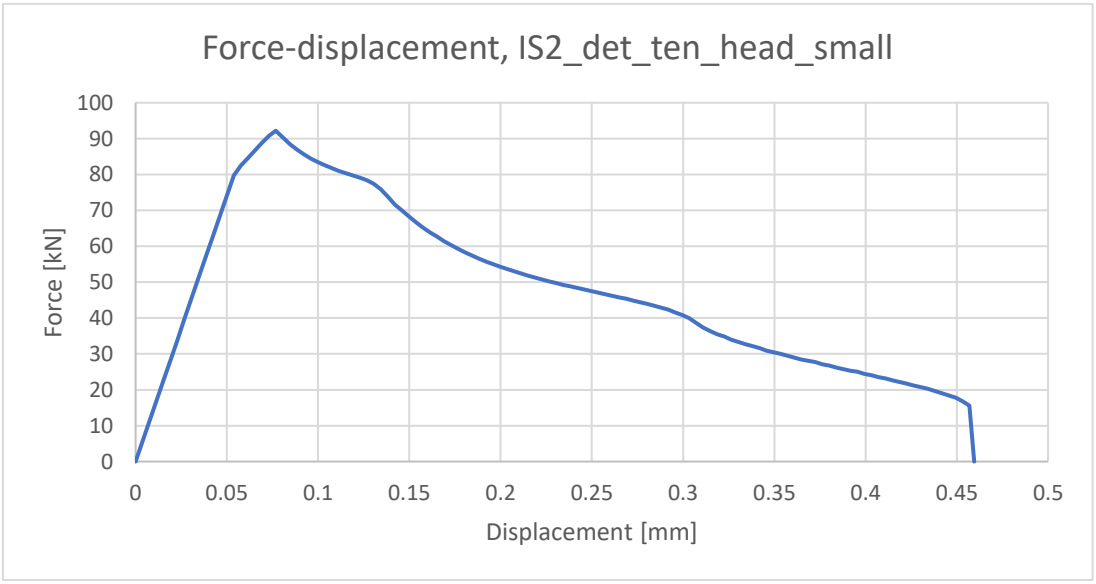

d)

Average element size [mm]		20x20
Number of elements	HX24L	3131
	PY15L	40
	TE12L	16
	TP18L	46
	Q24IF	276
Total number of nodes		6689

e)

Iteration method	Newton-Raphson	
Convergence norms	Displacement	Force
Convergence tolerances	0.01	0.01
Step size	0.008(125)	
Maximum number of iterations per step	100	
All norms satisfied	No	

Figure B.1: Results of finite element analysis IS2_det_ten_head_small. a-e: structure (a), finite element mesh (b), force-displacement curve (c), overview elements and nodes (d), overview iterative scheme (e)

a) 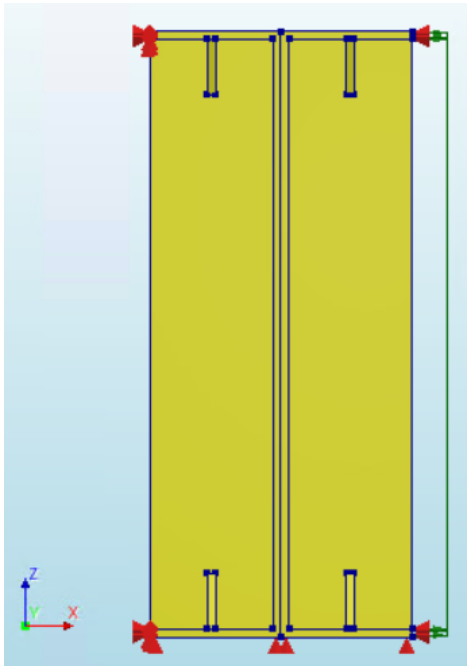

b) 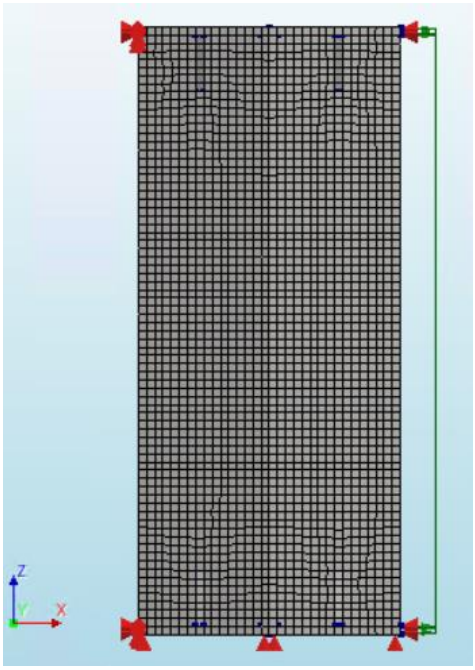

c) 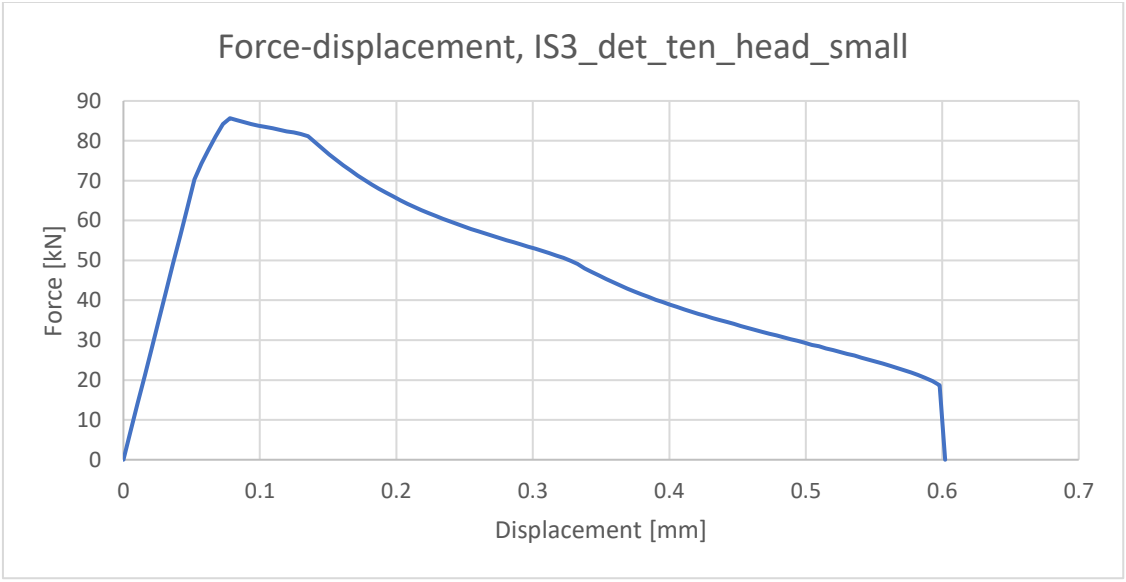

d)

Average element size [mm]		20x20
Number of elements	HX24L	3028
	TP18L	12
	Q24IF	296
Total number of nodes		6432

e)

Iteration method	Newton-Raphson	
Convergence norms	Displacement	Force
Convergence tolerances	0.01	0.01
Step size	0.008(125)	
Maximum number of iterations per step	100	
All norms satisfied	No	

Figure B.2: Results of finite element analysis IS3_det_ten_head_small. a-e: structure (a), finite element mesh (b), force-displacement curve (c), overview elements and nodes (d), overview iterative scheme (e)

a)

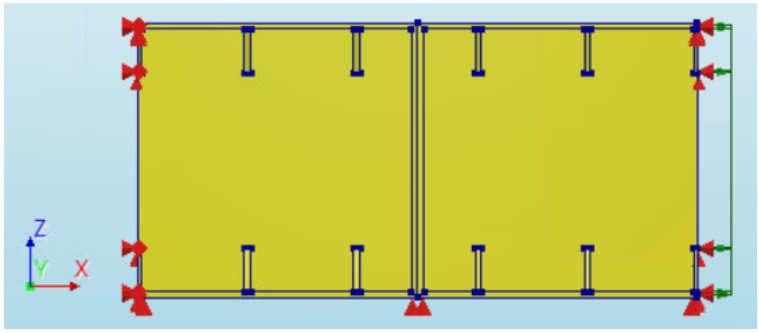

b)

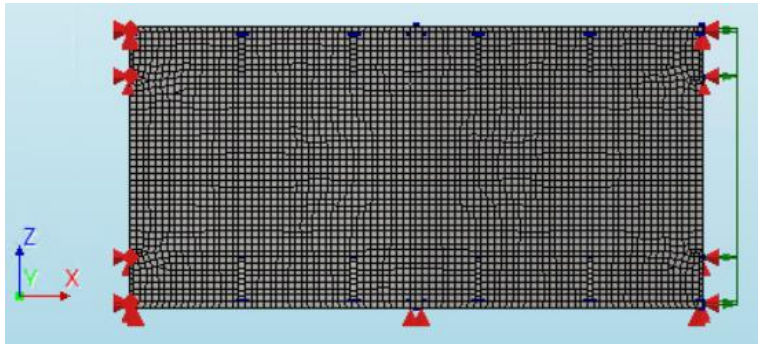

c)

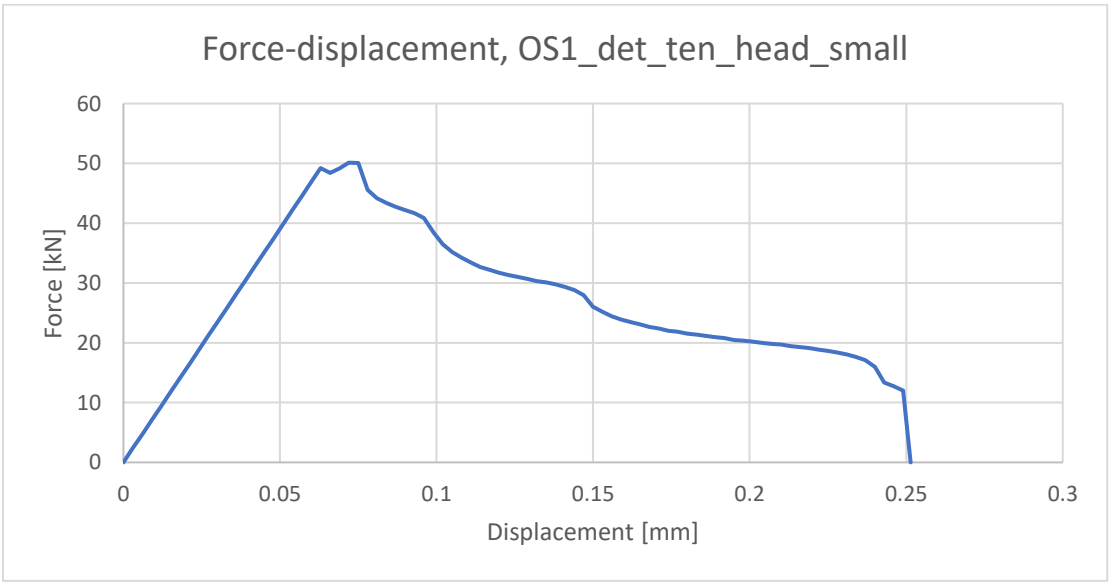

d)

Average element size [mm]		20x20
Number of elements	HX24L	8637
	PY15L	1407
	TE12L	1129
	TP18L	430
	Q24IF	220
Total number of nodes		14962

e)

Iteration method	Newton-Raphson	
Convergence norms	Displacement	Force
Convergence tolerances	0.01	0.01
Step size	0.01(100)	
Maximum number of iterations per step	100	
All norms satisfied	No	

Figure B.3: Results of finite element analysis OS1_det_ten_head_small. a-e: structure (a), finite element mesh (b), force-displacement curve (c), overview elements and nodes (d), overview iterative scheme (e)

a)

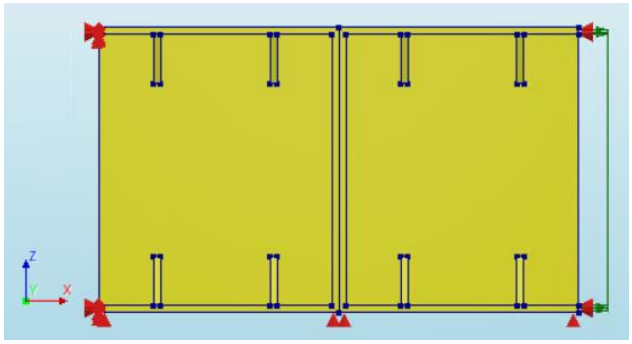

b)

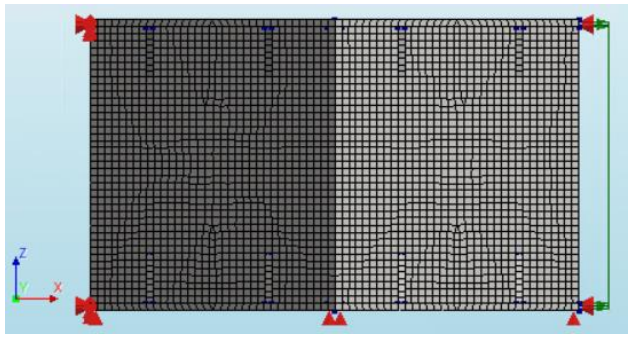

c)

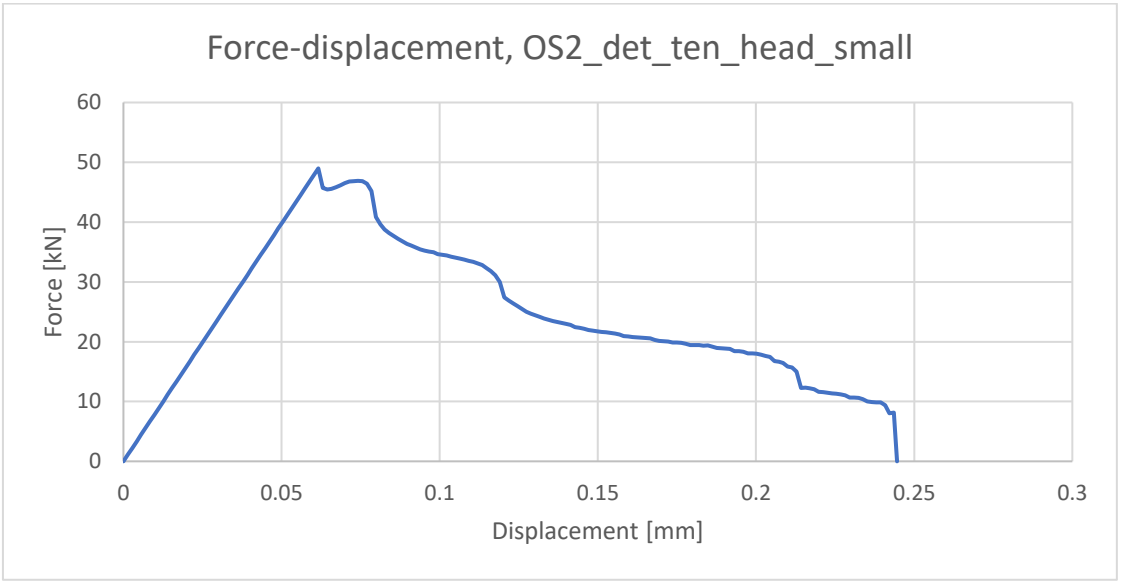

d)

Average element size [mm]		20x20
Number of elements	HX24L	4757
	PY15L	132
	TE12L	88
	TP18L	192
	Q24IF	164
Total number of nodes		8805

e)

Iteration method	Newton-Raphson	
Convergence norms	Displacement	Force
Convergence tolerances	0.01	0.01
Step size	0.005(200)	
Maximum number of iterations per step	100	
All norms satisfied	No	

Figure B.4: Results of finite element analysis OS2_det_ten_head_small. a-e: structure (a), finite element mesh (b), force-displacement curve (c), overview elements and nodes (d), overview iterative scheme (e)

a) b)

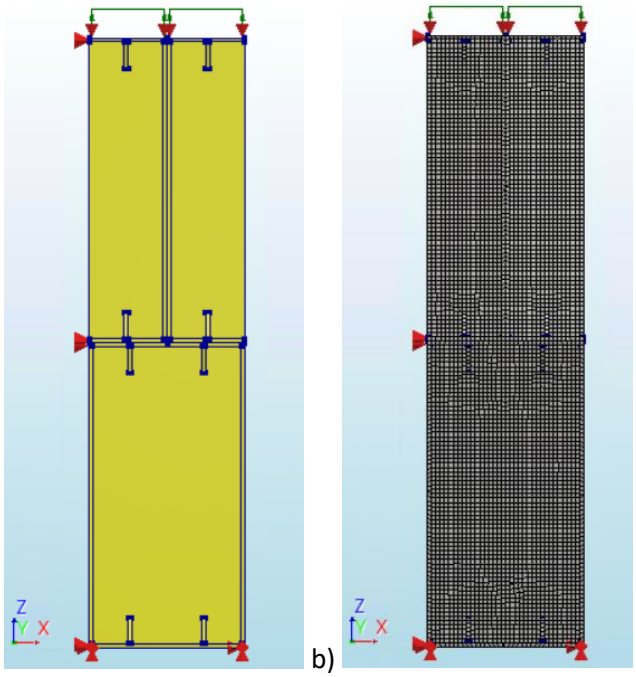

c)

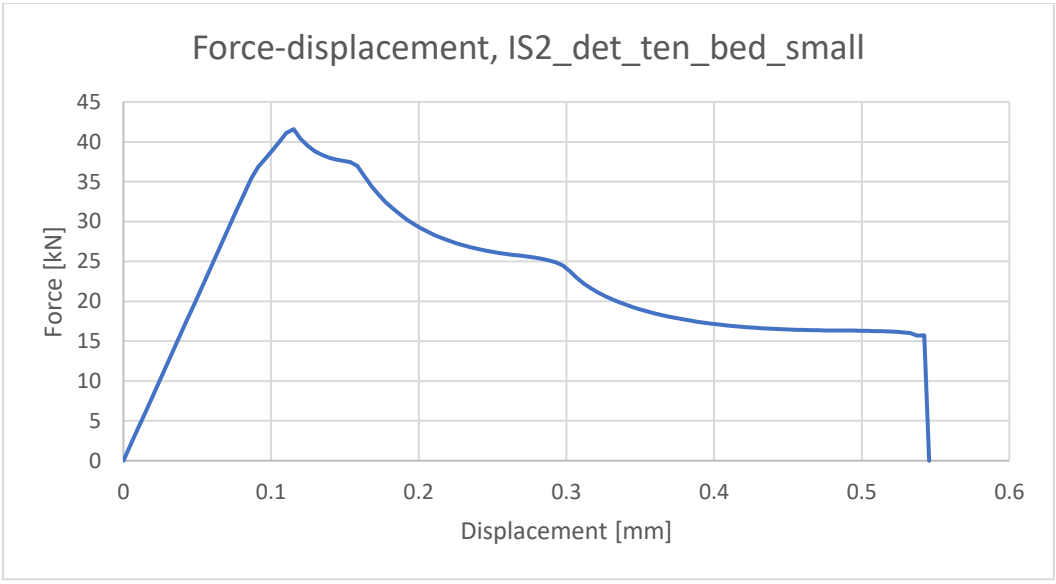

d)

Average element size [mm]		20x20
Number of elements	HX24L	7108
	PY15L	3908
	TE12L	3159
	TP18L	844
	Q24IF	420
Total number of nodes		16219

e)

Iteration method	Newton-Raphson	
Convergence norms	Displacement	Force
Convergence tolerances	0.01	0.01
Step size	0.008(125)	
Maximum number of iterations per step	100	
All norms satisfied	No	

Figure B.5: Results of finite element analysis IS2_det_ten_bed_small. a-e: structure (a), finite element mesh (b), force-displacement curve (c), overview elements and nodes (d), overview iterative scheme (e)

a) b)

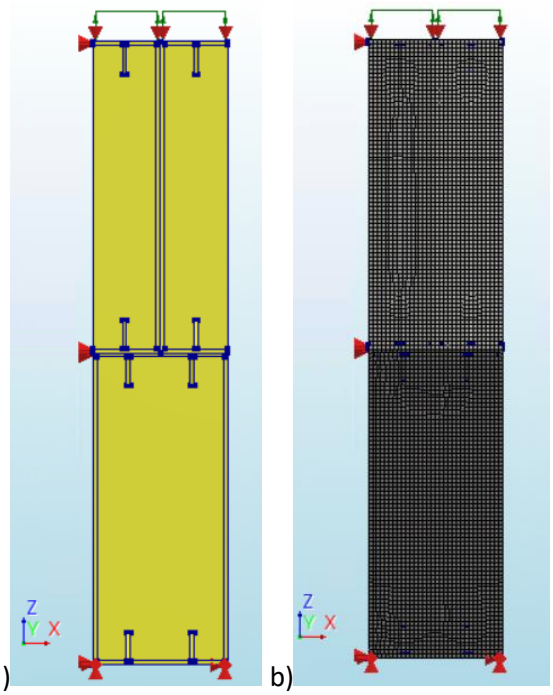

c)

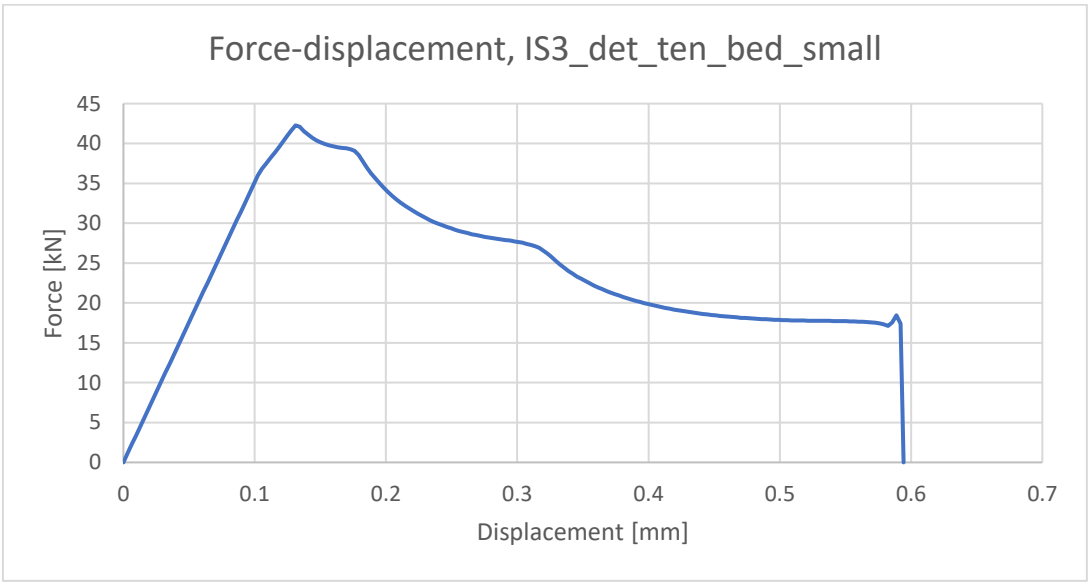

d)

Average element size [mm]		20x20
Number of elements	HX24L	6303
	PY15L	4769
	TE12L	3389
	TP18L	637
	Q24IF	424
Total number of nodes		15359

e)

Iteration method	Newton-Raphson	
Convergence norms	Displacement	Force
Convergence tolerances	0.01	0.01
Step size	0.005(200)	
Maximum number of iterations per step	100	
All norms satisfied	No	

Figure B.6: Results of finite element analysis IS3_det_ten_bed_small. a-e: structure (a), finite element mesh (b), force-displacement curve (c), overview elements and nodes (d), overview iterative scheme (e)

a) b)

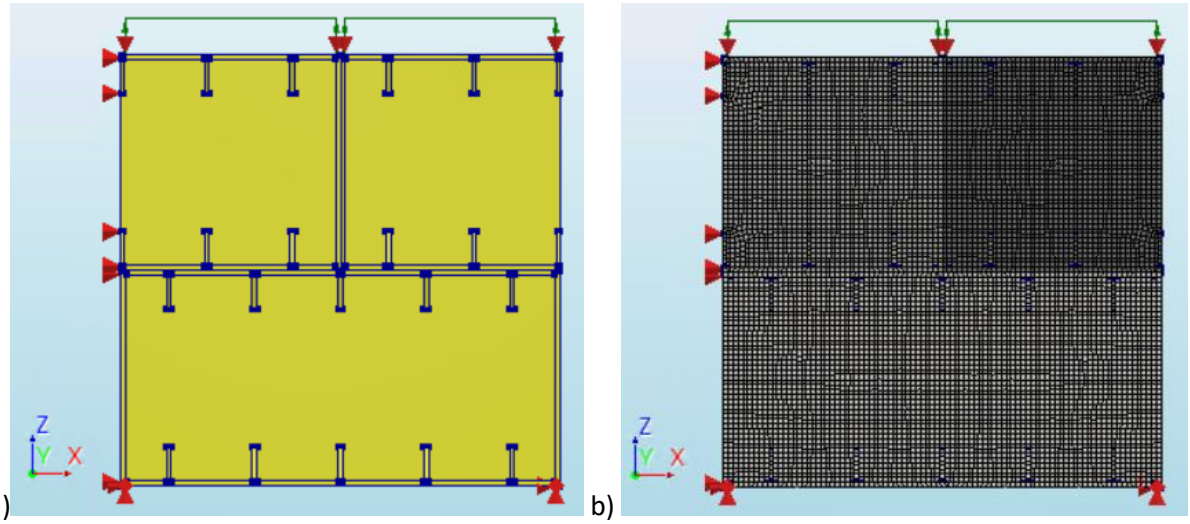

c)

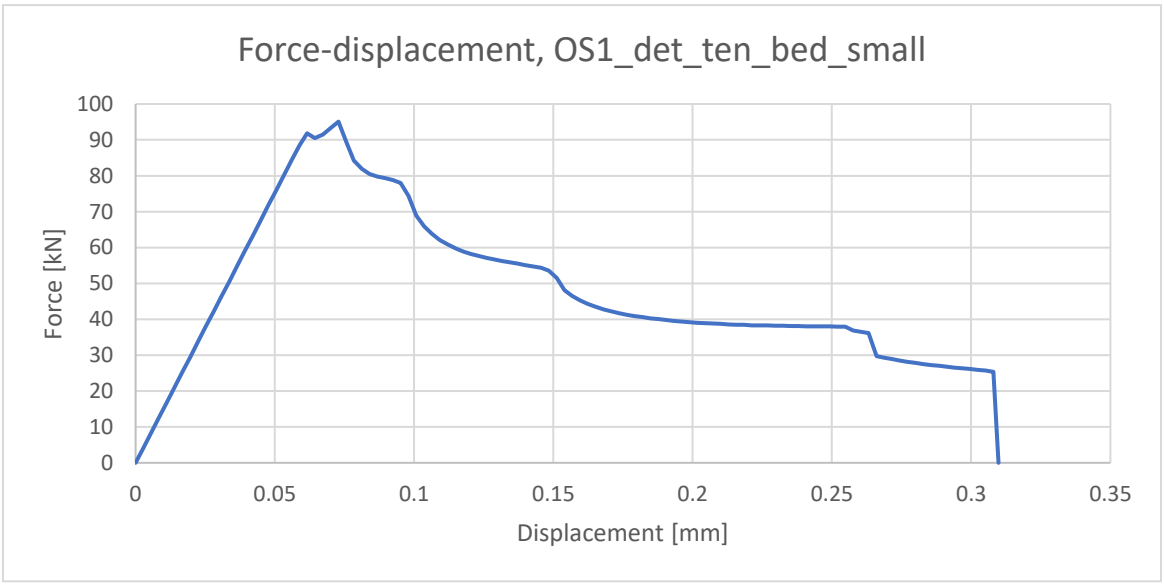

d)

Average element size [mm]		20x20
Number of elements	HX24L	9094
	PY15L	1032
	TE12L	769
	TP18L	454
	Q24IF	436
Total number of nodes		17423

e)

Iteration method	Newton-Raphson	
Convergence norms	Displacement	Force
Convergence tolerances	0.01	0.01
Step size	0.01(100)	
Maximum number of iterations per step	100	
All norms satisfied	No	

Figure B.7: Results of finite element analysis OS1_det_ten_bed_small. a-e: structure (a), finite element mesh (b), force-displacement curve (c), overview elements and nodes (d), overview iterative scheme (e)

a) b)

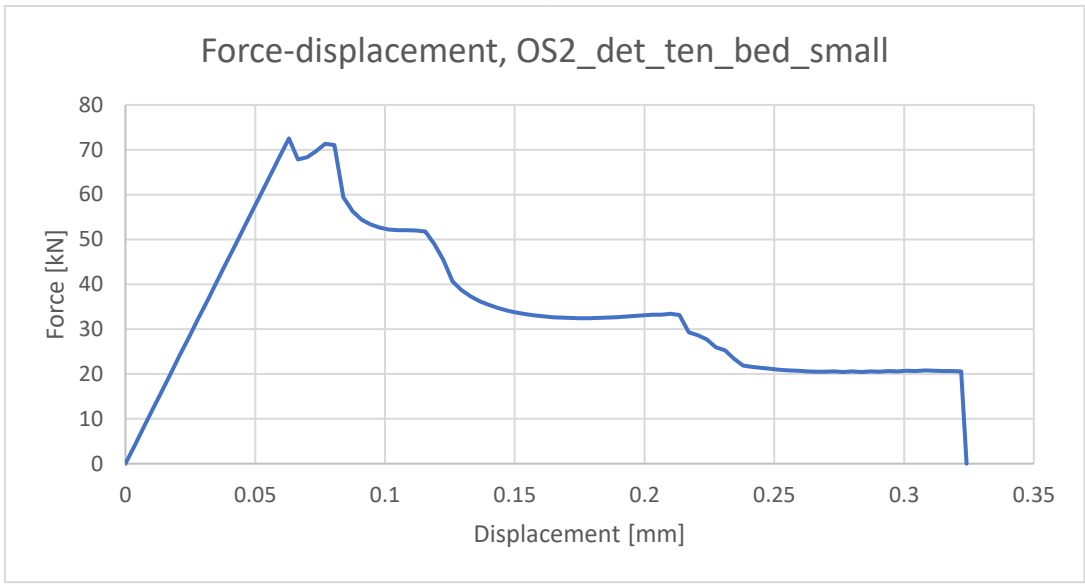

c)

Average element size [mm]		20x20
Number of elements	HX24L	9094
	PY15L	1032
	TE12L	769
	TP18L	454
	Q24IF	436
Total number of nodes		17423

d)

Iteration method	Newton-Raphson	
Convergence norms	Displacement	Force
Convergence tolerances	0.01	0.01
Step size	0.01(100)	
Maximum number of iterations per step	100	
All norms satisfied	No	

e)

Figure B.8: Results of finite element analysis OS2_det_ten_bed_small. a-e: structure (a), finite element mesh (b), force-displacement curve (c), overview elements and nodes (d), overview iterative scheme (e)

a) b)

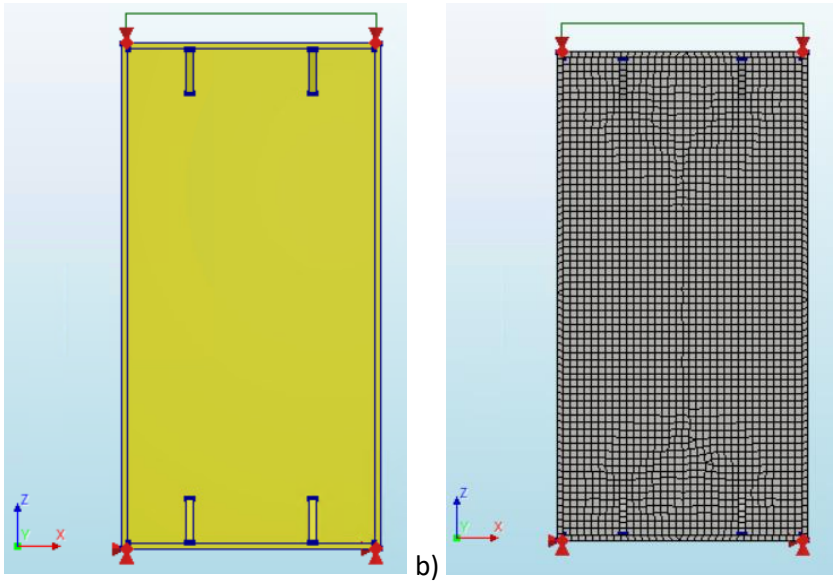

c)

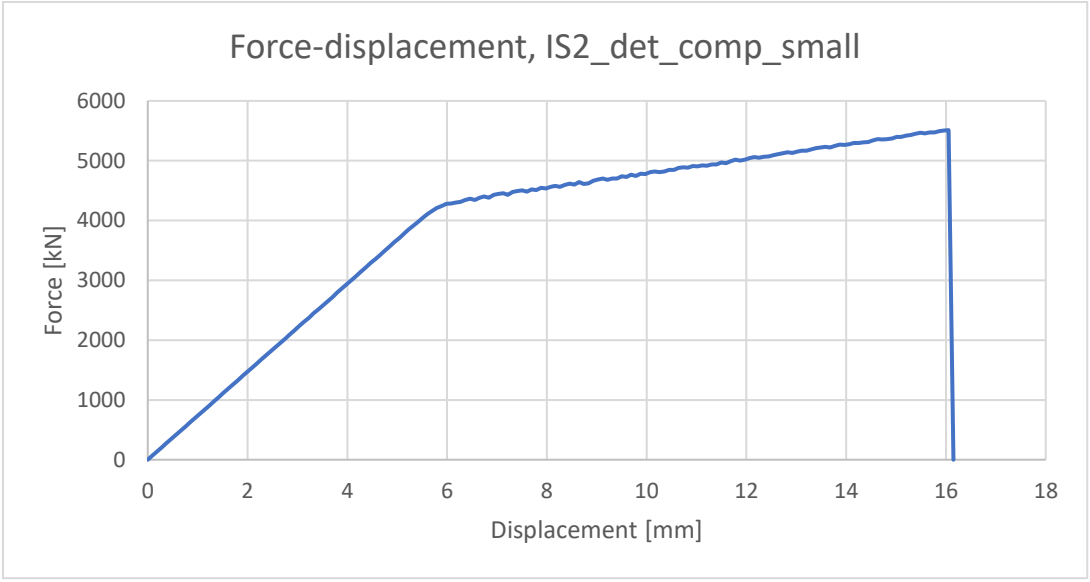

d)

Average element size [mm]		20x20
Number of elements	HX24L	2952
	PY15L	6433
	TE12L	5514
	TP18L	901
Total number of nodes		9752

e)

Iteration method	Newton-Raphson	
Convergence norms	Displacement	Force
Convergence tolerances	0.01	0.01
Step size	0.005(200)	
Maximum number of iterations per step	100	
All norms satisfied	No	

Figure B.9: Results of finite element analysis IS2_det_comp_small. a-e: structure (a), finite element mesh (b), force-displacement curve (c), overview elements and nodes (d), overview iterative scheme (e)

a) b)

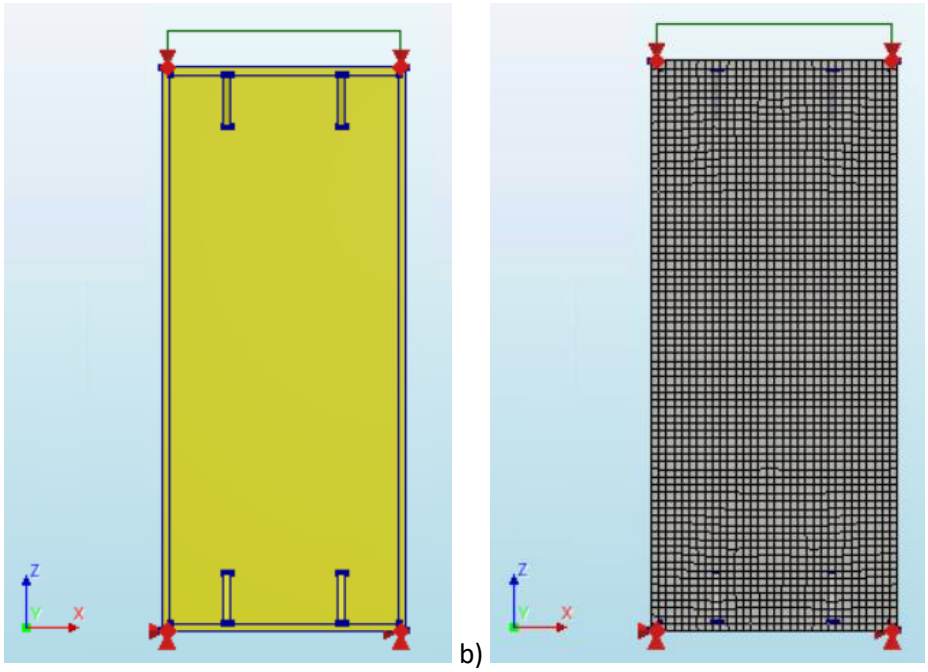

c)

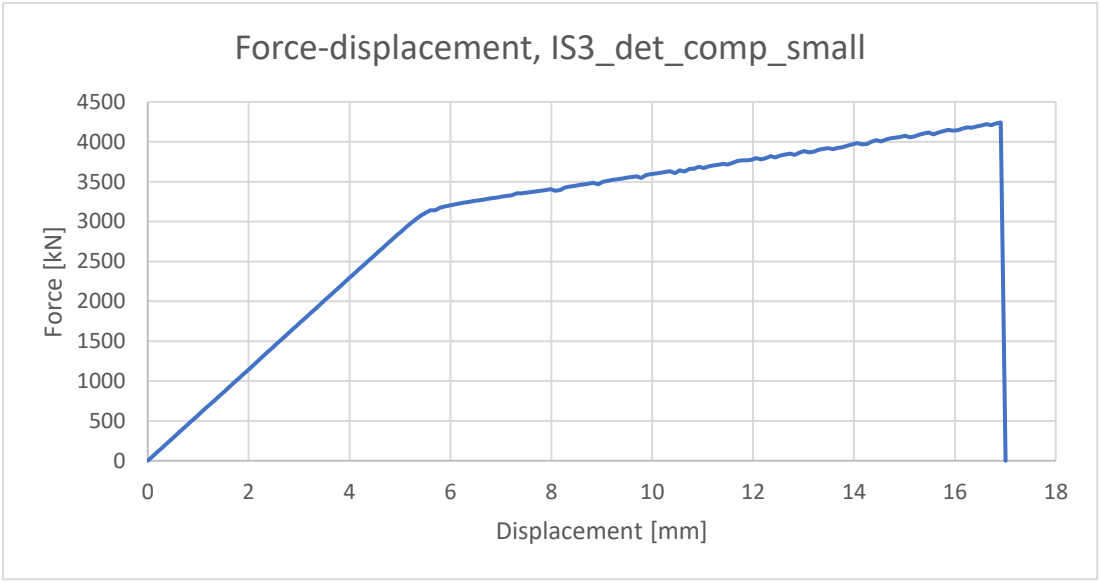

d)

Average element size [mm]		20x20
Number of elements	HX24L	3880
	PY15L	2862
	TE12L	2003
	TP18L	568
Total number of nodes		8657

e)

Iteration method	Newton-Raphson	
Convergence norms	Displacement	Force
Convergence tolerances	0.01	0.01
Step size	0.005(200)	
Maximum number of iterations per step	100	
All norms satisfied	No	

Figure B.10: Results of finite element analysis IS3_det_comp_small. a-e: structure (a), finite element mesh (b), force-displacement curve (c), overview elements and nodes (d), overview iterative scheme (e)

a)

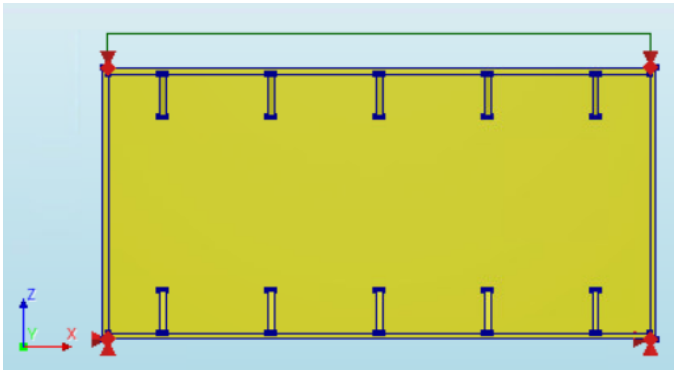

b)

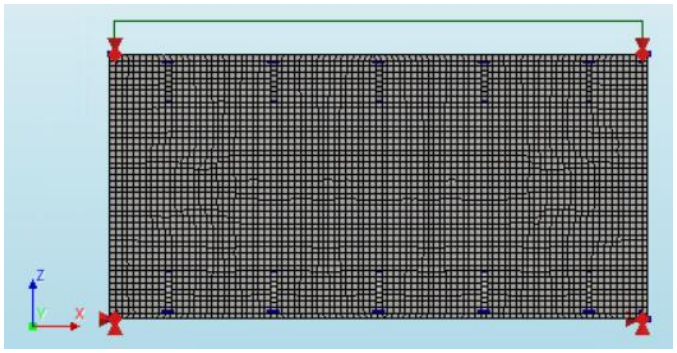

c)

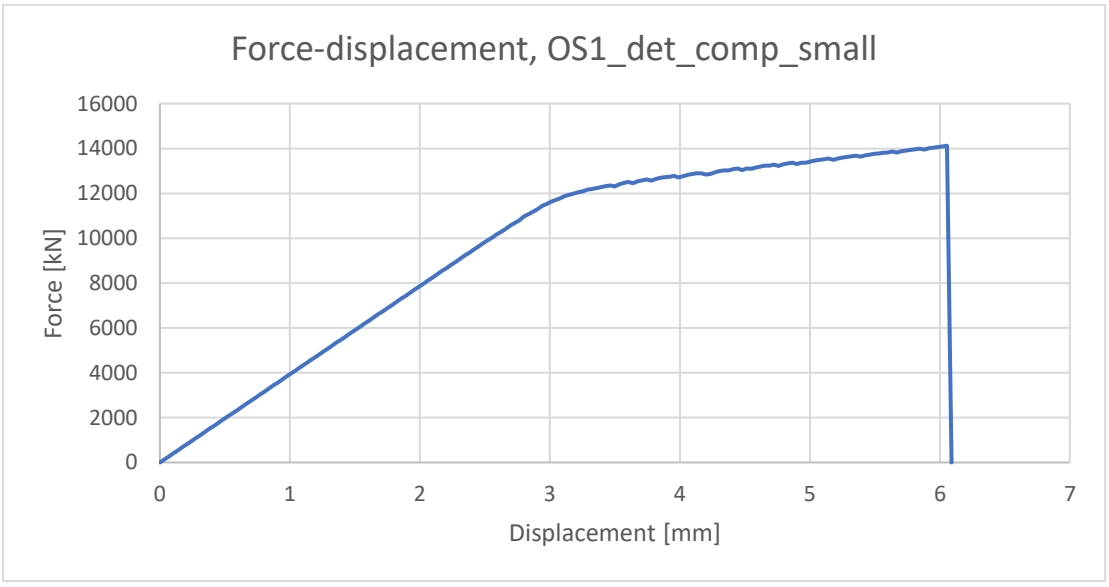

d)

Average element size [mm]		20x20
Number of elements	HX24L	8553
	PY15L	898
	TE12L	597
	TP18L	240
Total number of nodes		14351

e)

Iteration method	Newton-Raphson	
Convergence norms	Displacement	Force
Convergence tolerances	0.01	0.01
Step size	0.005(200)	
Maximum number of iterations per step	100	
All norms satisfied	No	

Figure B.11: Results of finite element analysis OS1_det_comp_small. a-e: structure (a), finite element mesh (b), force-displacement curve (c), overview elements and nodes (d), overview iterative scheme (e)

a)

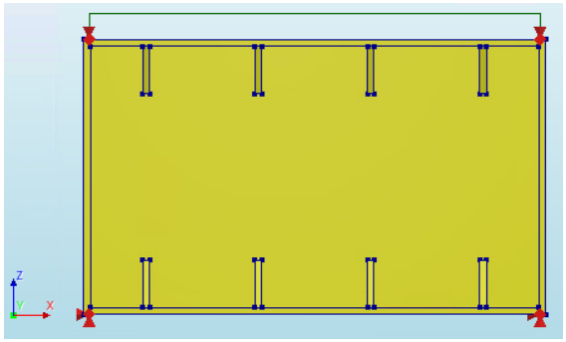

b)

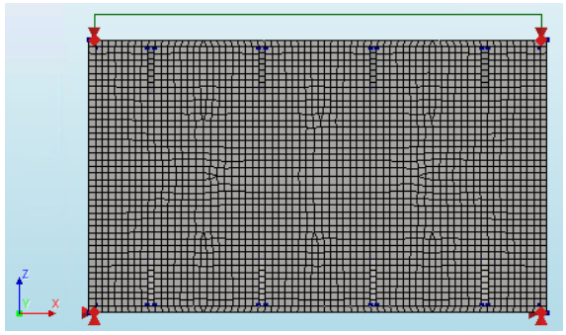

c)

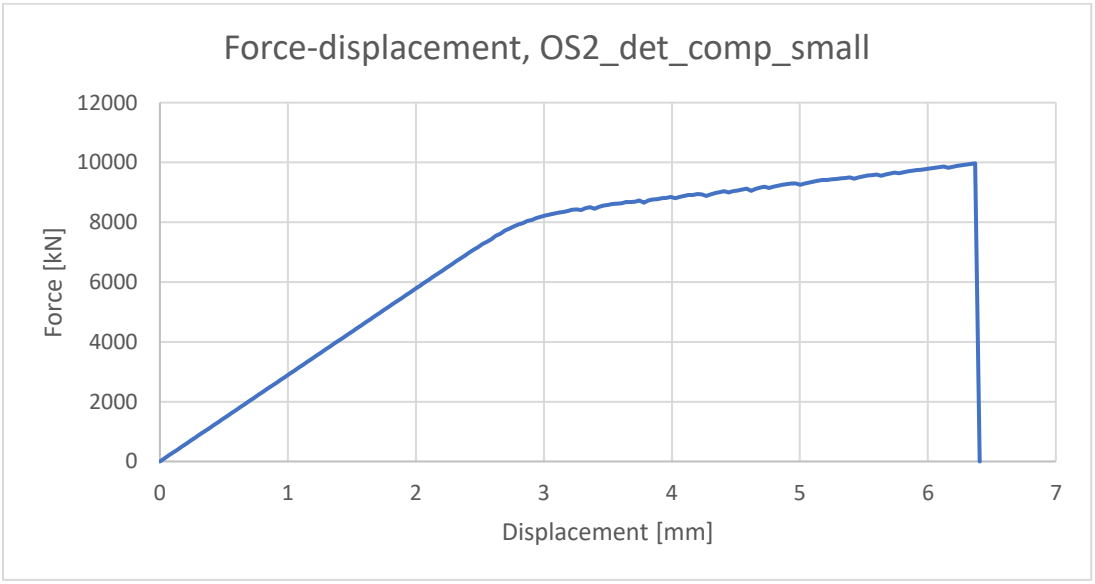

d)

Average element size [mm]		20x20
Number of elements	HX24L	4560
	PY15L	392
	TE12L	326
	TP18L	250
Total number of nodes		8609

e)

Iteration method	Newton-Raphson	
Convergence norms	Displacement	Force
Convergence tolerances	0.01	0.01
Step size	0.005(200)	
Maximum number of iterations per step	100	
All norms satisfied	No	

Figure B.12: Results of finite element analysis OS2_det_comp_small. a-e: structure (a), finite element mesh (b), force-displacement curve (c), overview elements and nodes (d), overview iterative scheme (e)

a) b)

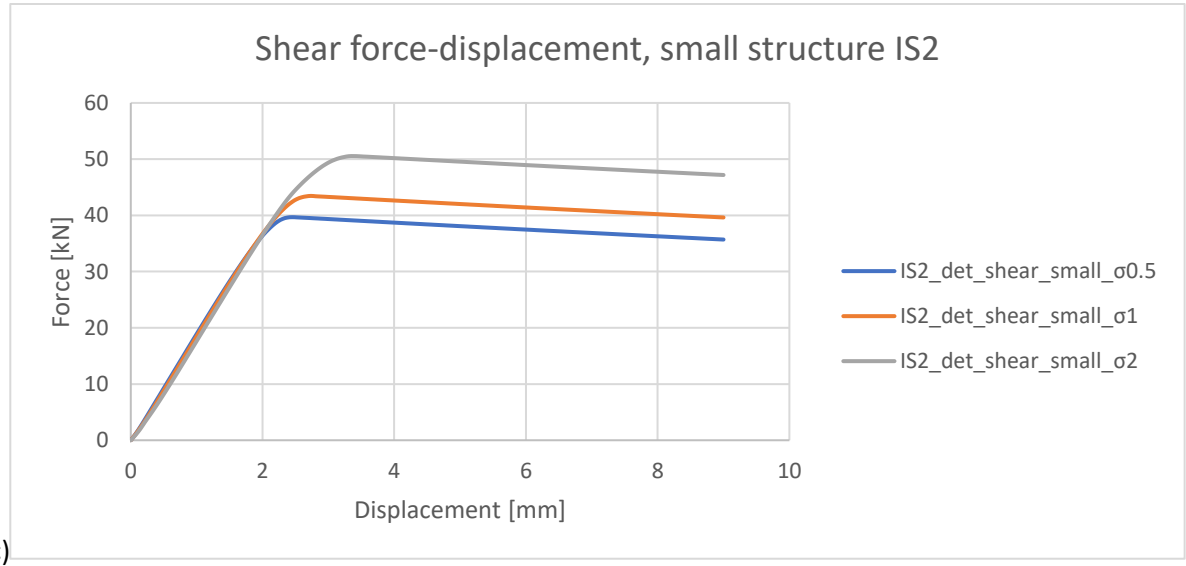

c)

Average element size [mm]		20x20
Number of elements	HX24L	7108
	PY15L	3908
	TE12L	3159
	TP18L	844
	Q24IF	420
Total number of nodes		16219

d)

Load	Compression		Translation	
Iteration method	Newton-Raphson		Newton-Raphson	
Convergence norms	Force	Displacement	Force	Displacement
Convergence tolerances	0.01	0.01	0.01	0.01
Step size	0.2(5)		0.008(125)	
Maximum number of iterations per step	100			
All norms satisfied	No			

e)

Figure B.13: Results of finite element analysis IS2_det_shear_small_σ0.5, σ1 & σ2. a-e: structure (a), finite element mesh (b), force-displacement curve (c), overview elements and nodes (d), overview iterative scheme (e)

a) b)

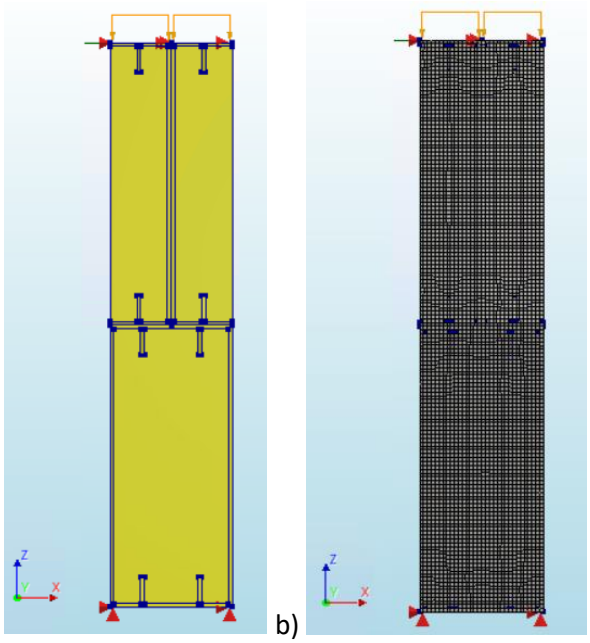

c)

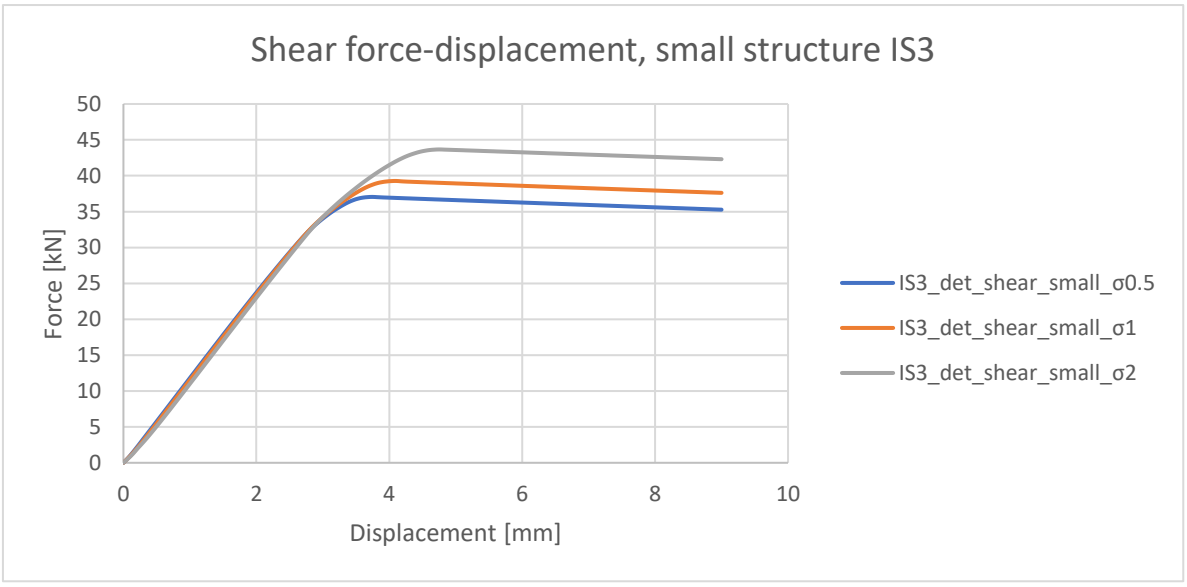

d)

Average element size [mm]		20x20
Number of elements	HX24L	6303
	PY15L	4769
	TE12L	3389
	TP18L	637
	Q24IF	424
Total number of nodes		15359

e)

Load	Compression		Translation	
Iteration method	Newton-Raphson		Newton-Raphson	
Convergence norms	Force	Displacement	Force	Displacement
Convergence tolerances	0.01	0.01	0.01	0.01
Step size	0.2(5)		0.008(125)	
Maximum number of iterations per step	100			
All norms satisfied	No			

Figure B.14: Results of finite element analysis IS3_det_shear_small_σ0.5, σ1 & σ2. a-e: structure (a), finite element mesh (b), force-displacement curve (c), overview elements and nodes (d), overview iterative scheme (e)

a)

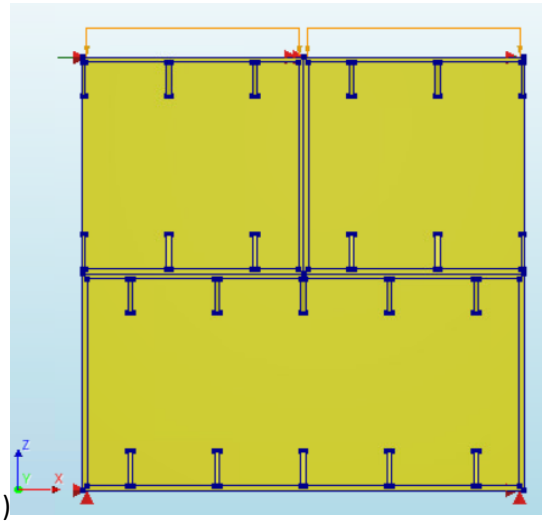

b)

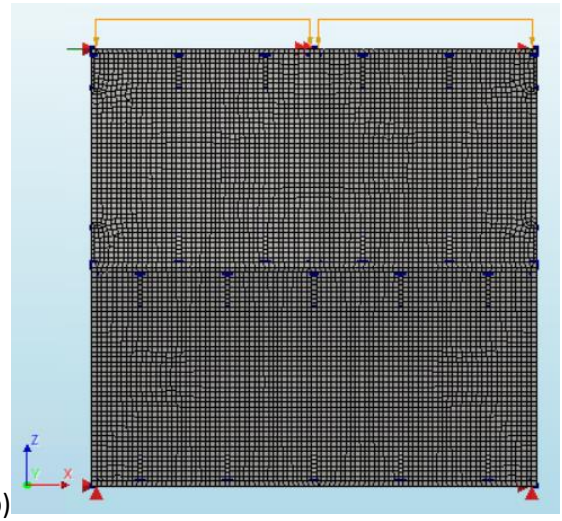

c)

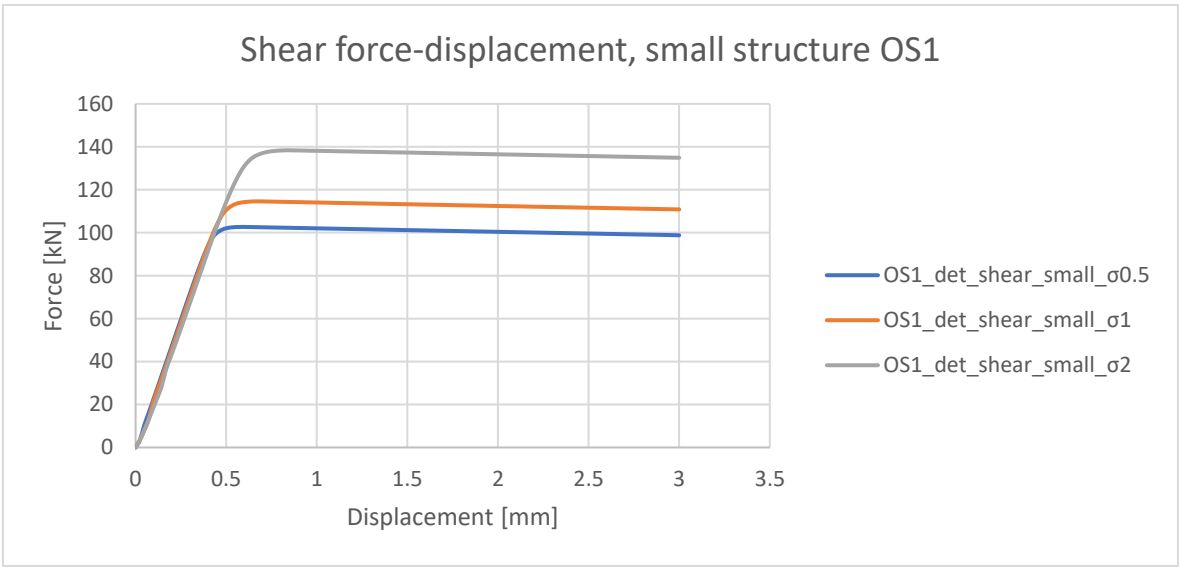

d)

Average element size [mm]		20x20
Number of elements	HX24L	17182
	PY15L	2366
	TE12L	1772
	TP18L	649
	Q24IF	670
Total number of nodes		29317

e)

Load	Compression		Translation	
Iteration method	Newton-Raphson		Newton-Raphson	
Convergence norms	Force	Displacement	Force	Displacement
Convergence tolerances	0.01	0.01	0.01	0.01
Step size	0.2(5)		0.008(125)	
Maximum number of iterations per step	100			
All norms satisfied	No			

Figure B.15: Results of finite element analysis OS1_det_shear_small_σ0.5, σ1 & σ2. a-e: structure (a), finite element mesh (b), force-displacement curve (c), overview elements and nodes (d), overview iterative scheme (e)

a) b)

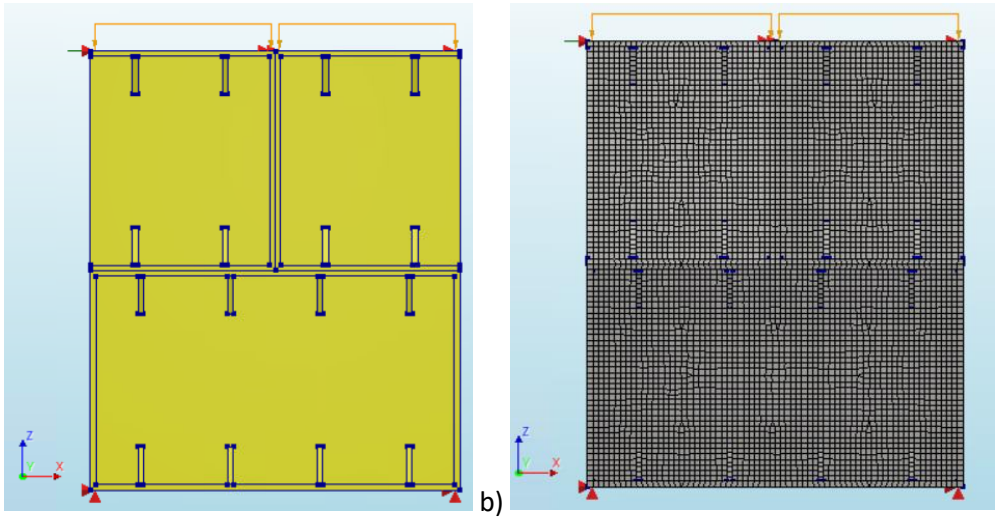

c)

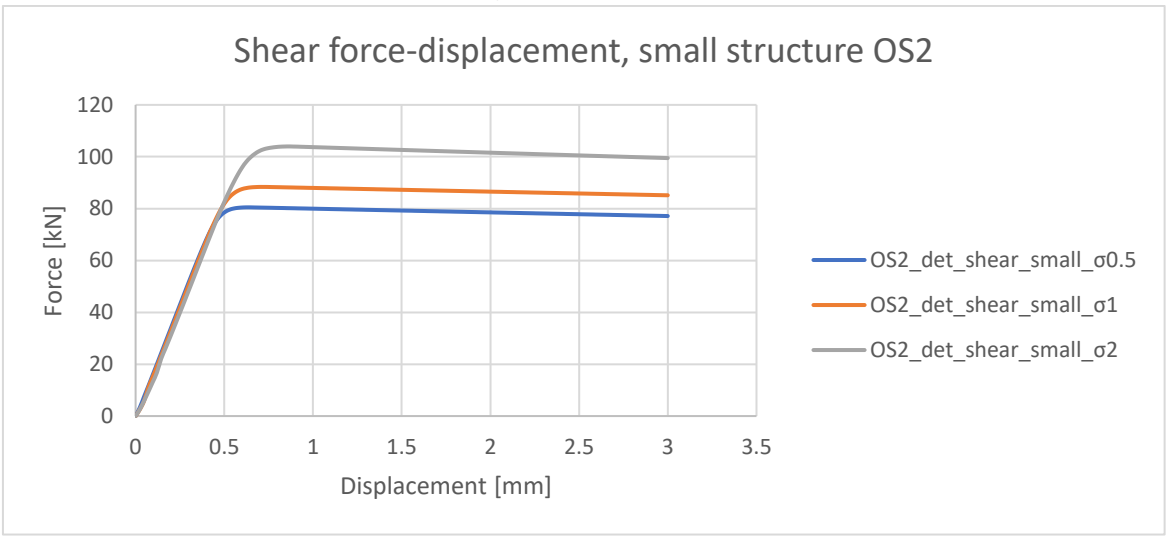

d)

Average element size [mm]		20x20
Number of elements	HX24L	9094
	PY15L	1032
	TE12L	769
	TP18L	454
	Q24IF	436
Total number of nodes		17423

e)

Load	Compression		Translation	
Iteration method	Newton-Raphson		Newton-Raphson	
Convergence norms	Force	Displacement	Force	Displacement
Convergence tolerances	0.01	0.01	0.01	0.01
Step size	0.2(5)		0.008(125)	
Maximum number of iterations per step	100			
All norms satisfied	No			

Figure B.16: Results of finite element analysis OS2_det_shear_small_σ0.5, σ1 & σ2. a-e: structure (a), finite element mesh (b), force-displacement curve (c), overview elements and nodes (d), overview iterative scheme (e)

C. Results equivalent EMM models of chapter 5

a)

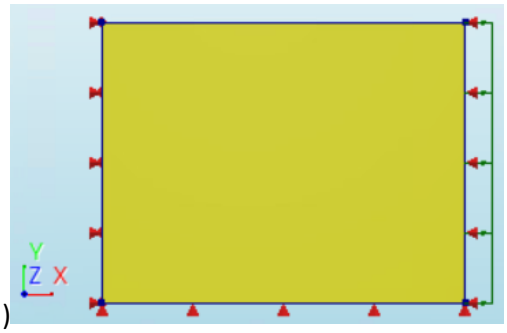

c)

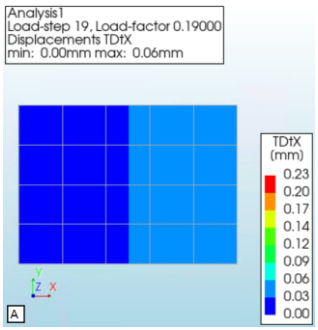

d)

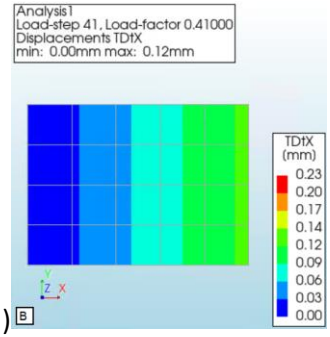

b)

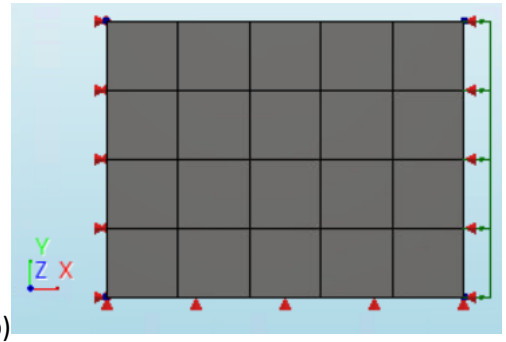

e)

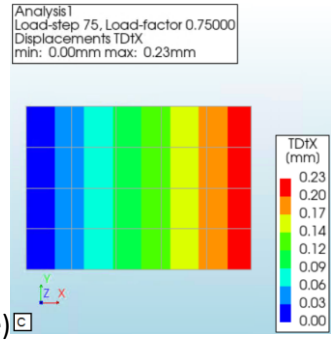

f)

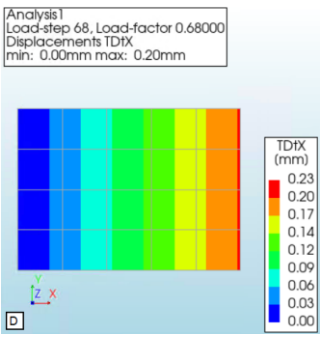

g)

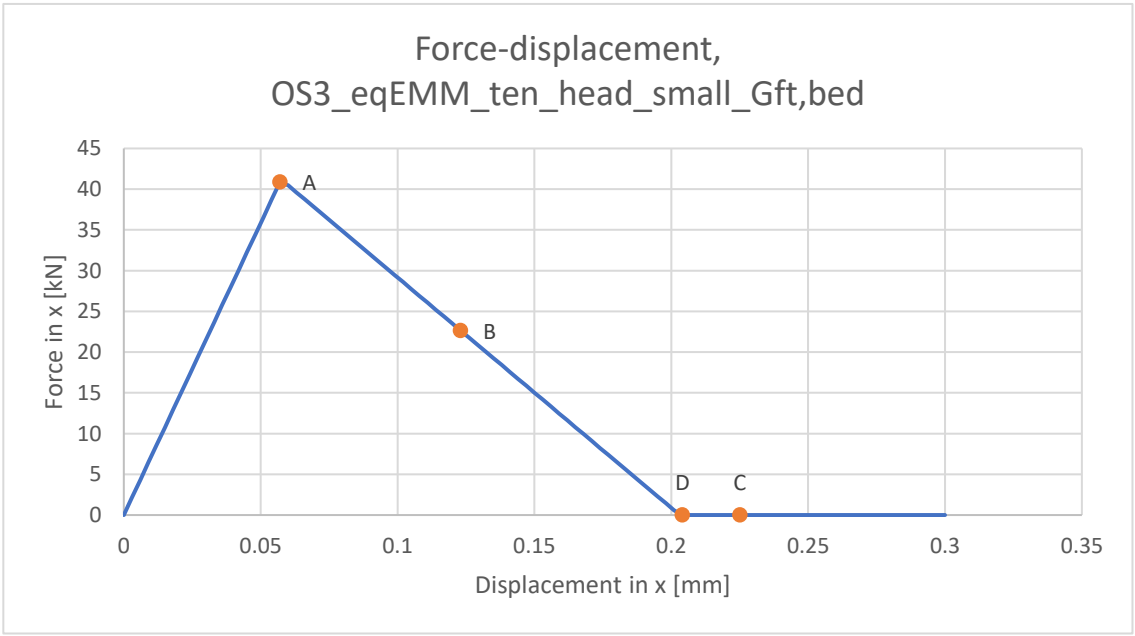

h)

Average element size [mm]		194x187.5
Number of elements	Q20SH	20
Total number of nodes		30

i)

Iteration method	Secant (Quasi-Newton)	
Convergence norms	Displacement	Force
Convergence tolerances	0.01	0.01
Step size	0.01(100)	
Maximum number of iterations per step	100	
All norms satisfied	No	

Figure C.1: Results of finite element analysis OS3_eqEMM_ten_head_small_$G_{ft,bed}$. a-i: structure (a), finite element mesh (b), displacement at point A (c), displacement at point B (d), displacement at point C (e), displacement at point D (f), force-displacement curve (g), overview elements and nodes (h), overview iterative scheme (i)

a)

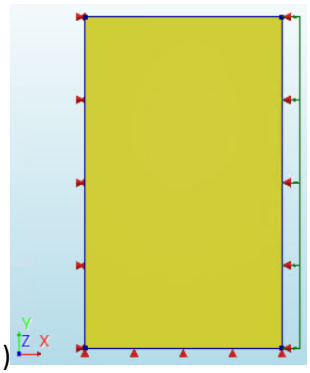

c)

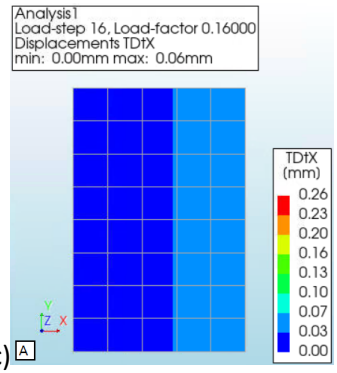

d)

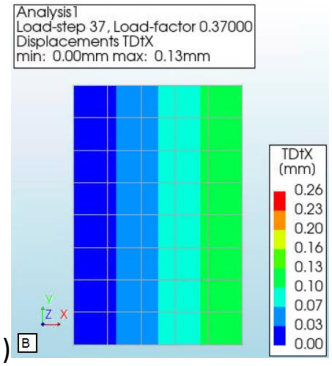

b)

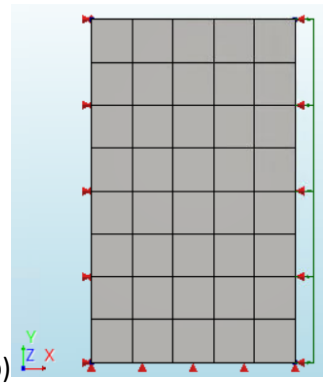

e)

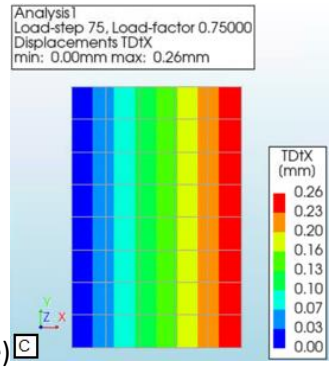

f)

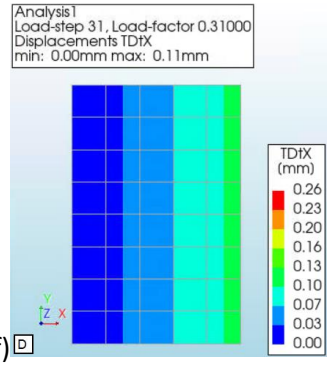

g)

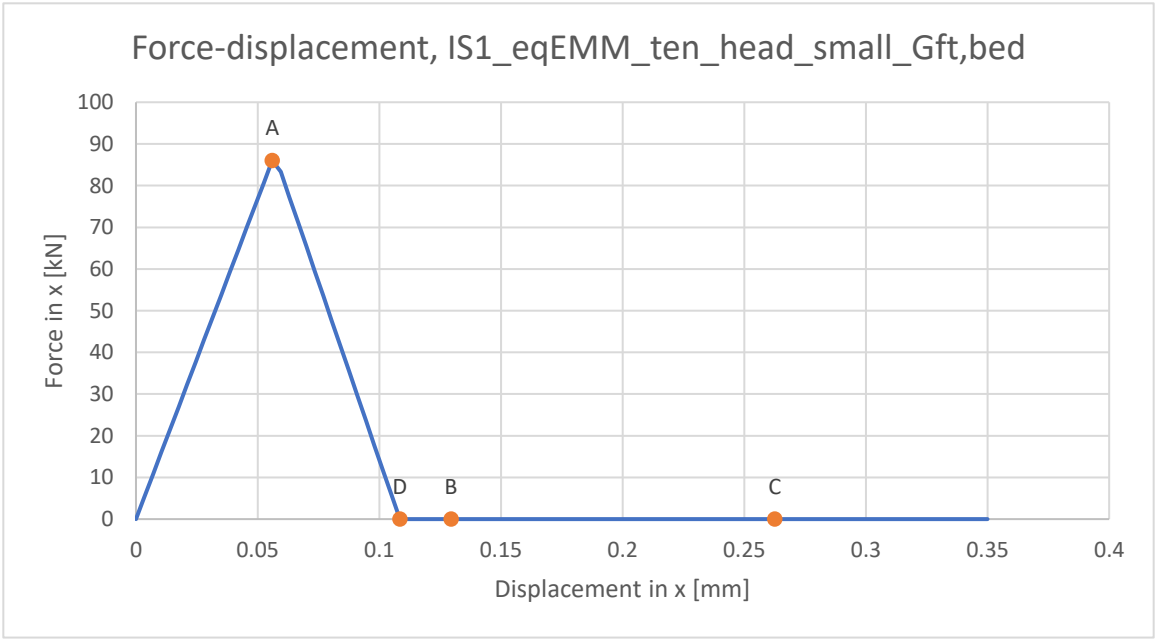

h)

Average element size [mm]		210.2x221.25
Number of elements	Q20SH	40
Total number of nodes		54

i)

Iteration method	Secant (Quasi-Newton)	
Convergence norms	Displacement	Force
Convergence tolerances	0.01	0.01
Step size	0.01(100)	
Maximum number of iterations per step	100	
All norms satisfied	No	

Figure C.2: Results of finite element analysis IS1_eqEMM_ten_head_small_$G_{ft,bed}$. a-i: structure (a), finite element mesh (b), displacement at point A (c), displacement at point B (d), displacement at point C (e), displacement at point D (f), force-displacement curve (g), overview elements and nodes (h), overview iterative scheme (i)

a)

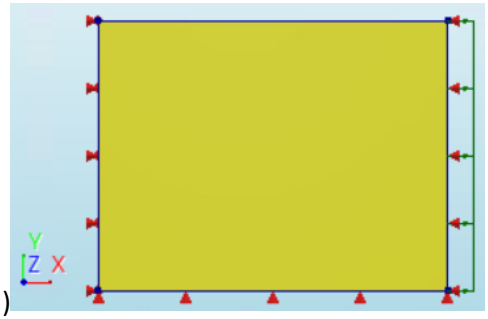

c)

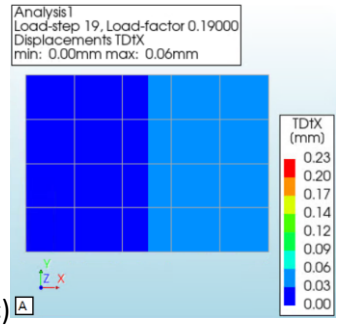

d)

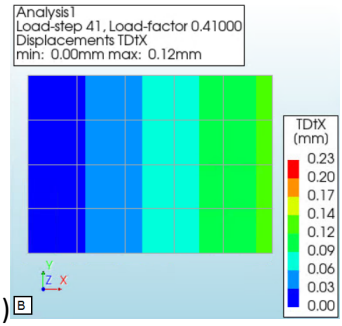

b)

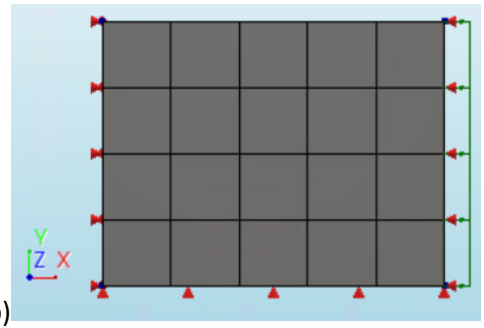

e)

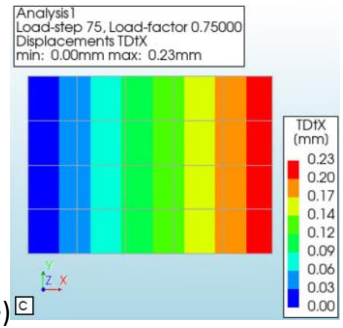

f)

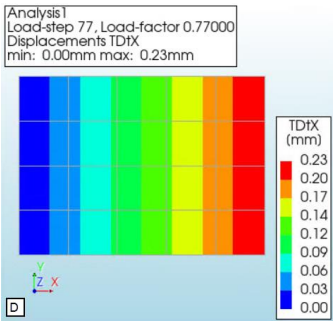

g)

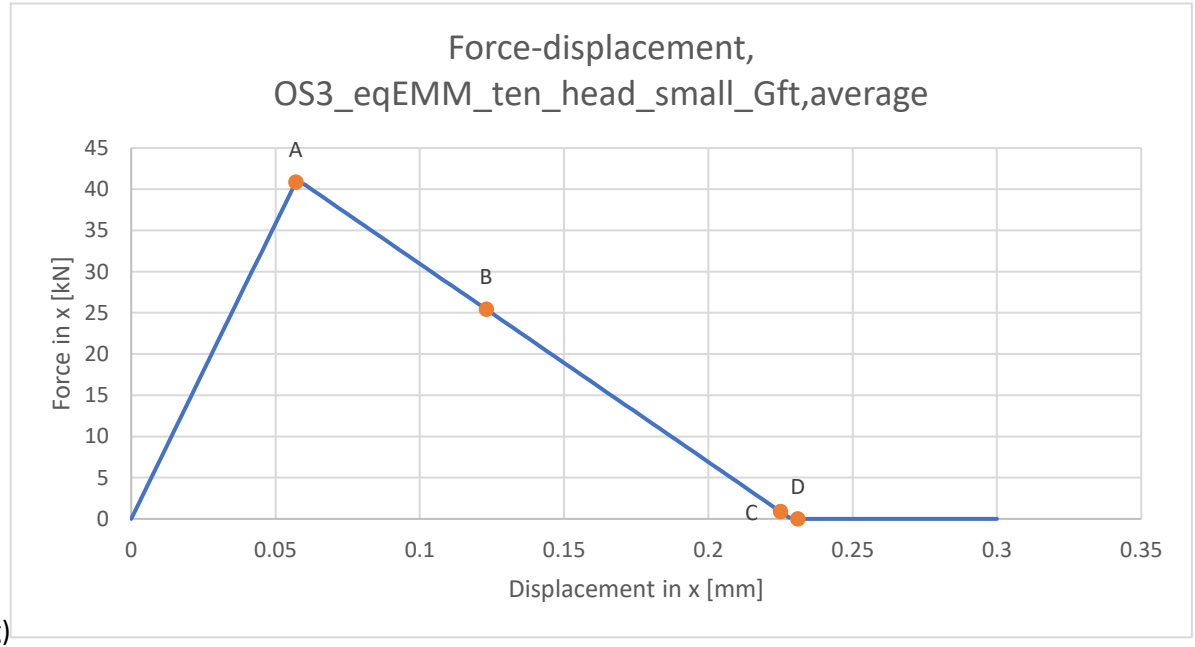

h)

Average element size [mm]		194x187.5
Number of elements	Q20SH	20
Total number of nodes		30

i)

Iteration method	Secant (Quasi-Newton)	
Convergence norms	Displacement	Force
Convergence tolerances	0.01	0.01
Step size	0.01(100)	
Maximum number of iterations per step	100	
All norms satisfied	No	

Figure C.3: Results of finite element analysis OS3_eqEMM_ten_head_small_$G_{ft,average}$. a-i: structure (a), finite element mesh (b), displacement at point A (c), displacement at point B (d), displacement at point C (e), displacement at point D (f), force-displacement curve (g), overview elements and nodes (h), overview iterative scheme (i)

a)

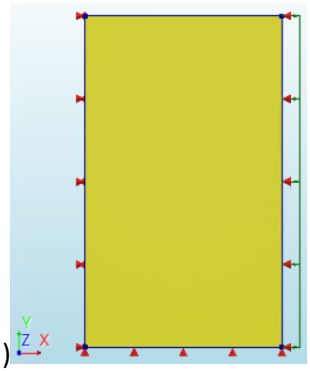

c)

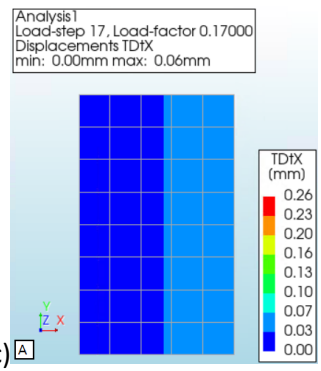

d)

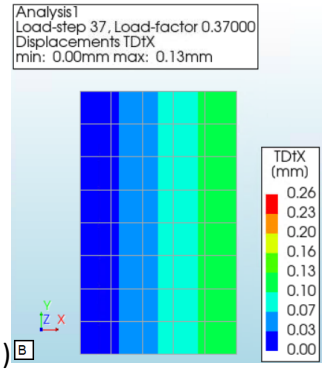

b)

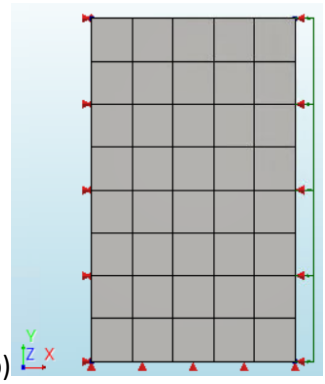

e)

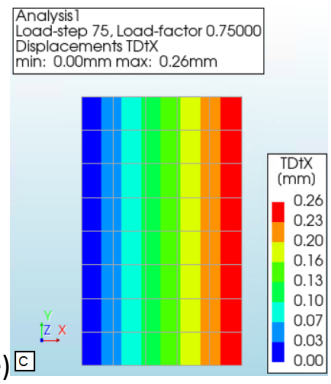

f)

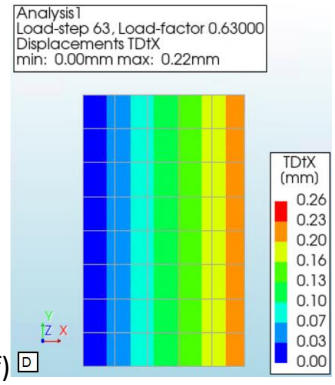

g)

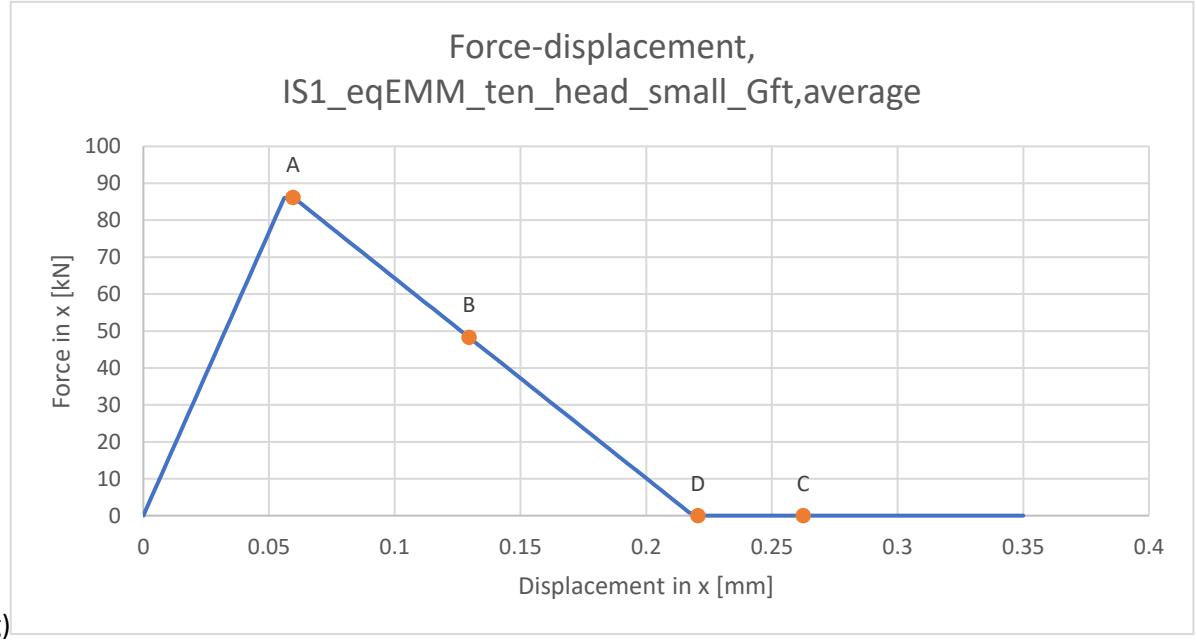

h)

Average element size [mm]		210.2x221.25
Number of elements	Q20SH	40
Total number of nodes		54

i)

Iteration method	Secant (Quasi-Newton)	
Convergence norms	Displacement	Force
Convergence tolerances	0.01	0.01
Step size	0.01(100)	
Maximum number of iterations per step	100	
All norms satisfied	No	

Figure C.4: Results of finite element analysis IS1_eqEMM_ten_head_small_$G_{ft,average}$. a-i: structure (a), finite element mesh (b), displacement at point A (c), displacement at point B (d), displacement at point C (e), displacement at point D (f), force-displacement curve (g), overview elements and nodes (h), overview iterative scheme (i)

a)

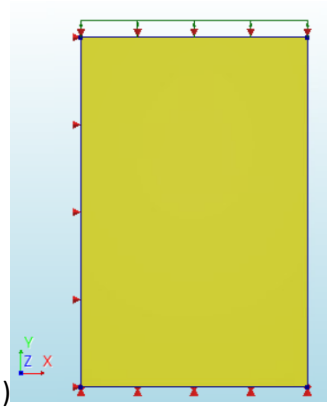

c)

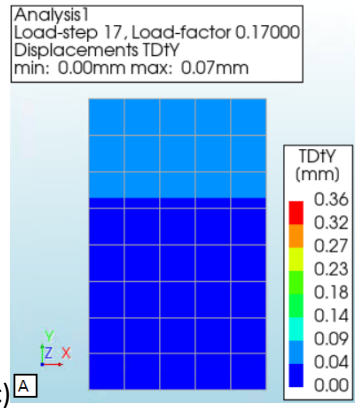

d)

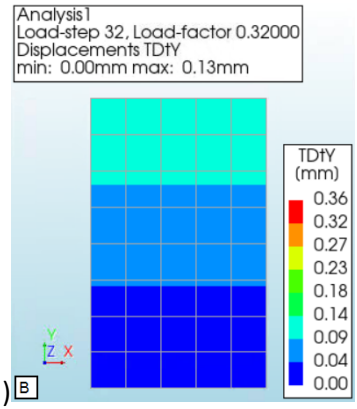

b)

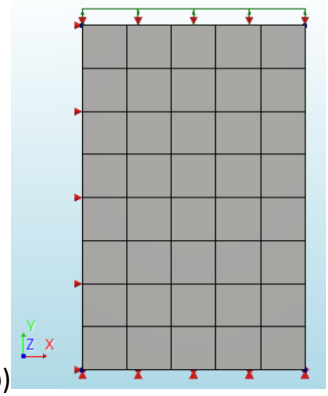

e)

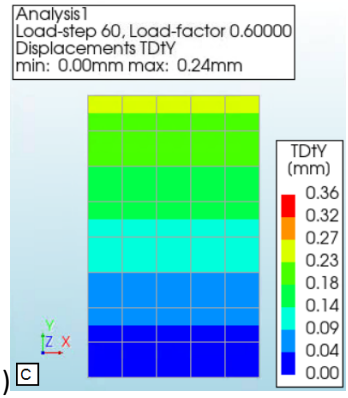

f)

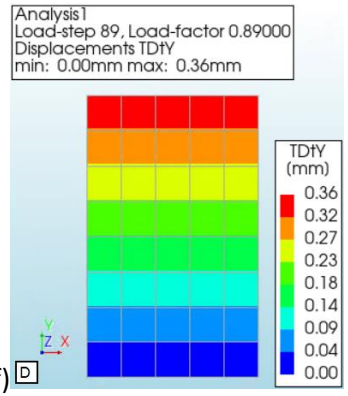

g)

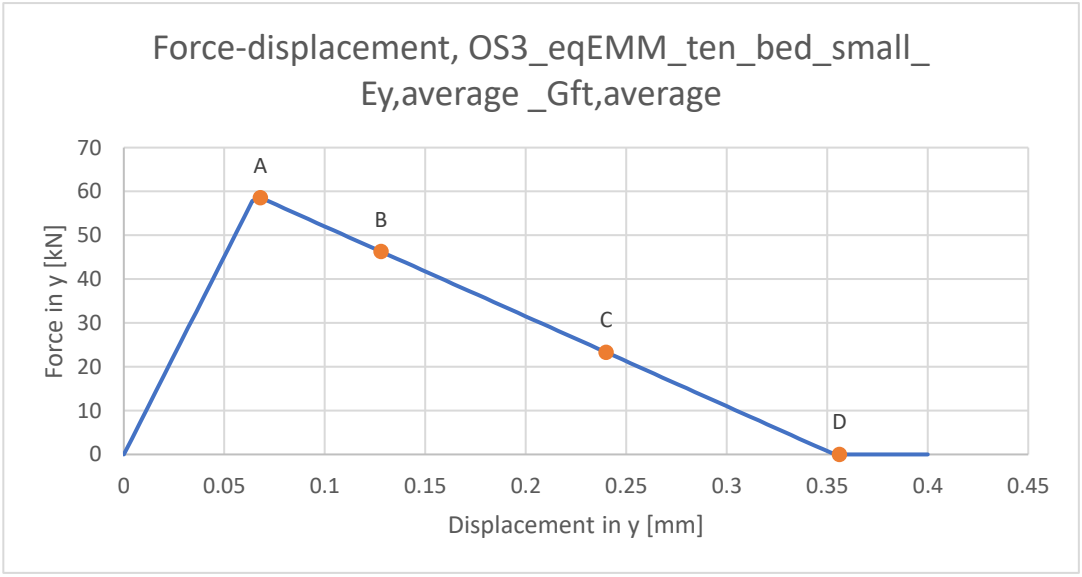

h)

Average element size [mm]		194x187.5
Number of elements	Q20SH	40
Total number of nodes		54

i)

Iteration method	Secant (Quasi-Newton)	
Convergence norms	Displacement	Force
Convergence tolerances	0.01	0.01
Step size	0.01(100)	
Maximum number of iterations per step	100	
All norms satisfied	No	

Figure C.5: Results of finite element analysis OS3_eqEMM_ten_bed_small_$E_{y,average}$_$G_{ft,average}$. a-i: structure (a), finite element mesh (b), displacement at point A (c), displacement at point B (d), displacement at point C (e), displacement at point D (f), force-displacement curve (g), overview elements and nodes (h), overview iterative scheme (i)

a) b)

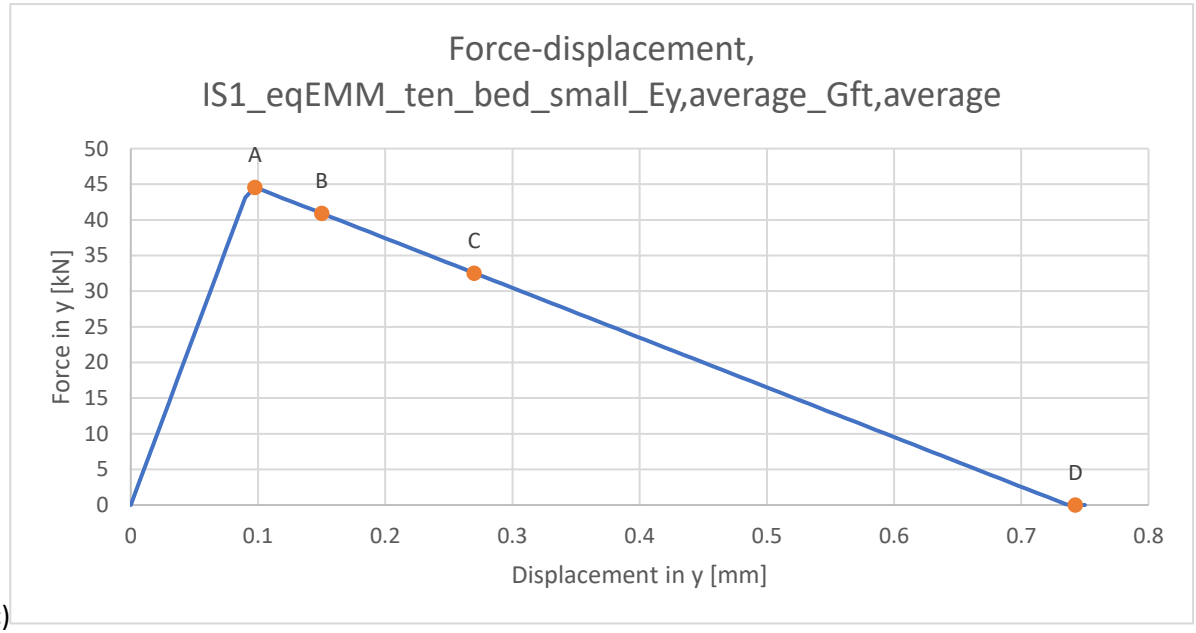

c)

h)

Average element size [mm]		210.2x221.25
Number of elements	Q20SH	80
Total number of nodes		102

i)

Iteration method	Secant (Quasi-Newton)	
Convergence norms	Displacement	Force
Convergence tolerances	0.01	0.01
Step size	0.01(100)	
Maximum number of iterations per step	100	
All norms satisfied	No	

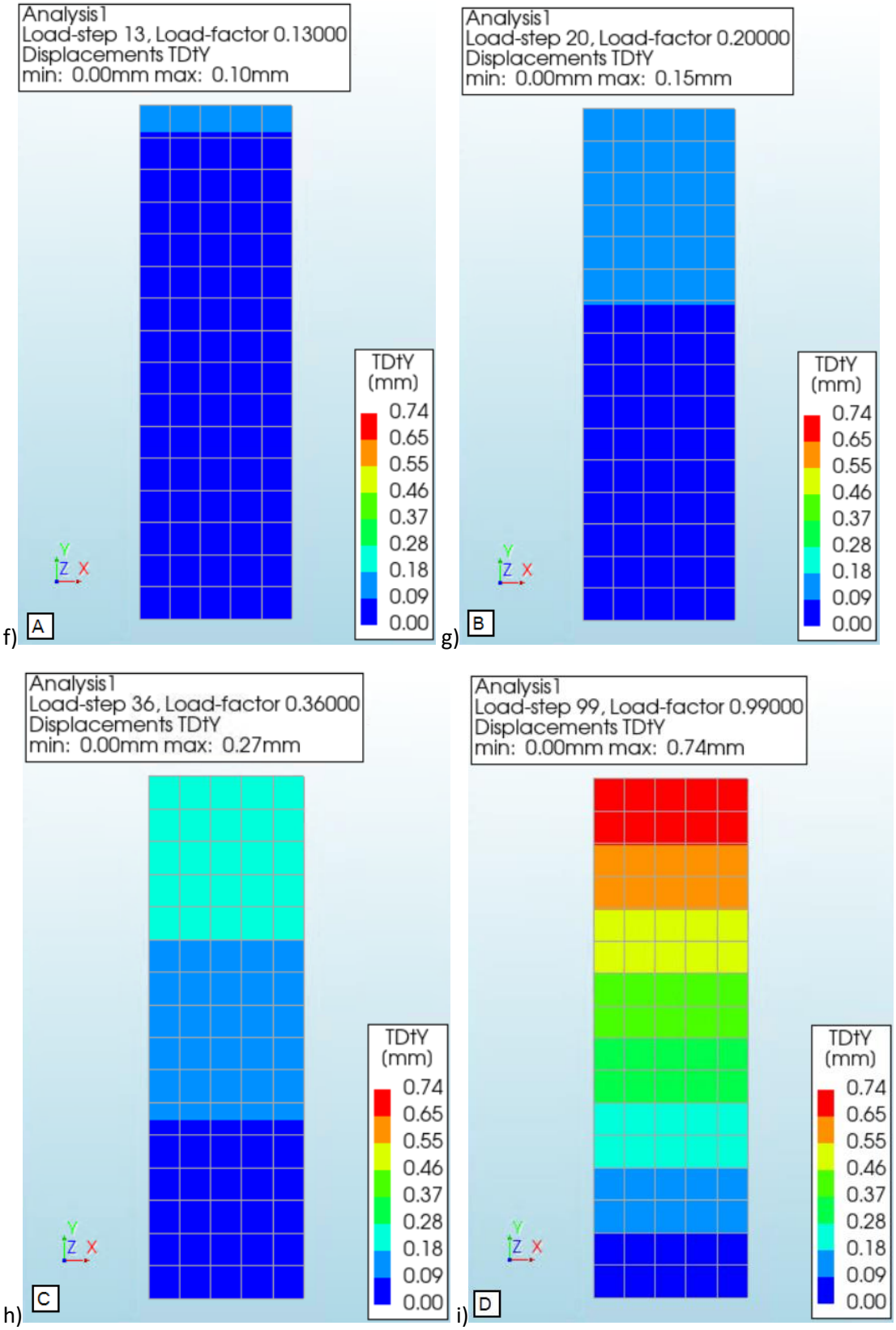

Figure C.6: Results of finite element analysis IS1_eqEMM_ten_bed_small_$E_{y,average}$_$G_{ft,average}$. a-i: structure (a), finite element mesh (b), force-displacement curve (c), overview elements and nodes (d), overview iterative scheme (e), displacement at point A (f), displacement at point B (g), displacement at point C (h), displacement at point D (i)

D. Results remaining detailed finite element models chapter 6

In this appendix, there are no contour plots in the results presentation, as the failure modes of these structures are identical to those of the structures of sections OS3 & IS1.

a) b)

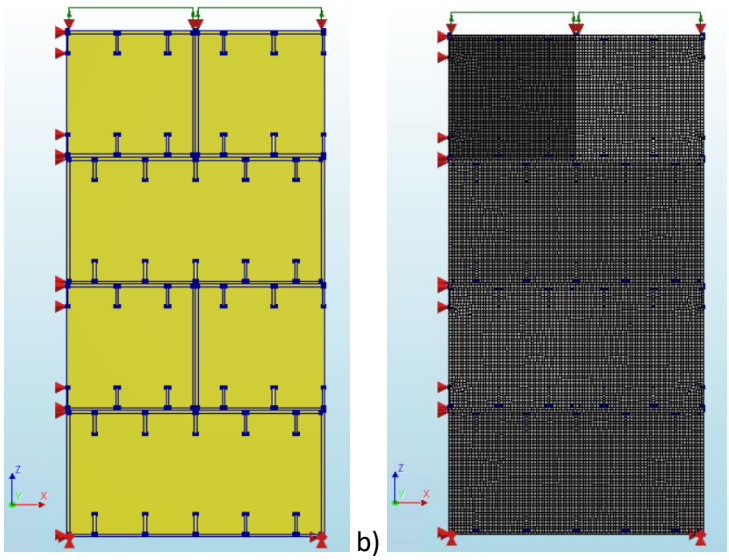

c)

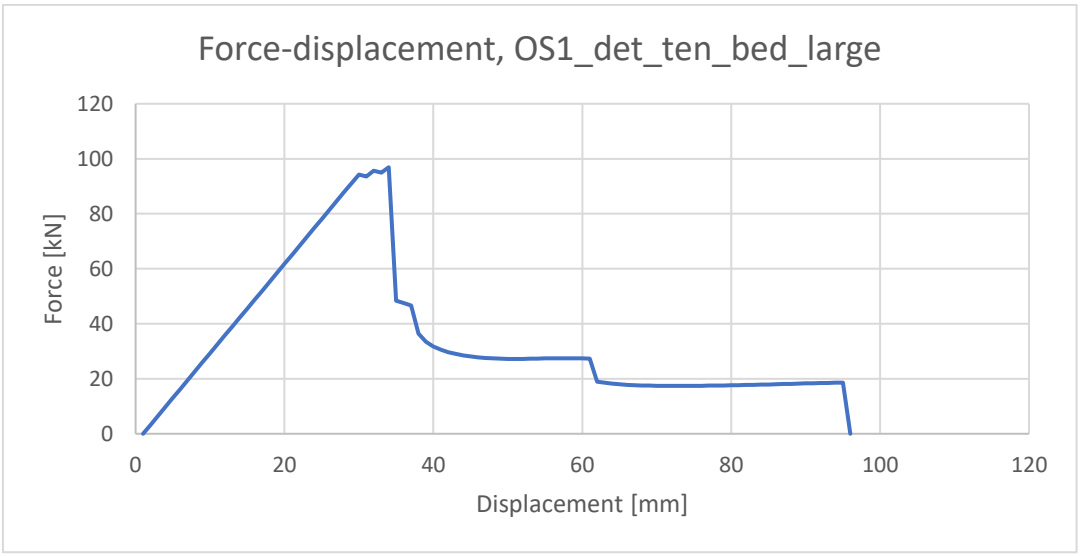

d)

Average element size [mm]		20x20
Number of elements	HX24L	34314
	PY15L	4765
	TE12L	3483
	TP18L	1211
	Q24IF	1790
Total number of nodes		58543

e)

Iteration method	Newton-Raphson	
Convergence norms	Displacement	Force
Convergence tolerances	0.01	0.01
Step size	0.008(125)	
Maximum number of iterations per step	100	
All norms satisfied	No	

Figure D.1: Results of finite element analysis OS1_det_ten_bed_large. a-e: structure (a), finite element mesh (b), force-displacement curve (c), overview elements and nodes (d), overview iterative scheme (e)

a) 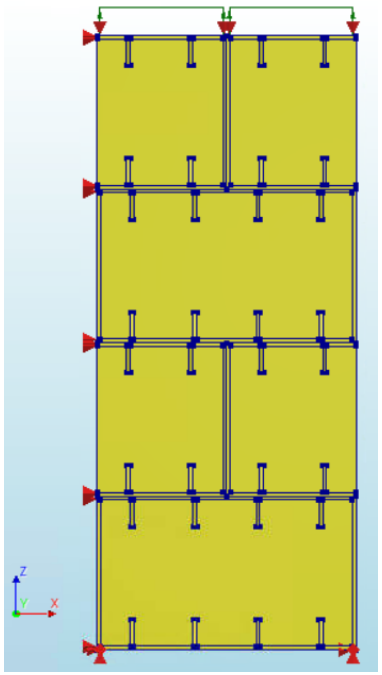

b) 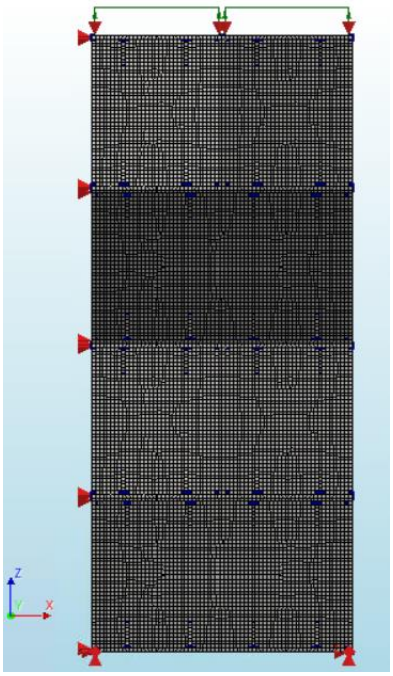

c) 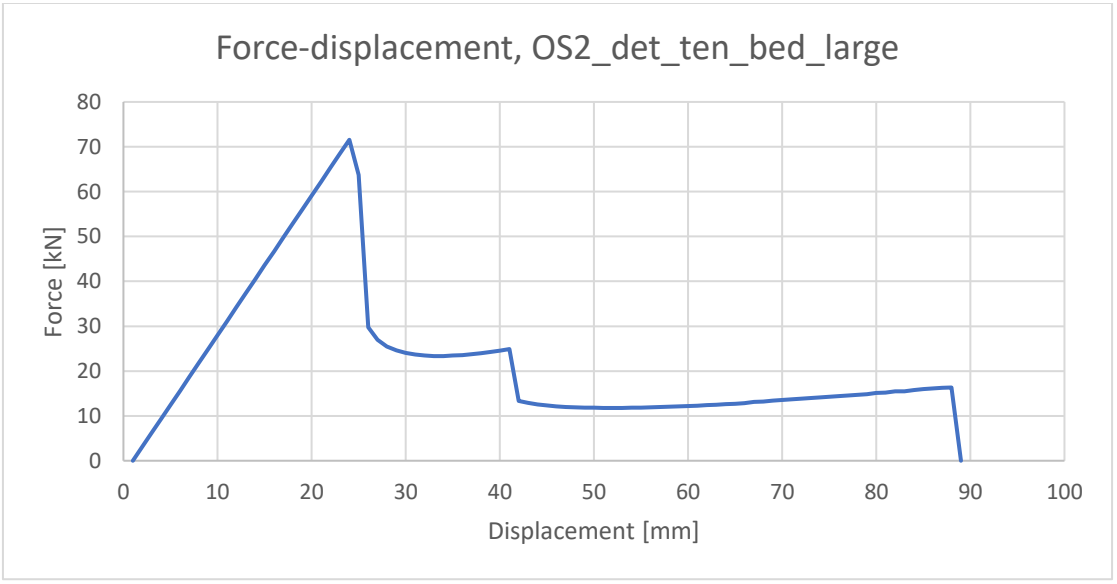

d)

Average element size [mm]		20x20
Number of elements	HX24L	18184
	PY15L	2040
	TE12L	1487
	TP18L	918
	Q24IF	1144
Total number of nodes		34833

e)

Iteration method	Newton-Raphson	
Convergence norms	Displacement	Force
Convergence tolerances	0.01	0.01
Step size	0.008(125)	
Maximum number of iterations per step	100	
All norms satisfied	No	

Figure D.2: Results of finite element analysis OS2_det_ten_bed_large. a-e: structure (a), finite element mesh (b), force-displacement curve (c), overview elements and nodes (d), overview iterative scheme (e)

a) b)

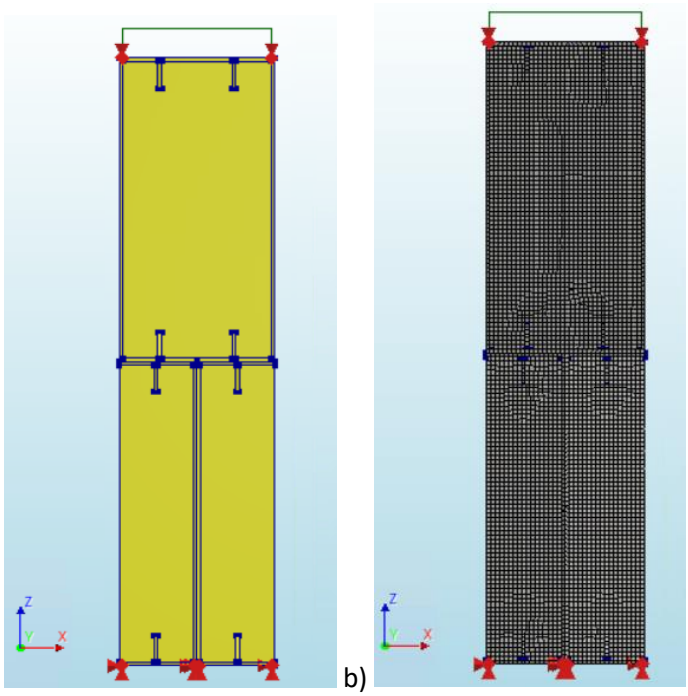

c)

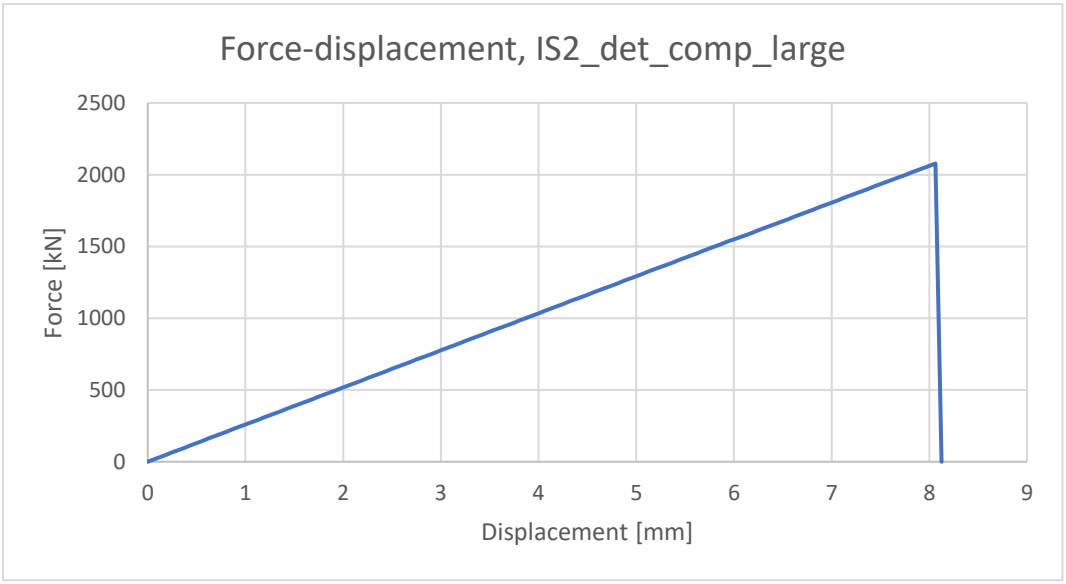

d)

Average element size [mm]		20x20
Number of elements	HX24L	7240
	PY15L	3768
	TE12L	2833
	TP18L	766
	Q24IF	420
Total number of nodes		16204

e)

Iteration method	Newton-Raphson	
Convergence norms	Displacement	Force
Convergence tolerances	0.01	0.01
Step size	0.00625(160)	
Maximum number of iterations per step	100	
All norms satisfied	No	

Figure D.3: Results of finite element analysis IS2_det_comp_large. a-e: structure (a), finite element mesh (b), force-displacement curve (c), overview elements and nodes (d), overview iterative scheme (e)

a) b)

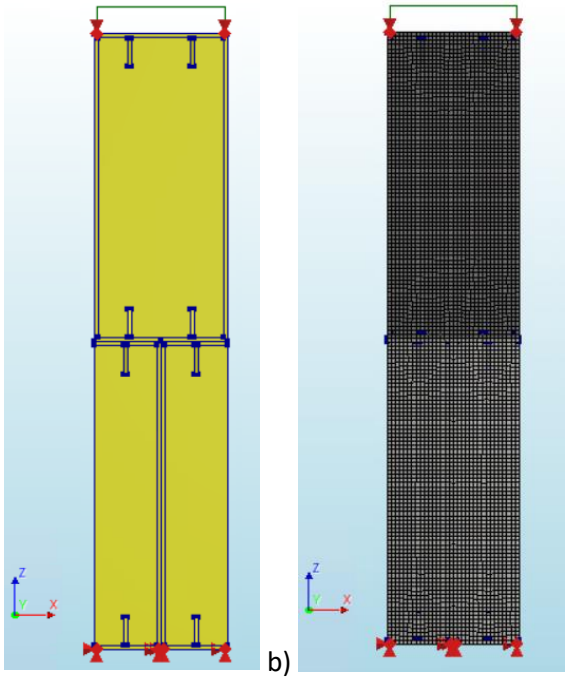

c)

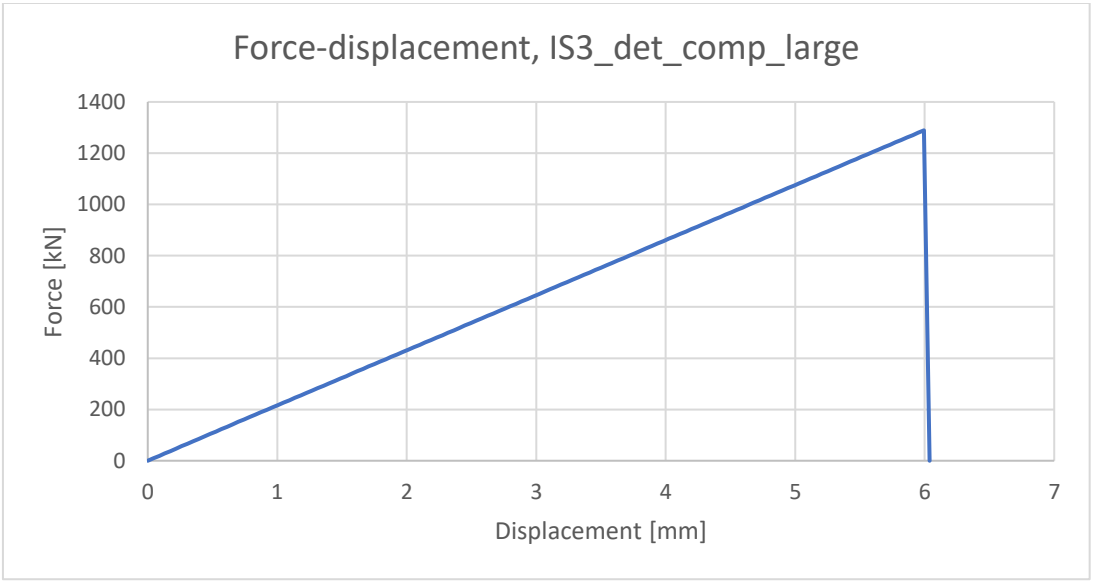

d)

Average element size [mm]		20x20
Number of elements	HX24L	6854
	PY15L	3009
	TE12L	2181
	TP18L	551
	Q24IF	424
Total number of nodes		15093

e)

Iteration method	Newton-Raphson	
Convergence norms	Displacement	Force
Convergence tolerances	0.01	0.01
Step size	0.00625(160)	
Maximum number of iterations per step	100	
All norms satisfied	No	

Figure D.4: Results of finite element analysis IS3_det_comp_large. a-e: structure (a), finite element mesh (b), force-displacement curve (c), overview elements and nodes (d), overview iterative scheme (e)

a) 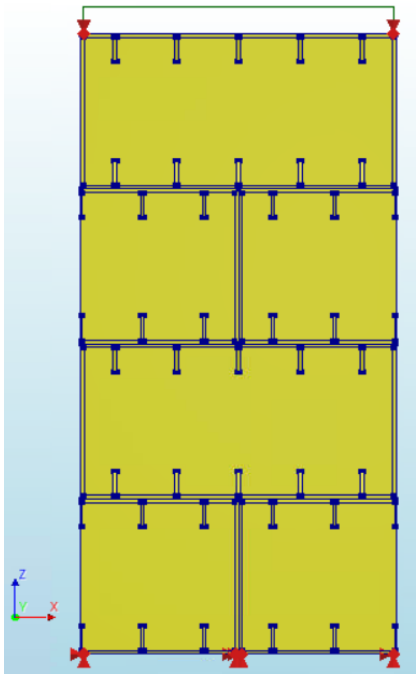

b) 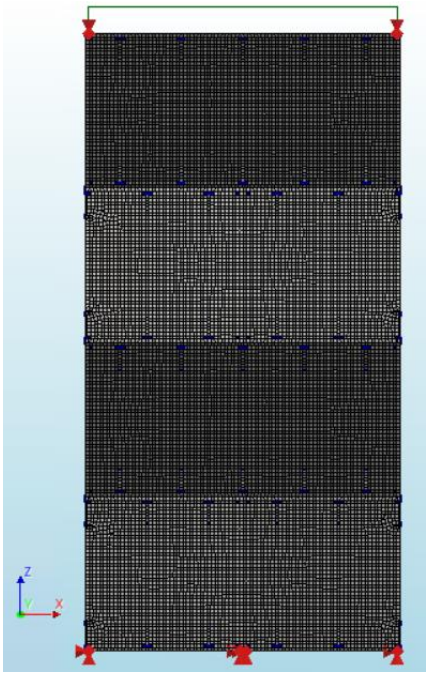

c) 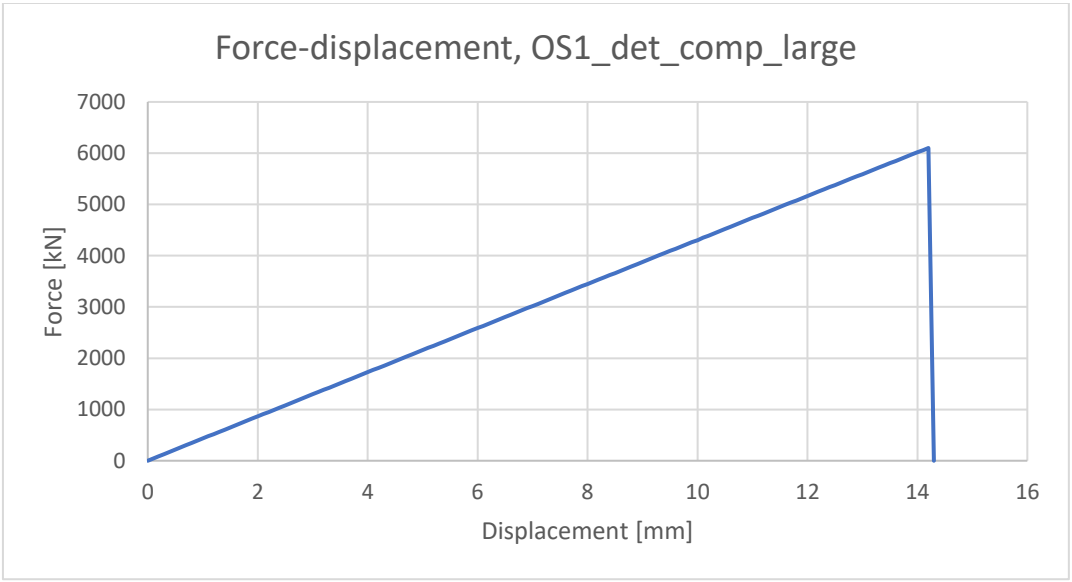

d)

Average element size [mm]		20x20
Number of elements	HX24L	34335
	PY15L	4709
	TE12L	3443
	TP18L	1197
	Q24IF	1790
Total number of nodes		58537

e)

Iteration method	Newton-Raphson	
Convergence norms	Displacement	Force
Convergence tolerances	0.01	0.01
Step size	0.00625(160)	
Maximum number of iterations per step	100	
All norms satisfied	No	

Figure D.5: Results of finite element analysis OS1_det_comp_large. a-e: structure (a), finite element mesh (b), force-displacement curve (c), overview elements and nodes (d), overview iterative scheme (e)

a) b)

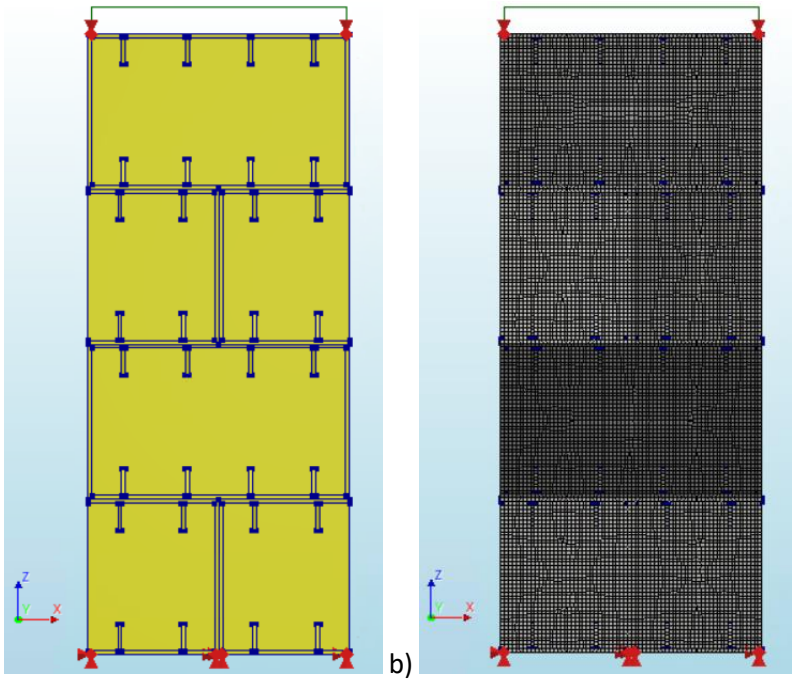

c)

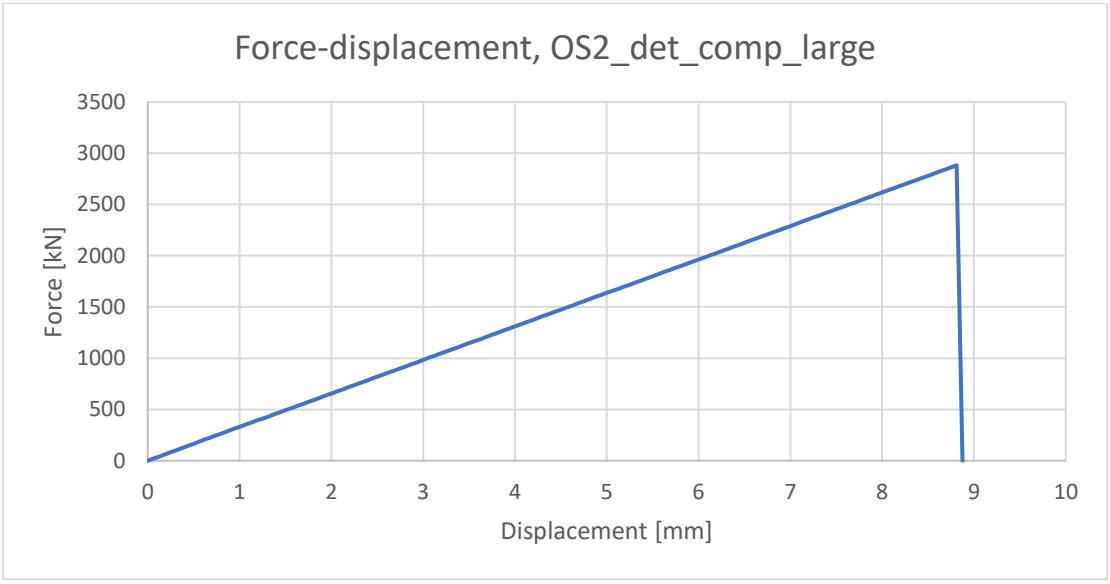

d)

Average element size [mm]		20x20
Number of elements	HX24L	18382
	PY15L	1693
	TE12L	1164
	TP18L	931
	Q24IF	1144
Total number of nodes		34869

e)

Iteration method	Newton-Raphson	
Convergence norms	Displacement	Force
Convergence tolerances	0.01	0.01
Step size	0.00625(160)	
Maximum number of iterations per step	100	
All norms satisfied	No	

Figure D.6: Results of finite element analysis OS2_det_comp_large. a-e: structure (a), finite element mesh (b), force-displacement curve (c), overview elements and nodes (d), overview iterative scheme (e)

a) b)

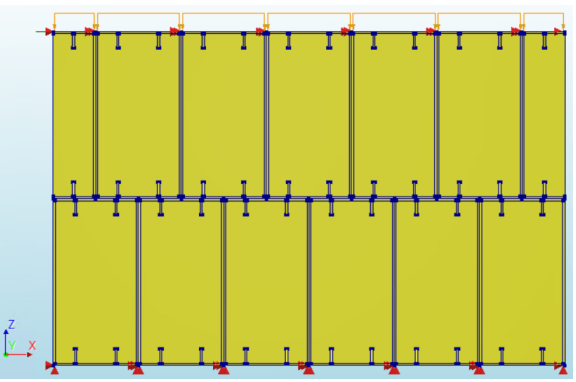

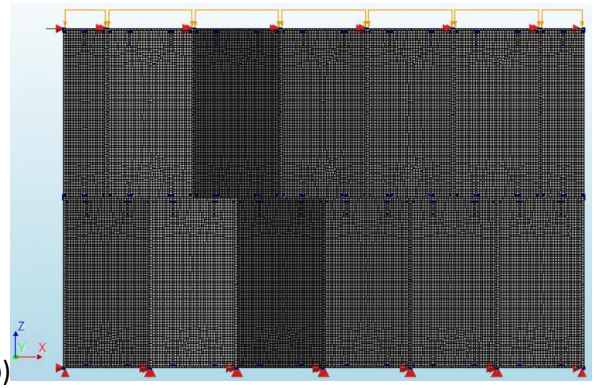

c)

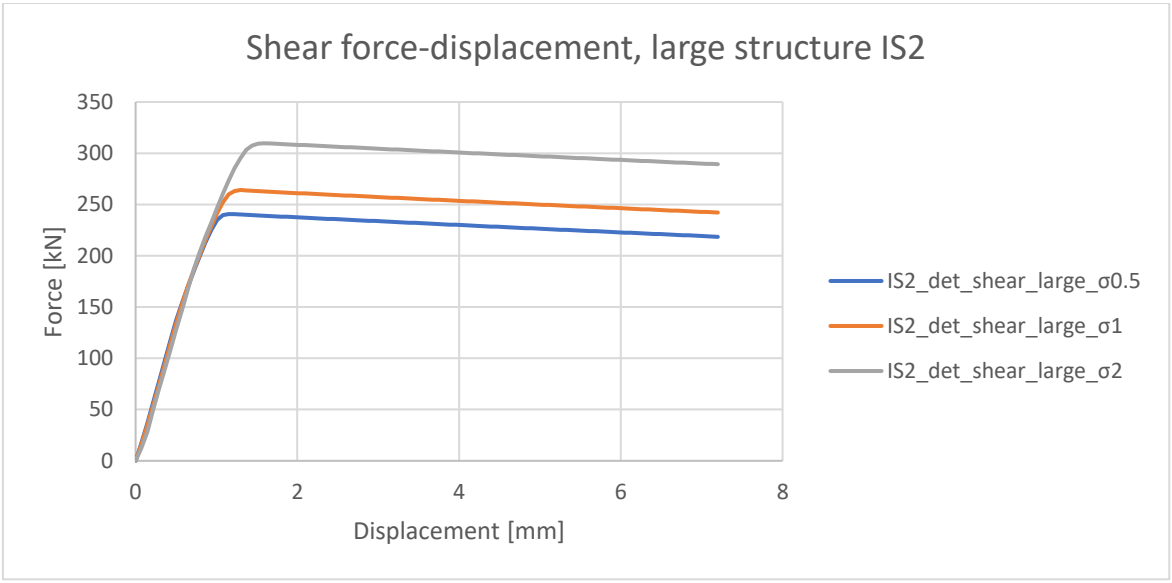

d)

Average element size [mm]		20x20
Number of elements	HX24L	46358
	PY15L	46362
	TE12L	36070
	TP18L	8042
	Q24IF	3900
Total number of nodes		112105

e)

Load	Compression		Translation	
Iteration method	Newton-Raphson		Newton-Raphson	
Convergence norms	Force	Displacement	Force	Displacement
Convergence tolerances	0.01	0.01	0.01	0.01
Step size	0.2(5)		0.008(125)	
Maximum number of iterations per step	100			
All norms satisfied	No			

Figure D.7: Results of finite element analysis IS2_det_shear_large_σ0.5, σ1 & σ2. a-e: structure (a), finite element mesh (b), force-displacement curve (c), overview elements and nodes (d), overview iterative scheme (e)

a) b)

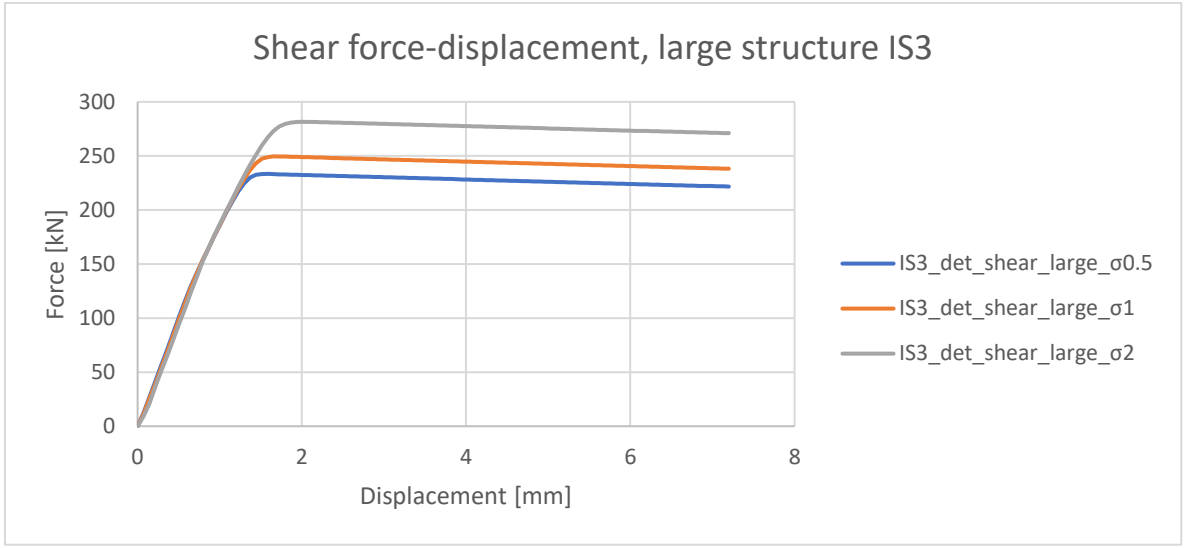

c)

Average element size [mm]		20x20
Number of elements	HX24L	43842
	PY15L	39949
	TE12L	26954
	TP18L	6223
	Q24IF	4024
Total number of nodes		103305

d)

Load	Compression		Translation	
Iteration method	Newton-Raphson		Newton-Raphson	
Convergence norms	Force	Displacement	Force	Displacement
Convergence tolerances	0.01	0.01	0.01	0.01
Step size	0.2(5)		0.008(125)	
Maximum number of iterations per step	100			
All norms satisfied	No			

e)

Figure D.8: Results of finite element analysis IS3_det_shear_large_σ0.5, σ1 & σ2. a-e: structure (a), finite element mesh (b), force-displacement curve (c), overview elements and nodes (d), overview iterative scheme (e)

a)

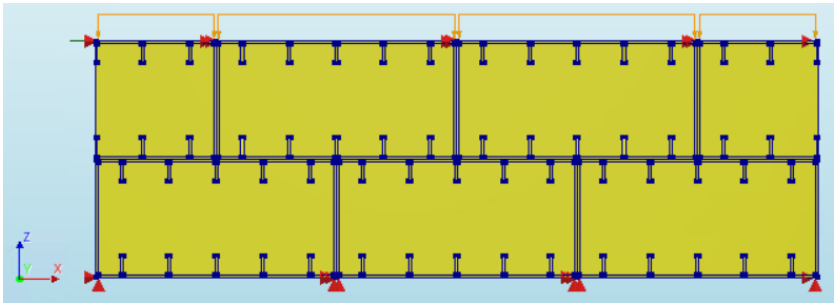

b)

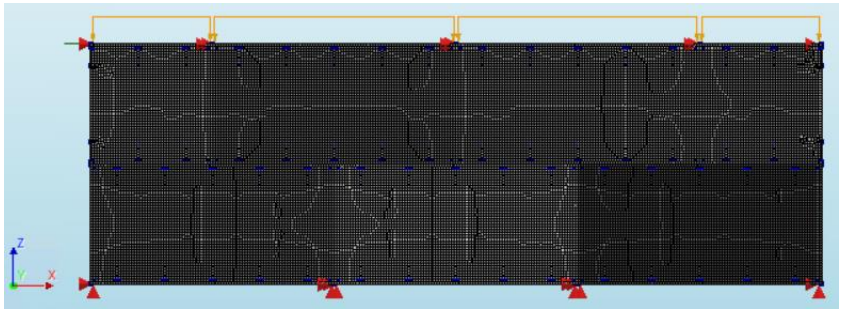

c)

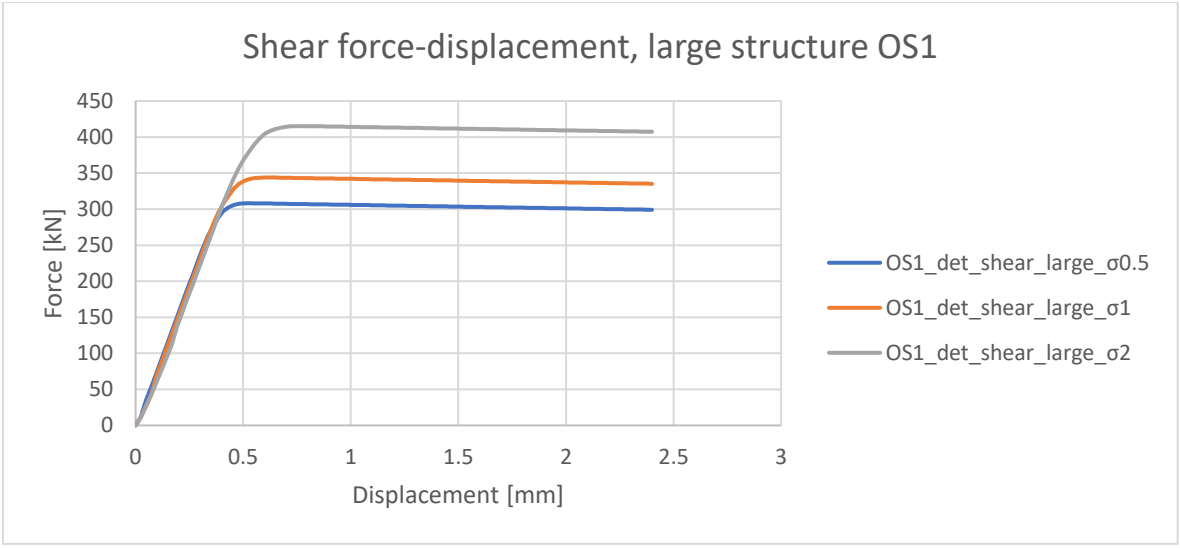

d)

Average element size [mm]		20x20
Number of elements	HX24L	51430
	PY15L	5929
	TE12L	4012
	TP18L	1547
	Q24IF	2450
Total number of nodes		86686

e)

Load	Compression		Translation	
Iteration method	Newton-Raphson		Newton-Raphson	
Convergence norms	Force	Displacement	Force	Displacement
Convergence tolerances	0.01	0.01	0.01	0.01
Step size	0.2(5)		0.008(125)	
Maximum number of iterations per step	100			
All norms satisfied	No			

Figure D.9: Results of finite element analysis OS1_det_shear_large_σ0.5, σ1 & σ2. a-e: structure (a), finite element mesh (b), force-displacement curve (c), overview elements and nodes (d), overview iterative scheme (e)

a)

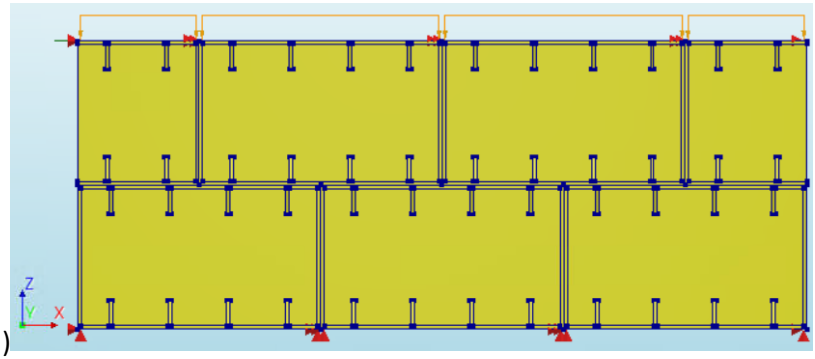

b)

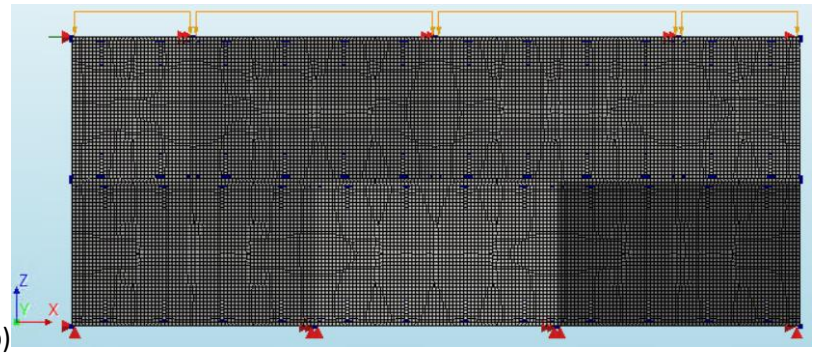

c)

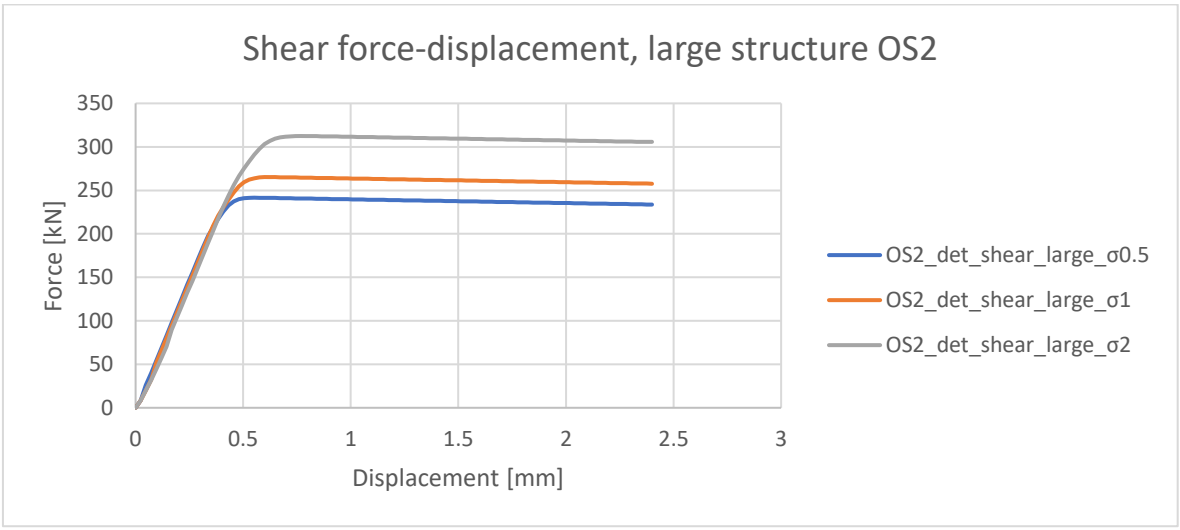

d)

Average element size [mm]		20x20
Number of elements	HX24L	26233
	PY15L	3413
	TE12L	2289
	TP18L	1445
	Q24IF	1636
Total number of nodes		51037

e)

Load	Compression		Translation	
Iteration method	Newton-Raphson		Newton-Raphson	
Convergence norms	Force	Displacement	Force	Displacement
Convergence tolerances	0.01	0.01	0.01	0.01
Step size	0.2(5)		0.008(125)	
Maximum number of iterations per step	100			
All norms satisfied	No			

Figure D.10: Results of finite element analysis OS2_det_shear_large_σ0.5, σ1 & σ2. a-e: structure (a), finite element mesh (b), force-displacement curve (c), overview elements and nodes (d), overview iterative scheme (e)

E. Results equivalent EMM models with final parameters, section 6.5

a) b)

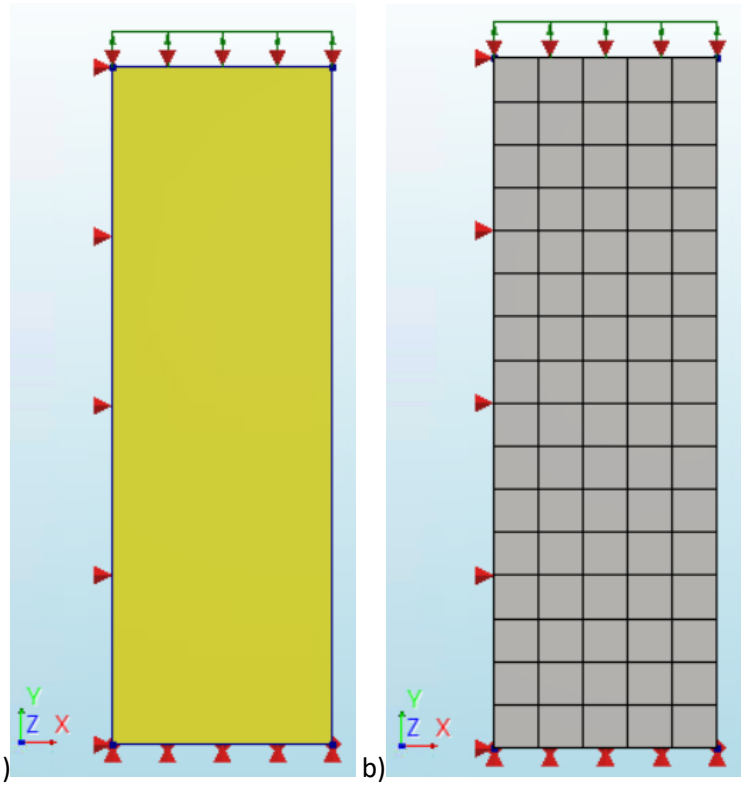

c)

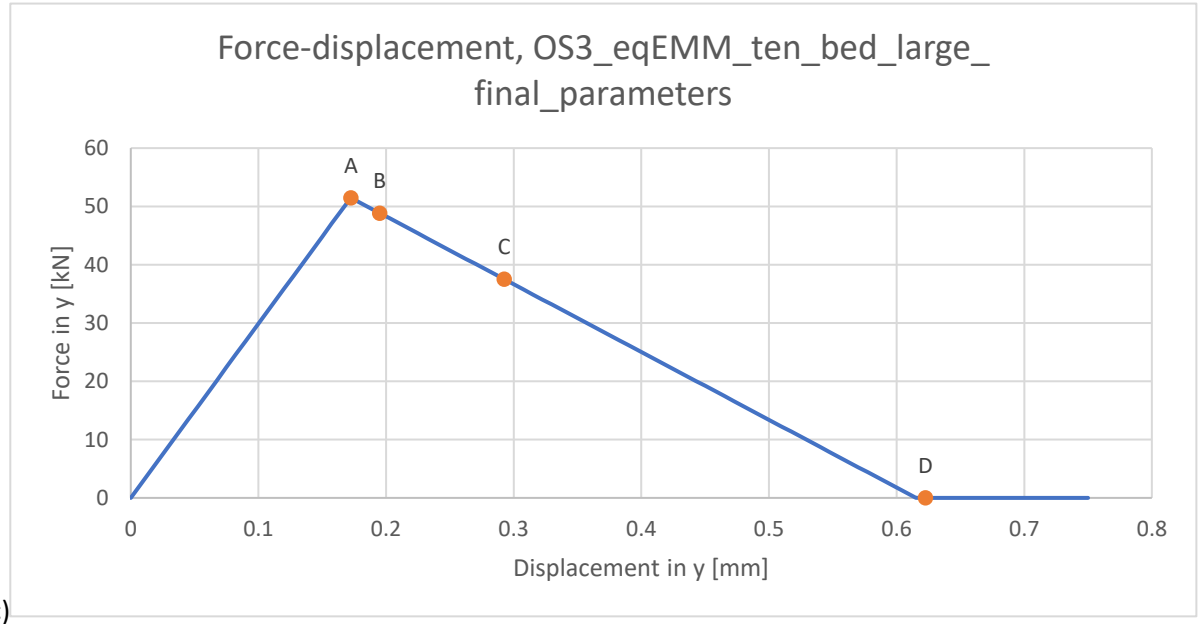

d)

Average element size [mm]		194x187.5
Number of elements	Q20SH	80
Total number of nodes		102

e)

Iteration method	Secant (Quasi-Newton)	
Convergence norms	Displacement	Force
Convergence tolerances	0.01	0.01
Step size	0.01(100)	
Maximum number of iterations per step	100	
All norms satisfied	No	

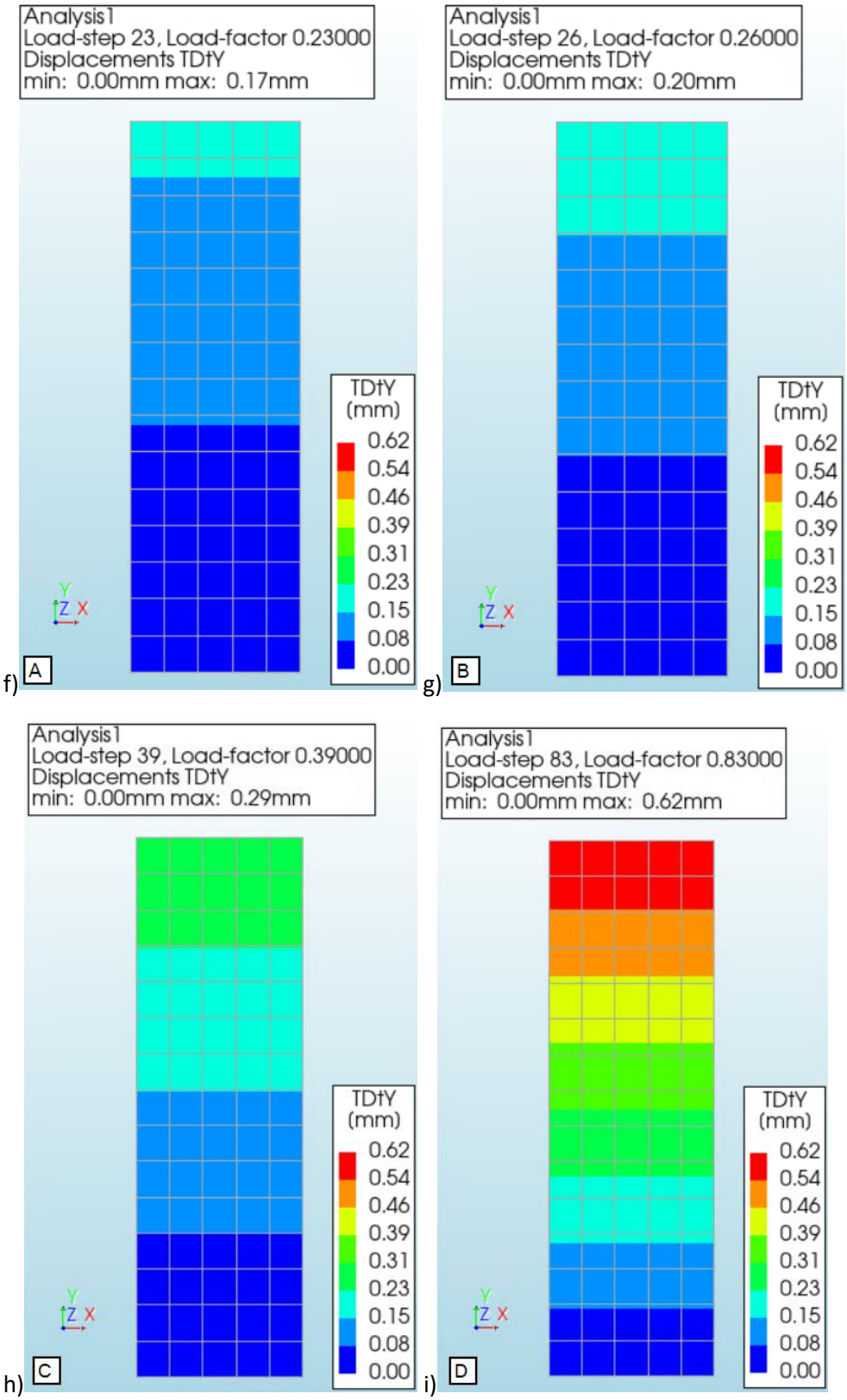

Figure E.1: Results of finite element analysis OS3_eqEMM_ten_bed_large_ final_parameters. a-i: structure (a), finite element mesh (b), force-displacement curve (c), overview elements and nodes (d), overview iterative scheme (e), displacement at point A (f), displacement at point B (g), displacement at point C (h), displacement at point D (i)

a) b)

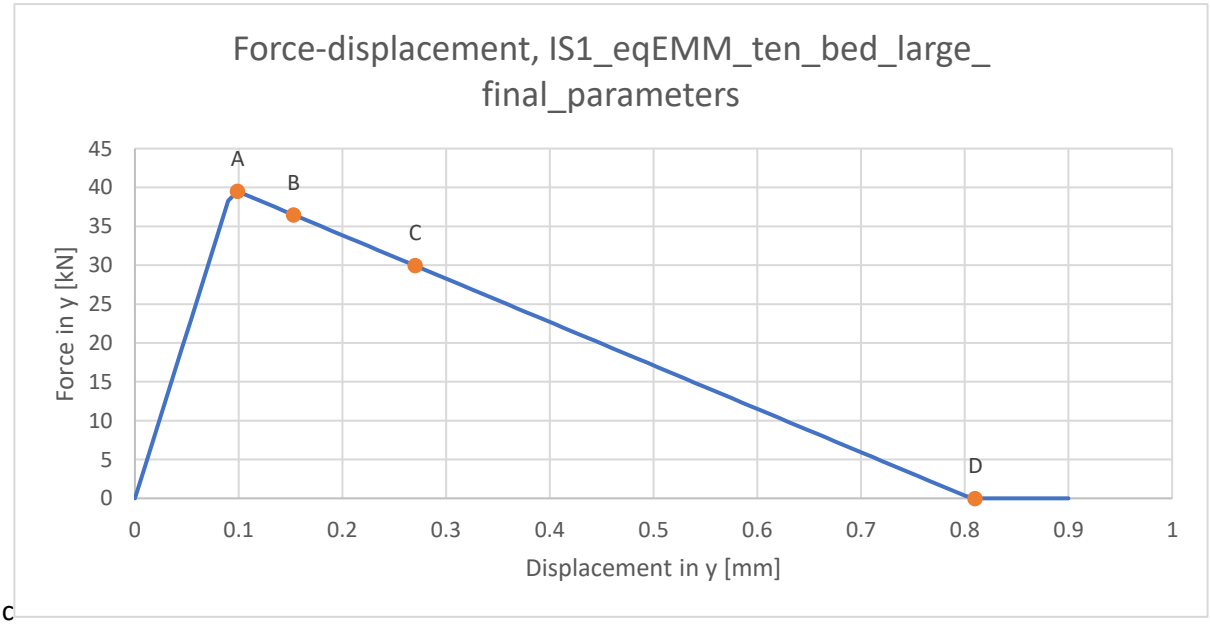

c

h)

Average element size [mm]		210.2x221.25
Number of elements	Q20SH	80
Total number of nodes		102

i)

Iteration method	Secant (Quasi-Newton)	
Convergence norms	Displacement	Force
Convergence tolerances	0.01	0.01
Step size	0.01(100)	
Maximum number of iterations per step	100	
All norms satisfied	No	

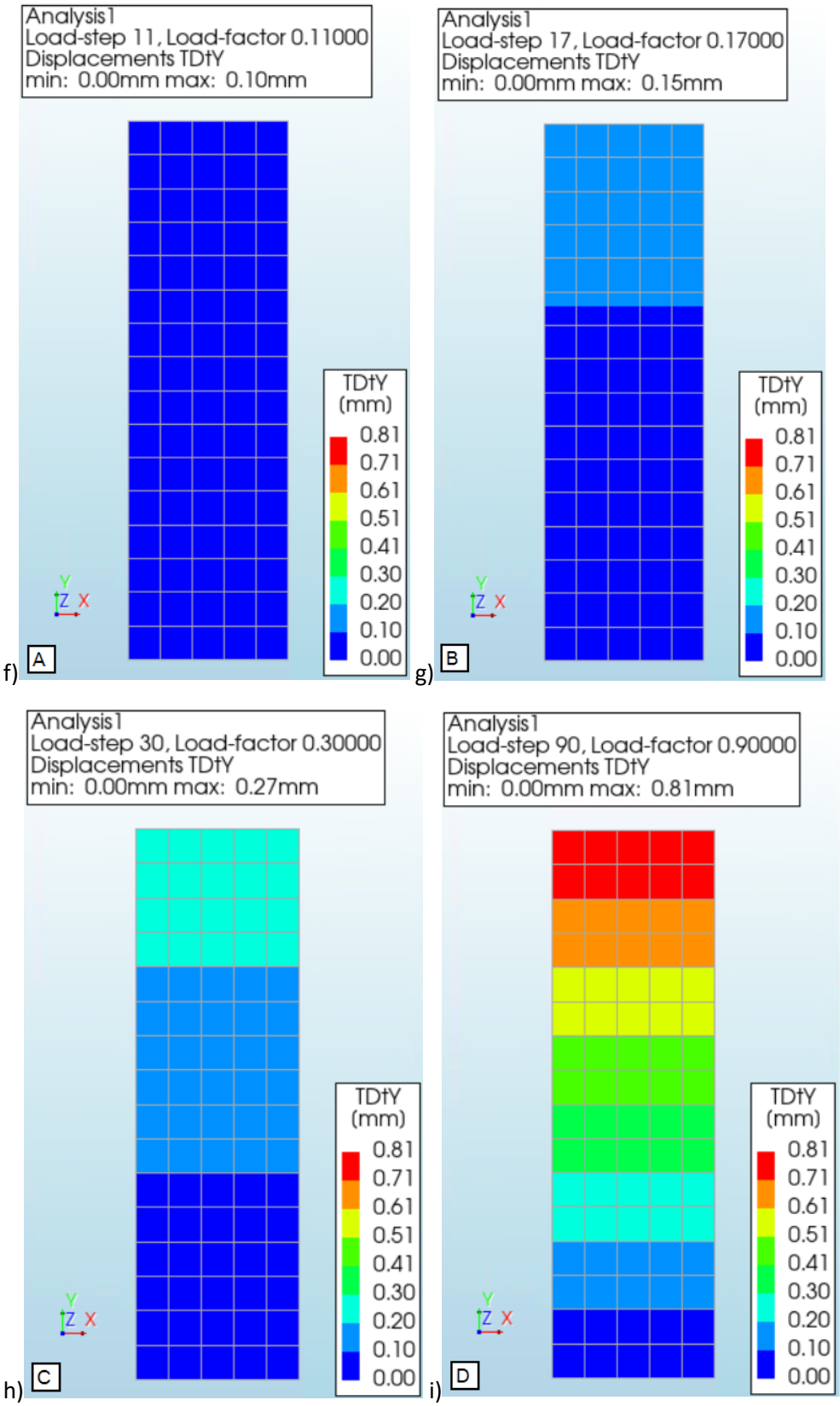

Figure E.2: Results of finite element analysis IS1_eqEMM_ten_bed_large_final_parameters. a-i: structure (a), finite element mesh (b), force-displacement curve (c), overview elements and nodes (d), overview iterative scheme (e), displacement at point A (f), displacement at point B (g), displacement at point C (h), displacement at point D (i)

a)

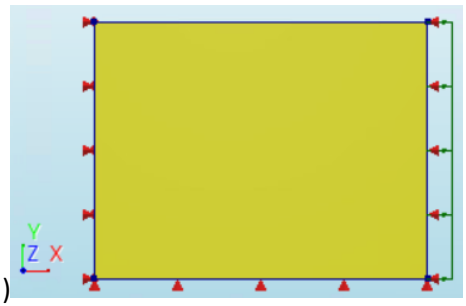

c)

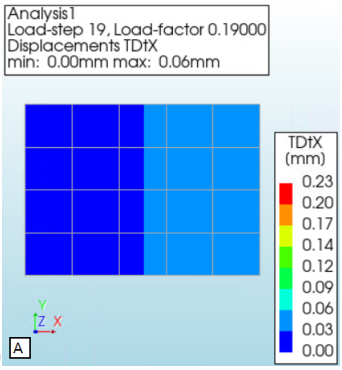

d)

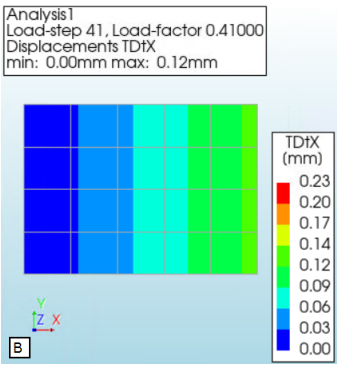

b)

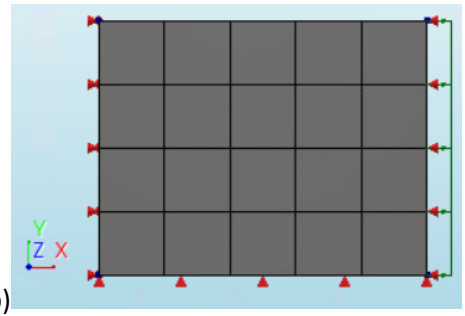

e)

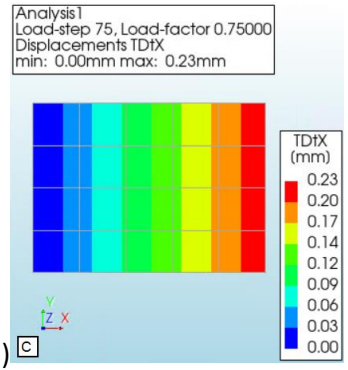

f)

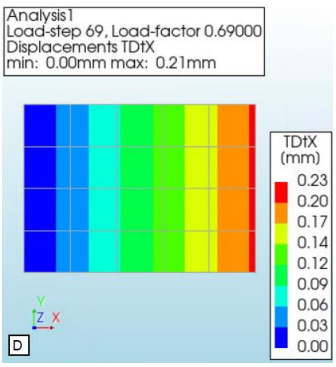

g)

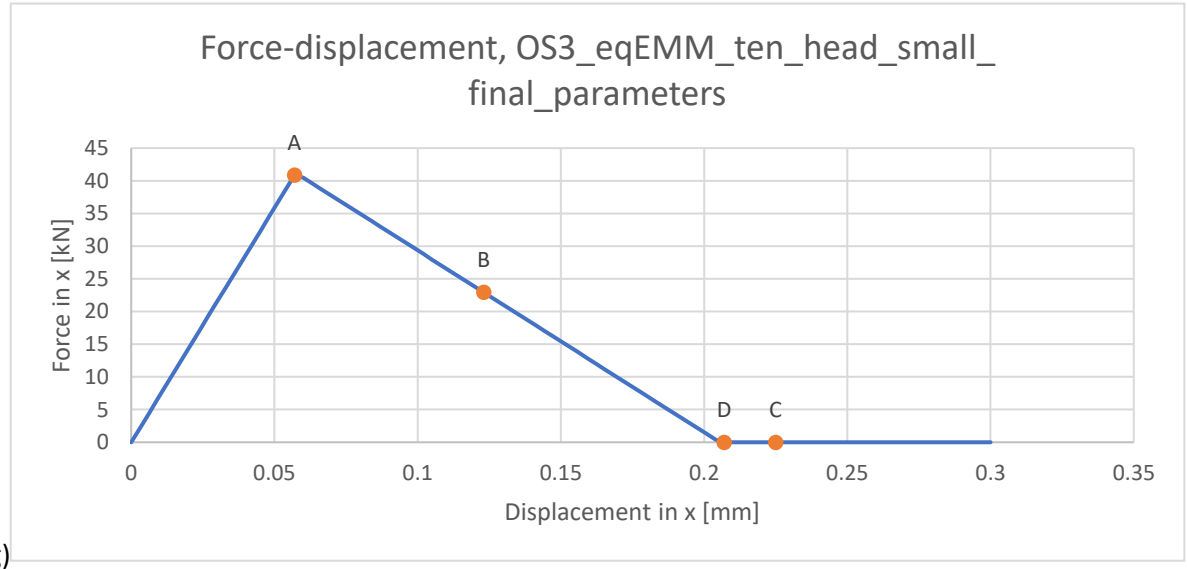

h)

Average element size [mm]		194x187.5
Number of elements	Q20SH	20
Total number of nodes		30

i)

Iteration method	Secant (Quasi-Newton)	
Convergence norms	Displacement	Force
Convergence tolerances	0.01	0.01
Step size	0.01(100)	
Maximum number of iterations per step	100	
All norms satisfied	No	

Figure E.3: Results of finite element analysis OS3_eqEMM_ten_head_small_final_parameters. a-i: structure (a), finite element mesh (b), displacement at point A (c), displacement at point B (d), displacement at point C (e), displacement at point D (f), force-displacement curve (g), overview elements and nodes (h), overview iterative scheme (i)

a)

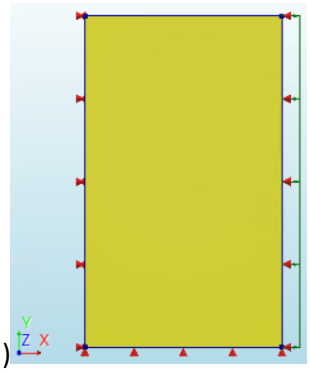

b)

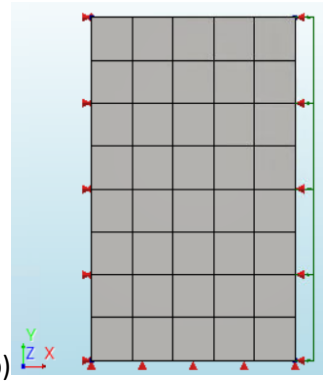

c)

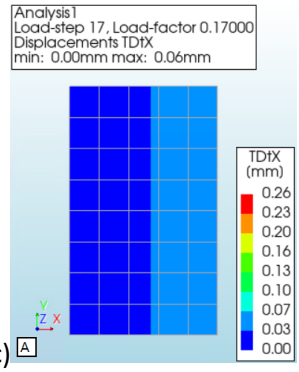

d)

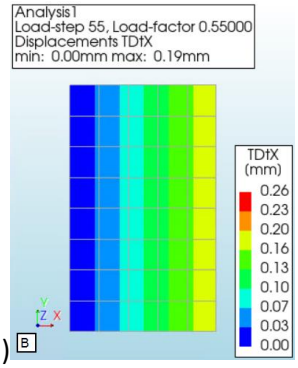

e)

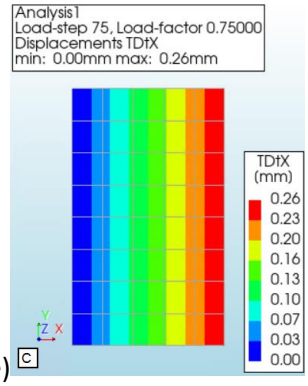

f)

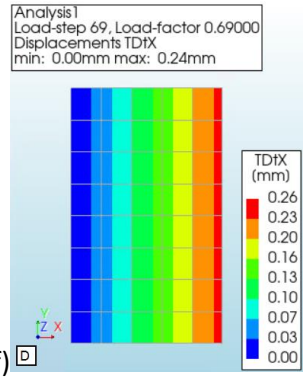

g)

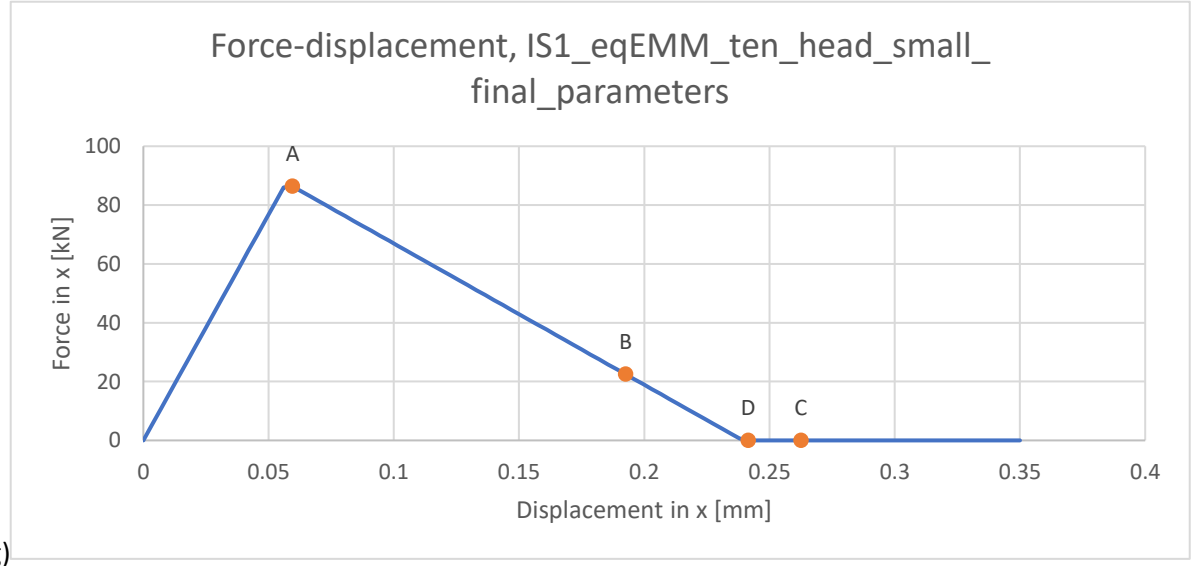

h)

Average element size [mm]		210.2x221.25
Number of elements	Q20SH	40
Total number of nodes		54

i)

Iteration method	Secant (Quasi-Newton)	
Convergence norms	Displacement	Force
Convergence tolerances	0.01	0.01
Step size	0.01(100)	
Maximum number of iterations per step	100	
All norms satisfied	No	

Figure E.4: Results of finite element analysis IS1_eqEMM_ten_head_small_final_parameters. a-i: structure (a), finite element mesh (b), displacement at point A (c), displacement at point B (d), displacement at point C (e), displacement at point D (f), force-displacement curve (g), overview elements and nodes (h), overview iterative scheme (i)

a) b)

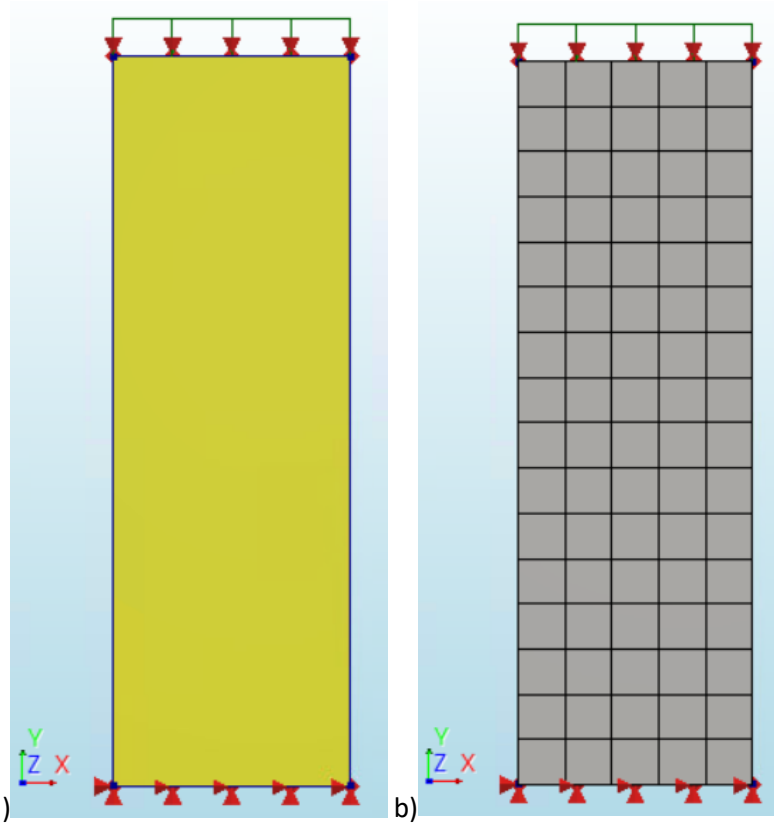

c)

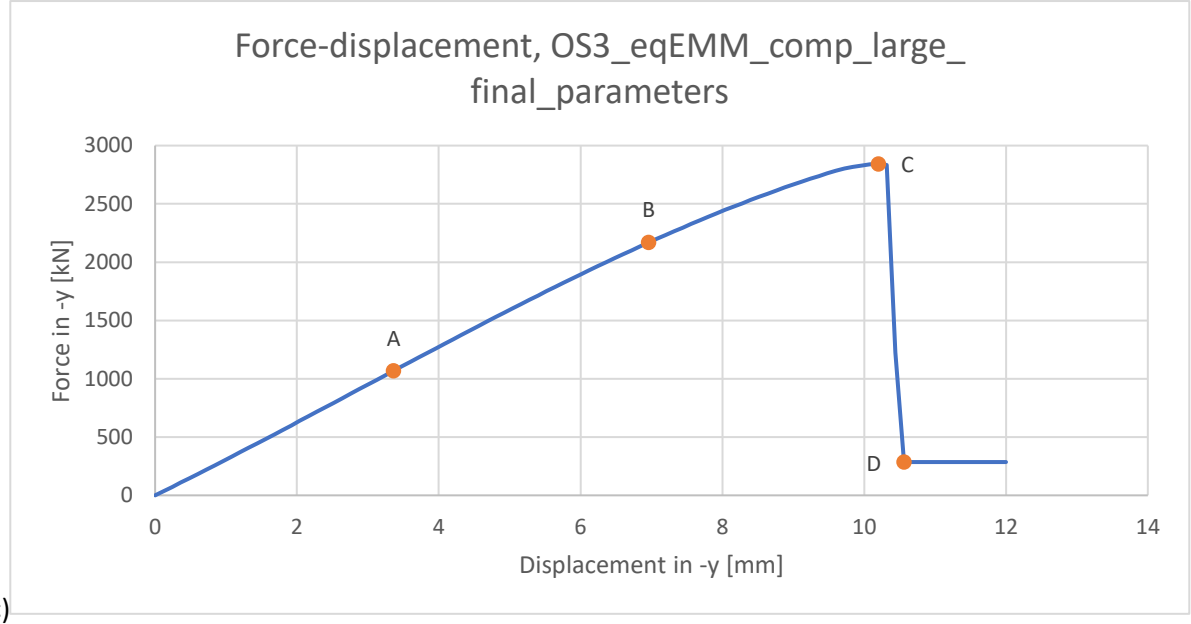

d)

Average element size [mm]		194x187.5
Number of elements	Q20SH	80
Total number of nodes		102

e)

Iteration method	Secant (Quasi-Newton)	
Convergence norms	Displacement	Force
Convergence tolerances	0.01	0.01
Step size	0.01(100)	
Maximum number of iterations per step	100	
All norms satisfied	No	

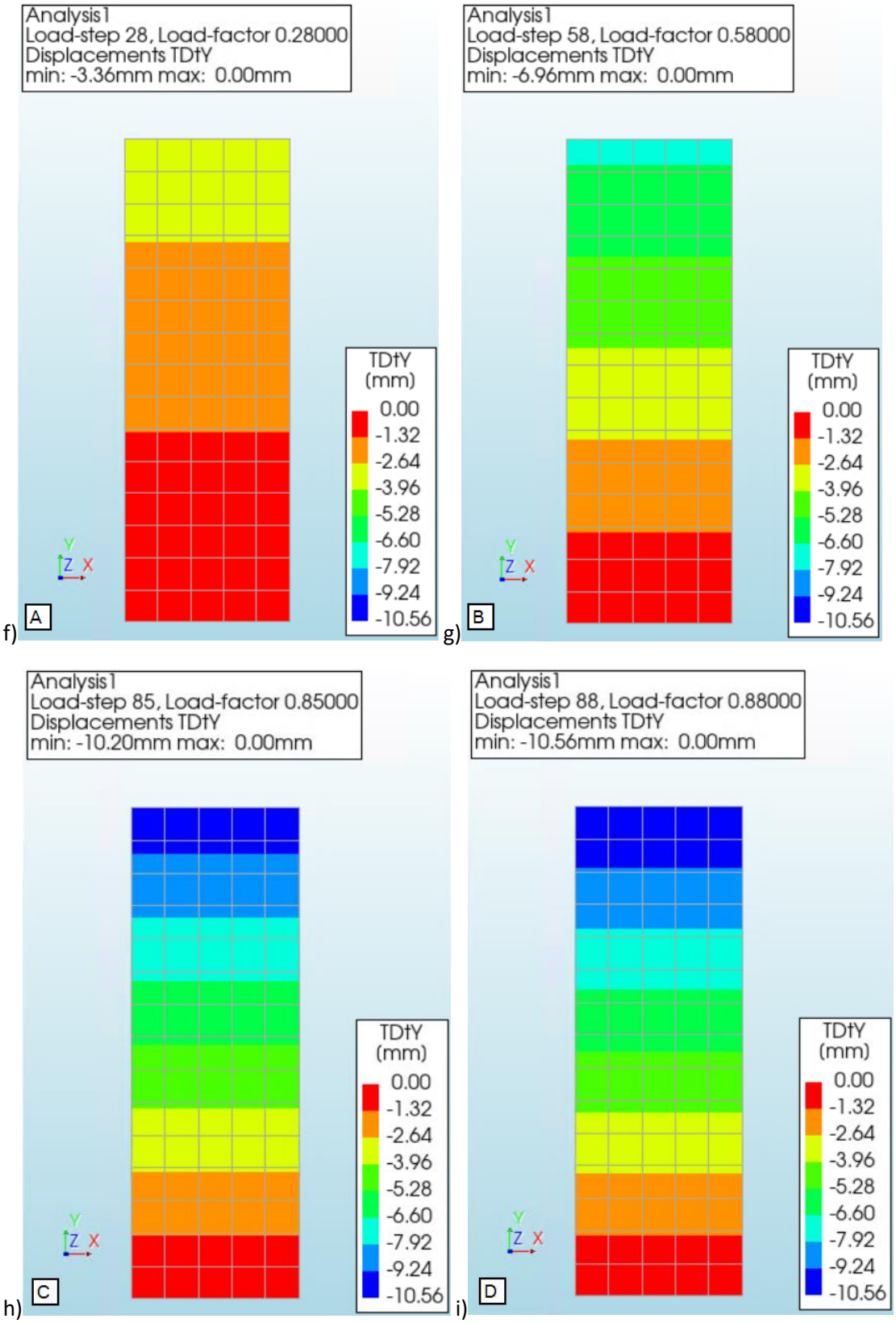

Figure E.5: Results of finite element analysis OS3_eqEMM_comp_large_ final_parameters. a-i: structure (a), finite element mesh (b), force-displacement curve (c), overview elements and nodes (d), overview iterative scheme (e), displacement at point A (f), displacement at point B (g), displacement at point C (h), displacement at point D (i)

a) b)

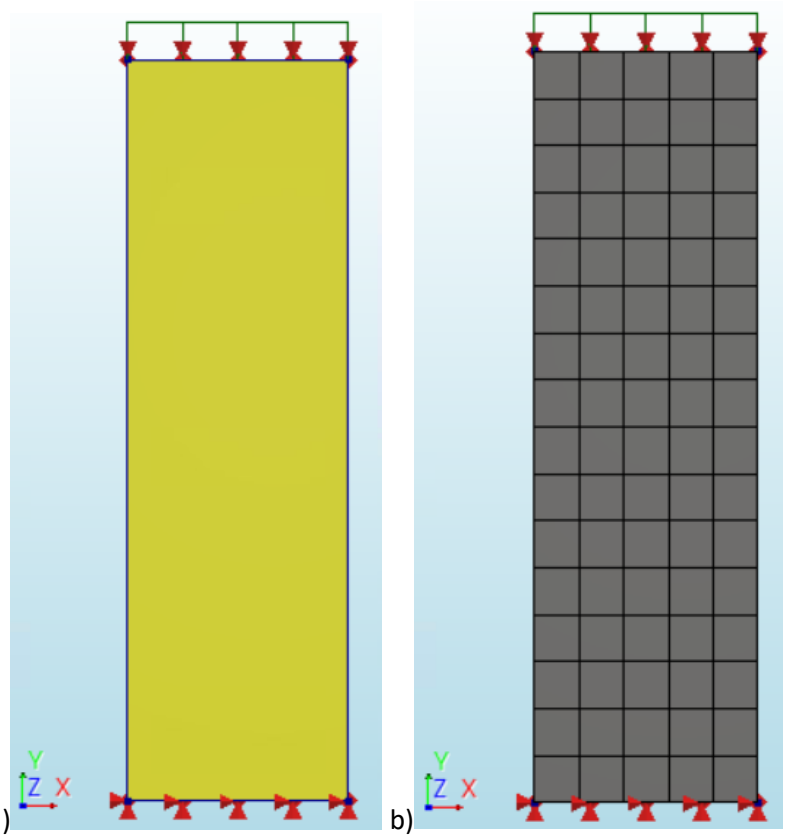

c)

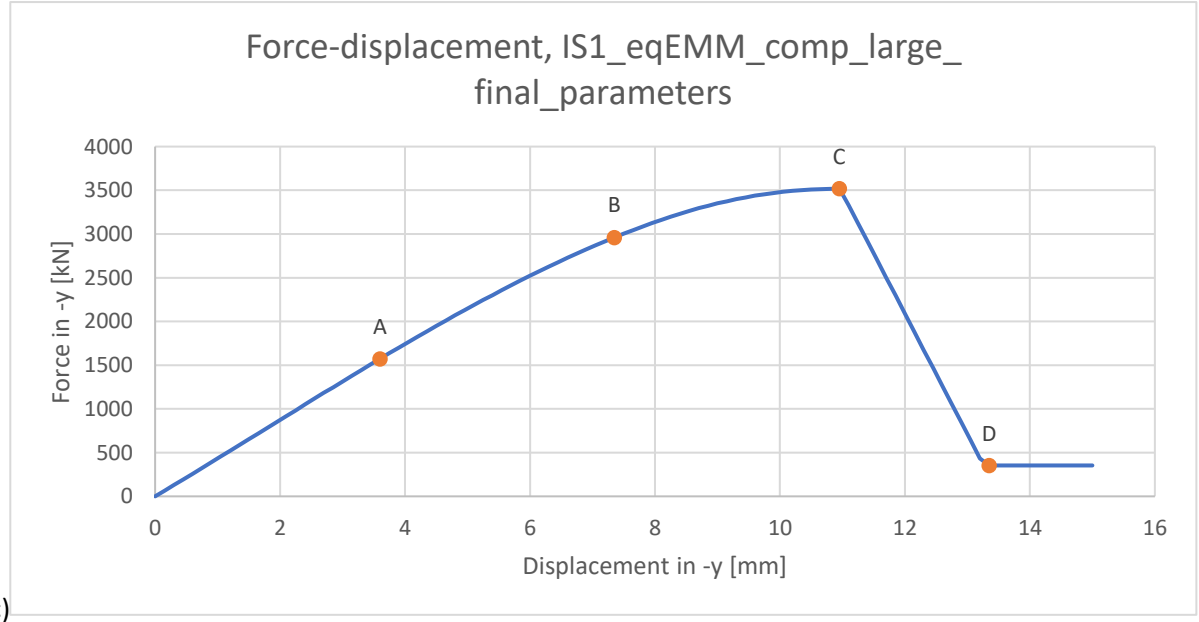

h)

Average element size [mm]		210.2x221.25
Number of elements	Q20SH	80
Total number of nodes		102

i)

Iteration method	Secant (Quasi-Newton)	
Convergence norms	Displacement	Force
Convergence tolerances	0.01	0.01
Step size	0.01(100)	
Maximum number of iterations per step	100	
All norms satisfied	No	

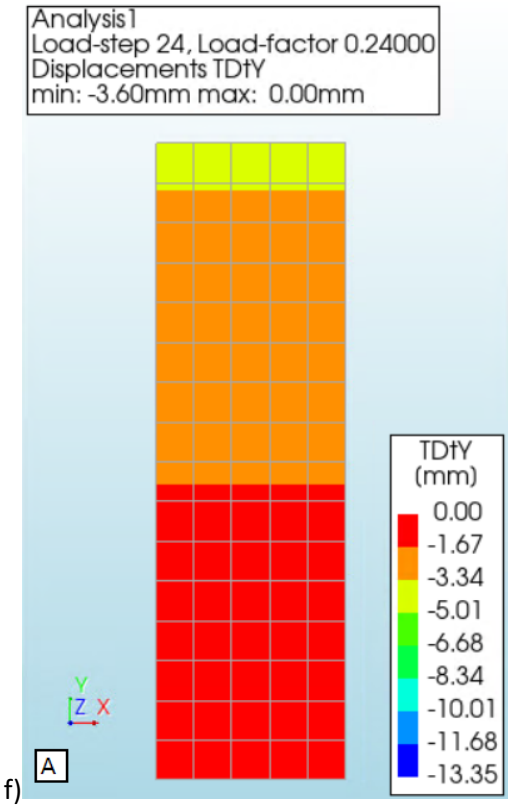

f)

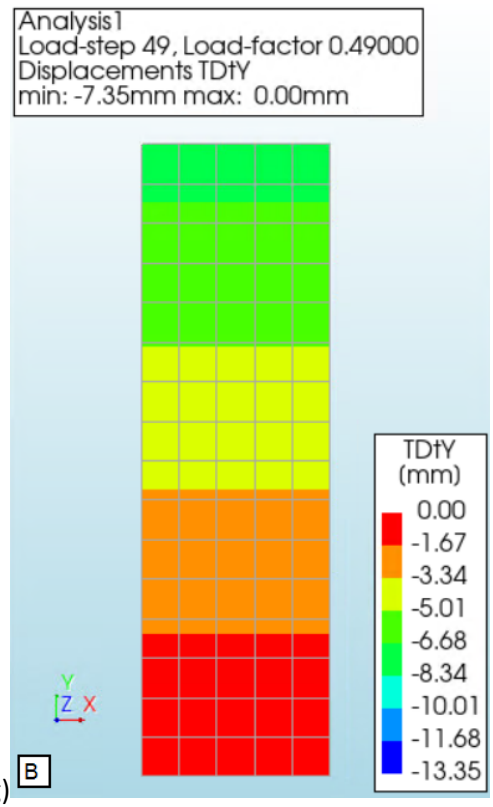

g)

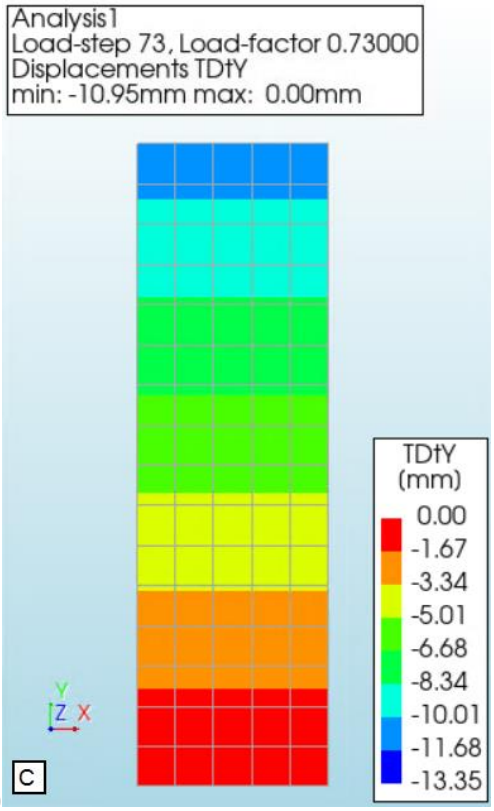

h)

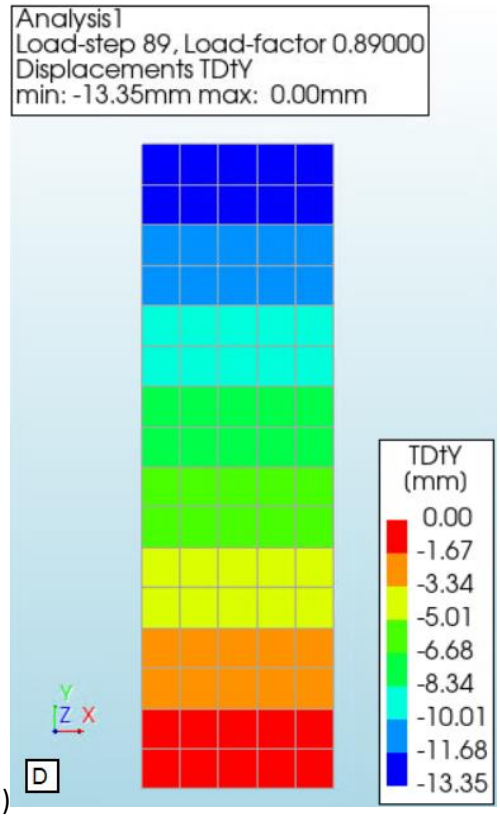

i)

Figure E.6: Results of finite element analysis IS1_eqEMM_comp_large_final_parameters. a-i: structure (a), finite element mesh (b), force-displacement curve (c), overview elements and nodes (d), overview iterative scheme (e), displacement at point A (f), displacement at point B (g), displacement at point C (h), displacement at point D (i)

a)

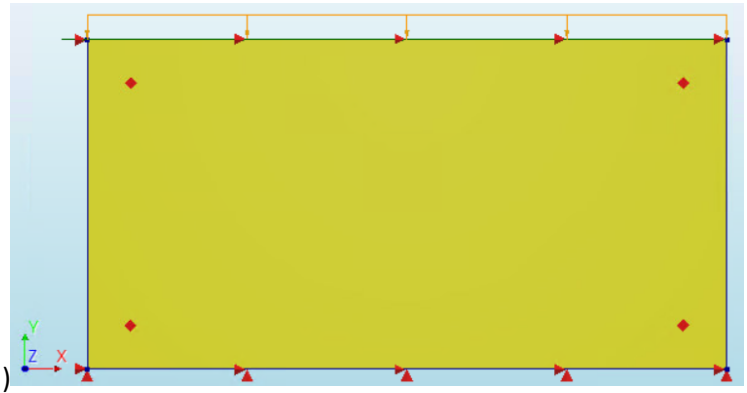

b)

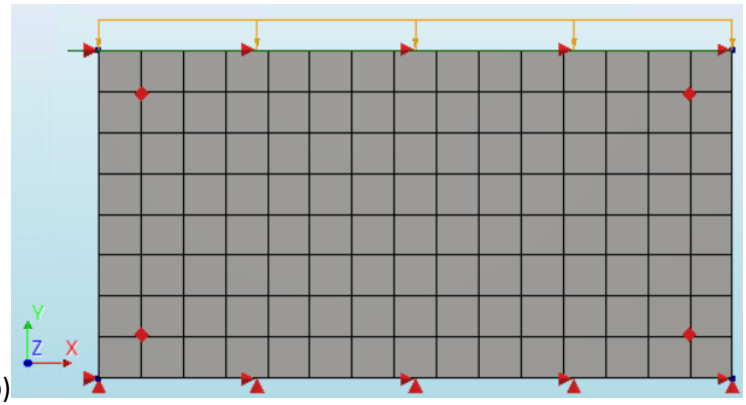

c)

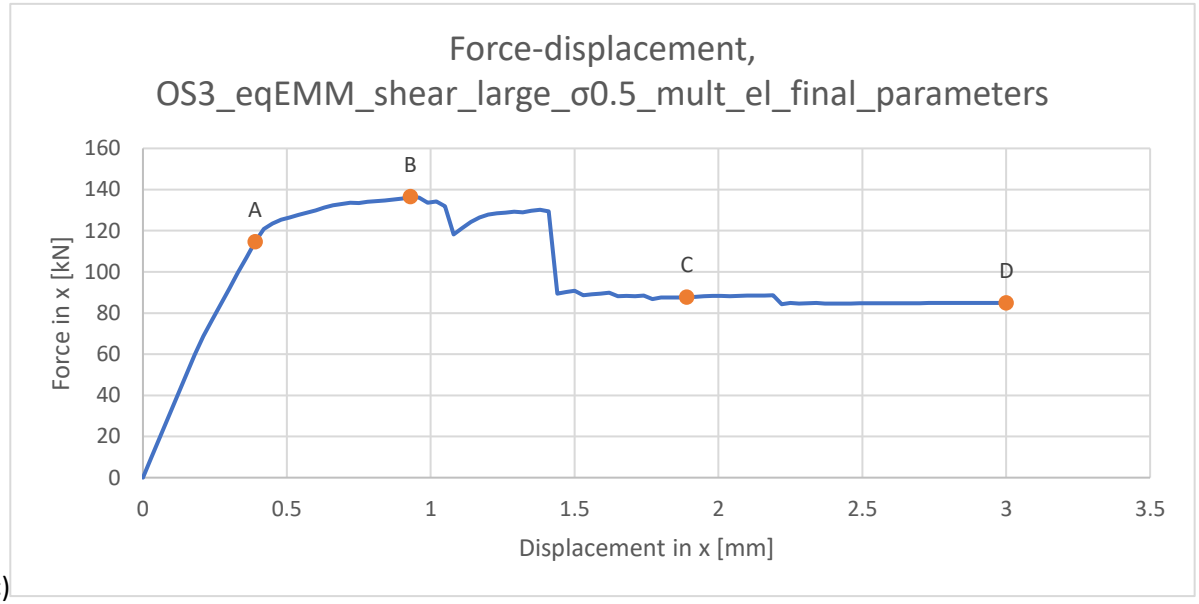

h)

Average element size [mm]		194x187.5
Number of elements	Q20SH	120
Total number of nodes		144

i)

Load	Compression		Translation	
Iteration method	Secant (Quasi-Newton)		Secant (Quasi-Newton)	
Convergence norms	Force	Displacement	Force	Displacement
Convergence tolerances	0.01	0.01	0.01	0.01
Step size	0.1(10)		0.01(100)	
Maximum number of iterations per step	100		100	
All norms satisfied	No		No	

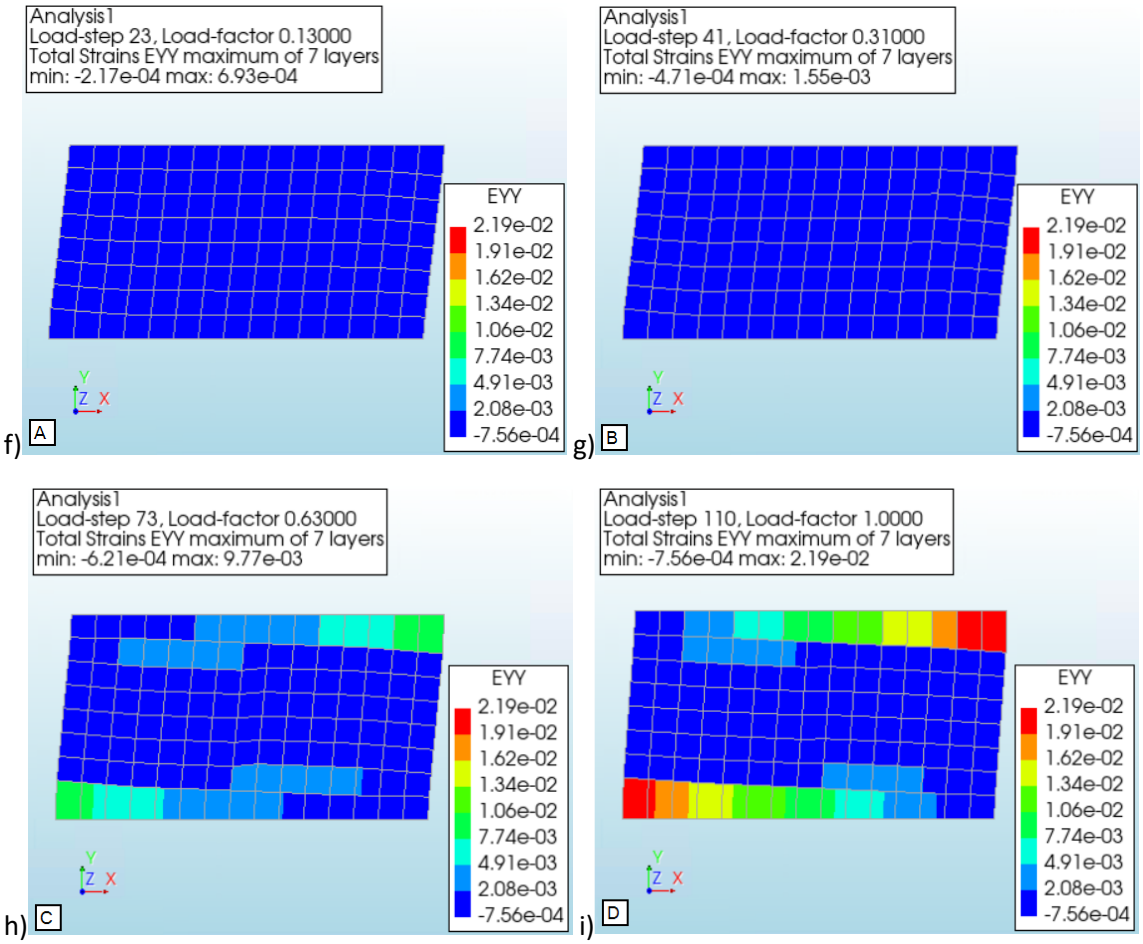

f) g) h) i)

Figure E.7: Results of finite element analysis OS3_eqEMM_shear_large_α0.5_mult_el_final_parameters. a-i: structure (a), finite element mesh (b), force-displacement curve (c), overview elements and nodes (d), overview iterative scheme (e), strain at point A (f), strain at point B (g), strain at point C (h), strain at point D (i)

a)

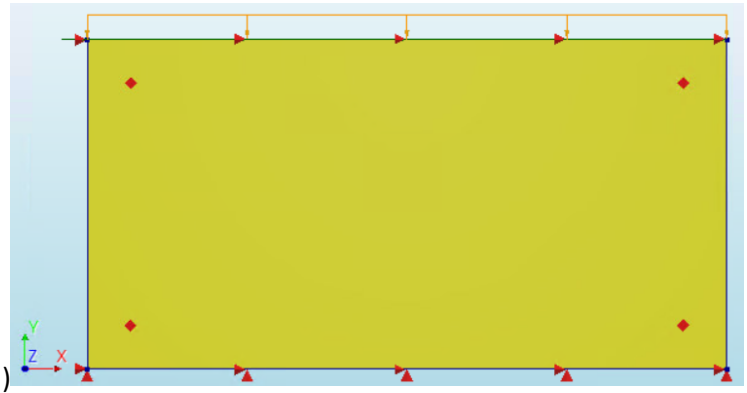

b)

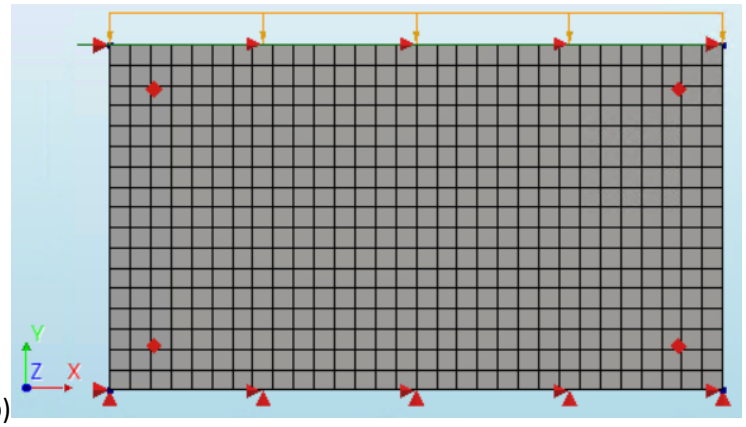

c)

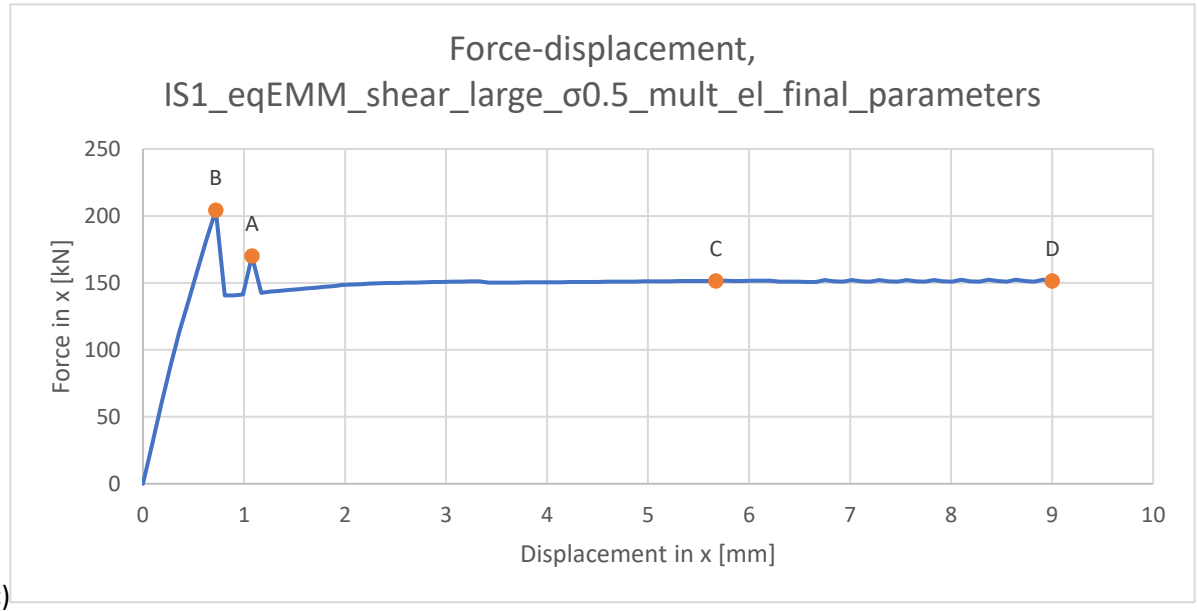

h)

Average element size [mm]		210.2x221.25
Number of elements	Q20SH	510
Total number of nodes		558

i)

Load	Compression		Translation	
Iteration method	Secant (Quasi-Newton)		Secant (Quasi-Newton)	
Convergence norms	Force	Displacement	Force	Displacement
Convergence tolerances	0.01	0.01	0.01	0.01
Step size	0.1(10)		0.01(100)	
Maximum number of iterations per step	100		100	
All norms satisfied	No		No	

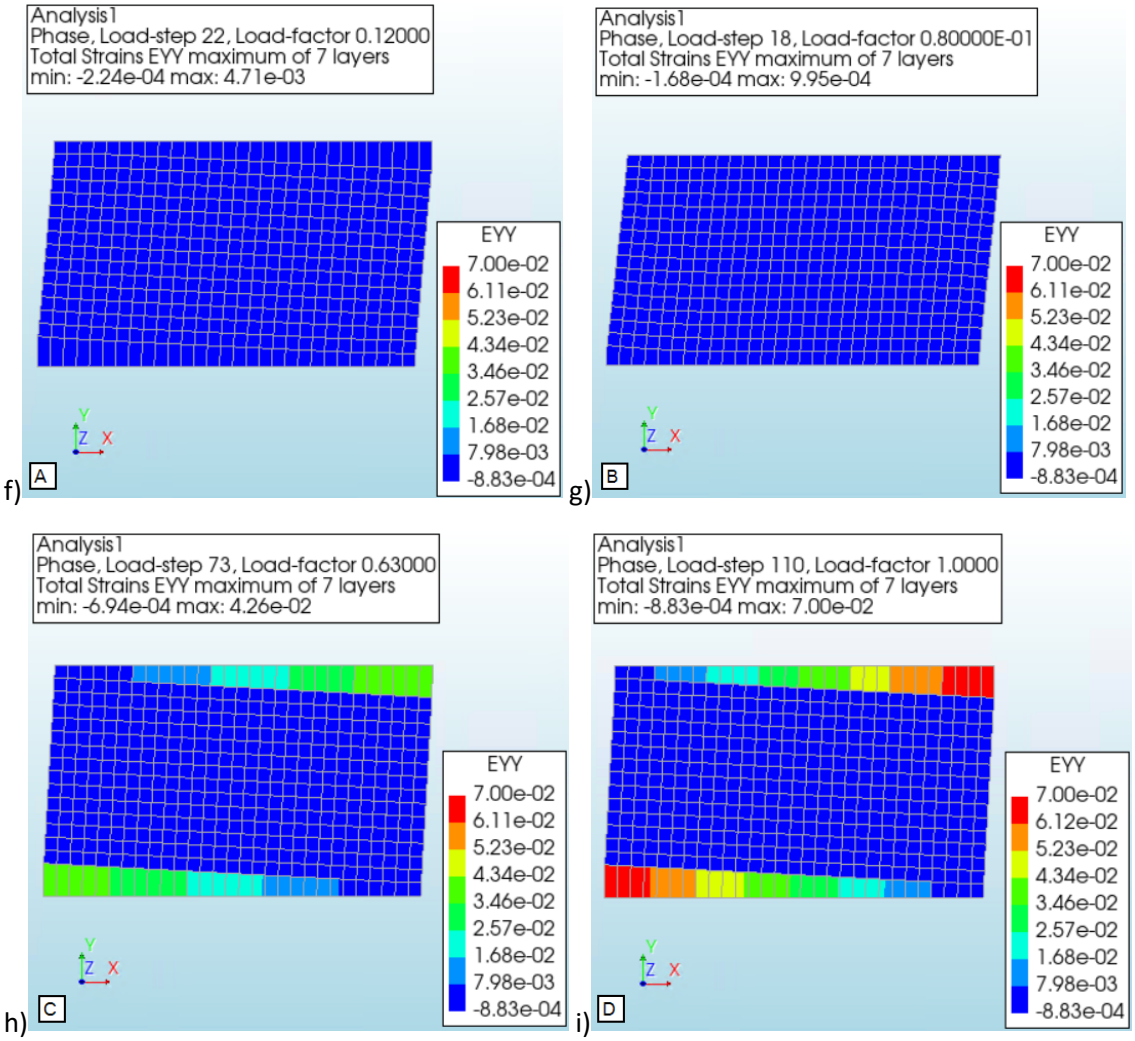

Figure E.8: Results of finite element analysis IS1_eqEMM_shear_large_σ0.5_mult_el_final_parameters. a-i: structure (a), finite element mesh (b), force-displacement curve (c), overview elements and nodes (d), overview iterative scheme (e), strain at point A (f), strain at point B (g), strain at point C (h), strain at point D (i)